University of Southampton

FACULTY OF PHYSICAL SCIENCES AND ENGINEERING
School of Physics and Astronomy

Inclusive semileptonic $B_{(s)}$-meson decays from Lattice QCD

by

Alessandro Barone

ORCiD: 0000-0002-0036-2517

A thesis for the degree of
Doctor of Philosophy

January 2024

University of Southampton

Abstract

FACULTY OF PHYSICAL SCIENCES AND ENGINEERING
School of Physics and Astronomy

Doctor of Philosophy

Inclusive semileptonic $B_{(s)}$-meson decays from Lattice QCD

by Alessandro Barone

The Standard Model (SM) is the most comprehensive framework to describe our current understanding of the known particle physics world. However, its limitations are well known as it cannot explain all observed phenomena. Discrepancies between measurements of SM observables and theoretical predictions guide us in the search for new physics and in extending the Standard Model.

One intriguing puzzle is the long-standing tension between the inclusive and exclusive determinations of the Cabibbo-Kobayashi-Maskawa (CKM) matrix elements $|V_{cb}|$ and $|V_{ub}|$, respectively. Semileptonic decays of B mesons constitute the main channel for the extraction of these parameters, and therefore represent crucial processes to address and investigate this tension. As B-physics experiments perform measurements and collect new data to study the B-meson properties, it becomes essential to address and understand the tension, and to provide more precise theoretical inputs to further improve our predictions.

In this work we address the nonperturbative calculation of the inclusive decay rate of semileptonic $B_{(s)}$-meson decays from lattice QCD. This type of computation may eventually provide new insight into the aforementioned tension in the determination of $|V_{cb}|$ and $|V_{ub}|$. We also address the computation of lepton energy and hadronic mass moments, which may provide ground for comparing lattice techniques with continuum approaches such as OPE and perturbation theory. We present results from a pilot lattice computation for $B_s \to X_c\, l \nu_l$, where the initial b quark described by the relativistic-heavy-quark (RHQ) formalism on the lattice and other valence quarks discretised with domain-wall fermions are simulated approximately at their physical quark masses. We compare different methods for computing the decay rate and the moments from lattice data of Euclidean four-point functions, namely approaches based on expansions in Chebyshev polynomials, approaches based on the Backus-Gilbert technique and also combinations of both. We find that the results we obtain are in excellent agreement. We further test our setup studying the ground-state meson limit and how much it dominates the

inclusive decay rate. We indicate possible strategies towards a computation with a more comprehensive error budget, and leave a proper determination of the systematics effects for future studies.

CONTENTS

LIST OF FIGURES

LIST OF TABLES

LIST OF ADDITIONAL MATERIAL

Dataset DOI: 10.5258/SOTON/D2798

Declaration of Authorship

I, Alessandro Barone, declare that this thesis and the work presented in it is my own and has been generated by me as the result of my own original research.

I confirm that:

1. This work was done wholly or mainly while in candidature for a research degree at this University;
2. Where any part of this thesis has previously been submitted for a degree or any other qualification at this University or any other institution, this has been clearly stated;
3. Where I have consulted the published work of others, this is always clearly attributed;
4. Where I have quoted from the work of others, the source is always given. With the exception of such quotations, this thesis is entirely my own work;
5. I have acknowledged all main sources of help;
6. Where the thesis is based on work done by myself jointly with others, I have made clear exactly what was done by others and what I have contributed myself;
7. Parts of this work have been published as: [1], [2] and [3].

Signed:..... Date:.....

Acknowledgements

First and foremost, I would like to thank my supervisor Prof. Andreas Jüttner for his exceptional guidance and constant support throughout my entire PhD journey. I am deeply grateful for introducing me to the field of Lattice QCD and for all the patience in our discussions. Secondly, I would like to thank Prof. Shoji Hashimoto for his guidance in this project and for hosting me as a JSPS fellow at KEK. I also wish to extend my gratitude to my collaborators Ryan Kellermann and Prof. Takashi Kaneko at KEK, as well as all the members of the lattice group in Southampton, particularly Prof. Jonathan Flynn and Prof. Chris Sachrajda, for all the useful comments and physics discussions.

These four years would have not been the same without the friends I made in Southampton, who provided me with much-needed balance and support. In no particular order, I wish to thank my flatmates and office mates Vlad and Mauricio, as well as the honorary flatmate Rajnandini, for all the enjoyable chats, random calls and fun moments we shared. A huge *grazie* goes to my friends Giorgio, Ivan, Valentina, Nikolaos and Hao, who became a second Italian family in this foreign city.

I cannot conclude my acknowledgements without thanking my parents, who always supported me in any way they could throughout my whole academic path.

DEFINITIONS AND ABBREVIATIONS

Chap(s).	Chapter(s)
Sec(s).	Section(s)
App(s).	Appendix(ces)
Eq(s).	Equation(s)
Fig(s).	Figure(s)
Tab(s).	Table(s)

INTRODUCTION

The Standard Model (SM) of particle particle physics is a renormalisable quantum field theory (QFT) that describes three of the four known fundamental forces of Nature, i.e. electromagnetic, weak and strong forces. It encodes information about all the known elementary particles and their interactions. Over the past decades, it allowed us to predict a wide variety of new particles and explain their behaviour and interactions. While this model has proven to be extremely successful in understanding a huge range of phenomena, it still fails to answer a large number of questions. Therefore, it cannot be considered a fundamental theory of the Universe, but only an effective theory valid at low energies. Some of the modern physics puzzles that are not taken into account by SM are:

- quantum gravity: the SM describes three of the four fundamental interactions at quantum level, but it does not include gravity, for which no satisfactory treatment of a QFT is known;
- hierarchy problem: it is not clear why there are vastly different energy and mass scales into the SM, namely the electroweak scale $M_{\rm EW} \sim 10^2\,\text{GeV}$ and the reduced Planck scale $M_{\rm P} \sim 10^{18}\,\text{GeV}$ (with $M_{\rm P} = 1/\sqrt{8\pi G}$ in natural units);
- mass generation problem: while SM successfully explains how particles acquire mass, it does not explain why they have the masses they do and why there is such a wide range of masses in the particle spectrum;
- cosmological constant: the vacuum energy density predicted by the SM is much smaller than the observed cosmological constant of the universe.

These are only few of the puzzling problems we face; other issues concern for example the strong CP problem, the origin of the parameters of the SM, the mass of the Higgs boson, the nature of dark matter and dark energy, and others.

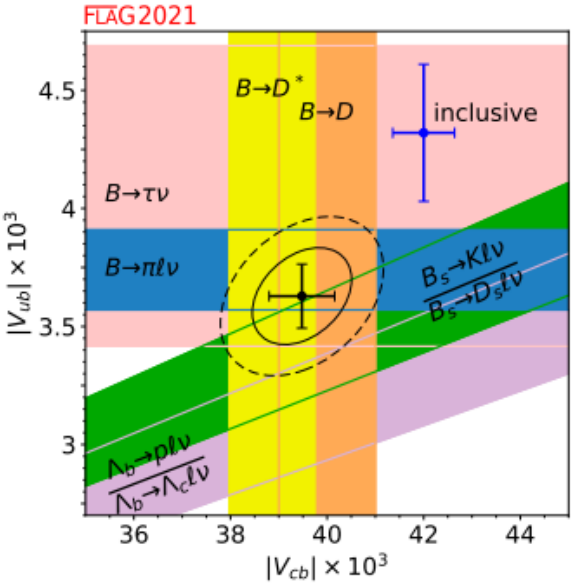

FIGURE 1: Summary of current status of $|V_{cb}|$ and $|V_{ub}|$ determination [5]. The black solid and dashed lines correspond to 68% and 95% C.L. contours, respectively. The lattice and experimental results are took from various groups, see [5] for full reference.

There are several different ways in which the SM could be extended, from *ad hoc* addition of new physics guided by experimental constraints to theoretical extensions suggested by first principles. However, the SM's physical predictions that can be tested in experiments are so far very robust: there are many extensions of the model which give acceptable descriptions now, but may no longer do so once more constraining data becomes available. A crucial task is therefore to increase precision from both theoretical predictions and experimental measurements to look for a signal or inconsistencies indicating New Physics. One area of particular interest is *quark-flavour physics*, which involves weak processes characterised by flavour-changing currents and aim to study the transitions and interactions among quarks. Indeed, some of these processes have been shown some tensions of the order of 2–3 σ (with σ being the standard deviation) between different determinations [4]. For example, tensions arise from extractions of the same SM parameters from different processes, e.g. the CKM-matrix elements [4,5], or from discrepancies between SM's theoretical predictions and experimental results as in the case of the ratio $R_{D^{(*)}}$ [6–11], to name a few. Any such anomalies could be an indicator of new effects: while new particles may be too heavy to be produced with energies achievable by current experimental facilities, quantum effects could leave detectable traces in flavour-physics processes.

In this thesis we focus in particular on the b-quark sector of particle physics. Indeed, the study of processes involving the bottom quark remains an exciting arena of precision physics, in which intriguing tensions between observations and SM predictions have been found [6,7,10,12–14]. One of these long standing tensions involves the measured values of the CKM-matrix elements $|V_{cb}|$ and $|V_{ub}|$ between exclusive and inclusive decays. The

former refer to decays with a single hadron in the final state (usually the ground state), whereas the latter refer to the case where all possible final states allowed by the decay are accounted for. Considering the semileptonic channel (i.e. a weak force mediated process where both hadrons and leptons are produced in the final state), $|V_{cb}|$ and $|V_{ub}|$ can be determined, for example, from the decay of a B into a $D^{(*)}$ (or π), or through the measurement of their inclusive decay rate. Other processes are indicated in the plot in Fig. 1 and a more general and complete review can be found in [4,5]. One of the most recent determination of $|V_{cb}|$ is

$$\begin{aligned} |V_{cb}| &= (42.19 \pm 0.78) \times 10^{-3} \quad \text{inclusive} \quad [4,15], \\ |V_{cb}| &= (39.36 \pm 0.68) \times 10^{-3} \quad \text{exclusive} \quad [5,16\text{–}19]\,, \end{aligned}$$

which shows a tension of $\simeq 2.7\sigma$, for which the corresponding summary plot of lattice results from the latest FLAG review [5] is shown in Fig. 1. In this work we focus on semileptonic meson decays, and in particular on their inclusive version.

While many SM predictions can be obtained from analytical calculations and perturbation theory, low-energy processes involving the strong force require the computation of nonperturbative contributions. Lattice Quantum Chromodynamics (LQCD) plays a central role in these computations: in particular, lattice calculations provide a solid framework to address the determination of hadronic form factors, which parametrise exclusive decay channels. In fact, the required lattice techniques to address exclusive decays are well established (see reviews [5, 20]).

On the other hand, the existing results for the inclusive decay are based on perturbative QCD and Operator Product Expansion (OPE) [15,21,22]. Given the described tensions, an independent theoretical prediction is therefore very timely. First viable theoretical proposals for how to accomplish the computation of the inclusive decay rate on the lattice have appeared only recently [23]. The idea relies on the extraction of a forward-scattering matrix element through analytic continuation of lattice results obtained in an unphysical kinematical region. In [24] it was then proposed to address decay and transition rates of multi-hadron processes through finite-volume Euclidean four-point functions provided that a method to extract the associated spectral function exists.

In this thesis, we present work towards an improved understanding of the calculation of the inclusive decay rate by means of a pilot study of semileptonic decays of B_s mesons into charmed particles, namely $B_s \to X_c\, l\nu_l$, following [25], where the extraction of the spectral function is bypassed, and the decay rate is evaluated directly. Part of this work has been presented and published in [1–3]. In particular, we improve and compare two existing methods, namely Chebyshev [25–27] and Backus-Gilbert [28,29] reconstructions.

In particular, this work provides a flexible setup to study inclusive decays on the lattice, relying on the pilot study of [25]. We find that the two techniques used for the analysis

are in agreement at the current statistical resolution for all the observables considered. We also obtain reliable predictions for the ground-state limit of the inclusive decay, which is found to reproduce the results of the exclusive channel evaluated with more conventional methods.

This thesis is organised as follows. In Chap. 1 we briefly review the building blocks of the Standard Model, highlighting in particular the electroweak and strong sector, together with the basics of Heavy Quark Effective Theory. In Chap. 2 we introduce the formalism of Lattice QCD, presenting the essential features adopted in this work. In Chap. 3 we present the continuum formulation specific to both exclusive and inclusive semileptonic B_s-mesons decay, and subsequently specialise to the lattice formalism for inclusive decays in Chap. 4. We give the details of the computations in Chap. 5 and present and discuss the result of our pilot study in Chap. 6. We summarise our findings and outline future work in the Conclusions.

CHAPTER 1

STANDARD MODEL

The Standard Model describes three of the four known fundamental forces and all the elementary particles that have been observed in Nature. In particular, it includes the quantum field theory of the strong, weak and electromagnetic interactions. It has been developed in the second half of the 20th century, thanks to (but not limited to) the central works of Yang and Mills [30], Glashow [31, 32], Salam and Ward [33, 34], Weinberg [35], Higgs [36, 37], Brout and Englert [38], Gell-Mann [39, 40], Politzer [41], Gross and Wilczek [42].

In this chapter, we describe some of the core aspects of the Standard Model, and refer to other textbooks for a more complete overview [43–45]. We introduce the particle content of the model in Sec. 1.1 and describe the main mathematical aspects of gauge theories in Sec. 1.2. We then review the electroweak and strong interactions in Sec. 1.3 and Sec. 1.4, respectively. For completeness, we conclude with some brief notes on Heavy Quark Effective Theory in Sec. 1.5, which represent a common framework to study some of the processes connected with this work.

1.1 Symmetries and particle content

A basic guiding principle to build particle physics models is given by *symmetries*: these are transformations of fields of the theory that leave the physics equations invariant. Symmetries can be *discrete* or *continuous*, *global* or *local*.

There are two general classes of transformations, *space-time symmetries* and *internal symmetries*. Space-time symmetries transform the coordinate $x^\mu \in \mathcal{M}$, with $\mathcal{M}$ being

the four-dimensional Minkowski space, as

$$x^\mu \rightarrow x'^\mu(x^\nu)\,, \quad \mu,\nu = 0,1,2,3\,. \tag{1.1}$$

Examples of these are Lorentz and Poincaré continuous transformations, but also discrete ones like parity or time-reversal.

Internal symmetries, on the other hand, transform the given field $\Phi(x)$ and do not act on the space-time coordinates, but only on the field representation, i.e.

$$\Phi^a(x) \rightarrow \Phi'^a(x) = M^a_b\,\Phi^b(x)\,, \tag{1.2}$$

where M^a_b is a generic matrix and the sum over b is intended. If M^a_b is independent of x, the symmetry is said to be *global*, whereas if it depends on the space-time coordinate $M^a_b \equiv M^a_b(x)$ it is said to be *local*. Local symmetries involve internal transformations which depend on the space-time and are key to build gauge theories.

Symmetries are important for many reasons: we list some of the main ones here.

1. They classify the properties of all the known particles such as, e.g. spin, electric, colour charge,...etc. and they define conserved physical quantities through generalisations of Noether's theorem [46].

2. They determine the interaction among particles thanks to the *gauge principle* by promoting global symmetries to local ones, which gives rise to *gauge bosons* as mediators of the interactions.

3. Symmetries can be spontaneously broken: this is a natural way in which the mass scale of the theory arises.

Symmetries are not always exact, but can be spontaneously or explicitly broken, depending on how the Lagrangian $\mathcal{L}$ of the theory and the vacuum $|0\rangle$ (and more precisely the vacuum expectation value of the fields) are modified under the given transformations. In particular, for the purpose of this chapter we limit ourselves to consider three cases:

1. Unbroken symmetry. Both the Lagrangian and the vacuum are left unchanged, i.e. $\mathcal{L} \rightarrow \mathcal{L}' = \mathcal{L}$ and $|0\rangle \rightarrow |0\rangle' = |0\rangle$ under application of a symmetry transformation.

2. Spontaneously broken symmetry. The Lagrangian is invariant, $\mathcal{L} \rightarrow \mathcal{L}' = \mathcal{L}$, but the vacuum is not, i.e. $|0\rangle \rightarrow |0\rangle' \neq |0\rangle$.

3. Explicitly broken symmetry. This is the case where the transformations do not constitute a symmetry of the Lagrangian in the first place, i.e. $\mathcal{L} \rightarrow \mathcal{L}' \neq \mathcal{L}$.

The Standard Model is a gauge theory based on the symmetry groups

$$SU(3)_C \times SU(2)_L \times U(1)_Y \,, \tag{1.3}$$

where C stands for *colour*, L refers to the *(left-handed) weak isospin* and Y is the *hypercharge*. $SU(3)_C$ describes the strong force through a QFT know as *Quantum Chromodynamics* (QCD), and $SU(2)_L \times U(1)_Y$ describes the electroweak force, which recovers the electromagnetic interaction described by the gauge group $U(1)_{EM}$ through a *spontaneous symmetry breaking* mechanism at the electroweak scale $M_{EW} \sim 10^2\,\text{GeV}$, as we will see in Sec. 1.3.1. The purely electromagnetic interaction can indeed be described by an abelian gauge theory based on the group $U(1)_{EM}$ known as *Quantum Electrodynamics* (QED) [47, 48].

The Standard Model Lagrangian $\mathcal{L}_{SM}$ can then be decomposed as

$$\mathcal{L}_{SM} = \mathcal{L}_{QCD} + \mathcal{L}_{EW} + \mathcal{L}_H + \mathcal{L}_Y \,, \tag{1.4}$$

where $\mathcal{L}_{QCD}$ describes the strong force and $\mathcal{L}_{EW}$ the electroweak one, whereas $\mathcal{L}_H$ account for the Higgs field and $\mathcal{L}_Y$ for the Yukawa couplings. We will discuss and clarify these components in more detail in the following sections of this chapter.

The matter content of the Standard model is given by two types of *fermions*, which are spin-1/2 particles. The first type are the *leptons*, which come in three generations given by the charged electron e, the muon μ and the tauon τ, and their neutral partners, i.e. the neutrinos ν_e, ν_μ and ν_τ. The second type are the *quarks*, also divided in three generations, which come in different *flavours*, given by up u and down d (first generation), charm c and strange s (second generation), bottom b and top t (third generation).

The interactions are carried by the gauge bosons, i.e. spin-1 particles that arise from the gauge groups of the Standard Model. In particular, the strong force is mediated by 8 gluons, which carry colour and anti-colour charges and interact only with quarks. The weak force is mediated by the positively and negatively charged $W^\pm$ bosons and by the neutral Z^0. Finally, the electromagnetic force is carried by the photon γ.

Quarks are charged with respect to all SM interactions and therefore interact with all the gauge bosons. Charged leptons interact both with the electroweak bosons and the photon, whereas the neutrinos interact only with the electroweak bosons.

The Higgs boson, the only spin-0 particle of the Standard Model, concludes the picture and is responsible for the mechanism that provide the particles with mass.

1.2 Non-abelian gauge theories

In this section, we briefly discuss the idea behind gauge theories and their construction [30]. We consider the general case of $SU(N)$ local symmetry, $SU(N)$ being the special unitary group of $N \times N$ matrices. This formulation can then be applied to the group of interest $SU(3)_C$ and $SU(2)_L$, as well the abelian group $U(1)_Y$. From a physical point of view, the request of local invariance corresponds to the fact that physical processes are unaltered by an arbitrary rotation under $SU(N)$ at each space-time point: for example, in the $SU(3)_C$ case, this means that one is free to redefine the colour charges at each space-time coordinate independently.

Let us consider a fermion field $\psi \equiv \psi(x)$ with a mass m, for which the free Lagrangian reads

$$\mathcal{L}_0 = \bar{\psi}(i\gamma^\mu \partial_\mu - m)\psi \,. \tag{1.5}$$

We now need to modify the above Lagrangian in order to make it invariant under the local transformation

$$\psi(x) \to \psi'(x) = U(x)\psi(x) \,, \tag{1.6}$$

$$\bar{\psi}(x) \to \bar{\psi}'(x) = \bar{\psi}(x)U^\dagger(x) \,, \tag{1.7}$$

where $U(x) \in SU(N)$ such that

$$U(x) = \exp\left(\frac{i}{2}\boldsymbol{t} \cdot \boldsymbol{\alpha}(x)\right) \tag{1.8}$$

where $\boldsymbol{t}/2$ is the vector containing the N^2-1 generators of $SU(N)$, i.e. $T^a = t^a/2$, which are represented by $N \times N$ unitary matrices living in the corresponding $su(n)$ algebra, and $\boldsymbol{\alpha}(x)$ is a vector of N^2-1 real components dependent on the space-time coordinate x. In particular, the generators satisfy the anticommutation relation

$$[T^a, T^b] = if^{abc}T^c \,, \tag{1.9}$$

where f^{abc} are the structure constant of the $SU(N)$ group. We will highlight the importance of this property of non-abelian groups at the end of the section.

Since U depends on x, the derivative term breaks the invariance, i.e.

$$\bar{\psi}\partial_\mu\psi \;\to\; \bar{\psi}'\partial_\mu\psi' \neq \bar{\psi}\partial_\mu\psi \,. \tag{1.10}$$

To fulfil the invariance request, we introduce the *covariant derivative*

$$D_\mu = \partial_\mu - igA_\mu \,, \tag{1.11}$$

where g is a constant that parametrises the strength of the interactions and A_μ is a $N \times N$ algebra-valued matrix

$$A_\mu = \frac{1}{2}\boldsymbol{t} \cdot \boldsymbol{A}_\mu = \frac{1}{2} t^a A^a_\mu \,, \tag{1.12}$$

with A^a_μ being the N^2-1 *gauge fields* (or *Yang-Mills fields*) which mediate the interaction associated with the $SU(N)$ group. The invariance requirement

$$\bar{\psi} D_\mu \psi \;\to\; \bar{\psi}' D'_\mu \psi' = \bar{\psi} D_\mu \psi \tag{1.13}$$

is now satisfied provided that the derivative and gauge fields transform as

$$D_\mu \;\to\; D'_\mu = \partial_\mu - i g A'_\mu \,, \tag{1.14}$$

$$A_\mu \;\to\; A'_\mu = U \left[A_\mu - \frac{i}{g} U^\dagger (\partial_\mu U) \right] U^\dagger \,. \tag{1.15}$$

We can now write the new Lagrangian as

$$\begin{aligned} \mathcal{L} &= \bar{\psi}(i\gamma^\mu D_\mu - m)\psi \\ &= \mathcal{L}_0 - g\bar{\psi}\gamma^\mu A_\mu \psi \\ &= \mathcal{L}_0 - \frac{g}{2} A^a_\mu \, \bar{\psi}\gamma^\mu t^a \psi \,, \end{aligned} \tag{1.16}$$

which can be split into the free Lagrangian $\mathcal{L}_0$ and an interaction part, which contains the interaction of the fermion currents $J^a_\mu = \bar{\psi}\gamma_\mu t^a \psi$ and the gauge fields A^a_μ.

The pure gauge Lagrangian $\mathcal{L}_G$, which contains the interactions among the gauge fields A^a_μ, is built as

$$\mathcal{L}_G = -\frac{1}{2} \operatorname{Tr}[F_{\mu\nu} F^{\mu\nu}] = -\frac{1}{4} F^a_{\mu\nu} F^{a\mu\nu} \,, \tag{1.17}$$

where the last line follows from $\operatorname{Tr}\left[t^a t^b\right] = 2\delta^{ab}$ and

$$F_{\mu\nu} = \frac{1}{2} F^a_{\mu\nu} t^a \tag{1.18}$$

with $F^a_{\mu\nu}$ being the field strength tensor. The latter can be built from the covariant derivatives as

$$F_{\mu\nu} = \frac{1}{ig}[D_\mu, D_\nu] = \partial_\mu A_\nu - \partial_\nu A_\mu - ig[A_\mu, A_\nu] \,, \tag{1.19}$$

and it transforms under $SU(N)$ as

$$F_{\mu\nu} \;\to\; F'_{\mu\nu} = U F_{\mu\nu} U^\dagger \,. \tag{1.20}$$

A key feature of non-abelian gauge theories is the presence of the non-trivial commutator $[A_\mu, A_\nu]$ in Eq. (1.19), as it follows from Eq. (1.9). Indeed, this implies that the gauge

Lagrangian contains terms that involve interactions among gauge fields (with 3 or 4 fields interacting at each vertex). This is a key feature of the weak and strong sectors of the Standard Model. These terms are absent in the case of an abelian group $U(1)$, as the structure constants of the group are zero and all the generators commute.

This concludes the discussion on non-abelian gauge theories, which represents the underlying fundamentals to build the Standard Model, as we will outline in the next sections. We showed how, starting from a free fermionic Lagrangian, it is possible to introduce interactions with a field carrying a given charge by requiring invariance under the corresponding local transformations of $SU(N)$. Finally, we showed how to introduce the Lagrangian $\mathcal{L}_G$ that contains the general kinetic terms for these gauge fields.

1.3 Electroweak theory

The electroweak theory is based on the $SU(2)_L \times U(1)_Y$ gauge groups, which correspond to the weak isospin and hypercharge quantum numbers, respectively. In particular, $SU(2)_L$ acts only on fermions with negative chirality (left-handed fermions), as determined by the quantum number associated with the chiral operator γ_5 (see an explicit representation in App. A.1). In particular, a fermion field ψ can be decomposed into its positive (right) and negative (left) chiral components as

$$\psi = P_R\psi + P_L\psi \equiv \psi_R + \psi_L \,, \tag{1.21}$$

where $P_{R,L} = (\mathrm{I} \pm \gamma_5)/2$ are the right- and left-handed chiral projectors, respectively.

Let us now discuss explicitly the construction of the model. Left-handed quark and leptons are introduced as $SU(2)_L$ doublets, defined as

$$L_1^l = \begin{pmatrix} \nu_{eL} \\ e_L \end{pmatrix} , \quad L_2^l = \begin{pmatrix} \nu_{\mu L} \\ \mu_L \end{pmatrix} , \quad L_3^l = \begin{pmatrix} \nu_{\tau L} \\ \tau_L \end{pmatrix} , \tag{1.22}$$

for the charged and neutral leptons and

$$L_1^q = \begin{pmatrix} u_L \\ d_L \end{pmatrix} , \quad L_2^q = \begin{pmatrix} c_L \\ s_L \end{pmatrix} , \quad L_3^q = \begin{pmatrix} t_L \\ b_L \end{pmatrix} , \tag{1.23}$$

for the quarks. The upper components of the doublets have weak isospin $1/2$, whereas the lower components have isospin $-1/2$. The doublets are also charged under $U(1)_Y$, with hypercharges $Y_L^l = -1$ and $Y_L^q = 1/3$. It is useful for later purposes (in particular in Sec. 1.3.2) to define in a compact notation these isospin components defining

$$L_i^{l,q} = \begin{pmatrix} L_{i+}^{l,q} \\ L_{i-}^{l,q} \end{pmatrix} , \tag{1.24}$$

for both leptons and quarks. The right-handed components are charged under $U(1)_Y$ and are singlets of $SU(2)_L$. For a compact and uniform notation we define

$$R^l_{1-} = e_R\,, \quad R^l_{2-} = \mu_R\,, \quad R^l_{3-} = \tau_R\,, \tag{1.25}$$

for the leptons, which have hypercharge $Y^l_{R-} = -2$, and

$$R^q_{1+} = u_R\,, \quad R^q_{2+} = c_R\,, \quad R^q_{3+} = t_R\,, \tag{1.26}$$

$$R^q_{1-} = d_R\,, \quad R^q_{2-} = s_R\,, \quad R^q_{3-} = b_R\,, \tag{1.27}$$

which carry hypercharge $Y^q_{R+} = 4/3$ and $Y^q_{R-} = -2/3$. Note that there are no right-handed neutrinos in the Standard Model: we will comment more about this in Sec. 1.3.2. The covariant derivatives with respect to the electroweak symmetry groups are

$$D^L_\mu = \partial_\mu - ig\frac{1}{2}\sigma^a W^a_\mu(x) - ig' Y B_\mu(x)\,, \quad D^R_\mu = \partial_\mu - ig' Y B_\mu(x) \tag{1.28}$$

where σ^a are the $SU(2)_L$ generators, i.e. the Pauli matrices, and Y is the generator of $U(1)_Y$. The coupling constant g and g' refers to the strength of interaction of the gauge fields W^a_μ of $SU(2)_L$ and the field $B_\mu(x)$ of $U(1)_Y$, respectively. The fermion electroweak Lagrangian $\mathcal{L}_{EW,F} = \mathcal{L}^l_{EW,F} + \mathcal{L}^q_{EW,F}$ is then given by

$$\mathcal{L}^l_{EW,F} = \sum_{i=1}^{3} \left[\bar{L}^l_i\, i\gamma^\mu D^L_\mu\, L^l_i + \bar{R}^l_{i-}\, i\gamma^\mu D^R_\mu\, R^l_{i-} \right]\,, \tag{1.29}$$

$$\mathcal{L}^q_{EW,F} = \sum_{i=1}^{3} \left[\bar{L}^q_i\, i\gamma^\mu D^L_\mu\, L^q_i + \bar{R}^q_{i+}\, i\gamma^\mu D^R_\mu R^q_{i+} + \bar{R}^q_{i-}\, i\gamma^\mu D^R_\mu\, R^q_{i-} \right]\,. \tag{1.30}$$

This Lagrangian contains now the kinetic terms for all the leptons and quarks together with their interaction terms with the gauge bosons W^1_μ, W^2_μ, W^3_μ and B_μ. The gauge Lagrangian for the latter can be constructed as in Eq. (1.17), i.e.

$$\mathcal{L}_{EW,G} = -\frac{1}{4} W^a_{\mu\nu} W^{a\mu\nu} - \frac{1}{4} B_{\mu\nu} B^{\mu\nu}\,, \tag{1.31}$$

where

$$W_{\mu\nu} = \partial_\mu W_\nu - \partial_\nu W_\mu - ig[W_\mu, W_\nu]\,, \tag{1.32}$$

$$B_{\mu\nu} = \partial_\mu B_\nu - \partial_\nu B_\mu\,, \tag{1.33}$$

are the field strength tensor for the fields $W_\mu = W^a_\mu\, \sigma^a/2$ and B_μ, respectively. We have then all the pieces to fully describe the $SU(2)_L \times U(1)_Y$ Lagrangian, which is given by

$$\mathcal{L}_{EW} = \mathcal{L}^l_{EW,F} + \mathcal{L}^q_{EW,F} + \mathcal{L}_{EW,G}\,. \tag{1.34}$$

However, this does not yet represent the physics we observe in nature. Indeed, it is

not possible to write any mass term for the leptons, quarks or gauge bosons, as such term would explicitly break gauge invariance. The Lagrangian $\mathcal{L}_{EW}$ presented here is therefore incomplete: we discuss in the next sections how to generate the mass terms for all the particles and how to relate the gauge fields W^i_μ and B_μ to the physical gauge bosons.

1.3.1 Spontaneous symmetry breaking and Higgs mechanism

As we just pointed out, gauge invariance forbids any mass term for leptons, quarks and gauge bosons: such a term would be an example of an explicitly breaking of the symmetry, as mentioned in Sec. 1.1. Instead, gauge bosons and fermions acquire mass through the Higgs field [36–38] and its spontaneous symmetry breaking mechanism, together with the Yukawa Lagrangian, which allows to generate the fermion masses through the interaction with the Higgs boson.

Let us start presenting the Higgs sector. We consider a $SU(2)_L$ doublet of complex scalar fields, that we indicate with

$$\Phi(x) = \begin{pmatrix} \phi_+(x) \\ \phi_0(x) \end{pmatrix} = \frac{1}{\sqrt{2}} \begin{pmatrix} \phi_1(x) + i\phi_2(x) \\ \phi_3(x) + i\phi_4(x) \end{pmatrix} , \tag{1.35}$$

where $\phi_i(x)$, $i = 1, 2, 3, 4$ are real scalar fields, and its Lagrangian

$$\mathcal{L}_H = \left[D^{L\,\mu}\Phi(x)\right]^\dagger \left[D^L_\mu \Phi(x)\right] + V(\Phi(x)) \,, \tag{1.36}$$

with D^L_μ in Eq. (1.28) and where $V(\Phi)$ is the Higgs potential associated with the field $\Phi(x)$

$$V(\Phi(x)) = -\mu^2 \Phi(x)^\dagger \Phi(x) + \lambda \left[\Phi(x)^\dagger \Phi(x)\right]^2 . \tag{1.37}$$

This potential has the peculiarity of having a negative mass term $-\mu^2$. It follows that $V(\Phi)$ possesses a set of minima given by

$$\Phi^\dagger \Phi = \frac{\mu^2}{2\lambda} \equiv \frac{v^2}{2} \,, \tag{1.38}$$

where we defined the vacuum $v^2 = \frac{\mu^2}{\lambda}$. This relation defines a set of equivalent *vacuum expectation values* (vev) for the scalar field Φ. This implies that in the four-dimensional space spanned by the real fields $(\phi_1, \phi_2, \phi_3, \phi_4)$ there exists a three-dimensional sphere along which the vev is always the same. Exploiting this observation, we can choose a vev for the field $\langle\Phi\rangle$ and re-parametrise the scalar doublet as fluctuations around it in terms of three real fields $\theta^a(x)$, which corresponds to the three directions tangent to the three-dimensional sphere that leave the vacuum invariant, and a real field $h(x)$, which

parametrises the fluctuations in the orthogonal direction, i.e.

$$\langle\Phi\rangle = \frac{1}{\sqrt{2}}\begin{pmatrix}0\\ v\end{pmatrix}, \quad \Phi(x) = \frac{1}{\sqrt{2}}e^{i\frac{1}{2v}\sigma^a\theta^a(x)}\begin{pmatrix}0\\ v+h(x)\end{pmatrix}. \tag{1.39}$$

Note that the real scalar fields $\theta^a(x)$ correspond to massless particles known as Nambu-Goldstone bosons [49, 50]. It is now possible to perform a gauge transformation that removes the fields $\theta^a(x)$ from the parametrisation of the scalar field using the so called *unitary gauge* [51, 52], for which the field $\Phi(x)$ reads

$$\Phi(x) = \frac{1}{\sqrt{2}}\begin{pmatrix}0\\ v+h(x)\end{pmatrix}. \tag{1.40}$$

The degrees of freedom carried by the fields $\theta^a(x)$ get in this way reabsorbed into the longitudinal degrees of freedom of the massive electroweak bosons, whose fields also undergo the gauge transformation. The field $h(x)$ corresponds to the Standard Model Higgs boson and its interaction with the gauge fields is responsible for generating the electroweak boson masses, as it can be seen by substituting Eq. (1.40) in Eq. (1.36). In Sec. 1.3.2 we will highlight how it is also responsible for all the fermion masses. Rewriting the field as in Eq. (1.40) in the Lagrangian Eq. (1.36) we obtain the required terms to connect the gauge fields with the physical massive bosons, which are expressed as

$$W^{\pm}_{\mu} \equiv \frac{1}{\sqrt{2}}(W^1_{\mu} \mp iW^2_{\mu}), \tag{1.41}$$

$$Z^0_{\mu} \equiv \frac{1}{\sqrt{g^2+g'^2}}(gW^3_{\mu} - g'B_{\mu}), \tag{1.42}$$

together with the massless photon field γ

$$A_{\mu} \equiv \frac{1}{\sqrt{g^2+g'^2}}(gW^3_{\mu} + g'B_{\mu}). \tag{1.43}$$

By inspection of the new mass term in the Lagrangian we can now see that they are related to the vacuum and the coupling constant as

$$M_{W^{\pm}} = \frac{gv}{2}, \tag{1.44}$$

$$M_{Z^0} = \frac{v}{2}\sqrt{g^2+g'^2}, \tag{1.45}$$

$$M_{\gamma} = 0. \tag{1.46}$$

Note that this mechanism leaves the photon massless. Indeed, the choice of the vev for the Higgs field leaves one unbroken generator $Q = \frac{1}{2}(\sigma^3 - \mathrm{I})$, which corresponds to the electric charge operator. The spontaneous symmetry breaking mechanism of $SU(2)_L \times U(1)_Y$ is therefore broken into the electromagnetic $U(1)_{EM}$, which remains a symmetry of the Lagrangian.

1.3.2 Yukawa interactions

We continue the discussion describing how to generate mass terms for leptons and quarks [35] through the Higgs field. We start introducing the *Yukawa Lagrangian* in the most general case for the three families of leptons as

$$\mathcal{L}_Y^l = -\sqrt{2}\sum_{i,j=1}^{3}\left[\bar{L}_i^l\Phi(m_{ij})R_{j-}^l + \bar{R}_{j-}^l(m_{ji}^*)\Phi^\dagger L_i^l\right], \tag{1.47}$$

where m_{ij} is a generic 3×3 matrix that mixes the left and right states. The spontaneous symmetry breaking mechanism allows us to rewrite the scalar field $\Phi(x)$ as in Eq. (1.40), which therefore generate mass term for the leptons in $\mathcal{L}_Y^l$, as well as their interaction terms with the Higgs field $h(x)$. Note that the fields in Eq. (1.47) are represented in their electroweak interaction basis: in order to obtain the mass eigenstates we need to diagonalise the matrix m_{ij}. This is possible through a biunitary transformation of the lepton fields

$$L_{i-}^l \rightarrow L_{i-}'^l = V_{ij}L_{j-}^l\,, \tag{1.48}$$

$$R_{i-}^l \rightarrow R_{i-}'^l = U_{ij}R_{j-}^l\,, \tag{1.49}$$

where V and U are unitary matrix, which allow to diagonalise the matrix m_{ij} as

$$m_{ij} \rightarrow m'_{ij} = V_{il}^\dagger m_{lk}U_{kj} \equiv \mathrm{diag}(\lambda_1,\lambda_2,\lambda_3)\,, \tag{1.50}$$

where $\lambda_i \equiv m'_{ii}$ are the *Yukawa couplings* and m'_{ij} is now proportional to the mass matrix. With $\lambda_i \equiv m'_{ii}$, and $\lambda_e \equiv \lambda_1$, $\lambda_\mu \equiv \lambda_2$ and $\lambda_\tau \equiv \lambda_3$, we see that the masses of the leptons e, μ and τ are given by

$$m_e = \lambda_e v\,, \tag{1.51}$$

$$m_\mu = \lambda_\mu v\,, \tag{1.52}$$

$$m_\tau = \lambda_\tau v\,. \tag{1.53}$$

The values of λ_i cannot be predicted by hand, but can (at present) only be fixed with the help of experimental inputs for the mass of the leptons. Note again that, since there are no right-handed neutrinos, neutrinos are massless in the Standard Model. While it is experimentally known that neutrinos do have masses, it is not clear by which mechanism they acquire mass in QFT. A possible extension to include neutrino masses is given by the see-saw mechanism [53–59], which introduces sterile right-handed neutrinos with extremely large masses that mix with the Standard Model left-handed ones, causing the latter to become extremely light.

We now turn to discuss the Yukawa Lagrangian for quarks

$$\mathcal{L}_Y^q = -\sqrt{2}\sum_{i,j=1}^{3}\Big[\bar{L}_i^q\Phi(m_{ij}^-)R_{j-}^q + \bar{R}_{j-}^q(m_{ji}^{-*})\Phi^\dagger L_i^q + \bar{L}_i^q\tilde{\Phi}(m_{ij}^+)R_{j+}^q + \bar{R}_{j+}^q(m_{ji}^{+*})\tilde{\Phi}^\dagger L_i^q\Big], \tag{1.54}$$

which includes all terms for left- and right-handed quarks with all six flavours thanks to the introduction of the field

$$\tilde{\Phi}(x)_i = \epsilon_{ij}\Phi_j^*(x)\,, \quad \tilde{\Phi}(x) = \begin{pmatrix}\phi_0^*(x)\\ -\phi_+^*(x)\end{pmatrix}, \tag{1.55}$$

where ϵ_{ij} is the two-dimensional Levi-Civita tensor. This new definition allows to give mass to the 1/2 weak isospin components, i.e. the up-type quarks, since under reparametrisation around the vev and unitary gauge transformation we obtain

$$\tilde{\Phi}(x) = \frac{1}{\sqrt{2}}\begin{pmatrix}v+h(x)\\ 0\end{pmatrix}. \tag{1.56}$$

After spontaneous symmetry breaking, recalling Eq. (1.24), the Yukawa Lagrangian gives the mass terms

$$\mathcal{L}_Y^q \supset -v\sum_{i,j=1}^{3}\Big[\bar{L}_{i-}^q(m_{ij}^-)R_{j-}^q + \bar{R}_{j-}^q(m_{ji}^{-*})L_{i-}^q + \bar{L}_{i+}^q(m_{ij}^+)R_{j+}^q + \bar{R}_{j+}^q(m_{ji}^{+*})L_{i+}^q\Big]. \tag{1.57}$$

Similarly to the lepton case, to find the actual masses we need to rotate the field in their mass eigenstates by diagonalising the matrices m_{ij}^+ and m_{ij}^- through the biunitary transformations

$$L_{i\pm}^l \to L_{i\pm}^{\prime l} = V_{ij}^\pm L_{j\pm}^l\,, \tag{1.58}$$

$$R_{i\pm}^l \to R_{i\pm}^{\prime l} = U_{ij}^\pm R_{j\pm}^l\,, \tag{1.59}$$

such that we obtain

$$m_{ij}^+ \to m_{ij}^{\prime +} = V_{il}^{+\dagger} m_{lk}^+ U_{kj}^+\,, \tag{1.60}$$

$$m_{ij}^- \to m_{ij}^{\prime -} = V_{il}^{-\dagger} m_{lk}^- U_{kj}^-\,, \tag{1.61}$$

The unitary matrices $V^\pm$ and $U^\pm$ then connect the physical mass eigenstates with the weak interaction eigenstates. In the next section we point out what this implies for the interactions among quarks of different flavours and generations.

1.3.3 Cabibbo-Kobayashi-Maskawa matrix

The transformations in Eqs. (1.58) and (1.59) have been introduced to find the mass matrices m'^{+}_{ij} of the up-type and m'^{-}_{ij} of the down-type quarks. However, these rotations apply to the whole Lagrangian, and affect the interaction between quarks and electroweak bosons. After spontaneous symmetry breaking, the interaction terms in Eq. (1.30) between quarks and $W^{\pm}$ bosons read

$$\mathcal{L}^{q}_{EW,F} \supset \frac{g}{\sqrt{2}} \sum_{i=1}^{3} \left(J^{\mu}_{+i} W^{-}_{\mu} + J^{\mu}_{-i} W^{+}_{\mu} \right) = \frac{g}{\sqrt{2}} \sum_{i=1}^{3} \left(J^{\mu}_{+i} W^{-}_{\mu} + \text{h.c.} \right) \tag{1.62}$$

where h.c. stands for "hermitian conjugate", $W^{\pm}_{\mu}$ are given in Eq. (1.41) and the left-handed charged quark currents $J^{\mu}_{\pm i}$ are defined (after evaluating explicitly the products between the $SU(2)_L$ doublets and Pauli matrices in the first term of Eq. (1.30)) as

$$\sum_{i=1}^{3} J^{\mu}_{+i} \equiv \sum_{i=1}^{3} \bar{L}^{q}_{i-} \gamma^{\mu} L^{q}_{i+} = \begin{pmatrix} \bar{d}_L & \bar{s}_L & \bar{b}_L \end{pmatrix} \gamma^{\mu} \begin{pmatrix} u_L \\ c_L \\ t_L \end{pmatrix} , \tag{1.63}$$

$$\sum_{i=1}^{3} J^{\mu}_{-i} \equiv \sum_{i=1}^{3} \bar{L}^{q}_{i+} \gamma^{\mu} L^{q}_{i-} = \begin{pmatrix} \bar{u}_L & \bar{c}_L & \bar{t}_L \end{pmatrix} \gamma^{\mu} \begin{pmatrix} d_L \\ s_L \\ b_L \end{pmatrix} . \tag{1.64}$$

After rotating into the mass eigenstates (indicated again with prime) the currents transform as

$$J^{\mu}_{+i} \to J'^{\mu}_{+i} = \bar{L}'^{q}_{i-} \gamma^{\mu} L'^{q}_{i+} = \sum_{k} \bar{L}^{q}_{i-} V^{-\dagger}_{ik} V^{+}_{ki} \gamma^{\mu} L^{q}_{i+} , \tag{1.65}$$

$$J^{\mu}_{-i} \to J'^{\mu}_{-i} = \bar{L}'^{q}_{i+} \gamma^{\mu} L'^{q}_{i-} = \sum_{k} \bar{L}^{q}_{i+} V^{+\dagger}_{ik} V^{-}_{ki} \gamma^{\mu} L^{q}_{i-} , \tag{1.66}$$

which explicitly gives

$$\sum_{i=1}^{3} J'^{\mu}_{+i} = \begin{pmatrix} \bar{d}'_L & \bar{s}'_L & \bar{b}'_L \end{pmatrix} V^{-\dagger} V^{+} \gamma^{\mu} \begin{pmatrix} u'_L \\ c'_L \\ t'_L \end{pmatrix} , \tag{1.67}$$

$$\sum_{i=1}^{3} J'^{\mu}_{-i} = \begin{pmatrix} \bar{u}'_L & \bar{c}'_L & \bar{t}'_L \end{pmatrix} V^{+\dagger} V^{-} \gamma^{\mu} \begin{pmatrix} d'_L \\ s'_L \\ b'_L \end{pmatrix} . \tag{1.68}$$

From these equations we define the Cabibbo-Kobayashi-Maskawa (CKM) matrix [60,61]

$$V_{CKM} = V^{+\dagger} V^{-} = (V^{-\dagger} V^{+})^{\dagger} = \begin{pmatrix} V_{ud} & V_{us} & V_{ub} \\ V_{cd} & V_{cs} & V_{cb} \\ V_{td} & V_{ts} & V_{tb} \end{pmatrix} , \tag{1.69}$$

which by construction is a unitary matrix that mixes the quarks (the physical quarks in their mass eigenstates) of different flavours and generations, allowing for charged flavour-changing currents in the Standard Model. Therefore, the entries $V_{qq'}$ of the matrix indicate how strongly each up-type flavour q mixes with the down-type quark q'. Thanks to unitarity and the global symmetries of the Lagrangian (in particular $U(1)$ global symmetry), the CKM matrix has only four degrees of freedom, which can be parametrised as three angles and a complex phase. Note in particular that the complex phase has been introduced in [61] to allow for direct CP-violating processes in Standard Model.

The CKM matrix can be represented in other ways. A very convenient parametrisation is given by the Wolfenstein parametrisation [62], which is particularly useful to obtain a first insight into the magnitude of the coupling between quarks of different generations. It reads

$$V_{CKM} = \begin{pmatrix} 1-\frac{\lambda^2}{2} & \lambda & A\lambda^3(\rho-i\eta) \\ -\lambda & 1-\frac{\lambda^2}{2} & A\lambda^2 \\ A\lambda^3(1-\rho-i\eta) & -A\lambda^2 & 1 \end{pmatrix} + \mathcal{O}(\lambda^4)\,. \tag{1.70}$$

where $A \sim \rho \sim \eta \sim \mathcal{O}(1)$ and $\lambda = 0.22500 \pm 0.00067$ [63–65]. This then shows the hierarchical structure of the matrix: the magnitude of the interaction is stronger for quarks of the same generation (the diagonal elements) and weaker for the coupling with the other generations.

The values of the CKM-matrix elements cannot be predicted from first principles, but can only be extracted from a combination of experimental measurements and theoretical predictions. Therefore, the study of flavour physics processes represents an interesting subject to thoroughly test the Standard Model through, e.g., test of the unitarity of the CKM matrix. For example, considering $|V_{ub}|$ and $|V_{cb}|$ (which are of particular interest in this thesis), some processes to extract the corresponding matrix elements are given by leptonic decays of $B \to \tau\nu_\tau$, non-leptonic decays of $B^0 \to \pi\pi$ or exclusive and inclusive semileptonic decays $B_{(s)} \to D_{(s)}^{(*)}\, l\nu_l$ and $B_{(s)} \to X_c\, l\nu_l$, respectively. Results and constraints for the CKM matrix are collected and constantly updated by different working groups such as FLAG [5], PDG [63], HFLAV [4], CKMfitter [66] and UTfit [67].

To conclude, we point out that there is no equivalent matrix for leptons due to the fact that neutrinos in the EW model are massless. Indeed, this implies that neutrinos are always zero-mass eigenstates and therefore couple only with charged leptons of the same generation. However, it is experimentally well-known that neutrinos are massive and they oscillate between different flavours: this phenomenon can described in the Standard Model in a similar way to what discussed in this section through the Pontecorvo–Maki–Nakagawa–Sakata (PMNS) matrix [68, 69].

1.4 Quantum Chromodynamics

Quantum Chromodynamics is the gauge theory that describes the strong force. It is based on the $SU(3)_C$ gauge group, which accounts for the colour charge of the quarks, conventionally called red, blue and green. In this section we refer to the quark field with the notation q_f, where f stands for the flavour. In particular, under $SU(3)_C$ the quark field is written as a triplet

$$q_f = \begin{pmatrix} q_f^r \\ q_f^b \\ q_f^g \end{pmatrix} , \tag{1.71}$$

where the superscripts refer to the colour charges.

The Lagrangian can be directly build from the procedure described in Sec. 1.2 for the $SU(3)_C$ group. In particular, in this case the 8 generators are given by the Gell-Mann matrices λ^a [70], i.e. $T^a = \lambda^a/2$. The Lagrangian reads

$$\mathcal{L}_{QCD} = \sum_f \bar{q}_f (i\gamma^\mu D_\mu - m) q_f - \frac{1}{4} G^a_{\mu\nu} G^{a\mu\nu} , \tag{1.72}$$

where $G^a_{\mu\nu}$ are the gluon field strength tensors and the covariant derivate is

$$D_\mu = \partial_\mu - i g_s \frac{1}{2} \lambda^a G^a_\mu , \tag{1.73}$$

where G^a_μ, $a = 1, 2, \dots 8$ are the 8 gluon fields. Note that they carry both a colour and an anti-colour charge and interact only with quarks.

1.4.1 Confinement and asymptotic freedom

QCD has some essential features originating from the non-abelian nature of the theory known as *confinement* and *asymptotic freedom*, which we briefly discuss in this section to highlight the peculiarity of the strong force. These are directly related to the properties on the strong coupling

$$\alpha_s(\mu) = \frac{g_s(\mu)}{4\pi} , \tag{1.74}$$

where μ indicates the renormalisation scale. Indeed, the coupling is not fixed, but it depends on the energy scale Q at which the given process is considered. The *running* of the coupling is governed by its renormalisation group equation, obtained through the solution of the QCD beta function. For instance, using perturbation theory at one loop

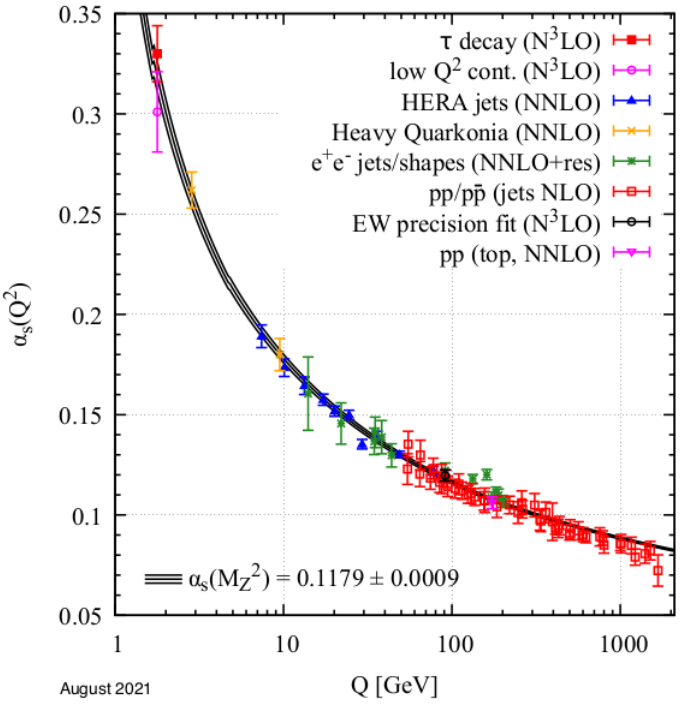

FIGURE 1.1: Experimental measurement of the running of the strong coupling constant $\alpha_s \equiv \alpha_s(Q^2)$, where Q is the energy scale. The plot is taken from [63].

[71, 72] (altough it is now known also at higher order) we obtain

$$\alpha_s(Q^2) = \frac{\alpha_s(\mu^2)}{1 - b_0 \ln(Q^2/\mu^2)\alpha_s(\mu^2)}\,, \quad b_0 = -\frac{33 - 2n_f}{12\pi} \tag{1.75}$$

where n_f is the number of flavours. This expression can be further manipulated introducing the QCD scale parameter Λ_{QCD}

$$\alpha_s(Q^2) = \frac{1}{-b_0 \ln\left(Q^2/\Lambda^2_{QCD}\right)}\,. \tag{1.76}$$

Λ_{QCD} denotes the scale at which the renormalisation group improved perturbation theory ceases to be valid. Its numerical value can be determined experimentally or on the lattice [5], and the latest estimate gives $\Lambda_{QCD} \sim 300\,\text{MeV}$ [63], which is roughly of the same order of the hadron masses. Therefore, Λ_{QCD} also indicates the change of regime of QCD: from the above equations we can see that $\alpha_s \ll 1$ for $Q \to \infty$, whereas $\alpha_s \sim \mathcal{O}(1)$ for $Q \to \Lambda_{QCD}$. This implies that the energy scale at which we probe QCD processes determines a substantially different behaviour of the theory: for small values of α_s, standard tools such as perturbation theory allow to extract analytical prediction for the physics considered, whereas for large value of α_s we enter in a nonperturbative regime where other techniques must be employed, such as for example Lattice QCD (see Chap. 2). The experimental measurement of the running of α_s is shown in Fig. 1.1.

Let us now turn to confinement. It refers to the fact that quarks at low energy cannot

propagate freely. Instead, they are constrained in colour-neutral bound states known as *hadrons*. Hadrons are further categorised in *mesons*, i.e. bound states of a quark-antiquark pair, and *baryons*, i.e. states of three quarks. More exotic states such as tetraquarks [73–76] and pentaquarks [77, 78] have also been observed recently, although their structure is still under study. Confinement is related to the fact that at low transferred momenta Q^2 (i.e. at long distances), the coupling constant of QCD α_s becomes increasingly large, generating a stronger attraction between quarks. On a more intuitive level, this is due to the fact that as two quarks separate, the energy density between them increases and the gluons mediating the interaction give rise to a quark-antiquark pair, which induces the creation of hadrons through a process called *hadronisation*. The confinement property for a simple quark-antiquark system can be modelled using the *Cornell* (or *funnel*) *potential* [79, 80]

$$V(r) = -\frac{4}{3}\frac{\alpha_s}{r} + \sigma r\,, \tag{1.77}$$

which empirically describes interactions among a pair of quarks at a distance r, with $\sigma \simeq 0.18\,\text{GeV}^2$ [81]. Indeed, while at distances $r \lesssim 0.1\,\text{fm}$ the first Coulomb-type term dominates, as r increases the second linear term becomes more and more relevant and leads to a creation of a "flux tube" of gluonic field lines responsible for the quark confinement. This second term is therefore valid until string breaking, which leads to the hadronisation process.

The asymptotic freedom property refers to the regime where α_s is small and perturbation theory can be applied, i.e. when we consider high energy scales. In particular, the coupling constant asymptotically approaches zero for $Q \to \infty$. At these scales, the quarks inside the hadrons effectively behave like free point-like particles: this was first observed in proton-electron elastic scattering, which at high energies can be understood as a electron-quark elastic scattering, which is at the base of Feynman parton model [82].

Finally, we point out that the behaviour of the running coupling α_s strictly depends on the non-abelian nature of the group and the sign of b_0 in Eq. (1.75), which is negative for the number of quark flavours present in the Standard Model $n_f = 6$. This is different for an abelian theory such as Quantum Electrodynamics (QED), for which b_0 has an opposite sign such that the denominator in Eq. (1.75) is always positive.

1.5 Heavy Quark Effective Theory

We now discuss the Heavy Quark Effective Theory (HQET), which provide a useful analytical framework commonly adopted to study some of the processes considered in this work. We briefly present the general features and refer to other sources [83–86] for more detailed reviews.

The key observation for this effective theory relies on the fact that the b and c quark masses are larger than the nonperturbative QCD scale

$$m_b \gg m_c \gg \Lambda_{\rm QCD}\,. \tag{1.78}$$

It is then convenient to separate the heavy quarks explicitly in the Lagrangian and treat them within the framework of an effective theory. For simplicity, we consider only one heavy flavour that we indicate with Q. The QCD Lagrangian then reads

$$\mathcal{L}^{(Q)}_{\rm QCD} = \mathcal{L}_Q + \mathcal{L}_{u,d,s} + \mathcal{L}_{QCD,G}\,, \tag{1.79}$$

$$\mathcal{L}_Q = \bar{Q}(i\gamma^\mu D_\mu - m_Q)Q(x)\,, \tag{1.80}$$

where $\mathcal{L}_Q$ contains the heavy quark, $\mathcal{L}_{u,d,s}$ contains the light quarks up, down and strange and $\mathcal{L}_{QCD,G}$ is the gauge Lagrangian. This is enough to describe a hadron H with a single heavy quark. In this hadron, sea-quark fluctuations of $Q\bar{Q}$ are suppressed by a power $1/(2m_Q)$ due to the large mass of the heavy quark. Our goal is then to find an effective Lagrangian for the heavy quark Q that can be expanded in powers of $1/m_Q$ and that recovers a lowest order Lagrangian in the static limit $m_Q \to \infty$. This limit corresponds to the case where the momentum of the hadron is carried almost entirely by the heavy quark. Given a mass M_H and a momentum p_H for the hadron, we introduce the four-velocity $v = \frac{p_H}{M_H}$, which in the rest frame is given by $v = (1,0,0,0)$. We can further decompose the momentum as

$$p_H = m_Q v + k\,, \tag{1.81}$$

where we separated the large fraction of momentum $m_Q v$ carried by the heavy quark from the subdominant component k, which contains contributions from the lighter flavours. A key aspect is that k is not altered significantly by the value of m_Q as long as $m_Q \gg \Lambda_{\rm QCD}$: this is due to the fact that the hadronic dynamics is dominated by nonperturbative quark-gluon interactions. Indeed, we can write

$$M_H = \sqrt{p_H^2} = \sqrt{(m_Q v + k)^2} = m_Q + \bar{\Lambda} + O(\Lambda^2_{\rm QCD}/m_Q)\,, \tag{1.82}$$

where $\bar{\Lambda} = v \cdot k$ is the residual energy in the rest frame of H. This parameter is not affected by flavour due to flavour independence of the quark-gluon interactions: this lead to an approximate *heavy-quark flavour symmetry*.

The above discussion suggests the following decomposition induced by the two orthogonal projectors $(1 \pm \not{v})/2$

$$Q(x) = \frac{1+\not{v}}{2}Q(x) + \frac{1-\not{v}}{2}Q(x) \equiv \phi_v(x) + \chi_v(x)\,, \tag{1.83}$$

$$\bar{Q}(x) = \bar{Q}(x)\frac{1+\not{v}}{2} + \bar{Q}(x)\frac{1-\not{v}}{2} \equiv \bar{\phi}_v(x) + \bar{\chi}_v(x) \tag{1.84}$$

such that the new fields

$$\phi_v(x) = \frac{1+\not{v}}{2} Q(x)\,, \qquad \chi_v(x) = \frac{1-\not{v}}{2} Q(x) \tag{1.85}$$

are eigenvectors of the $\not{v}$ operator

$$\not{v}\phi_v = \phi_v\,, \quad \not{v}\chi_v = -\chi_v\,, \tag{1.86}$$

and similarly for $\bar{\phi}_v(x)$ and $\bar{\chi}_v(x)$. It is now convenient to decompose the covariant derivative in its longitudinal and transverse components as $D_\mu = D_\mu^{\parallel} + D_\mu^{\perp}$, such that $v \cdot D = v \cdot D^{\parallel}$ and $v \cdot D^{\perp} = 0$, i.e.

$$D_\mu^{\parallel} = v_\mu (v \cdot D)\,, \quad D_\mu^{\perp} = (g_{\mu\nu} - v_\mu v_\nu) D^\nu\,, \tag{1.87}$$

where $g_{\mu\nu}$ is the space-time metric tensor in Eq. (A.1). In particular, in the rest frame $v = (1, \mathbf{0})$ we have $D^{\perp} = (0, -\boldsymbol{D})$ as well as the anticommutator

$$\{\not{D}^{\perp}, \not{v}\} = 0\,. \tag{1.88}$$

The final step is now to factor out a phase that carries the major contribution of the momentum $m_Q v$ as

$$\phi_v = e^{-im_Q(v\cdot x)} h_v(x)\,, \quad \chi_v = e^{-im_Q(v\cdot x)} H_v(x)\,, \tag{1.89}$$

where the new field $h_v(x)$ and $H_v(x)$ are still eigenvectors of $\not{v}$ as the original ones. The final Lagrangian then reads

$$\begin{aligned} \mathcal{L}_Q =& \bar{h}_v(x) i(v \cdot D) h_v(x) - \bar{H}_v(x) \left[i(v \cdot D) + 2m_Q \right] H_v(x) \\ &+ \bar{h}_v(x) i\not{D}^{\perp} H_v(x) + \bar{H}_v(x) i\not{D}^{\perp} h_v(x)\,. \end{aligned} \tag{1.90}$$

It is clear the $h_v(x)$ describes the massless modes of the heavy quark field, whereas $H_v(x)$ accounts for the $Q\bar{Q}$ fluctuations. Starting from the Dirac equation for $Q(x)$, substituting the new fields and projecting to $(1 \pm \not{v})/2$ we arrive at a system of two coupled equations for $h_v(x)$ and $H_v(x)$

$$\begin{cases} i\not{D}^{\perp} H_v(x) &= -i(v \cdot D) h_v(x) \\ i\not{D}^{\perp} h_v(x) &= \left[i(v \cdot D) + 2m_Q \right] H_v(x) \end{cases}. \tag{1.91}$$

From the latter we get

$$H_v(x) = \left(\frac{1}{i(v \cdot D) + 2m_Q} \right) i\not{D}^{\perp} h_v(x)\,, \tag{1.92}$$

where the operator on the right is now non-local as it involves an infinite series of derivative terms after expanding in powers of $1/m_Q$. From this we finally arrive at the

equation of motion for the massless field

$$i(v\cdot D)h_v(x) = -i\not{D}^{\perp}\left(\frac{1}{i(v\cdot D)+2m_Q}\right)i\not{D}^{\perp}h_v(x)\,. \tag{1.93}$$

We can now write down the final Lagrangian of this EFT

$$\mathcal{L}^{(Q)}_{\mathrm{HQET}} = \mathcal{L}_h + \mathcal{L}_{u,d,s} + \mathcal{L}_G\,, \tag{1.94}$$

with

$$\mathcal{L}_h = \bar{h}_v(x)i(v\cdot D)h_v(x) + \bar{h}_v(x)i\not{D}^{\perp}\left(\frac{1}{i(v\cdot D)+2m_Q}\right)i\not{D}^{\perp}h_v(x)\,. \tag{1.95}$$

This formulation allows to describe hadrons with a heavy quark Q in terms of the field $h_v(x)$. The Lagrangian $\mathcal{L}_h$ can be now expanded in powers of $1/m_Q$, and it recovers the leading term for the massless field $h_v(x)$ in the static limit $m_Q \to \infty$.

The hadron states can be described by replacing the four-momentum p_H with the velocity $v = p_H/m_H$, which is now the variable that encodes their kinematics. The states read

$$|H(v)\rangle = \frac{1}{m_H}\,|H(p_H)\rangle\ , \tag{1.96}$$

with normalisation

$$\big\langle H(v')\big|H(v)\big\rangle = 2(2\pi)^3\frac{p_{H,0}}{m_H}\delta^{(3)}(\boldsymbol{p}'_H - \boldsymbol{p}_H)\,. \tag{1.97}$$

Together with the above effective Lagrangian, these transformations allow to redefine important physical quantities such as, e.g., matrix elements for decay processes, into the framework provided by HQET, and allow to treat them with the corresponding parametrisation and expansion in $1/m_Q$.

CHAPTER 2

LATTICE QCD

At low energies $\mu \lesssim 1\,\text{GeV}$ quantum chromodynamics is a strongly coupled theory governed by a large value of the strong coupling $\alpha_s \sim \mathcal{O}(1)$. In this nonperturbative regime, standard methods such as perturbation theory are not reliable. Various approaches exist to address nonperturbative calculations, as for example (but not limited to) QCD sum rules [87,88] (see [86,89] for more extensive reviews), chiral perturbation theory [90], or effective field theories such as HQET, briefly discussed in Sec. 1.5.

In this chapter, we introduce the basics of Lattice QCD, which provides a fully nonperturbative approach to QCD and enables us to make accurate predictions for low energy processes through the use of numerical simulations on supercomputers. The core of this formulation lies in the discretisation of four-dimensional space-time on a finite-volume Euclidean lattice Λ of size $L^3 \times T$, where L denotes the spatial extent and T the temporal one. Note that the use of Euclidean space-time is crucial to perform Lattice QCD calculations, as we will show in Sec. 2.1. In the rest of this manuscript, we therefore assume to be in Euclidean space unless explicitly stated otherwise. The physical distance between sites, the *lattice spacing* a, and the lenght L of the sides of the spatial cubic volume $V = L^3$ are crucial parameters that regulate the theory, acting as ultraviolet and infrared cutoff, respectively. This formulation is then well suited for numerical simulations, and physical predictions are obtained removing the regulators by considering the continuum limit $a \to 0$ and the infinite-volume limit $L \to \infty$.

This chapter is organised as follows. We present the core ideas for calculating observables on a lattice in Sec. 2.1 and address the strategy for the discretisation in Sec. 2.2, highlighting the actions relevant for this work. In Secs. 2.3 and 2.4 we discuss the strategies for computing observables, addressing the construction of propagators and correlation functions.

2.1 Path integrals

The starting point for calculating observables in Lattice QCD is the path-integral formulation of QFT in Minkowski space, which allows to address the evaluation of *correlation functions*, which are crucial objects in QFT and Lattice QCD. A n-point correlation function is defined as the expectation value of the time-ordered product

$$C_{\text{npt}}(x_1, x_2, \dots, x_n) = \langle T\{\mathcal{O}_1(x_1)\mathcal{O}_2(x_2)\dots\mathcal{O}_n(x_n)\}\rangle\,, \tag{2.1}$$

where $\mathcal{O}_i(x_i)$ are interpolating operators with the quantum numbers of the physics process we are interested in and T is the time-ordering operator. For simplicity, in the rest of this section we indicate with $\mathcal{O}$ the time-ordered product of the operators $\mathcal{O}_i(x_i)$. The path integral then reads

$$\langle\mathcal{O}\rangle = \frac{1}{Z}\int \mathcal{D}[\Phi]\,\mathcal{O}\,e^{iS_M[\Phi]}\,, \tag{2.2}$$

with $\Phi \equiv (\Psi, \bar{\Psi}, U)$, where Ψ collects the fermion fields and U collects the gauge fields, $S_M = \int \mathrm{d}^4x\mathcal{L}_{QCD}$ is the (Minkowski) QCD action and Z is the partition function defined as

$$Z = \int \mathcal{D}[\Phi]\,e^{iS_M[\Phi]}\,. \tag{2.3}$$

Note that the expectation value is intended to be evaluated over both the fermionic fields Ψ ("F") and the gauge fields U ("G"), i.e. $\langle\dots\rangle \equiv \langle\dots\rangle_{F,G}$, as clear from the measure $\mathcal{D}[\Phi] \equiv \mathcal{D}[\Psi, \bar{\Psi}]\mathcal{D}[U]$ in Eq. (2.2). In order to make use of this expression for numerical calculations, we need to follow a few steps, listed here schematically.

1. Wick-rotate the path integral into Euclidean space such that $iS_M \to -S_E$, where the Euclidean discretised action S_E must reproduce the correct one in the continuum limit $a \to 0$.
2. Replace the continuum space-time with a four-dimensional Euclidean lattice Λ with size $L^3 \times T$ and a given lattice spacing a.
3. Consider (classical) Euclidean operators and build the relevant correlators accordingly.

Note that the degrees of freedom are now classical Euclidean field variables defined on the lattice. The path integral becomes

$$\langle\mathcal{O}\rangle_T = \frac{1}{Z_T}\int \mathcal{D}[\Phi]\,\mathcal{O}\,e^{-S[\Phi]}\,, \tag{2.4}$$

with

$$Z_T = \int \mathcal{D}[\Phi]\, e^{-S[\Phi]}\,, \tag{2.5}$$

where T indicate the finite-volume prescription and where we dropped the "E" subscript for simplicity. In the remainder of the chapter we assume to be in Euclidean space; see App. A for a brief discussion of the relation between Minkowski and Euclidean space.

The minus sign in $e^{-S[\Phi]}$ allows us to interpret the exponential as a Boltzmann factor, as long as $S[\Phi]$ is real. This implies that Eq. (2.4) can be interpreted as a weighted average over field configurations with weight $e^{-S[\Phi]}$. This enables us to use a Monte Carlo procedure to evaluate the multidimensional integrals by generating a large number of N_{config} configurations Φ_α with probability

$$P[\Phi_\alpha] \propto e^{-S[\Phi_\alpha]}\,, \tag{2.6}$$

and estimate the path integral as

$$\langle \mathcal{O} \rangle_T \simeq \frac{1}{N_{\text{config}}} \sum_{\alpha=1}^{N_{\text{config}}} \mathcal{O}\Big|_{\Phi_\alpha}\,, \tag{2.7}$$

where the operator $\mathcal{O}$ on the r.h.s. has now been evaluated on the configuration Φ_α. Note that the QCD action can be split as $S[\Psi, \bar{\Psi}, U] = S_F[\Psi, \bar{\Psi}, U] + S_G[U]$, where S_F contains the fermion fields and S_G represents the pure gauge part. Since S_F is quadratic in the fermion fields Ψ, we can integrate out the fermionic part "F" [91, 92] and get

$$\langle \mathcal{O} \rangle_{T,F} = \int \mathcal{D}[\Psi, \bar{\Psi}] \mathcal{O} e^{-S[\Phi]} \equiv \det[D] \mathcal{O}[U] e^{-S_G[\Phi]}\,, \tag{2.8}$$

$$Z_{T,F} = \int \mathcal{D}[\Psi, \bar{\Psi}]\, e^{-S[\Phi]} \equiv \det[D] e^{-S_G[\Phi]} \tag{2.9}$$

where D is the Dirac operator of the S_F action, cf. with Eq. (2.13). The path integral then reduces to

$$\langle \mathcal{O} \rangle_T = \frac{\int \mathcal{D}[U] \det[D] \mathcal{O}[U]\, e^{-S_G[U]}}{\int \mathcal{D}[U] \det[D]\, e^{-S_G[U]}}\,. \tag{2.10}$$

The gauge field U is, therefore, the only field we need to generate an ensemble of configurations for in order to evaluate the correlation function. This final equation represents therefore the key ingredient to perform lattice computations.

2.2 Discretised QCD actions

We now describe how to build a discretised QCD action and in particular how to treat fermions on the lattice. We only report some of the central aspects and refer to other sources [93,94] for more details. We consider a lattice Λ of size $L^3 \times T$, with L being the spatial extension and T the temporal one, and lattice spacing a. Considering $L = aN_L$, $T = aN_T$, where N_L and N_T are the number of sites along the spatial and temporal direction, respectively, and writing $x_\mu = an_\mu$, $n_\mu \in \mathbb{N}$, the lattice is given by

$$\Lambda = \{n = (n_1, n_2, n_3, n_4) \,|\, n_1, n_2, n_3 = 0, 1, \ldots, N_L - 1; n_4 = 0, 1, \ldots N_T - 1\} \,. \quad (2.11)$$

There is no unique way to proceed with the discretisation. All meaningful discretisation have in common that the continuum limit $a \to 0$ recovers the correct QCD Lagrangian. Such procedure comes with discretisation effects of order $\mathcal{O}(a^n)$, which can be further improved through methods like, e.g., the Symanzik improvement program [95–97].

We present the key ideas for the discretisation of the quark fermion field $q(x)$ in Sec. 2.2.1 through the *naive fermions* formulation. We then show how to build a pure gauge theory in Sec. 2.2.2 and discuss Wilson-type quarks and the specific actions relevant for this work in the remaining sections. We consider a single quark flavour for simplicity, but the generalisation is straightforward as it just requires summing over all flavours involved.

2.2.1 Naive fermions and gauge invariance on the lattice

The naive action relies on the discretisation of the derivative

$$\partial_\mu q(x) \;\to\; \frac{1}{2a}\left(q(x + a\hat{\mu}) - q(x - a\hat{\mu})\right) \,, \quad (2.12)$$

which is valid up to $\mathcal{O}(a)$ discretisation errors, as it can be seen by Taylor expanding $q(x \pm a\hat{\mu})$. The generic discretised action can be written as

$$S[q, \bar{q}] = a^4 \sum_{x,y} \bar{q}(y) D(y, x) q(x) \,, \quad (2.13)$$

where D is the Dirac operator, which contains the kinetic and mass term, as it will be clear in the following discussion. Requiring gauge invariance under $SU(3)$ transformations for the discrete theory with $\Omega(x) \in SU(3)$

$$q(x) \;\to q'(x) = \Omega(x) q(x) \,, \quad (2.14)$$

$$\bar{q}(x) \;\to \bar{q}'(x) = \bar{q}(x) \Omega^\dagger(x) \,, \quad (2.15)$$

$$U_\mu(x) \;\to \bar{U}'_\mu(x) = \Omega(x) U_\mu(x) \Omega(x + a\hat{\mu}) \,, \quad (2.16)$$

we can build the discretised version of the covariant derivatives

$$D_\mu q(x) \;\to\; \frac{1}{2a}\left(U_\mu(x)q(x+a\hat{\mu}) - U_{-\mu}(x)q(x-a\hat{\mu})\right)\,, \tag{2.17}$$

where U_μ is the gauge field, with $U_{-\mu}(x) = U_\mu^\dagger(x-a\hat{\mu})$. The gauge field $U_\mu(x)$ connects the lattice point x to $x+a\hat{\mu}$ and is therefore referred to as *link variable*. The interacting naive Dirac operator takes the form

$$D_F(y,x) = \sum_{\mu=1}^{4}\gamma_\mu \frac{U_\mu(y)\delta_{y+a\hat{\mu},x} - U_{-\mu}(y)\delta_{y-a\hat{\mu},x}}{2a} + m_q\,, \tag{2.18}$$

which represents the massive kinetic term of the action, with m_q being the bare quark mass. Note that the free theory can be recovered setting $U_\mu(x) = \mathrm{I}$.

In a finite volume we need to impose boundary conditions on the fields to specify their behaviour at the edges of the four-dimensional volume. In particular, the conditions are given by

$$q(x + aN_\mu\hat{\mu}) = e^{i2\pi\theta_\mu}q(x)\,, \tag{2.19}$$

where N_μ is the number of lattice points in the direction $\hat{\mu}$, i.e. $N_1 = N_2 = N_3 = N_L$ and $N_4 = N_T$, and θ_μ is the phase which is referred to as *twist*. Setting $\theta_\mu = 0\ \forall\mu$ corresponds to the *periodic boundary conditions* case: in this scenario, the volume is equivalent to a torus. On the other hand, the case with $\theta_\mu \neq 0$ corresponds to imposing *twisted boundary conditions* [98,99]. From a physical point of view, boundary conditions imply that the momentum space is restricted to the discrete values

$$p_\mu = \frac{2\pi}{aN_\mu}(k_\mu + \theta_\mu) \quad k_\mu \in \mathbb{N}, \tag{2.20}$$

such that the accessible momenta on the lattice are given by

$$\tilde{\Lambda} = \left\{ p \,|\, p_\mu = \frac{2\pi}{aN_\mu}(k_\mu+\theta_\mu), k_\mu = -\frac{N_\mu}{2}+1,\ldots,\frac{N_\mu}{2}\right\}\,. \tag{2.21}$$

2.2.2 Pure gauge action

From the naive formulation of Sec. 2.2.1 we see that the gauge fields are now elements of the group $SU(3)$ instead of the corresponding algebra as in the continuum. In particular, the gauge link can be written as

$$U_\mu(x) = e^{iaA_\mu(x)}\,, \tag{2.22}$$

with $A_\mu(x)$ being the algebra-valued lattice gauge field. It can be shown that in the limit $a \to 0$ Eq. (2.22) allows to recover the correct continuum interactive action from Eqs. (2.18) and (2.13).

We now proceed to build a lattice gauge action which recovers the continuum one in the limit $a \to 0$. Considering that the fundamental objects on a lattice are gauge links, which connect the adjacent sites and are related to the fields $A_\mu(x)$ through an exponential, we can think of building the lattice version of the continuum Wilson line W on a path γ and Wilson loop W_L on a closed path $\tilde{\gamma}$

$$W[\gamma] = \mathcal{P} e^{i \int_\gamma \mathrm{d}x^\mu A_\mu} , \qquad W_L[\tilde{\gamma}] = \mathrm{Tr} \left[\mathcal{P} e^{i \oint_{\tilde{\gamma}} \mathrm{d}x^\mu A_\mu} \right] , \tag{2.23}$$

where $\mathcal{P}$ is the path-ordering operator. In a similar way, we can build the corresponding lattice object that connects two lattice point x and y through a ordered path $\mathcal{C}$

$$P[U] = \prod_{(z,\mu) \in \mathcal{C}} U_\mu(z) , \tag{2.24}$$

which, following Eq. (2.16), transforms under $SU(3)$ as

$$P[U] \;\to\; P[U'] = \Omega(x) P[U] \Omega^\dagger(y) . \tag{2.25}$$

We can then consider the trace of path products along a closed loop $\tilde{\mathcal{C}}$ to build the gauge invariant quantity

$$L[U] = \mathrm{Tr} \left[\prod_{(z,\mu) \in \tilde{\mathcal{C}}} U_\mu(z) \right] , \tag{2.26}$$

which is the analogous of the continuum Wilson loop. An arbitrary closed loop can be used to build the QCD action, as long as it suitably treated in order to reproduce the correct space-time symmetries. The simplest non-trivial path that can be constructed from the gauge links is the *plaquette*

$$U_{\mu\nu}(x) = U_\mu(x) U_\nu(x + a\hat{\mu}) U_\mu^\dagger(x + a\hat{\nu}) U_\nu^\dagger(x) , \tag{2.27}$$

which represents a closed loop in the two-dimensional plane $(\hat{\mu}, \hat{\nu})$ that connects the points x, $x + a\hat{\mu}$, $x + a\hat{\mu} + a\hat{\nu}$ and $x + a\hat{\nu}$.

We can finally build the *Wilson gauge action* as a sum over plaquettes, each of which is counted with only one orientation

$$S_G[U] = \frac{2}{g^2} \sum_x \sum_{\mu<\nu} \mathrm{Re}\, \mathrm{Tr} \left[\mathrm{I} - U_{\mu\nu}(x) \right] . \tag{2.28}$$

Taylor expanding the plaquette $U_{\mu\nu}(x)$ in the lattice spacing a, it can be shown that $S_G[U]$ reproduces the correct gauge action up to $\mathcal{O}(a^2)$ effects that vanishes in the limit $a \to 0$.

This action can be improved to further eliminate lattice artefacts and obtain smaller discretisation errors, as in the case, for example, of the Iwasaki gauge action [100, 101], which is the one specifically considered in this work.

2.2.3 Wilson action

The naive action discussed in Sec. 2.2.1 presents however some problems. Indeed, let us consider the free theory $U_\mu(x) = \mathrm{I}$ and consider the Dirac operator in momentum space

$$\tilde{D}(p,q) = \sum_{x,y} e^{-ip\cdot y} D(y,x) e^{iq\cdot x} = \tilde{D}(p)\delta(p-q)\,, \tag{2.29}$$

$$\tilde{D}(p) = m_q \mathrm{I} + \frac{i}{a}\sum_{\mu=1}^{4} \gamma_\mu \sin(p_\mu a)\,. \tag{2.30}$$

The propagator in momentum space $\tilde{\Lambda}$ (given in Eq. (2.21)), is

$$\tilde{D}^{-1}(p) = \frac{m_q \mathrm{I} - i a^{-1} \sum_\mu \gamma_\mu \sin(p_\mu a)}{m_q^2 + a^{-2}\sum_\mu \sin^2(p_\mu a)}\,. \tag{2.31}$$

From this expression it is immediate to see that in the massless limit $m_q = 0$ the propagator has not only a pole in $p = 0$ as in the continuum theory, but it also has extra 15 poles for all the combinations of $p_\mu \in \{0, \pi/a\}$. This implies that the naive action describes unphysical particles, called *doublers*, that we have to remove from the theory.

A possible solution to the doubler problem has been suggested by Wilson [102], who proposed to add an irrelevant dimension-five term, the *Wilson term*, that lifts the doubler modes to higher masses of order $E \sim 1/a$, which then decouple from the theory as $a \to 0$. The Wilson operator is

$$\mathcal{O}_W(y,x) = -ar \sum_{\mu=1}^{4} \frac{U_\mu(y)\delta_{y+a\hat{\mu},x} - 2\delta_{y,x} + U_{-\mu}(y)\delta_{y-a\hat{\mu},x}}{2a^2}\,, \tag{2.32}$$

and it corresponds to the discretised version of the Laplace operator $-ar/2\,\partial_\mu\partial_\mu$, which indeed vanishes as $a \to 0$. While the Wilson term fixes the doubler problem, it comes at the cost of breaking chiral symmetry. This is understood in general thanks to the Nielsen-Ninomiya no-go theorem [103], which states that no local action in an even-dimensional Euclidean space-time can be constructed such that it simultaneously removes the doublers and preserves chiral symmetry. Chiral symmetry is a central feature of QCD: for

example, pions corresponds to the Goldstone bosons of this symmetry, and its spontaneous breaking mechanism explain their small mass. We will discuss one of the possible formulations to implement chiral symmetry on a lattice in Sec. 2.2.6.

The Wilson action is then

$$S_W[q,\bar{q},U] = a^4 \sum_{x,y} \bar{q}(y) D_W(y,x) q(x)\,, \tag{2.33}$$

where the Dirac operator $D_W(y,x) = D_F(y,x) + \mathcal{O}_W(y,x)$ is

$$D_W(y,x) = \left(m_q + \frac{4}{a}r\right)\delta_{y,x} - \frac{1}{2a}\sum_{\mu=\pm1}^{\pm4}(1-\gamma_\mu)\,U_\mu(y)\delta_{y+a\hat{\mu},x}\,. \tag{2.34}$$

where $\gamma_{-\mu} = -\gamma_\mu$ and $U_{-\mu}(x) = U_\mu^\dagger(x - a\hat{\mu})$. This action represents the starting point to build the actions considered in the next sections. The fermions discretised through actions based on the Wilson one are therefore referred to as *Wilson-type fermions*.

2.2.4 Clover action

The Sheikholeslami-Wohlert action (or *clover action*), is a $\mathcal{O}(a)$-improved Wilson action of the form

$$S_{SW} = S_W + c_{sw} a^5 \sum_x \sum_{\mu<\nu} \frac{1}{2}\bar{q}(x)\sigma_{\mu\nu}\hat{F}_{\mu\nu}(x)q(x)\,, \tag{2.35}$$

where $\sigma_{\mu\nu} = -i[\gamma_\mu,\gamma_\nu]/2$ and c_{sw} is the *Sheikholeslami-Wohlert coefficient*, which is a real coefficient that has to be tuned nonperturbatively in order to remove the $\mathcal{O}(a)$ discretisation errors. The improvement is achieved through the addition of the dimension-five term

$$S_C = \bar{q}(x)\sigma_{\mu\nu}\hat{F}_{\mu\nu}(x)q(x)\,, \tag{2.36}$$

which is a magnetic moment term with

$$\hat{F}_{\mu\nu}(x) = \frac{-i}{8a^2}(C_{\mu\nu}(x) - C_{\nu\mu}(x))\,, \tag{2.37}$$

and where $C_{\mu\nu}(x)$ is the sum of plaquettes in Eq. (2.27)

$$C_{\mu\nu}(x) = U_{\mu\nu}(x) + U_{\nu-\mu}(x) + U_{-\mu-\nu}(x) + U_{-\nu\mu}(x)\,, \tag{2.38}$$

which represents a discretisation of the continuum field strength tensor. The name "clover" comes from the fact that $C_{\mu\nu}(x)$ represent a sum of loops in a two-dimensional plane that reminds the shape of a clover leaf.

2.2.5 Relativistic Heavy Quark action

The Relativistic Heavy Quark (RHQ) action is an anisotropic version of the clover action, formulated with the intent of treating heavy quarks on a lattice through the help of nonperturbative parameters that reduce the discretisation errors. While the previous actions can be used to study light, strange and charm quarks, the bottom quark requires the use of effective theories. Indeed, today typical lattice spacings range between $a^{-1} \sim \mathcal{O}(2 - 4\,\text{GeV})$: in order to keep the discretisation errors under control, the quark bare mass m_q needs to satisfy the relation

$$m_q \ll \frac{1}{a} \implies m_q a \ll 1\,, \tag{2.39}$$

which is violated in the case of the b quark mass $m_b = 4.18^{+0.03}_{-0.02}\,\text{GeV}$ [63], which corresponds to the "running mass" $(m_b(\mu = m_b))$ in the $\overline{\text{MS}}$-scheme.

In this work we consider the Columbia formulation [104, 105] of the RHQ action, which is based on the Fermilab heavy quark action [106]. In particular, this action allows to reduce the discretisation effects of order $\mathcal{O}((m_q a)^n)$, $\mathcal{O}(\boldsymbol{p}a)$ and $\mathcal{O}((\boldsymbol{p}a)(m_q a)^n)$ by tuning three nonperturbative parameters [107], one of them being the bare mass m_q. The approach considered is similar to the one of HQET, where the heavy quark mass is assumed to be much larger than its spatial momentum.

The action reads

$$\begin{aligned} S_{RHQ} = a^4 \sum_{x,y} \bar{Q}(x) \Big[& m_q + \gamma_0 D_0 + \zeta \gamma_i \cdot D_i - \frac{a}{2} (D_0)^2 - \frac{a}{2} (\boldsymbol{D})^2 \\ & + c_{\text{sw}} \sum_{\mu<\nu} \frac{ia}{2} \sigma_{\mu\nu} \hat{F}_{\mu\nu} \Big] Q(y) \end{aligned} \tag{2.40}$$

where we indicate with Q the heavy quark and where we defined the covariant derivatives

$$D_\mu Q(x) = \frac{1}{2a} \left[U_\mu(x) Q(x + a\hat{\mu}) - U_{-\mu}(x) Q(x - a\hat{\mu}) \right], \tag{2.41}$$

$$D^2_\mu Q(x) = \frac{1}{a^2} \left[U_\mu(x) Q(x + a\hat{\mu}) - U_{-\mu}(x) Q(x - a\hat{\mu}) - Q(x) \right]. \tag{2.42}$$

In this work we will consider heavy-light currents of the form $J_\mu(x) = \bar{Q}(x) \Gamma^J_\mu q(x)$, where q is a Wilson-type light quark (in practice a domain-wall fermion as in Sec. 2.2.6). We report the construction of the $\mathcal{O}(a)$-improved current [108]: while we don't make explicit use of them for the purpose of the present work, they may become important

for future phenomenology studies. The improved terms are

$$J^1_\mu(x) = \bar{Q}(x) 2\,\Gamma^J \overrightarrow{D}_\mu q(x)\,, \tag{2.43}$$
$$J^2_\mu(x) = \bar{Q}(x) 2\,\Gamma^J \overleftarrow{D}_\mu q(x)\,, \tag{2.44}$$
$$J^3_\mu(x) = \bar{Q}(x) 2\,\Gamma^J_\mu \gamma_i \overrightarrow{D}_i q(x)\,, \tag{2.45}$$
$$J^4_\mu(x) = \bar{Q}(x) 2\,\Gamma^J_\mu \gamma_i \overleftarrow{D}_i q(x)\,, \tag{2.46}$$

where the gamma-matrices are defined in App. A.1 and the covariant derivatives $\overrightarrow{D}_\mu$ and $\overleftarrow{D}_\mu$ are defined through their action on the quark fields as

$$\overrightarrow{D}_\mu q(x) = \frac{1}{2}\left[U_\mu(x) q(x + a\hat{\mu}) - U^\dagger_\mu(x - a\hat{\mu}) q(x - a\hat{\mu})\right]\,, \tag{2.47}$$
$$\bar{Q}(x)\overleftarrow{D}_\mu = \frac{1}{2}\left[\bar{Q}(x + a\hat{\mu}) U^\dagger_\mu(x) - \bar{Q}(x - a\hat{\mu}) U_\mu(x - a\hat{\mu})\right]\,. \tag{2.48}$$

The improved current then reads

$$J^{\text{imp}}_\mu(x) = J_\mu(x) + c^{J,1}_\mu J^1_\mu(x) + c^{J,2}_\mu J^2_\mu(x) + c^{J,3}_\mu J^3_\mu(x) + c^{J,4}_\mu J^4_\mu(x)\,, \tag{2.49}$$

where the coefficients $c^{J,i}_\mu$ can be computed through one-loop lattice perturbation theory [109].

2.2.6 Domain-Wall Fermion action

The Domain-Wall Fermion (DWF) formulation, introduced in [110] and further developed in [111–114], makes use of a five-dimensional theory in order to circumvent the Nielsen-Ninomiya no-go theorem [103] and preserve chiral symmetry. A chirally-symmetric lattice action is characterised by the fact that it satisfies the Ginsparg-Wilson equation [115]

$$\{D, \gamma_5\} = a D \gamma_5 D\,, \tag{2.50}$$

which recovers the continuum chiral symmetry relation $\{D, \gamma_5\} = 0$ as $a \to 0$. An example of such an action is given by the overlap formulation [116–119], which has explicitly been shown to satisfy the Ginsparg-Wilson relation [120].

Let us now briefly describe the DWF action in Shamir's formulation [111, 113], and refer to other reviews for more details [121, 122]. We consider a five-dimensional lattice $\Lambda_5 = \Lambda \times L_s$, whose coordinates are given by $X = (x, x_5)$, with $x \in \Lambda$ and $x_5 \in L_s$, and the fermionic fields

$$\mathcal{Q}(X)\,, \quad \bar{\mathcal{Q}}(X)\,. \tag{2.51}$$

The 5D action can be written in the usual way as

$$S_{DWF}[\mathcal{Q},\bar{\mathcal{Q}},U] = \sum_{X,Y} \bar{\mathcal{Q}}(Y) D_{DWF}(Y,X) \mathcal{Q}(X) \tag{2.52}$$

where the Dirac operator is decomposed into a Wilson-like operator and a one-dimensional operator on the fifth dimension

$$D_{DWF}(Y,X) = \delta_{y_5,x_5} D_W(y,x) + \delta_{y,x} D_5(y_5,x_5)\,, \tag{2.53}$$

which are respectively parallel and perpendicular components with respect the 4D space-time. In particular, D_W reads

$$D_W(y,x) = (4 - M_5)\,\delta_{y,x} - \frac{1}{2a} \sum_{\mu=\pm1}^{\pm4} (1-\gamma_\mu)\, U_\mu(y) \delta_{y+a\hat{\mu},x}\,, \tag{2.54}$$

where M_5 corresponds to the height of the domain wall, which separates the points $x_5 = 0$ and $x_5 = L_s - 1$, and D_5 reads

$$\begin{aligned} D_5(y_5,x_5) =& \delta_{y_5,x_5} - (1-\delta_{y_5,L_s-1}) P_L \delta_{y_5+1,x_5} - (1-\delta_{y_5,0}) P_R \delta_{y_5-1,x_5} \\ &+ m_q (P_L \delta_{y_5,L_s-1} \delta_{0,x_5} + P_R \delta_{y_5,0} \delta_{L_s-1,x_5})\,, \end{aligned} \tag{2.55}$$

where m_q is the mass of the four-dimensional quark field and $P_{R,L} = (\mathrm{I} \pm \gamma_5)/2$ are the right and left chiral projectors acting on the Dirac indices. Note that the gauge links do not appear in D_5 and they are therefore only defined on the 4D space as usual. The physical four-dimensional fields live on the 4D boundary of Λ_5 (in particular on the first and the last 4D slice) and they are defined as

$$q(x) = P_L \mathcal{Q}(x,0) + P_R \mathcal{Q}(x,L_s-1)\,, \quad \bar{q}(x) = \bar{\mathcal{Q}}(x,L_s-1) P_L + \bar{\mathcal{Q}}(x,0) P_R\,, \tag{2.56}$$

which shows that the right-handed modes are generated on the slice $x_5 = 0$ and the left-handed modes on the slice $x_5 = L_s - 1$. These four-dimensional quark fields can now be used to construct the observables of interest, e.g. the scalar density $\bar{q}(x)q(x)$.

Exact chiral symmetry is recovered for $L_s \to \infty$, since the Ginsparg-Wilson equation is satisfied in this limit. It can also be shown that in this case the DWF formulation is equivalent to the overlap one [123, 124]. However, in practical cases L_s takes a finite value: as a consequence, the 4D fields contain some small mixing between right and left modes, which leads to a residual chiral symmetry breaking effect. This effect is parametrised by the *residual mass* m_{res} that manifests as an additive renormalisation term to the bare quark mass. Chiral symmetry is then recovered in good approximation as long as the choice of L_s produces a small value of m_{res}.

2.3 Propagators

Let us now turn to discuss practical aspects of lattice computations, starting from how to build propagators and consequently correlation functions. Propagators are essential objects in QFT and they are the building blocks to compute correlators on a lattice, as we will see in Sec. 2.4. They are formally defined as a the vacuum expectation value of the time-ordered product of two given fields at different space-time points and correspond to Green functions, i.e. the inverse of the kinetic operator for the given theory. For example, considering a quark field q, the propagator $G(y,x)$ from x to y reads

$$G(y,x) = \langle q(y)\bar{q}(x)\rangle\,, \tag{2.57}$$

where $\bar{q} = q^\dagger\gamma^4$ is the adjoint field in Euclidean space-time. Propagators relate to the amplitude of a particle travelling between the two space-time points. On a discretised finite-volume space-time, the propagator assumes the form of a $N \times N$ matrix, with $N = 3 \times 4 \times N_L^3 \times N_T$, where 3 refers to the $SU(3)$ structure of QCD (colour), 4 to the Dirac structure (spin) and $N_L^3 \times N_T$ to the size of the lattice. Considering a discretised action with a Dirac operator D, the propagator G is obtained by solving the equation

$$DG = S\,, \quad G = D^{-1}S\,, \tag{2.58}$$

where all the operators are written in their compact matrix form and S is a *source* operator. The source can be thought as the equivalent of Dirac delta function in the continuum version of the above equation; possible different choices for the source will be discussed in the following sections.

Concerning the propagator, the variable dependence is explicitly given by

$$G(y,x)^{\beta\alpha}_{ba} = \sum_{z,\mu,c} D^{-1}(y,z)^{\beta\mu}_{bc}\, S(z,x)^{\mu\alpha}_{ca}\,, \tag{2.59}$$

where the Greek characters indicate the Dirac structure and the Roman characters indicate the $SU(3)$ QCD structure. The propagator $G(y,x)^{\beta\alpha}_{ba}$ connects then the lattice site (x,α,a) to the site (y,β,b) and has to be computed for every gauge field configuration we are interested in. The expression in Eq. (2.58) is intended in its full matrix form, i.e. it contains information about propagation from all possible sites x to all possible sites y and it is referred to as *all-to-all* propagator. However, the operator D is typically large (with a size N of order $\mathcal{O}(10^6)$ for small lattices, e.g. $L^3 \times T = 16^3 \times 24$) and the evaluation of its inverse is computationally very expensive and requires a lot of disk space. Instead, we can consider the propagator from a fixed point x_0 and indices α_0 and a_0 using a vector source $S^{(x_0,\alpha_0,a_0)}(z)^{\mu}_{c}$, i.e. a column of the matrix source $S(z,x)^{\mu\alpha}_{ca}$

in Eq. (2.59), such that

$$G(y,x_0)^{\beta\alpha_0}_{ba_0} = \sum_{z,\mu,c} D^{-1}(y,z)^{\beta\mu}_{bc}\, S^{(x_0,\alpha_0,a_0)}(z)^{\mu}_{c}\,, \tag{2.60}$$

The above expression must be evaluated for 12 sources for all the combination of Dirac and colour indices α_0 and a_0 respectively, and it corresponds to a single column of the inverse of the matrix D associated with the point (column) x_0. We use the subscript "0" to indicate that the source is intended to be a column vector fixed at that point and indices and that the propagator is intended to be a column of the full propagator: we refer to it as *one-to-all* propagator. This is the case that will be considered in the whole manuscript. The propagator can be evaluated at multiple values of x_0, which can be averaged thanks to translational invariance to reduce the overall noise of the final correlator. The matrix inversion can be performed through the help of numerical methods such as the Conjugate Gradient (CG) algorithm [125]; we refer to other sources, e.g. [126], for a more comprehensive review on possible approaches to the numerical problem.

2.3.1 Point sources

Point sources are the most straightforward choice and are given by

$$S_{\text{pt}}^{(x_0,\alpha_0,a_0)}(z)^{\mu}_{c} = \delta(z-x_0)\,\delta_{\alpha_0\mu}\,\delta_{a_0c}\,, \tag{2.61}$$

following the convention of the previous section. They correspond to the standard Dirac delta function that appears in the most conventional Green equation in the continuum. They are placed at specific lattice sites and they are therefore sensitive to local fluctuations of the gauge field. To maximise the information extracted and reduce the statistical noise one would then need to place many sources across the lattice sites, perform many inversion of the kinetic operator and average the results obtained.

2.3.2 Stochastic sources

Stochastic sources have been introduced to reduce the overall noise of the final observables in lattice QCD [127], but also in other different fields of physics [128–130]. Following the standard notation, we introduce N stochastic vector η^n with $n = 1, 2, \ldots, N$ such that

$$\langle \eta_i \rangle = 0\,, \quad \langle \eta_i \eta_j^\dagger \rangle = \frac{1}{N}\sum_{n=1}^{N} \eta_i^n \eta_j^{n\dagger} = \delta_{ij}\,. \tag{2.62}$$

where η_i^n is the i-th entry of the vector η^n and the average $\langle\cdot\rangle$ is intended over the whole set of noise vectors. We refer to it as a set of *hits* of stochastic sources. It can be

shown that the expectation value of the matrix element $E[G_{ij}]$ can be easily found by solving Eq. (2.58) for all the N hits. Indeed

$$E[G_{ij}] = \langle \eta_i^\dagger (D^{-1}\eta)_j \rangle = \sum_k D^{-1}_{jk} \langle \eta_i^\dagger \eta_k \rangle = D^{-1}_{ij} \,. \tag{2.63}$$

While different choices of noise are possible, e.g. Gaussian noise, in this work we make use of $\mathbb{Z}_2$ sources, which in some cases have been shown to produce minimum variance [127]. Indeed, the use of stochastic sources has the advantage of making use of the full volume, in contrast to what happens with point sources. In our case, following [131], the i-th entry corresponds to a site z of the lattice and explicitly to a $\mathbb{Z}_2 \times \mathbb{Z}_2$ complex number

$$\eta^n(z) \in \left\{ \frac{1}{\sqrt{2}}(\pm 1 \pm i) \right\} \,, \tag{2.64}$$

which is drawn randomly for every source vector. The source reads

$$S^{(n,\alpha_0,a_0)}_{\mathbb{Z}_2}(z)_{\mu c} = \eta^n(z) \delta_{\alpha_0 \mu} \delta_{a_0 c} \,, \tag{2.65}$$

where in this case there is no dependence on any fixed lattice site but only on a single hit n. For this reason, the propagator in (2.60) now reads

$$G^n(y)_{\substack{\beta\alpha_0 \\ ba_0}} \equiv \sum_{z,\mu,c} D^{-1}(y,z)_{\substack{\beta\mu \\ bc}} S^{(n,\alpha_0,a_0)}_{\mathbb{Z}_2}(z)_{\substack{\mu \\ c}} \,. \tag{2.66}$$

For a large number of hits $N \to \infty$ we have

$$\sum_{\mu,c} \langle S^{(n,\alpha,a)}_{\mathbb{Z}_2}(y)_{\mu c} \, S^{(n,\beta,b)\dagger}_{\mathbb{Z}_2}(x)_{\mu c} \rangle = \frac{1}{N} \sum_{n=1}^{N} \eta^n(y) \eta^n(x)^\dagger \delta_{\alpha\beta} \delta_{ab} \quad \longrightarrow \quad \delta(x-y) \delta_{\alpha\beta} \delta_{ab} \,, \tag{2.67}$$

which reproduces the behaviour of the standard point sources. In particular, in this work we make use of $\mathbb{Z}_2$-*wall sources* [132], where the time dependence of the stochastic source is fixed at a given time t_0, i.e.

$$\eta(z; t_0) = \eta(z) \delta(z_4 - t_0) \,. \tag{2.68}$$

2.3.3 Smearing

The sources discussed so far rely on quark fields q that are placed on specific sites of the lattice. However, this implies that the overlap with the physical wavefunction is not optimal. We can then consider more general *smeared fields* to optimise the physical signal we are interested in. For example, a common trick is to introduce a smearing function that maximises the overlap of the wavefunction with the ground state and reduces the excited-states contamination.

Introducing the notation, we write $G \to G^{XY}$ with $X, Y \in \{S, L\}$, where S stands for "smeared" and L stands for "local". We introduce the smearing operator H^X that acts on the quark field as $q^X = H^X q^L$ as

$$\begin{aligned} q^X(x)^{\alpha}_{a} &= \sum_y H^X(x,y)^{\alpha\beta}_{ab}\, q^L(y)^{\beta}_{b} \\ \bar{q}^Y(x)^{\alpha}_{a} &= \sum_y \bar{q}^L(y)^{\beta}_{b}\, H^{Y\dagger}(y,x)^{\beta\alpha}_{ba}\,, \end{aligned} \tag{2.69}$$

where

$$\left[H^X(y,x)\right]^{\dagger\,\alpha\beta}_{ab} = H^{X*}(x,y)^{\beta\alpha}_{ba} \qquad \text{and} \qquad H^L(x,y)^{\alpha\beta}_{ab} = \delta(x-y)\delta_{\alpha\beta}\delta_{ab}\,. \tag{2.70}$$

Note that the field is smeared only on the three-dimensional space on a given time plane t, and the smearing operator depends on $H^S \equiv H^S(\boldsymbol{x}, \boldsymbol{y}; t)$ with $x = (\boldsymbol{x}, x_4) = (\boldsymbol{x}, t)$. Here we chose to keep the discussion general as in the previous section to keep the notation as light as possible. The standard discussion (see for example the appendix of [133]) can be easily recovered simply considering $H^S(x,y) \equiv H^S(\boldsymbol{x}, \boldsymbol{y})\delta(x_4 - t)\delta(y_4 - t)$.

Given a propagator $G^{XY}(y,x) = \langle q^X(y)\bar{q}^Y(x)\rangle$, it is clear that the smearing can be applied independently both at the *source* point x or at then *sink* point y, adopting the conventional terminology. The general expression then reads

$$G^{XY}(y,x) = \sum_{z,w} H^X(y,z) G^{LL}(z,w) H^{Y\dagger}(w,x)\,. \tag{2.71}$$

In practice, the propagator smeared at the source can be obtained by applying the smearing operator directly at the point source, i.e.

$$DG^{LS} = SH^{S\dagger}\,. \tag{2.72}$$

Note that explicitly this implies

$$G^{LS}(y,x) = \sum_{z,w} D^{-1}(y,z) S(z,w) H^S(w,x)^\dagger = \sum_w G^{LL}(y,w) H^S(w,x)^\dagger\,. \tag{2.73}$$

On the other hand, the propagator smeared at the sink can be easily obtained by applying the operator H^S on the propagator G^{LL} as

$$G^{SL} = H^S G^{LL}\,. \tag{2.74}$$

Finally, the smearing can also be applied simultaneously at both source and sink by combining the previous operations

$$G^{SS}(y,x) = \sum_{z,w} H^S(y,z) G^{LL}(z,w) H^S(w,x)^\dagger = \sum_z H^S(y,z) G^{LS}(z,x)\,, \tag{2.75}$$

where we made use of Eq. (2.73). Note that in principle it is also possible to employ different smearing, i.e. different choices of the operator H^S, at source or sink.

Let us conclude discussing explicitly how to build a smeared source $H^S(\boldsymbol{y}, \boldsymbol{x}_0)$, where we are now considering explicitly a smearing operator that depends only on the spatial coordinates. While in this work we make use of Jacobi smearing, here we briefly present the the Wuppertal approach [134, 135] as a pedagogical introduction to smearing. Let us consider the equation

$$\sum_{\boldsymbol{y}} K(\boldsymbol{x}, \boldsymbol{y}) H^S(\boldsymbol{y}, \boldsymbol{x}_0) = \delta(\boldsymbol{x} - \boldsymbol{x}_0)\,, \tag{2.76}$$

where we defined

$$\begin{cases} K(\boldsymbol{x}, \boldsymbol{y}) = \delta(\boldsymbol{x} - \boldsymbol{y}) - \kappa_s U(\boldsymbol{x}, \boldsymbol{y}) \\ U(\boldsymbol{x}, \boldsymbol{y}) = \sum_{j=1}^{3} \left[U_j(\boldsymbol{x}) \delta_{\boldsymbol{x}+\hat{\jmath}, \boldsymbol{y}} + U_j^\dagger(\boldsymbol{x} - \hat{\jmath}) \delta_{\boldsymbol{x}-\hat{\jmath}, \boldsymbol{y}} \right] \end{cases}, \tag{2.77}$$

and κ_s is a parameter that controls the smearing width. The effect of the smearing is to build a sort of "shell-model" wavefunction with each quark centred on $\boldsymbol{x}_0$ in a region of radius

$$r^2 = \frac{\sum_{\boldsymbol{y}} |\boldsymbol{y}|^2 |H^S(\boldsymbol{y}, \boldsymbol{x}_0)|^2}{\sum_{\boldsymbol{y}} |H^S(\boldsymbol{y}, \boldsymbol{x}_0)|^2} \tag{2.78}$$

controlled by the value of κ_s. Since inverting $K = \mathrm{I} - \kappa_s U$ is computationally expensive, we can make use of Jacobi iteration to obtain $H^S = K^{-1}$. Considering

$$H^S = (1 - \kappa_s U)^{-1} = \sum_{n=0}^{\infty} \kappa_s^n U^n = K^{-1}\,, \tag{2.79}$$

we can define the matrix

$$H^{S(N)} = \sum_{n=0}^{N} \kappa_s^n U^n \quad \overset{N\to\infty}{\longrightarrow} \quad K^{-1}\,, \tag{2.80}$$

which converges to the desired matrix K^{-1} for a large enough value of N. In practice, starting from $H^{S(0)} = H^L$, we repeat the following step

$$H^{S\,(n+1)} = H^L + \kappa_s U H^{S\,(n)}\,,$$

for a large enough number of iterations N such that $H^{S(N)}$ approximate H^S well enough.

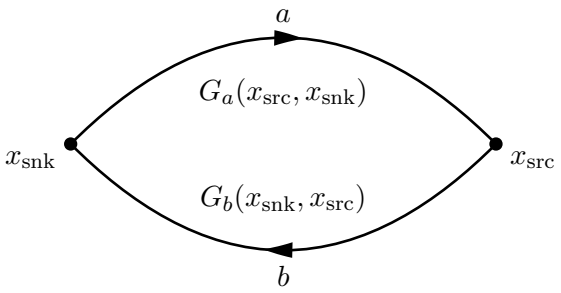

FIGURE 2.1: Two-point correlator diagram (connected) corresponding to the meson interpolator $\mathcal{O} = \bar{q}_a(x)\Gamma q_b(x)$. The quark q_a is propagated from $x_{\rm snk}$ to $x_{\rm src}$ through the propagator $G_a(x_{\rm src}, x_{\rm snk})$, whereas the quark q_b is propagated from $x_{\rm src}$ to $x_{\rm snk}$ by $G_b(x_{\rm snk}, x_{\rm src})$.

2.4 Interpolators and correlation functions

We now discuss how to build correlators on the lattice focusing on meson interpolators, which are the ones of interest in this work. We consider operators of the form

$$\mathcal{O}(x) = \bar{q}_b(x)\Gamma q_a(x)\,, \tag{2.81}$$

where a, b label the flavours and $\Gamma \in \{\Gamma^J, \Gamma^J_\mu\}$ (see App. A.1 for definition). In this way we aim to keep track of all the possibilities for all scalar, pseudoscalar, vector and axial operators with any combination of flavours. While we kept the discussion and notation general in the previous sections, we will now adopt the standard nomenclature for this sort of computations. We then refer to the source point as $x_{\rm src}$ and the sink point as $x_{\rm snk}$. For simplicity, in order to expose the momentum flow, the following discussion is specific to the case of the point source. Note that in practice we will use $\mathbb{Z}_2$ sources with twisted boundary conditions as detailed in Chap. 5.

2.4.1 Two-point correlators

Let us consider the two-point correlator depicted in figure Eq. (2.1)

$$C_{\rm 2pt}(x_{\rm snk}, x_{\rm src}) = \langle T\{\mathcal{O}_{\rm snk}(x_{\rm snk})\,\mathcal{O}^\dagger_{\rm src}(x_{\rm src})\}\rangle\,, \tag{2.82}$$

where the interpolating operators are

$$\mathcal{O}^\dagger_{\rm src}(x_{\rm src}) = \bar{q}_b(x_{\rm src})\Gamma^\dagger_{\rm src}\, q_a(x_{\rm src})\,, \tag{2.83}$$

$$\mathcal{O}_{\rm snk}(x_{\rm snk}) = \bar{q}_a(x_{\rm snk})\Gamma_{\rm snk}\, q_b(x_{\rm snk})\,. \tag{2.84}$$

This notation makes it easy to keep track of the position of the gammas when constructing the correlator. Note that a common case (as the ones considered in this work) is

given by $\mathcal{O}_{\text{src}} = \mathcal{O}_{\text{snk}}$ and $\Gamma_{\text{src}} = -\gamma^4\Gamma_{\text{snk}}\gamma^4 = \pm\,\Gamma_{\text{snk}}$, where the last sign depends on the commutation relation between γ^4 and Γ_{snk}. We are then creating a particle at the source with the quark content $q_b\bar{q}_a$ that is then destroyed at the sink (recall that the field $\bar{q}(x)$ creates a quark q, or equivalently destroys an antiquark $\bar{q}$, in position x, and vice versa for the field operator $q(x)$).

We can now write the components explicitly and apply Wick's theorem [136] to get

$$C_{2\text{pt}}(x_{\text{snk}}, x_{\text{src}}) = \langle T\{\bar{q}_a(x_{\text{snk}})_\alpha\,(\Gamma_{\text{snk}})_{\alpha\beta}\,q_b(x_{\text{snk}})_\beta\;\bar{q}_b(x_{\text{src}})_{\alpha'}\,(\Gamma^\dagger_{\text{src}})_{\alpha'\beta'}\,q_a(x_{\text{src}})_{\beta'}\}\rangle \tag{2.85}$$

which is given by the sum

$$C_{2\text{pt}}(x_{\text{snk}}, x_{\text{src}}) = C^{\text{conn}}_{2\text{pt}}(x_{\text{snk}}, x_{\text{src}}) + \delta_{ab}\,C^{\text{disc}}_{2\text{pt}}(x_{\text{snk}}, x_{\text{src}}) \tag{2.86}$$

of a connected diagram

$$\begin{aligned} C^{\text{conn}}_{2\text{pt}}(x_{\text{snk}}, x_{\text{src}}) &= -\langle(\Gamma_{\text{snk}})_{\alpha\beta}\,(\Gamma^\dagger_{\text{src}})_{\alpha'\beta'}\,\langle q_b(x_{\text{snk}})_\beta\,\bar{q}_b(x_{\text{src}})_{\alpha'}\rangle_F\,\langle q_a(x_{\text{src}})_{\beta'}\,\bar{q}_a(x_{\text{snk}})_\alpha\rangle_F\rangle_G \\ &= -\langle(\Gamma_{\text{snk}})_{\alpha\beta}\,(\Gamma^\dagger_{\text{src}})_{\alpha'\beta'}\,G_b(x_{\text{snk}}, x_{\text{src}})_{\beta\alpha'}\,G_a(x_{\text{src}}, x_{\text{snk}})_{\beta'\alpha}\rangle_G \\ &= -\left\langle \text{Tr}\left[\Gamma_{\text{snk}}G_b(x_{\text{snk}}, x_{\text{src}})\Gamma^\dagger_{\text{src}}G_a(x_{\text{src}}, x_{\text{snk}})\right]\right\rangle_G , \end{aligned} \tag{2.87}$$

and disconnected diagram

$$\begin{aligned} C^{\text{disc}}_{2\text{pt}}(x_{\text{snk}}, x_{\text{src}}) &= \langle(\Gamma_{\text{snk}})_{\alpha\beta}\,(\Gamma^\dagger_{\text{src}})_{\alpha'\beta'}\,\langle q_a(x_{\text{src}})_{\beta'}\,\bar{q}_a(x_{\text{src}})_{\alpha'}\rangle_F\,\langle q_a(x_{\text{snk}})_\beta\,\bar{q}_a(x_{\text{snk}})_\alpha\rangle_F\rangle_G \\ &= \langle(\Gamma_{\text{snk}})_{\alpha\beta}\,(\Gamma^\dagger_{\text{src}})_{\alpha'\beta'}\,G_a(x_{\text{src}}, x_{\text{src}})_{\beta'\alpha'}\,G_a(x_{\text{snk}}, x_{\text{snk}})_{\beta\alpha}\rangle_G \\ &= \left\langle \text{Tr}\left[\Gamma^\dagger_{\text{src}}G_a(x_{\text{src}}, x_{\text{src}})\right]\,\text{Tr}\left[\Gamma_{\text{snk}}G_a(x_{\text{snk}}, x_{\text{snk}})\right]\right\rangle_G , \end{aligned} \tag{2.88}$$

In the above steps we reordered the Grassman variables and used the fact that the fermionic expectation value $\langle\ldots\rangle_F$ factorises with respect to the flavour. Note that the disconnected piece enters only in the case of equal flavours $a = b$. We will focus only on connected diagrams as these are the only ones relevant for this work. Using γ_5-hermiticity (see App. B.4) on G_a we finally get

$$C^{\text{conn}}_{2\text{pt}}(x_{\text{snk}}, x_{\text{src}}) = -\left\langle \text{Tr}\left[\gamma_5\Gamma_{\text{snk}}G_b(x_{\text{snk}}, x_{\text{src}})\Gamma^\dagger_{\text{src}}\gamma_5 G^\dagger_a(x_{\text{snk}}, x_{\text{src}})\right]\right\rangle_G . \tag{2.89}$$

This allows to always compute one-to-all propagators from a fixed x_{src} and reduce the computational cost, as also clear in Eq. (2.91), where only a sum over $\boldsymbol{x}_{\text{snk}}$ is performed.

The final step is to project the correlators in momentum space. In particular, thanks to momentum conservation, it is enough to project just one of the two interpolators (typically the one at the sink)

$$\tilde{\mathcal{O}}_{\text{snk}}(\boldsymbol{p}_{\text{snk}}, t) = \sum_{\boldsymbol{x}_{\text{snk}}} e^{-i\boldsymbol{p}_{\text{snk}}\cdot\boldsymbol{x}_{\text{snk}}}\,\mathcal{O}_{\text{snk}}(\boldsymbol{x}_{\text{snk}}, t_{\text{snk}}) , \tag{2.90}$$

where we used the discrete Fourier transform in three dimensions such that the final correlator reads

$$\begin{aligned} C_{2\mathrm{pt}}(\boldsymbol{p}_{\mathrm{snk}}, t_{\mathrm{snk}}, t_{\mathrm{src}}) &= \langle T\{\tilde{\mathcal{O}}_{\mathrm{snk}}(\boldsymbol{p}_{\mathrm{snk}}, t_{\mathrm{snk}})\, \mathcal{O}^{\dagger}_{\mathrm{src}}(\boldsymbol{x}_{\mathrm{src}}, t_{\mathrm{src}})\}\rangle \\ &= \sum_{\boldsymbol{x}_{\mathrm{snk}}} e^{-i\boldsymbol{p}_{\mathrm{snk}}\cdot(\boldsymbol{x}_{\mathrm{snk}}-\boldsymbol{x}_{\mathrm{src}})} \langle T\{\mathcal{O}_{\mathrm{snk}}(\boldsymbol{x}_{\mathrm{snk}}, t_{\mathrm{snk}})\, \mathcal{O}^{\dagger}_{\mathrm{src}}(\boldsymbol{x}_{\mathrm{src}}, t_{\mathrm{src}})\}\rangle \\ &= -\sum_{\boldsymbol{x}_{\mathrm{snk}}} e^{-i\boldsymbol{p}_{\mathrm{snk}}\cdot(\boldsymbol{x}_{\mathrm{snk}}-\boldsymbol{x}_{\mathrm{src}})} \left\langle \mathrm{Tr}\left[\gamma_5 \Gamma_{\mathrm{snk}} G_b(x_{\mathrm{snk}}, x_{\mathrm{src}}) \Gamma^{\dagger}_{\mathrm{src}} \gamma_5 G^{\dagger}_a(x_{\mathrm{snk}}, x_{\mathrm{src}})\right]\right\rangle_G . \end{aligned} \tag{2.91}$$

Note that we used translation invariance to include a dependence on $\boldsymbol{x}_{\mathrm{src}}$ in the exponential with the intent to show explicitly the momentum flow. We will adopt the same convention in the rest of the manuscript.

We can now insert a complete set of states $I = \sum_n \frac{|H_n\rangle\langle H_n|}{2E_n}$, and defining $t = t_{\mathrm{snk}} - t_{\mathrm{src}}$ thanks to time-translation invariance, and $\boldsymbol{p} = \boldsymbol{p}_{\mathrm{snk}} = \boldsymbol{p}_{\mathrm{src}}$ we get

$$C_{2\mathrm{pt}}(\boldsymbol{p}, t) = \sum_n \frac{Z_{\mathrm{snk,n}}\, Z^{*}_{\mathrm{src,n}}}{2E_n} \left[e^{-(T-t)E_n} \pm e^{-tE_n}\right] , \tag{2.92}$$

where $E_n \equiv E_n(\boldsymbol{p})$, $Z_{\mathrm{snk,n}} = \langle 0|\, \mathcal{O}_{\mathrm{snk}}\, |H_n(\boldsymbol{p})\rangle$ and $Z^{*}_{\mathrm{src,n}} = \langle H_n(\boldsymbol{p})|\, \mathcal{O}^{\dagger}_{\mathrm{src}}\, |0\rangle$, and where $|H_n(\boldsymbol{p})\rangle$ is the n-th hadronic energy state with momentum $\boldsymbol{p}$. Note that the relative sign depends on the property of the time-reversal of the specific operators considered.

It is often useful to consider the case where the ground state dominates, e.g. to extract the hadron mass associated with the ground state of the given interpolator. Focusing on the positive sign in Eq. (2.92), we can then consider the case $t \gg 0$ such that

$$\begin{aligned} C_{2\mathrm{pt}}(\boldsymbol{p}, t) &\overset{t\gg 0}{=} \frac{Z_{\mathrm{snk,0}}\, Z^{*}_{\mathrm{src,0}}}{2E_0} \left[e^{-(T-t)E_0} + e^{-tE_0}\right] \\ &= 2A_0 e^{-T/2} \cosh\left((T/2 - t)E_0\right) , \end{aligned} \tag{2.93}$$

where $A_0 = Z_{\mathrm{snk,0}}\, Z^{*}_{\mathrm{src,0}}/(2E_0)$. The analysis of two-point functions is then particularly useful to obtain the energies of the ground states and, in some cases, of some of the excited states. It allows in this way to determine the basic properties of the gauge ensemble considered for the computations.

2.4.2 Three-point correlators

We now focus on the construction of a generic three-point correlator. Similar to the previous case, we consider the generic operators

$$\mathcal{O}^{\dagger}_{\mathrm{src}}(x_{\mathrm{src}}) = \bar{q}_b(x_{\mathrm{src}}) \Gamma^{\dagger}_{\mathrm{src}}\, q_a(x_{\mathrm{src}}) , \tag{2.94}$$

$$J_\mu(x) = \bar{q}_c(x) \Gamma^{J}_{\mu}\, q_b(x) , \tag{2.95}$$

$$\mathcal{O}_{\mathrm{snk}}(x_{\mathrm{snk}}) = \bar{q}_a(x_{\mathrm{snk}}) \Gamma_{\mathrm{snk}}\, q_c(x_{\mathrm{snk}}) . \tag{2.96}$$

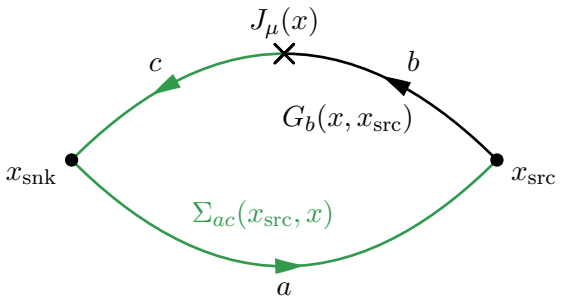

FIGURE 2.2: Three-point correlator diagram. The black propagator G_b propagates the quark q_b from $x_{\rm src}$ to x, whereas the green line is a sequential propagator that propagates the quark q_c from x to $x_{\rm snk}$ (with a fixed $t_{\rm snk}$) and the then the quark q_a from $x_{\rm snk}$ to $x_{\rm src}$.

Note that the current operator J_μ depends on the index μ because of the Γ^J_μ matrix. This is the case relevant for this work, but the treatment can be generalised trivially considering a generic matrix Γ.

The correlation function, represented in Fig. 2.2, is given by

$$C_{3{\rm pt},\mu}(x_{\rm snk}, x, x_{\rm src}) = \langle T\{\mathcal{O}_{\rm snk}(x_{\rm snk})\, J_\mu(x)\, \mathcal{O}^\dagger_{\rm src}(x_{\rm src})\}\rangle\,. \tag{2.97}$$

Expanding the representation it can be divided in connected and disconnect contributions as for the two-point functions. For simplicity, we will consider only the connected contribution, which is the only one relevant in this work since we consider processes where $a \neq b \neq c$. We then get

$$\begin{aligned} C_{3{\rm pt},\mu}(x_{\rm snk}, x, x_{\rm src}) &= \langle \bar q_a(x_{\rm snk})\Gamma_{\rm snk}\, q_c(x_{\rm snk})\bar q_c(x)\Gamma^J_\mu\, q_b(x)\bar q_b(x_{\rm src})\Gamma^\dagger_{\rm src}\, q_a(x_{\rm src})\rangle \\ &= -\langle(\Gamma_{\rm snk})_{\alpha\beta}(\Gamma^J_\mu)_{\gamma\delta}(\Gamma^\dagger_{\rm src})_{\epsilon\zeta}\times \\ &\quad \langle q_a(x_{\rm src})_\zeta\, \bar q_a(x_{\rm snk})_\alpha\rangle_F \langle q_b(x)_\delta\, \bar q_b(x_{\rm src})_\epsilon\rangle_F \langle q_c(x_{\rm snk})_\beta\, \bar q_c(x)_\gamma\rangle_F\rangle_G \\ &= -\left\langle {\rm Tr}\left[\Gamma^J_\mu G_b(x, x_{\rm src})\Gamma^\dagger_{\rm src} G_a(x_{\rm src}, x_{\rm snk})\Gamma_{\rm snk} G_c(x_{\rm snk}, x)\right]\right\rangle_G . \end{aligned} \tag{2.98}$$

We can then project into momentum space as before the operators $\tilde{\mathcal{O}}_{\rm snk}(\boldsymbol{p}_{\rm snk}, t_{\rm snk}) = \sum_{\boldsymbol{x}_{\rm snk}} e^{-i\boldsymbol{p}_{\rm snk}\cdot\boldsymbol{x}_{\rm snk}}\mathcal{O}_{\rm snk}(\boldsymbol{x}_{\rm snk}, t_{\rm snk})$ and $\tilde J_\mu(\boldsymbol{q}, t) = \sum_{\boldsymbol{x}} e^{-i\boldsymbol{q}\cdot\boldsymbol{x}} J_\mu(\boldsymbol{x}, t)$, where $\boldsymbol{q} = \boldsymbol{p}_{\rm src} - \boldsymbol{p}_{\rm snk}$ is the momentum transfer, such that

$$\begin{aligned} C_{3{\rm pt},\mu}(x_{\rm snk}, x, x_{\rm src}) &= \sum_{\boldsymbol{x}_{\rm snk},\boldsymbol{x}} e^{-i\boldsymbol{p}_{\rm snk}\cdot(\boldsymbol{x}_{\rm snk}-\boldsymbol{x}_{\rm src})} e^{-i\boldsymbol{q}\cdot(\boldsymbol{x}-\boldsymbol{x}_{\rm src})}\times \\ &\quad \langle T\{\mathcal{O}_{\rm snk}(x_{\rm snk})\, J_\mu(x)\, \mathcal{O}^\dagger_{\rm src}(x_{\rm src})\}\rangle \\ &= -\sum_{\boldsymbol{x}_{\rm snk},\boldsymbol{x}} e^{-i\boldsymbol{p}_{\rm snk}\cdot(\boldsymbol{x}_{\rm snk}-\boldsymbol{x}_{\rm src})} e^{-i\boldsymbol{q}\cdot(\boldsymbol{x}-\boldsymbol{x}_{\rm src})}\times \\ &\quad \left\langle {\rm Tr}\left[\Gamma^J_\mu G_b(x, x_{\rm src})\Gamma^\dagger_{\rm src} G_a(x_{\rm src}, x_{\rm snk})\Gamma_{\rm snk} G_c(x_{\rm snk}, x)\right]\right\rangle_G . \end{aligned} \tag{2.99}$$

The practical evaluation of the above expression requires a lot of computational resources, since each inversion of the kinetic operator uses a significant amount of computer time. To overcome this we can introduce the *sequential source method* [137], defining the *sequential propagator* as

$$\Sigma_{ac}(x_{\mathrm{src}}, x) = \sum_{\boldsymbol{x}_{\mathrm{snk}}} e^{-i\boldsymbol{p}_{\mathrm{snk}}\cdot(\boldsymbol{x}_{\mathrm{snk}}-\boldsymbol{x}_{\mathrm{src}})} G_a(x_{\mathrm{src}}, x_{\mathrm{snk}})\Gamma_{\mathrm{snk}} G_c(x_{\mathrm{snk}}, x)\,. \tag{2.100}$$

such that the final expression simplifies as

$$\begin{aligned} C_{3\mathrm{pt},\mu}(\boldsymbol{q}, \boldsymbol{p}_{\mathrm{snk}}, t_{\mathrm{snk}}, t, t_{\mathrm{src}}) &= -\sum_{\boldsymbol{x}} e^{-i\boldsymbol{q}\cdot(\boldsymbol{x}-\boldsymbol{x}_{\mathrm{src}})} \left\langle \mathrm{Tr}\left[\Gamma^J_\mu G_b(x, x_{\mathrm{src}})\Gamma^\dagger_{\mathrm{src}}\Sigma_{ac}(x_{\mathrm{src}}, x)\right]\right\rangle_G \\ &= \pm\sum_{\boldsymbol{x}} e^{-i\boldsymbol{q}\cdot(\boldsymbol{x}-\boldsymbol{x}_{\mathrm{src}})} \left\langle \mathrm{Tr}\left[\gamma_5\Gamma^J_\mu G_b(x, x_{\mathrm{src}})\Gamma^\dagger_{\mathrm{src}}\gamma_5\Sigma^\dagger_{ca}(x, x_{\mathrm{src}})\right]\right\rangle_G , \end{aligned} \tag{2.101}$$

with exactly the same structure of the two-point function in Eq. (2.91), where we used γ_5-hermiticity on the sequential propagator

$$\begin{aligned} \Sigma_{ac}(x_{\mathrm{src}}, x) &= \gamma_5 \left(\sum_{\boldsymbol{x}_{\mathrm{snk}}} e^{i\boldsymbol{p}_{\mathrm{snk}}\cdot(\boldsymbol{x}_{\mathrm{snk}}-\boldsymbol{x}_{\mathrm{src}})} G_c(x, x_{\mathrm{snk}})\gamma_5\Gamma^\dagger_{\mathrm{snk}}\gamma_5 G_a(x_{\mathrm{snk}}, x_{\mathrm{src}})\right)^\dagger \gamma_5 \\ &= \pm\gamma_5 \left(\sum_{\boldsymbol{x}_{\mathrm{snk}}} e^{i\boldsymbol{p}_{\mathrm{snk}}\cdot(\boldsymbol{x}_{\mathrm{snk}}-\boldsymbol{x}_{\mathrm{src}})} G_c(x, x_{\mathrm{snk}})\Gamma^\dagger_{\mathrm{snk}} G_a(x_{\mathrm{snk}}, x_{\mathrm{src}})\right)^\dagger \gamma_5 \\ &= \pm\,\gamma_5\Sigma^\dagger_{ca}(x, x_{\mathrm{src}})\gamma_5\,, \end{aligned} \tag{2.102}$$

and where the sign has to be determined from the commutation or anticommutation relation of Γ_{snk} and γ_5. It is then clear from this expression that instead of computing all the all-to-all propagators we can simply compute $G_a(x_{\mathrm{snk}}, x_{\mathrm{src}})$ with a fixed source in x_{src} as described in Sec. 2.3, fix the value of t_{snk} and compute the sequential propagator $\Sigma_{ca}(x, x_{\mathrm{src}})$ as

$$\begin{cases} \displaystyle\sum_x D_c(y, x)\Sigma_{ca}(x, x_{\mathrm{src}}) = S_{\mathrm{seq}}(y, x_{\mathrm{src}}) \\ S_{\mathrm{seq}}(y, x_{\mathrm{src}}) = e^{i\boldsymbol{p}_{\mathrm{snk}}\cdot(\boldsymbol{y}-\boldsymbol{x}_{\mathrm{src}})}\Gamma^\dagger_{\mathrm{snk}} G_a(y, x_{\mathrm{src}})\delta(y_4 - t_{\mathrm{snk}}) \end{cases} . \tag{2.103}$$

This requires us to invert the kinetic operators D_a and D_c only once each instead of multiple times for all the possible values of x_{snk}, provided that we fix the value of t_{snk}. Note that while the sequential propagator Σ_{ca} depends on the momentum $\boldsymbol{p}_{\mathrm{snk}}$, we omit its dependence in the arguments for consistency with the notation for the other propagators.

The complete insertion of states $I = \sum_n \frac{|H_n\rangle\langle H_n|}{2E_n}$ between $\mathcal{O}_{\rm snk}$ and J_μ, and between J_μ and $\mathcal{O}^\dagger_{\rm src}$ gives

$$C_{3{\rm pt},\mu}(\boldsymbol{q}, \boldsymbol{p}_{\rm snk}, t_{\rm snk}, t, t_{\rm src}) = \sum_{n,m} \frac{Z_{{\rm snk,n}} Z^*_{{\rm src,m}}}{4E_{{\rm snk,n}} E_{{\rm src,m}}} \langle H_{{\rm snk,n}}(\boldsymbol{p}_{\rm snk})| J_\mu |H_{{\rm src,m}}(\boldsymbol{p}_{\rm src})\rangle \times \Big[\theta(t_{\rm snk} - t)\theta(t - t_{\rm src}) e^{-E_{{\rm snk,n}}(t_{\rm snk} - t)} e^{-E_{{\rm src,m}}(t - t_{\rm src})} - \theta(T + t_{\rm src} - t)\theta(t - t_{\rm snk}) e^{-E_{{\rm src,m}}(T + t_{\rm src} - t)} e^{-E_{{\rm snk,n}}(t - t_{\rm snk})}\Big], \quad (2.104)$$

where the definitions of energies and states follow from the conventions used for the two-point functions.

The interest of three-point function often relies on the extraction of the matrix element associated with the hadronic process $H_{\rm src,0} \to H_{\rm snk,0}$ mediated by the current J_μ, where the subscript "0" indicate the ground state. It is then convenient to fix $t_{\rm snk}$ such that the excited states in Eq. (2.104) are suppressed for suitable value of t, i.e. $t_{\rm snk} - t \gg 0$, $t - t_{\rm src} \gg 0$. In this regime, and with $t_{\rm snk} \geq t \geq t_{\rm src}$, the three-point correlator reads

$$C_{3{\rm pt},\mu}(\boldsymbol{q}, \boldsymbol{p}_{\rm snk}, t_{\rm snk}, t, t_{\rm src}) = \frac{Z_{{\rm snk},0} Z^*_{{\rm src},0}}{4E_{{\rm snk},0} E_{{\rm src},0}} \langle H_{{\rm snk},0}(\boldsymbol{p}_{\rm snk})| J_\mu |H_{{\rm src},0}(\boldsymbol{p}_{\rm src})\rangle \times e^{-E_{{\rm snk},0}(t_{\rm snk} - t)} e^{-E_{{\rm src},0}(t - t_{\rm src})}. \quad (2.105)$$

2.4.3 n-point correlators

The treatment of Secs. 2.4.1 and 2.4.2 can be further extended and generalised to arbitrary n-point correlation functions. In particular, quantities of interests in this work are four-point functions, which address the extraction of matrix elements of the form

$$\langle H| J^2 J^1 |H\rangle \quad (2.106)$$

where $|H\rangle$ is the initial hadronic states and $J^{1,2}$ are current operators that mediate a given physical process. To avoid further complications in this chapter, we discuss their construction directly in connection to the process of interest in Sec. 4.1.

CHAPTER 3

$B_{(S)}$ SEMILEPTONIC DECAYS

In this chapter we review the formalism to describe semileptonic decays involving $B_{(s)}$ mesons, focusing in particular on the exclusive decay $B_s \to D_s^{(*)} l\nu_l$ and its inclusive version $B_s \to X_c\, l\nu_l$ in Fig. 3.1. However, the formalism can be applied more in general to other channels such as, e.g., $B \to X\, l\nu_l$ or $D_{(s)} \to X l\nu_l$ [2]. We start in Sec. 3.1 recalling the kinematic relations of an exclusive three-body decay and extending them to the inclusive case. In Sec. 3.2 we describe the quantities relevant for the exclusive processes $B_s \to D_s^{(*)} l\nu_l$. We finally address the inclusive case in Sec. 3.3, where we derive all the equations necessary to study these decays, focusing in particular on the computation of the decay rate, the lepton energy moments and the hadronic mass moments.

In this work we consider the case where the lepton is represented by an electron or a muon, $l = e, \mu$, and we therefore focus on the limit $m_l = 0$. Note that, as opposed to the rest of the manuscript, the physics processes described here are treated in Minkowski space as in Chap. 1.

The B_s decay under study is triggered by an effective weak interaction $\bar{b} \to \bar{c}$. The tree-level Hamiltonian for the process is given by

$$\mathcal{H}_W = \frac{G_F}{\sqrt{2}} V_{cb} \left[\bar{\nu}_{lL} \gamma_\mu l_L\right] J_\mu \,, \quad J_\mu = \bar{b}_L \gamma^\mu c_L \,, \tag{3.1}$$

where G_F is the Fermi constant and V_{cb} is the CKM-matrix element for the charged-current flavour-changing quark transition, and J_μ is the electroweak quark current for this process. We can also decompose $J_\mu = V_\mu - A_\mu$ with $V_\mu = \bar{b}\gamma_\mu c$ and $A_\mu = \bar{b}\gamma_\mu\gamma_5 c$ being the vector and axial currents, respectively.

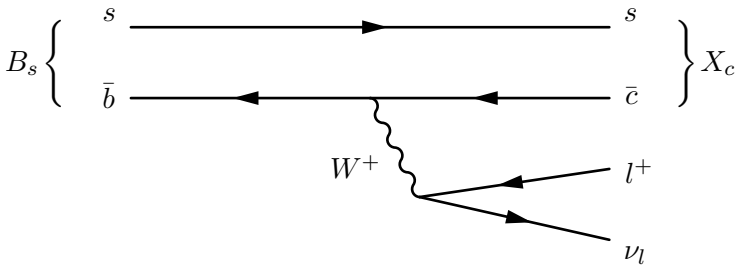

FIGURE 3.1: Feynman diagram for $B_s \to X_c\, l\nu_l$.

3.1 Kinematics

We first review the kinematics of a three-particle decay. Let us consider a particle of mass m with four-momentum p that decays into three particles with masses m_i and four-momenta p_i, $i = 1, 2, 3$. The basic conservation law is

$$p = p_1 + p_2 + p_3\,, \quad s = p^2 = m^2\,, \tag{3.2}$$

where s is the Mandelstam variable. We can define additional invariants as

$$\begin{cases} s_1 &= (p - p_1)^2 = (p_2 + p_3)^2\,, \\ s_2 &= (p - p_2)^2 = (p_1 + p_3)^2\,,\,, \\ s_3 &= (p - p_3)^2 = (p_1 + p_2)^2\,, \end{cases} \tag{3.3}$$

which are related to the subsystem of two particles 23, 13 and 12 respectively. These quantities are not independent, since

$$s_1 + s_2 + s_3 = m^2 + m_1^2 + m_2^2 + m_3^2\,. \tag{3.4}$$

If we consider the rest frame of the decaying particle, the invariants s_i read explicitly

$$s_i = (p - p_i)^2 = m^2 + m_i^2 - 2mE_i\,, \tag{3.5}$$

where $E_i = \sqrt{m_i^2 + \boldsymbol{p}_i^2}$ can range between $E_i\big|_{\min} = m_i$ and $E_i\big|_{\max} = \sqrt{m_i^2 + \boldsymbol{p}_i^2\big|_{\max}}$. The maximum value $E_i|_{\max}$ corresponds to the limiting case where all the momentum flows into the particle m_i, whereas the other two particles m_j and m_k with $j \neq k \neq i$ are produced at rest. The range for s_i is then

$$\begin{cases} s_i\big|_{\min} = m^2 + m_i^2 - 2mE_i\big|_{\max} = (p_j\big|_{\min} + p_k\big|_{\min})^2 = (m_j + m_k)^2 \\ s_i\big|_{\max} = m^2 + m_i^2 - 2mE_i\big|_{\min} = (m - m_i)^2 \end{cases}. \tag{3.6}$$

Incidentally, this also shows that

$$E_i\big|_{\max} = \frac{1}{2m}\left[m^2 + m_i^2 - (m_j + m_k)^2\right]\,. \tag{3.7}$$

However, not all these values of s_i are accessible, as we still need to take into account the full kinematic constraints. Imposing momentum conservation and integrating over all the possible angular distributions for the three particles, we see that the whole kinematics relies on only two independent variables: we can take, for example, $s_3 = (p_1 + p_2)^2$ and E_2. Typically, $s_3 \equiv q^2$ would be the momentum of a mediator particle. For these two we have

$$(m_1 + m_2)^2 \leq q^2 \leq (m - m_3)^2 \,, \qquad m_2 \leq E_2 \leq \frac{1}{2m}\left[m^2 + m_2^2 - (m_1 + m_3)^2\right] \,. \tag{3.8}$$

These relations would represent a box in the phase space (q^2, E_2). However, they are related to each other and must then obey further constraints. In particular, we have

$$\begin{cases} q^2 = (p_1 + p_2)^2 = m_1^2 + m_2^2 + 2p_1 \cdot p_2 \,, \\ q^2 = (p - p_3)^2 = m^2 + m_3^2 - 2mE_3 \,, \end{cases} \qquad \begin{cases} q_0 = E_1 + E_2 \,, \\ q_0 = m - E_3 \,. \end{cases} \tag{3.9}$$

Combining these expressions we can work out the relations for E_1 and E_3

$$E_3 = \frac{m^2 + m_3^2 - q^2}{2m} \,, \qquad E_1 = \frac{m^2 - m_3^2 + q^2}{2m} - E_2 \,. \tag{3.10}$$

If we assume E_2 fixed, for q^2 we get

$$\begin{aligned} q^2 = m_1^2 + m_2^2 + 2\Bigg\{ & E_2 \left[\frac{m^2 - m_3^2 + q^2}{2m} - E_2\right] \\ & - \cos\theta_{12}\sqrt{E_2^2 - m_2^2}\sqrt{\left[\frac{m^2 - m_3^2 + q^2}{2m} - E_2\right]^2 - m_1^2}\Bigg\} \,, \end{aligned} \tag{3.11}$$

where the term inside the brackets corresponds to $p_1 \cdot p_2$ and $\cos\theta_{12} = \boldsymbol{p}_1 \cdot \boldsymbol{p}_2/(|\boldsymbol{p}_1||\boldsymbol{p}_2|)$ is the angle between $\boldsymbol{p}_1$ and $\boldsymbol{p}_2$. This final formula shows the relation between the two independent variables q^2 and E_2, which, together with the ranges in Eq. (3.8), fully determines the phase space of the three-body decay.

Let us now extend the previous discussion to the kinematics of inclusive B_s-meson semileptonic decays $B_s \to X_c\, l \nu_l$ in the B_s rest frame, i.e $p_{B_s} = (M_{B_s}, 0, 0, 0)$, which can be obtained by extending the previous discussion. Since X_c represents all possible final states allowed by conservation laws, there are three independent kinematic variables, one more compared to the exclusive case. We can choose q^2, E_l and M_{X_c}, which correspond to s_3, E_2 and m_3 from the previous derivation, with

$$q = p_{B_s} - p_{X_c} = p_l + p_{\nu_l} \,, \qquad \begin{cases} q_0 = M_{B_s} - E_{X_c} = E_l + E_{\nu_l} \,, \\ \boldsymbol{q} = -\boldsymbol{p}_{X_c} = \boldsymbol{p}_l + \boldsymbol{p}_{\nu_l} \,. \end{cases} \tag{3.12}$$

In the limit of massless leptons $m_l = m_{\nu_l} = 0$, from Eq. (3.8) it follows that the kinematic variables must lie in the following ranges

$$\begin{cases} 0 \leq q^2 \leq (M_{B_s} - M_{X_c})^2 \,, \\ 0 \leq E_l \leq \dfrac{1}{2M_{B_s}}(M_{B_s}^2 - M_{X_c}^2) \,, \\ M_{D_s} \leq M_{X_c} \leq M_{B_s} \,. \end{cases} \tag{3.13}$$

The variables q^2 and E_l are related to one another by

$$\begin{aligned} q^2 &= 2p_l p_{\nu_l} = 2E_l E_{\nu_l}(1 - \cos\theta_{l\nu_l}) \\ &= (1 - \cos\theta_{l\nu_l})E_l \left[\frac{M_{B_s}^2 - M_{X_c}^2 + q^2}{M_{B_s}} - 2E_l \right] , \end{aligned} \tag{3.14}$$

where we used Eq. (3.10) for E_{ν_l}, and $\cos\theta_{l\nu_l} = \boldsymbol{p}_l \cdot \boldsymbol{p}_{\nu_l}/(|\boldsymbol{p}_l||\boldsymbol{p}_{\nu_l}|)$ is the angle between the electron and neutrino momenta. Rearranging for q^2 we get

$$q^2 = \frac{(1 - \cos\theta_{\nu l})E_l}{M_{B_s} - (1 - \cos\theta_{\nu l})E_l}(M_{B_s}^2 - M_{X_c}^2 - 2M_{B_s}E_l) \,. \tag{3.15}$$

Considering the minimum and maximum values for $\cos\theta_{\nu l}$, for every E_l fixed the corresponding q^2 lies in the range

$$0 \leq q^2 \leq \frac{2E_l}{M_{B_s} - 2E_l}(M_{B_s}^2 - M_{X_c}^2 - 2M_{B_s}E_l) \,. \tag{3.16}$$

This concludes the discussion on the inclusive kinematics: from the last two equations and the ranges in Eq. (3.13) we can now obtain the phase space in the plane (q^2, E_l) for any given value of M_{X_c}.

3.2 Exclusive semileptonic decays

We now review the standard formalism for treating the exclusive decays $B_s \to D_s^{(*)} l\nu_l$. QCD matrix elements associated with such decays can be described by *form factors*. Hadron form factors appear in any transition between an initial and final hadronic state induced by an electromagnetic or weak interaction of quarks. They are functions of the momentum transfer and fully describe the nonperturbative dynamics involved in the decay process.

3.2.1 Decay into pseudoscalar final state

Let us first consider the case $B_s \to D_s\, l\nu_l$, where the final-state hadron is the pseudoscalar D_s meson, $J^P = 0^-$. In this case, only the vector current V_μ contributes to the

decay because of parity conservation. The amplitude then reads

$$\mathcal{A}(B_s \to D_s l \nu_l) = \frac{G_F}{\sqrt{2}} V_{cb} \left[\bar{\nu}_{lL} \gamma_\mu l_L\right] \langle D_s(p_{D_s})| V^\mu |B_s(p_{B_s})\rangle \ . \tag{3.17}$$

The QCD matrix element $\mathcal{M}_{V_\mu}^{D_s B_s} \equiv \langle D_s(p_{D_s})| V_\mu |B_s(p_{B_s})\rangle$ can be decomposed as

$$\mathcal{M}_{V_\mu}^{D_s B_s} = (p_{B_s} + p_{D_s})_\mu \, f_{D_s B_s}^+(q^2) + (p_{B_s} - p_{D_s})_\mu \, f_{D_s B_s}^-(q^2) \,, \tag{3.18}$$

where $f_{D_s B_s}^+(q^2)$ and $f_{D_s B_s}^-(q^2)$ are the form factors for the given decay. On the other hand, the form factors can be related to the matrix elements as

$$f_{D_s B_s}^+(q^2) = \frac{p_{B_s}^s - p_{D_s}^s}{(E_{B_s} + E_{D_s})(p_{B_s}^s - p_{D_s}^s) - (E_{B_s} - E_{D_s})(p_{B_s}^s + p_{D_s}^s)} \times \left(\mathcal{M}_{V_0}^{D_s B_s} - \frac{(E_{B_s} - E_{D_s})}{p_{B_s}^s - p_{D_s}^s} \mathcal{M}_{V_s}^{D_s B_s} \right) , \tag{3.19}$$

$$f_{D_s B_s}^-(q^2) = \frac{p_{B_s}^s + p_{D_s}^s}{(E_{B_s} - E_{D_s})(p_{B_s}^s + p_{D_s}^s) - (E_{B_s} + E_{D_s})(p_{B_s}^s - p_{D_s}^s)} \times \left(\mathcal{M}_{V_0}^{D_s B_s} - \frac{(E_{B_s} + E_{D_s})}{p_{B_s}^s + p_{D_s}^s} \mathcal{M}_{V_s}^{D_s B_s} \right) , \tag{3.20}$$

where $\mathcal{M}_{V_s}^{D_s B_s} = 1/3 \sum_{k=1}^3 \mathcal{M}_{V_k}^{D_s B_s}$, $p_{D_s}^s = 1/3 \sum_{k=1}^3 p_{D_s,k}$ and $p_{B_s}^s = 1/3 \sum_{k=1}^3 p_{B_s,k}$ are the averages over the three spatial directions. The matrix element is commonly reformulated as

$$\begin{aligned} \mathcal{M}_{V_\mu}^{D_s B_s} = & \left[2p_{D_s,\mu} + \left(1 - \frac{M_{B_s}^2 - M_{D_s}^2}{q^2} \right) q_\mu \right] f_{D_s B_s}^+(q^2) \\ & + \frac{M_{B_s}^2 - M_{D_s}^2}{q^2} q_\mu f_{D_s B_s}^0(q^2) \,, \end{aligned} \tag{3.21}$$

where $f_{D_s B_s}^+(q^2)$ is referred to as *vector form factor* and

$$f_{D_s B_s}^0(q^2) = f_{D_s B_s}^+(q^2) + \frac{q^2}{M_{B_s}^2 - M_{D_s}^2} f_{D_s B_s}^-(q^2) \,, \tag{3.22}$$

is the *scalar form factor*. Note that $f_{D_s B_s}^0(0) = f_{D_s B_s}^+(0)$ such that there is no divergence at $q^2 = 0$ in Eq. (3.21). The name scalar form factor refers to its relation with the hadronic matrix elements involving the scalar current $\bar{c}b$, in particular

$$\langle D_s(p_{D_s})| (m_b - m_c) \bar{b}c |B_s(p_{B_s})\rangle = (M_{B_s}^2 - M_{D_s}^2) f_{D_s B_s}^0(q^2), \tag{3.23}$$

where m_b and m_c are the bottom and charm quark masses, respectively. Furthermore, the contraction of the matrix element with the transferred momentum q is proportional to the scalar form factor, i.e. $q^\mu \mathcal{M}_{V_\mu}^{D_s B_s} = (M_{B_s}^2 - M_{D_s}^2) f_{D_s B_s}^0(q^2)$.

A useful observable for this exclusive process is the differential decay rate

$$\begin{aligned}\frac{\mathrm{d}\Gamma(B_s \to D_s l\nu_l)}{\mathrm{d}q^2} =& \frac{G_F^2|V_{cb}|^2}{24\pi^3}\frac{(q^2-m_l^2)^2}{(q^2)^2}|\boldsymbol{p}_{D_s}|\Bigg\{\left(1+\frac{m_l^2}{2q^2}\right)|\boldsymbol{p}_{D_s}|^2|f^+_{B_sD_s}(q^2)|^2 \\ &+\frac{3m_l^2}{8q^2}\frac{(M_{B_s}^2-M_{D_s}^2)^2}{M_{B_s}^2}|f^0_{B_sD_s}(q^2)|^2\Bigg\}.\end{aligned} \tag{3.24}$$

Indeed, it is experimentally accessible by measuring the distribution in momenta of the D_s and can therefore be directly combined with the Standard-Model prediction for the r.h.s of the equation to extract the CKM-matrix element $|V_{cb}|$.

3.2.2 Decay into vector final state

Let us now consider the decay $B_s \to D_s^* l\nu_l$, where D_s^* is a vector particle $J^P = 1^-$. Vector mesons such as the D_s^* are unstable hadrons in QCD and they are observed indirectly as resonances. In order to describe them here, we assume that they can be treated as asymptotic final states with fixed masses, as supported by the experimentally determined mass of the D_s^* meson $M_{D_s^*} = 2112.2 \pm 0.4\,\mathrm{MeV}$ and its narrow width given by $\Gamma < 1.9\,\mathrm{MeV}$ [63].

Spin-1 particles are characterised by momentum and polarisation. Assuming the D_s^* three-momentum to be in the z-direction, $\boldsymbol{p}_{D_s^*} = (0,0,|\boldsymbol{p}_{D_s^*}|)$, the polarisation four-vectors are given by

$$\varepsilon_\pm^\mu = \frac{1}{\sqrt{2}}(0,\mp 1,-i,0)\,, \quad \varepsilon_0^\mu = \frac{1}{M_{D_s^*}}(|\boldsymbol{p}_{D_s^*}|,0,0,E_{D_s^*})\,, \tag{3.25}$$

where $\varepsilon_\pm^\mu$ are the transverse vectors with positive and negative helicity, and ε_0^μ is the longitudinal one. They all fulfil $\varepsilon\cdot\varepsilon^* = 1$ and are orthogonal to the D_s^* four-momentum, i.e. $p_{D_s^*}\cdot\varepsilon = 0$, where we suppressed the polarisation index for simplicity.

Both vector and axial currents contribute to the decay into a vector final state. In particular, following the notation in [138] and defining

$$\mathcal{M}_{V_\mu}^{D_s^* B_s} \equiv \left\langle D_s^*(p_{D_s^*},\varepsilon)\right| V_\mu \left|B_s(p_{B_s})\right\rangle\,, \quad \mathcal{M}_{A_\mu}^{D_s^* B_s} \equiv \left\langle D_s^*(p_{D_s^*},\varepsilon)\right| A_\mu \left|B_s(p_{B_s})\right\rangle\,, \tag{3.26}$$

we have

$$\mathcal{M}_{V_\mu}^{D_s^* B_s} = \epsilon_{\mu\nu\rho\sigma}\varepsilon^{*\nu}q^\rho p_{D_s^*}^\sigma \frac{2f_V(q^2)}{M_{B_s}+M_{D_s^*}}\,, \tag{3.27}$$

where $\epsilon_{\mu\nu\rho\sigma}$ is the Levi-Civita tensor and $f_V(q^2)$ is the vector form factor, and

$$\begin{aligned}\mathcal{M}_{A_\mu}^{D_s^* B_s} =& i\varepsilon_\mu^*(M_{B_s} + M_{D_s^*}) f_{A_1}(q^2) \\ &- i(2p_{D_s^*} + q)_\mu (\varepsilon^* \cdot q) \frac{f_{A_2}(q^2)}{M_{B_s} + M_{D_s^*}} \\ &- iq_\mu (\varepsilon^* \cdot q) \frac{2M_{D_s^*}}{q^2} \left(f_{A_3}(q^2) - f_{A_0}(q^2) \right) ,\end{aligned} \tag{3.28}$$

where $f_{A_0}(q^2)$, $f_{A_1}(q^2)$, $f_{A_2}(q^2)$ and $f_{A_3}(q^2)$ are the axial form factors. Note that there are only three independent form factors as

$$2M_{D_s^*} f_{A_3}(q^2) = (M_{B_s} + M_{D_s^*}) f_{A_1}(q^2) - (M_{B_s} - M_{D_s^*}) f_{A_2}(q^2) , \tag{3.29}$$

with $f_{A_0}(0) = f_{A_3}(0)$. The form factor $f_{A_0}(q^2)$ is the analogous of the scalar form factor $f_{B_s D_s}^0(q^2)$, as it is related to the pseudoscalar current $\bar{b}\gamma_5 c$ as

$$2M_{D_s^*} (\varepsilon^* \cdot q) f_{A_0}(q)^2 = \left\langle D_s^*(p_{D_s^*}, \varepsilon) \right| i(m_b + m_c) \bar{b}\gamma_5 c \left| B_s(p_{B_s}) \right\rangle . \tag{3.30}$$

3.3 Inclusive decays

Inclusive decays $B_s \to X_c\, l\nu_l$ are characterised by a sum over all the possible final states allowed by the kinematics of the given $\bar{b} \to \bar{c}$ weak transition. The state X_c can therefore include single-particle states, e.g. the D_s meson, but also multiparticle ones. Inclusive decays can be analytically studied in the framework of HQET [139–144]: this introduction closely follows [142, 143]. The matrix element (averaged over the spin) for the interaction is given by

$$|\mathcal{M}(B_s \to X_c\, l\nu_l)|^2 \propto \sum_{X_c} \sum_{l \text{ spin}} \frac{|\left\langle X_c\, l\nu_l \right| \mathcal{H}_W \left| B_s \right\rangle|^2}{2M_{B_s}} (2\pi)^3 \delta^{(4)}(p_{B_s} - q - p_{X_c}) , \tag{3.31}$$

where $q = p_l + p_{\nu_l} = p_{B_s} - p_{X_c}$ is the transferred momentum between the initial and final hadronic states. We consider the decay in the rest frame of the B_s meson, i.e. $p_{B_s} = (M_{B_s}, 0, 0, 0)$. The leptonic and hadronic contributions to the matrix element can be decomposed as

$$|\mathcal{M}(B_s \to X_c\, l\nu_l)|^2 = G_F^2 |V_{cb}|^2 M_{B_s} L_{\mu\nu} W^{\mu\nu} , \tag{3.32}$$

where $W^{\mu\nu} \equiv W^{\mu\nu}(p_{B_s}, q)$ is the hadronic tensor defined as

$$\begin{aligned} W^{\mu\nu}(p_{B_s}, q) =& \frac{1}{(2\pi)2M_{B_s}} \int \mathrm{d}^4x\, e^{-iq\cdot x} \langle B_s(\boldsymbol{p}_{B_s})| J^{\mu\dagger}(x) J^{\nu}(0) |B_s(\boldsymbol{p}_{B_s})\rangle \\ =& \frac{1}{2M_{B_s}} \sum_{X_c} (2\pi)^3 \delta^{(4)}(p_{B_s} - q - p_{X_c}) \\ & \times \langle B_s(\boldsymbol{p}_{B_s})| J^{\mu\dagger}(0) |X_c(\boldsymbol{p}_{X_c})\rangle \langle X_c(\boldsymbol{p}_{X_c})| J^{\nu}(0) |B_s(\boldsymbol{p}_{B_s})\rangle \ , \end{aligned} \tag{3.33}$$

where in the last line we inserted a sum over a complete set of charmed states X_c, with $\sum_{X_c} |X_c(\boldsymbol{p}_{X_c})\rangle \langle X_c(\boldsymbol{p}_{X_c})| \equiv \sum_{X_c} \int \frac{\mathrm{d}\boldsymbol{p}_{X_c}}{(2\pi)^3} \frac{1}{2E_{X_c}} |X_c(\boldsymbol{p}_{X_c})\rangle \langle X_c(\boldsymbol{p}_{X_c})|$, and $L^{\mu\nu}$ is the leptonic tensor defined as

$$L^{\mu\nu} = p_l^{\mu} p_{\nu_l}^{\nu} + p_l^{\nu} p_{\nu_l}^{\mu} - g^{\mu\nu} p_l \cdot p_{\nu_l} - i\varepsilon^{\mu\alpha\nu\beta} p_{l,\alpha} p_{\nu_l,\beta} \, . \tag{3.34}$$

The hadronic tensor can be further decomposed in terms of five real scalar structure functions $W_i \equiv W_i(q^2, p_{B_s} \cdot q/M_{B_s})$ as

$$W^{\mu\nu} = -g^{\mu\nu} W_1 + v^{\mu} v^{\nu} W_2 - i\varepsilon^{\mu\nu\alpha\beta} v_{\alpha} q_{\beta} W_3 + q^{\mu} q^{\nu} W_4 + (v^{\mu} q^{\nu} + v^{\nu} q^{\mu}) W_5 \, , \tag{3.35}$$

where v is the velocity of the B_s meson, $v = p_{B_s}/M_{B_s} = (1, 0, 0, 0)$ in its rest frame, and $q = (q_0, \boldsymbol{q}) = (M_{B_s} - \omega, -\boldsymbol{p}_{X_c})$. From now on, we will indicate with $\omega = E_{X_c}$ the energy of the final state hadron. The hadronic tensor contains all the information about the nonperturbative QCD effects. It can be directly related to the discontinuity of the forward-scattering matrix element

$$T_{\mu\nu} = -\frac{i}{2M_{B_s}} \int \mathrm{d}^4x e^{-iq\cdot x} \langle B_s| T\{J_{\mu}^{\dagger}(x) J_{\nu}(0)\} |B_s\rangle \ , \tag{3.36}$$

which can be decomposed into structure functions T_i in a similar way,

$$T_{\mu\nu} = -g^{\mu\nu} T_1 + v^{\mu} v^{\nu} T_2 - i\varepsilon^{\mu\nu\alpha\beta} v_{\alpha} q_{\beta} T_3 + q^{\mu} q^{\nu} T_4 + (v^{\mu} q^{\nu} + v^{\nu} q^{\mu}) T_5 \, . \tag{3.37}$$

Using the integral representation of the Heaviside step function

$$\theta(x) = \frac{1}{2\pi i} \int_{-\infty}^{\infty} \mathrm{d}z \, \frac{e^{ixz}}{z - i\epsilon} = -\frac{1}{2\pi i} \int_{-\infty}^{\infty} \mathrm{d}z \, \frac{e^{-ixz}}{z + i\epsilon} \, , \tag{3.38}$$

we can evaluate Eq. (3.36) and find

$$\begin{aligned} T_{\mu\nu} =& \frac{(2\pi)^3}{2M_{B_s}} \sum_{X_c} \frac{\langle B_s| J^{\mu\dagger} |X_c\rangle \langle X_c| J^{\nu} |B_s\rangle}{M_{B_s} - E_{X_c} - q_0 + i\epsilon} \delta^{(3)}(\boldsymbol{q} + \boldsymbol{p}_{X_c}) \\ & - \frac{(2\pi)^3}{2M_{B_s}} \sum_{X_{cbb}} \frac{\langle B_s| J^{\nu} |X_{cbb}\rangle \langle X_{cbb}| J^{\mu\dagger} |B_s\rangle}{E_{X_{cbb}} - M_{B_s} - q_0 - i\epsilon} \delta^{(3)}(\boldsymbol{q} - \boldsymbol{p}_{X_{cbb}}) \, , \end{aligned} \tag{3.39}$$

where we omitted the momentum dependence of the states for simplicity. X_{cbb} indicates a complete set of states containing two $\bar{b}$ quarks and a c quark. From this expression, it

can be seen that at a fixed value of the three-momentum $\boldsymbol{q}$ the tensor $T_{\mu\nu}$ presents two cuts in the complex plane of $q_0 = q \cdot v$ along the real axis in the regions

$$-\infty < q_0 < M_{B_s} - \sqrt{M^2_{X_c^{\min}} + \boldsymbol{q}^2} \quad \text{and} \quad -M_{B_s} + \sqrt{M^2_{X_{cbb}^{\min}} + \boldsymbol{q}^2} < q_0 < \infty\,, \tag{3.40}$$

where $M^2_{X^{\min}}$ correspond to the lowest possible value for the states X_c and X_{cbb}, respectively. Approximating the meson masses with that of the their heavy quarks, the minimum separation between the cuts (occurring at $\boldsymbol{q}^2 = 0$) is given by $2m_c$. The decay $B_s \to X_c\, l\nu_l$ occurs only in the lower cut, since the upper cut corresponds to the process $\bar{b} \to c\bar{b}\bar{b}$. To finally relate $T_{\mu\nu}$ to $W_{\mu\nu}$, we use the relation

$$\frac{1}{x \pm i\epsilon} = P\frac{1}{x} \mp i\pi\delta(x)\,, \tag{3.41}$$

with P being the principal value, and evaluate the imaginary part of $T_{\mu\nu}$ (the discontinuity across the cut) as

$$\begin{aligned}\frac{1}{\pi}\operatorname{Im} T_{\mu\nu} = &-\frac{(2\pi)^3}{2M_{B_s}} \sum_{X_c} \langle B_s|\, J^{\mu\dagger}\, |X_c\rangle \langle X_c|\, J^{\nu}\, |B_s\rangle\, \delta^{(4)}(p_{B_s} - q - p_{X_c}) \\ &-\frac{(2\pi)^3}{2M_{B_s}} \sum_{X_{cbb}} \langle B_s|\, J^{\nu}\, |X_{cbb}\rangle \langle X_{cbb}|\, J^{\mu\dagger}\, |B_s\rangle\, \delta^{(4)}(p_{B_s} + q - p_{X_{cbb}})\,.\end{aligned} \tag{3.42}$$

The first term of this equation corresponds to the hadronic tensor in Eq. (3.33), which then corresponds to the discontinuity across the cut. For the left-hand cut we have

$$-\frac{1}{\pi}\operatorname{Im} T_{\mu\nu} = W_{\mu\nu}\,, \quad -\frac{1}{\pi}\operatorname{Im} T_i = W_i\,, \tag{3.43}$$

which shows that the T_i are analytically continued from the structure functions W_i. Therefore, the integrals of W_i over q_0, necessary to obtain the total decay rate, are related to the integrals of T_i over a contour $\mathcal{C}$ in the complex plane of q_0 that encloses the physical (left-hand) cut such that the discontinuity of $T_{\mu\nu}$ is included. While in Lattice QCD it is possible to address the calculation of $W_{\mu\nu}$ directly, as we will see in Chap. 4, this last relation is central to apply QCD perturbation theory to inclusive decays (in the regime where the separation between the cuts is larger than Λ_{QCD} [139], as for $\bar{b} \to \bar{c}$ transitions). Indeed, inclusive observables admit a double expansion in α_s and $1/m_b$ [139–142], and techniques such as Operator Product Expansion (OPE) [145–147] can be applied to the time-ordered product of the form

$$t_{\mu\nu} = \frac{i}{2M_{B_s}} \int \mathrm{d}^4x e^{-iq\cdot x} T\{J^\dagger_\mu(x) J_\nu(0)\}\,, \tag{3.44}$$

which is directly related to $T_{\mu\nu}$, and can be expanded in a sum of local operators by performing a short distance expansion.

3.3.1 Decay rate

In this section, we work out explicitly the key quantities necessary to calculate the total decay rate. Since this is a central observable in this work, we report the full details of the calculations. The starting point is the differential decay rate, given by

$$\frac{\mathrm{d}\Gamma}{\mathrm{d}q^2\mathrm{d}q_0\mathrm{d}E_l} = \frac{G_F^2|V_{cb}|^2}{8\pi^3} L_{\mu\nu}W^{\mu\nu}\,. \tag{3.45}$$

We can calculate the expression for the total decay rate contracting the leptonic and hadronic tensors explicitly and integrating. Note that for the leptonic tensor $p_{\nu_l,\mu}L^{\mu\nu} = 0$ and $p_{l,\mu}L^{\mu\nu} = m_l^2 p^\nu_{\nu_l}$; it follows that $q_\mu L^{\mu\nu} = m_l^2 p^\nu_{\nu_l}$. We get

$$\begin{aligned} L_{\mu\nu}W^{\mu\nu} =& W_1\left[q^2 - m_l^2\right] + W_2\left[2E_lE_{\nu_l} - \frac{1}{2}(q^2 - m_l^2)\right] \\ &+ W_3\left[q^2(E_l - E_{\nu_l}) - m_l^2(E_l + E_{\nu_l})\right] + W_4\left[\frac{1}{2}m_l^2(q^2 - m_l^2)\right] \\ &+ W_5\left[2m_l^2E_{\nu_l}\right]\,. \end{aligned} \tag{3.46}$$

This expression can be split into a massless contribution

$$\begin{aligned} L_{\mu\nu}W^{\mu\nu}\Big|_{m_l=0} &= W_1q^2 + W_2\left(2E_l(q_0 - E_l) - \frac{q^2}{2}\right) + W_3q^2(2E_l - q_0) \\ &= q^2\left(W_1 - \frac{1}{2}W_2 - q_0W_3\right) + 2E_l(q_0W_2 + q^2W_3) - 2E_l^2W_2\,. \end{aligned} \tag{3.47}$$

and a massive one $\delta L_{\mu\nu}W^{\mu\nu}\Big|_{m_l\neq 0} = L_{\mu\nu}W^{\mu\nu} - L_{\mu\nu}W^{\mu\nu}\Big|_{m_l=0}$ as

$$\delta L_{\mu\nu}W^{\mu\nu}\Big|_{m_l\neq 0} = m_l^2\left[-W_1 + \frac{1}{2}W_2 - q_0W_3 + \frac{1}{2}(q^2 - m_l^2)W_4 + 2(q_0 - E_l)W_5\right]\,, \tag{3.48}$$

where we used $E_{\nu_l} = q_0 - E_l$. The next step is then to integrate Eq. (3.45) over the lepton energy E_l substituting Eq. (3.46). It is convenient to calculate beforehand the integral over E_l^n as

$$\Delta E_l^n = n\int_{E_l^{\min}}^{E_l^{\max}} \mathrm{d}E_l\, E_l^{n-1} = (E_l^{\max})^n - (E_l^{\min})^n\,. \tag{3.49}$$

where the maximum and minimum values for the electron energy can be obtained by squaring $p_{\nu_l} = q - p_l$, and solving for E_l considering the limit cases $\boldsymbol{q}\cdot\boldsymbol{p}_l = \pm|\boldsymbol{q}||\boldsymbol{p}_l|$. Assuming either electrons or muons in the final state, i.e. considering the massless case limit $m_l = 0$, we find

$$E_l^{\min} = \frac{q^2}{2(q_0 + |\boldsymbol{q}|)} = \frac{1}{2}(q_0 - |\boldsymbol{q}|)\,, \qquad E_l^{\max} = \frac{q^2}{2(q_0 - |\boldsymbol{q}|)} = \frac{1}{2}(q_0 + |\boldsymbol{q}|)\,. \tag{3.50}$$

The final expression for ΔE_l^n then becomes

$$\begin{aligned}\Delta E_l^n &= \frac{1}{2^n}\left[(q_0+|\boldsymbol{q}|)^n-(q_0-|\boldsymbol{q}|)^n\right] \\ &= \frac{1}{2^n}\sum_{k=0}^{n}\binom{n}{k}q_0^{n-k}\left[|\boldsymbol{q}|^k-(-|\boldsymbol{q}|)^k\right] \\ &= \frac{1}{2^{n-1}}\sum_{\substack{k=0\\ k\text{ odd}}}^{n}\binom{n}{k}q_0^{n-k}|\boldsymbol{q}|^k\,,\end{aligned} \tag{3.51}$$

with $|\boldsymbol{q}|=\sqrt{\boldsymbol{q}^2}=\sqrt{q_0^2-q^2}$, which leads us to the general expression

$$\int_{E_l^{\min}}^{E_l^{\max}}\mathrm{d}E_l\,E_l^{n-1}=\frac{1}{n}\Delta E_l^n=\frac{1}{2^{n-1}\,n}\sum_{\substack{k=0\\ k\text{ odd}}}^{n}\binom{n}{k}q_0^{n-k}|\boldsymbol{q}|^k\,. \tag{3.52}$$

In particular, we have explicitly

$$\begin{aligned}\Delta E_l &= |\boldsymbol{q}|\,,\\ \Delta E_l^2 &= q_0|\boldsymbol{q}|\,,\\ \Delta E_l^3 &= \frac{|\boldsymbol{q}|}{4}\left(3q_0^2+|\boldsymbol{q}|^2\right)\,,\\ \Delta E_l^4 &= \frac{q_0|\boldsymbol{q}|}{2}\left(q_0^2+|\boldsymbol{q}|^2\right)\,,\\ \Delta E_l^5 &= \frac{|\boldsymbol{q}|}{16}\left(5q_0^4+10q_0^2|\boldsymbol{q}|^2+|\boldsymbol{q}|^4\right)\,,\\ \Delta E_l^6 &= \frac{q_0|\boldsymbol{q}|}{16}\left(3q_0^4+10q_0^2|\boldsymbol{q}|^2+3|\boldsymbol{q}|^4\right)\,,\end{aligned} \tag{3.53}$$

which we will make use of in Sec. 3.3.4. In the remaining of this chapter we always consider only the case $m_l=0$. Proceeding with the calculations, the integration over the lepton energy E_l in the massless limit gives the double differential decay rate

$$\frac{\mathrm{d}\Gamma}{\mathrm{d}q^2\mathrm{d}q_0}=\frac{G_F^2|V_{cb}|^2}{8\pi^3}\sqrt{\boldsymbol{q}^2}\left[W_1q^2+\frac{1}{3}(q_0^2-q^2)W_2\right]\,. \tag{3.54}$$

Since on the lattice we can address the calculation of $W^{\mu\nu}$, as we will show in Chap. 4, we now need to rewrite the structure functions W_i in terms of the hadronic tensor $W_{\mu\nu}$. We then consider explicitly

$$W_{00}=-W_1+W_2+q_0^2W_4+2q_0W_5\,, \tag{3.55}$$

$$W_{ij}=\delta_{ij}W_1+q_iq_jW_4-i\varepsilon_{ij0k}q^kW_3\,, \tag{3.56}$$

$$W_{0i}=W_{i0}=q_i(q_0W_4+W_5)\,, \tag{3.57}$$

which we will have to invert and subsequently substitute in Eq. (3.54). Before proceeding, we recall that the structure functions are real and that $W_{\mu\nu}^\dagger=W_{\nu\mu}$, which implies

$\frac{1}{2}(W_{ij}+W_{ji}) = \mathrm{Re}(W_{ij})$ and $\frac{1}{2}(W_{ij}-W_{ji}) = \mathrm{Im}(W_{ij})$. Multiplying the spatial indices of the hadronic tensor by q_i and q_j and summing over the indices we get more general relations

$$\sum_i W_{ii} = 3W_1 + \boldsymbol{q}^2 W_4\,, \tag{3.58}$$

$$\sum_{i,j} q^i W_{ij} q^j = \boldsymbol{q}^2 W_1 + (\boldsymbol{q}^2)^2 W_4\,, \tag{3.59}$$

$$\sum_i q^i (W_{0i} + W_{i0}) = 2(q_0 W_4 + W_5)\boldsymbol{q}^2\,, \tag{3.60}$$

$$\sum_{i,j,k} W_{ij}\varepsilon^{ijk} q_k = -i\boldsymbol{q}^2 W_3\,, \tag{3.61}$$

where in the last line we used $\varepsilon^{ij0k} = \varepsilon^{0ijk} = \varepsilon^{ijk}$ and $\sum_{i,j}\varepsilon_{ijl}\varepsilon^{ijk} = 2\delta^k_l$, and the indices run over the spatial components $1,2,3$. We stress that these equations are general and hold for every $\boldsymbol{q}$. We can now invert these relations to express the structure functions in terms of the hadronic tensor. In the case $\boldsymbol{q} = \boldsymbol{0}$ we can only derive

$$W_1 = \frac{1}{3}\sum_i W_{ii}\,. \tag{3.62}$$

For all the other cases $\boldsymbol{q} \neq \boldsymbol{0}$ we can solve the system given by Eq. (3.58) and (3.59) and obtain

$$\begin{cases} \boldsymbol{q}^2 W_4 &= \dfrac{1}{\boldsymbol{q}^2}\displaystyle\sum_{i,j} q^i W_{ij} q^j - W_1 \\ W_1 &= \dfrac{1}{3}\left(\displaystyle\sum_i W_{ii} - \boldsymbol{q}^2 W_4\right) \end{cases}, \quad \rightarrow \quad \begin{cases} \boldsymbol{q}^2 W_4 &= \dfrac{3}{2}\dfrac{1}{\boldsymbol{q}^2}\displaystyle\sum_{i,j} q^i W_{ij} q^j - \dfrac{1}{2}\sum_i W_{ii} \\ W_1 &= \dfrac{1}{2}\displaystyle\sum_i W_{ii} - \dfrac{1}{2}\dfrac{1}{\boldsymbol{q}^2}\sum_{i,j} q^i W_{ij} q^j \end{cases}. \tag{3.63}$$

We can now determine W_5 from Eq. (3.60) as

$$\begin{aligned} W_5 &= \frac{1}{\boldsymbol{q}^2}\sum_i q^i \frac{1}{2}(W_{0i}+W_{i0}) - q_0 W_4 \\ &= \frac{1}{\boldsymbol{q}^2}\sum_i q^i \frac{1}{2}(W_{0i}+W_{i0}) - \frac{q_0}{\boldsymbol{q}^2}\left[\frac{3}{2}\frac{1}{\boldsymbol{q}^2}\sum_{i,j} q^i W_{ij} q^j - \frac{1}{2}\sum_i W_{ii}\right], \end{aligned} \tag{3.64}$$

as well as W_2 from Eq. (3.55)

$$W_2 = W_{00} - \frac{q_0}{\boldsymbol{q}^2}\sum_i q^i (W_{0i}+W_{i0}) + W_1 + q_0^2 W_4\,, \tag{3.65}$$

where we can further substitute W_1 and W_4 from the system (3.63) to get a full expression in terms of $W_{\mu\nu}$.

We summarise all the relations between the relevant structure functions and the hadronic tensor as

$$W_1 = \frac{1}{2}\sum_{i,j}\left[\delta_{ij} - \frac{q^i q^j}{\boldsymbol{q}^2}\right] W_{ij}\,, \tag{3.66}$$

$$\begin{aligned} W_2 = W_{00} - \frac{q_0}{\boldsymbol{q}^2}\sum_i q^i (W_{0i} + W_{i0}) + \frac{q_0^2}{(\boldsymbol{q}^2)^2}\sum_{i,j} q^i W_{ij} q^j \\ + \frac{1}{2}\left(1 - \frac{q_0^2}{\boldsymbol{q}^2}\right)\sum_{i,j}\left[\delta_{ij} - \frac{q^i q^j}{\boldsymbol{q}^2}\right] W_{ij}\,, \end{aligned} \tag{3.67}$$

$$W_3 = \frac{i}{\boldsymbol{q}^2}\sum_{i,j,k} W_{ij}\varepsilon^{ijk} q_k\,, \tag{3.68}$$

$$W_4 = \frac{1}{(\boldsymbol{q}^2)^2}\sum_{i,j} q^i W_{ij} q^j - \frac{1}{2}\frac{1}{\boldsymbol{q}^2}\sum_{i,j}\left[\delta_{ij} - \frac{q^i q^j}{\boldsymbol{q}^2}\right] W_{ij}\,, \tag{3.69}$$

$$\begin{aligned} W_5 = \frac{1}{\boldsymbol{q}^2}\sum_i q^i \frac{1}{2}(W_{0i} + W_{i0}) - \frac{q_0}{(\boldsymbol{q})^2}\sum_{i,j} q^i W_{ij} q^j \\ + \frac{q_0}{\boldsymbol{q}^2}\sum_{i,j}\left[\delta_{ij} - \frac{q^i q^j}{\boldsymbol{q}^2}\right] W_{ij}\,. \end{aligned} \tag{3.70}$$

We can now rewrite the differential decay rate with the change of variables $\omega = M_{B_s} - q_0$ and $\boldsymbol{q}^2 = q_0^2 - q^2$ (note that the Jacobian of the transformation is 1) as

$$\frac{\mathrm{d}\Gamma}{\mathrm{d}\boldsymbol{q}^2\mathrm{d}\omega} = \frac{G_F^2|V_{cb}|^2}{8\pi^3}\sqrt{\boldsymbol{q}^2}\left[W_1(q_0^2 - \boldsymbol{q}^2) + \frac{1}{3}\boldsymbol{q}^2 W_2\right]. \tag{3.71}$$

Substituting Eq. (3.66) and (3.67) we finally obtain the massless differential decay rate

$$\begin{aligned} \frac{\mathrm{d}\Gamma}{\mathrm{d}\boldsymbol{q}^2\mathrm{d}\omega} = \frac{G_F^2|V_{cb}|^2}{24\pi^3}\sqrt{\boldsymbol{q}^2}\Bigg\{\boldsymbol{q}^2\left[W_{00} - \sum_i W_{ii}\right] + \sum_{i,j} q^i W_{ij} q^j \\ - q_0\left[\sum_i q^i (W_{0i} + W_{i0})\right] \\ + q_0^2\left[\sum_i W_{ii}\right]\Bigg\}. \end{aligned} \tag{3.72}$$

From this expression we can now define the key quantities we use in this work. We can conveniently rewrite the differential decay rate in a compact form as

$$\frac{\mathrm{d}\Gamma}{\mathrm{d}\boldsymbol{q}^2\mathrm{d}\omega} = \frac{G_F^2|V_{cb}|^2}{24\pi^3}\sqrt{\boldsymbol{q}^2}X(\boldsymbol{q}^2,\omega)\,, \tag{3.73}$$

where we defined

$$X(\boldsymbol{q}^2,\omega) \equiv \frac{3}{\sqrt{\boldsymbol{q}^2}}\int_{E_l^{\min}}^{E_l^{\max}} \mathrm{d}E_l\, L_{\mu\nu} W^{\mu\nu}\,. \tag{3.74}$$

The function $X(\boldsymbol{q}^2, \omega)$ can be decomposed as

$$X(\boldsymbol{q}^2, \omega) = X^{(0)}(\boldsymbol{q}^2, \omega) + X^{(1)}(\boldsymbol{q}^2, \omega) + X^{(2)}(\boldsymbol{q}^2, \omega)\,, \tag{3.75}$$

where the superscripts distinguish the components in powers of $q_0 = M_{B_s} - \omega$, i.e.

$$X^{(0)}(\boldsymbol{q}^2, \omega) = \boldsymbol{q}^2 \left(W_{00} - \sum_i W_{ii} \right) + \sum_{i,j} q^i W_{ij} q^j\,, \tag{3.76}$$

$$X^{(1)}(\boldsymbol{q}^2, \omega) = -q_0 \sum_i q^i (W_{0i} + W_{i0})\,, \tag{3.77}$$

$$X^{(2)}(\boldsymbol{q}^2, \omega) = q_0^2 \sum_i W_{ii}\,. \tag{3.78}$$

Eventually, the total decay rate can be obtained integrating over ω and $\boldsymbol{q}^2$

$$\Gamma = \frac{G_F^2 |V_{cb}|^2}{24\pi^3} \int_0^{\boldsymbol{q}^2_{\max}} \mathrm{d}\boldsymbol{q}^2 \sqrt{\boldsymbol{q}^2} \sum_{l=0}^{2} \bar{X}^{(l)}(\boldsymbol{q}^2)\,, \quad \bar{X}^{(l)}(\boldsymbol{q}^2) \equiv \int_{\omega_{\min}}^{\omega_{\max}} \mathrm{d}\omega X^{(l)}(\boldsymbol{q}^2, \omega)\,, \tag{3.79}$$

with $\omega_{\min} = \sqrt{M_{D_s}^2 + \boldsymbol{q}^2}$, $\omega_{\max} = M_{B_s} - \sqrt{\boldsymbol{q}^2}$ and $\boldsymbol{q}^2_{\max} = (M_{B_s}^2 - M_{D_s}^2)^2/(4M_{B_s}^2)$, where the latter can be obtained solving $\boldsymbol{q}^2_{\max} = q_0^2 - q^2_{\min}$ with $q^2_{\min} = 0$. To summarise

$$\begin{aligned}
\Gamma &= \frac{G_F^2 |V_{cb}|^2}{24\pi^3} \int_0^{\boldsymbol{q}^2_{\max}} \mathrm{d}\boldsymbol{q}^2 \sqrt{\boldsymbol{q}^2} \sum_{l=0}^{2} \bar{X}^{(l)}(\boldsymbol{q}^2)\,, \qquad \bar{X}^{(l)}(\boldsymbol{q}^2) \equiv \int_{\omega_{\min}}^{\omega_{\max}} \mathrm{d}\omega X^{(l)}(\boldsymbol{q}^2, \omega)\,, \\
X^{(0)}(\boldsymbol{q}^2, \omega) &= \boldsymbol{q}^2 W_{00} + \sum_i (q_i^2 - \boldsymbol{q}^2) W_{ii} + \sum_{i \neq j} q^i W_{ij} q^j\,, \\
X^{(1)}(\boldsymbol{q}^2, \omega) &= -q_0 \sum_i q^i (W_{0i} + W_{i0})\,, \\
X^{(2)}(\boldsymbol{q}^2, \omega) &= q_0^2 \sum_i W_{ii}\,.
\end{aligned} \tag{3.80}$$

The above expressions constitute the central formulas used in this work. In particular, they allow to rewrite the total decay rate as an integral over the energy ω of the final-state hadron and its three-momentum $\boldsymbol{q}^2$ through the help of the functions $X^{(l)}(\boldsymbol{q}^2, \omega)$, which contains linear combinations of components of the hadronic tensor and kinematics factors. These expressions are particularly convenient to address the calculation on the lattice, as we will show in Chap. 4.

3.3.2 Longitudinal and transverse components

To further study the inclusive decay process, it is advantageous to decompose $X(\boldsymbol{q}^2, \omega)$ in its longitudinal and transverse components. Indeed, these components are useful to

isolate different physical channels, as e.g. in the case of the ground-state limit addressed in Sec. 3.3.3, but also for comparison with other approaches such as the OPE [29]. To this end, we define a basis $\boldsymbol{e}_\parallel$, $\boldsymbol{e}_1$ and $\boldsymbol{e}_2$ for the three-dimensional space such that

$$\boldsymbol{e}_\parallel = \frac{\boldsymbol{q}}{\sqrt{\boldsymbol{q}^2}}\,, \quad \boldsymbol{e}_a \cdot \boldsymbol{e}_\parallel = 0\,, \quad \boldsymbol{e}_a \cdot \boldsymbol{e}_b = \delta_{ab}\,, \quad a = \{1,2\}\,. \tag{3.81}$$

From the basis vectors we can build the longitudinal ($\parallel$) and transverse ($\perp$) projectors

$$\Pi_\parallel^{ij} = e_\parallel^i e_\parallel^j = \frac{q^i q^j}{\boldsymbol{q}^2}\,, \qquad \Pi_\perp^{ij} = \sum_{a=1}^{2} e_a^i e_a^j = \delta^{ij} - \frac{q^i q^j}{\boldsymbol{q}^2}\,, \qquad \delta^{ij} = \Pi_\parallel^{ij} + \Pi_\perp^{ij}\,. \tag{3.82}$$

Note that the restriction to the three-dimensional space is due to the fact that we are implicitly assuming to be in the rest frame of the B_s meson, and all the equations are then referring to that specific frame. While Lorentz-invariance is then non-explicit, it is clear that we are left with $SO(3)$ symmetry and we are free to rotate the frame with respect to the direction of the $\boldsymbol{q}$ momentum. We obtain for $X(\boldsymbol{q}^2,\omega)$ in Eq. (3.75)

$$\begin{aligned} X(\boldsymbol{q}^2,\omega) &= \boldsymbol{q}^2 W_{00} - q_0 \sum_i q^i (W_{0i} + W_{i0}) + (q_0^2 - \boldsymbol{q}^2) \sum_{i,j} \delta^{ij} W_{ij} + \boldsymbol{q}^2 \sum_{i,j} \frac{q^i q^j}{\boldsymbol{q}^2} W_{ij} \\ &= \boldsymbol{q}^2 W_{00} - q_0 \sum_i q^i (W_{0i} + W_{i0}) + (q_0^2 - \boldsymbol{q}^2) \sum_{i,j} \Pi_\parallel^{ij} W_{ij} + \boldsymbol{q}^2 \sum_{i,j} \Pi_\parallel^{ij} W_{ij} \\ &\quad + (q_0^2 - \boldsymbol{q}^2) \sum_{i,j} \Pi_\perp^{ij} W_{ij}\,, \end{aligned} \tag{3.83}$$

where we used $\delta^{ij} = \Pi_\parallel^{ij} + \Pi_\perp^{ij}$. Splitting the components with different projectors in the above equation as $X(\boldsymbol{q}^2,\omega) = X^\parallel(\boldsymbol{q}^2,\omega) + X^\perp(\boldsymbol{q}^2,\omega)$, the longitudinal and transverse contributions read

$$X^\parallel(\boldsymbol{q}^2,\omega) = \boldsymbol{q}^2 W_{00} - q_0 \sum_i q^i (W_{0i} + W_{i0}) + \frac{q_0^2}{\boldsymbol{q}^2} \sum_{i,j} q^i W_{ij} q^j\,, \tag{3.84}$$

$$\begin{aligned} X^\perp(\boldsymbol{q}^2,\omega) &= (q_0^2 - \boldsymbol{q}^2) \sum_{i,j} \left[\delta^{ij} - \frac{q^i q^j}{\boldsymbol{q}^2}\right] W_{ij} \\ &= \left(1 - \frac{q_0^2}{\boldsymbol{q}^2}\right) \left[\sum_i \left((q^i)^2 - \boldsymbol{q^2}\right) W_{ii} + \sum_{i \neq j} q^i W_{ij} q^j\right]\,. \end{aligned} \tag{3.85}$$

In term of the structure functions these corresponds to

$$X^\parallel(\boldsymbol{q}^2,\omega) = q^2 W_1 + \boldsymbol{q}^2 W_2\,, \tag{3.86}$$

$$X^\perp(\boldsymbol{q}^2,\omega) = 2 q^2 W_1\,. \tag{3.87}$$

We have then further decomposed $X(\boldsymbol{q}^2,\omega)$ into longitudinal and transverse components with respect to the three-momentum $\boldsymbol{q}^2$, as defined through the projectors in Eq. (3.82). We will show how to make practical use of these expressions in the next section.

3.3.3 Ground-state limit

In this section we consider the limit case where only the lowest-mass final state $D_s^{(*)}$ contributes to the inclusive decay, i.e.

$$W^{\mu\nu} \to \frac{1}{2M_{B_s}}\Bigg[\delta(\omega - E_{D_s})\frac{1}{2E_{D_s}}\langle B_s(\boldsymbol{p}_{B_s})|J^{\mu\dagger}|D_s(\boldsymbol{p}_{D_s})\rangle\langle D_s(\boldsymbol{p}_{D_s})|J^{\nu}|B_s(\boldsymbol{p}_{B_s})\rangle \\ +\delta(\omega - E_{D_s^*})\frac{1}{2E_{D_s^*}}\langle B_s(\boldsymbol{p}_{B_s})|J^{\mu\dagger}|D_s^*(\boldsymbol{p}_{D_s^*},\varepsilon)\rangle\langle D_s^*(\boldsymbol{p}_{D_s^*},\varepsilon)|J^{\nu}|B_s(\boldsymbol{p}_{B_s})\rangle\Bigg]\,. \tag{3.88}$$

In this limit we can reconstruct the inclusive process starting from simulations of the corresponding exclusive decays. This provides an ideal environment to further test the inclusive setup and analysis strategy, as well as to assess the contribution of the excited states contained in the inclusive decays.

For the following discussion it is convenient to assume the momentum to be in the z-direction, $\boldsymbol{q} = (0, 0, q^3)$ and label the parallel and perpendicular components explicitly as $q^1 = q^2 = q^\perp = 0$ and $q^3 = q^\parallel$. In a similar way, we also label the hadronic tensor as $W_{\perp\perp} = (W_{11} + W_{22})/2$, $W_{33} = W_{\parallel\parallel}$, $W_{03} = W_{0\parallel}$, $W_{30} = W_{\parallel 0}$; all the other components do not appear in this case. The final $X^{(l)}(\boldsymbol{q}^2, \omega)$ then read

$$X^{(0)}(\boldsymbol{q}^2,\omega) = \boldsymbol{q}^2(W_{00} - 2W_{\perp\perp})\,, \tag{3.89}$$
$$X^{(1)}(\boldsymbol{q}^2,\omega) = -q_0 q^\parallel(W_{0\parallel} + W_{\parallel 0})\,, \tag{3.90}$$
$$X^{(2)}(\boldsymbol{q}^2,\omega) = q_0^2(W_{\parallel\parallel} + 2W_{\perp\perp})\,, \tag{3.91}$$

together with the longitudinal and transverse contributions

$$X^\parallel(\boldsymbol{q}^2,\omega) = \boldsymbol{q}^2 W_{00} - q_0 q^\parallel(W_{0\parallel} + W_{\parallel 0}) + q_0^2 W_{\parallel\parallel}\,, \tag{3.92}$$
$$X^\perp(\boldsymbol{q}^2,\omega) = 2(q_0^2 - \boldsymbol{q}^2)W_{\perp\perp}\,. \tag{3.93}$$

In order to show the connection of these components with the underlying exclusive form factors, we first introduce the HQET basis: this is commonly used to study these processes and it simplifies the calculations we address in this section. In this framework, the form factors depend on the variable

$$w^{(*)} = v_{D_s^{(*)}} \cdot v_{B_s} = \frac{M_{B_s}^2 + M_{D_s^{(*)}}^2 - q^2}{2M_{B_s}M_{D_s^{(*)}}}\,, \tag{3.94}$$

which takes the place of the conventional momentum transfer q^2, and where

$$v_{D_s^{(*)}} = \frac{p_{D_s^{(*)}}}{M_{D_s^{(*)}}}\,, \quad v_{B_s} = \frac{p_{B_s}}{M_{B_s}}\,, \tag{3.95}$$

are the four-velocities of $D_s^{(*)}$ and B_s, respectively. In this picture, the matrix elements for the pseudoscalar final state D_s and the vector final state D_s^* are given by

$$\frac{\langle D_s(p_{D_s})|\, V_\mu \,|B_s(p_{B_s})\rangle}{\sqrt{M_{B_s} M_{D_s}}} = (v_{B_s} + v_{D_s})_\mu h^+(w) + (v_{B_s} - v_{D_s})_\mu h^-(w)\,, \tag{3.96}$$

$$\frac{\langle D_s^*(p_{D_s^*},\varepsilon)|\, V_\mu \,|B_s(p_{B_s})\rangle}{\sqrt{M_{B_s} M_{D_s}}} = \epsilon_{\mu\nu\alpha\beta}\, \varepsilon^{*\nu}\, v_{D_s^*}^\alpha v_{B_s}^\beta h_V(w^*)\,, \tag{3.97}$$

$$\begin{aligned}\frac{\langle D_s^*(p_{D_s^*},\varepsilon)|\, A_\mu \,|B_s(p_{B_s})\rangle}{\sqrt{M_{B_s} M_{D_s}}} &= i\varepsilon_\mu^*(1+w^*)h_{A_1}(w^*) - i(\varepsilon^*\cdot v_{B_s})v_{B_s,\,\mu} h_{A_2}(w^*) \\ &\quad - i(\varepsilon^*\cdot v_{B_s})v_{D_s^*\,\mu} h_{A_3}(w^*)\,,\end{aligned} \tag{3.98}$$

where $h^\pm(w)$, $h_V(w^*)$ and $h_{A_i}(w^*)$ are the HQET form factors. In particular, defining in a compact notation the matrix elements $\mathcal{M}_{J_\mu} = \langle D_s(p_{D_s})|J_\mu|B_s(p_{B_s})\rangle$ and $\mathcal{M}^*_{J_\mu} = \langle D_s^*(p_{D_s},\varepsilon)|J_\mu|B_s(p_{B_s})\rangle$, we can calculate explicitly the longitudinal and transverse components. Starting from the the pseudoscalar decays we have

$$\frac{\mathcal{M}_{V_0}}{\sqrt{M_{B_s} M_{D_s}}} = \left(1 + \frac{E_{D_s}}{M_{D_s}}\right) h^+ + \left(1 - \frac{E_{D_s}}{M_{D_s}}\right) h^-\,, \tag{3.99}$$

$$\frac{\mathcal{M}_{V_\parallel}}{\sqrt{M_{B_s} M_{D_s}}} = \frac{p^\parallel_{D_s}}{M_{D_s}}(h^+ - h^-)\,, \tag{3.100}$$

$$\frac{\mathcal{M}_{V_\perp}}{\sqrt{M_{B_s} M_{D_s}}} = 0\,. \tag{3.101}$$

For the D_s^* decay mediated by vector currents the only non-zero contribution is given by the transverse component

$$\frac{\mathcal{M}^*_{V_\perp}}{\sqrt{M_{B_s} M_{D_s^*}}} = \frac{p^\parallel_{D_s}}{M_{D_s}} h_V\,, \tag{3.102}$$

whereas for the axial currents we have

$$\frac{\mathcal{M}^*_{A_0}}{\sqrt{M_{B_s} M_{D_s^*}}} = -i\frac{q^\parallel}{M_{D_s^*}}\left[(1+w^*)h_{A_1} - \left(h_{A_2} + \frac{E_{D_s^*}}{M_{D_s^*}} h_{A_3}\right)\right]\,, \tag{3.103}$$

$$\frac{\mathcal{M}^*_{A_\parallel}}{\sqrt{M_{B_s} M_{D_s^*}}} = \frac{i}{M_{D_s^*}}\left[E_{D_s^*}(1+w^*)h_{A_1} - \frac{q^2_\parallel}{M_{D_s^*}} h_{A_3}\right]\,, \tag{3.104}$$

$$\frac{\mathcal{M}^*_{A_\perp}}{\sqrt{M_{B_s} M_{D_s^*}}} = i(1+w^*)h_{A_1}\,. \tag{3.105}$$

It is then useful to decompose the hadronic tensor $W^{\mu\nu} = W^{\mu\nu}_{VV} + W^{\mu\nu}_{AA} - W^{\mu\nu}_{VA} - W^{\mu\nu}_{AV}$ in order to disentangle contributions from different physical channels, such that X can also be rewritten in a way that exposes the $V-A$ structure of the charged current, namely

$$X = X_{VV} + X_{AA} - X_{VA} - X_{AV}\,. \tag{3.106}$$

Combining Eqs. (3.92) and (3.93) with (3.88) and the expressions above for the matrix elements we obtain $X^{\parallel}(\boldsymbol{q}^2,\omega)$ and $X^{\perp}(\boldsymbol{q}^2,\omega)$ in the ground-state limit

$$X^{\parallel}_{VV}(\boldsymbol{q}^2,\omega) = \frac{\boldsymbol{q}^2}{4M_{D_s}E_{D_s}}\left[(M_{D_s}+M_{B_s})h^+ + (M_{D_s}-M_{B_s})h^-\right]^2 , \tag{3.107}$$

$$X^{\perp}_{VV}(\boldsymbol{q}^2,\omega) = \frac{\boldsymbol{q}^2}{2M_{D_s}E_{D_s^*}}[(M_{B_s}-E_{D_s^*})^2-\boldsymbol{q}^2]h_V^2 , \tag{3.108}$$

$$X^{\parallel}_{AA}(\boldsymbol{q}^2,\omega) = \frac{1}{4M^*_{D_s}E^*_{D_s}}\Bigg\{E^*_{D_s}(M_{B_s}-E^*_{D_s})(1+w^*)h_{A_1} + \boldsymbol{q}^2\left[(1+w^*)h_{A_1}-h_{A_2}-\frac{M_{B_s}}{M^*_{D_s}}h_{A_3}\right]\Bigg\}^2 , \tag{3.109}$$

$$X^{\perp}_{AA}(\boldsymbol{q}^2,\omega) = \frac{M^*_{D_s}}{2E^*_{D_s}}\left[(M_{B_s}-E^*_{D_s})^2-\boldsymbol{q}^2)\right](1+w^*)^2h^2_{A_1} . \tag{3.110}$$

Note in particular that in the rest frame of the B_s the HQET form factors $h^{\pm}(w)$ are related to the standard $f^{\pm}_{D_sB_s}(q^2)$ as

$$h^{\pm}(w) = \frac{1}{2\sqrt{M_{B_s}M_{D_s}}}\left[(M_{B_s}\pm M_{D_s})f^+_{D_sB_s}(q^2)+(M_{B_s}\mp M_{D_s})f^-_{D_sB_s}(q^2)\right] , \tag{3.111}$$

from which we can write $X^{\parallel}_{VV}(\boldsymbol{q}^2,\omega)$ as

$$X^{\parallel}_{VV}(\boldsymbol{q}^2,\omega) = \frac{M_{B_s}}{E_{D_s}}\boldsymbol{q}^2|f^+_{D_sB_s}(q^2)|^2 . \tag{3.112}$$

We have in this way shown how the ground-state limit of the inclusive decays can be related to the underlying HQET form factors, in particular through the decomposition into longitudinal and transverse components, further divided according to the nature of the currents. This is in useful, for example, to compare the inclusive results with the exclusive one in different channels, which can be computed on the lattice with more conventional techniques [148–150]. Furthermore, a solid understanding of the ground state limit could provide a way to better assess the effect of the excited states, as for example in the P-wave contributions [151–153].

3.3.4 Moments

We conclude this chapter discussing *moments* of various kinematical quantities, which describe the distribution of the given kinematic variable in the decay process. Lattice calculations of moments are particularly interesting for comparison with experiments and with OPE approaches [154–160]: indeed, they can provide a way to test the validity of these analytical techniques [29], which heavily rely on perturbative expansions. In particular, we focus on *hadronic mass moments* and *lepton energy moments*, as they are the ones that have been studied experimentally [161–166].

We then define the hadronic mass moments $\langle (M_{X_c}^2)^n \rangle$, with $M_{X_c}^2 = (p_{B_s} - q)^2 = (\omega^2 - \boldsymbol{q}^2)$, through the ratio

$$\langle (M_{X_c}^2)^n \rangle = \frac{\Gamma_{H_n}}{\Gamma} = \frac{\int \mathrm{d}\boldsymbol{q}^2 \mathrm{d}\omega \mathrm{d}E_l \, (\omega^2 - \boldsymbol{q}^2)^n \left[\frac{\mathrm{d}\Gamma}{\mathrm{d}\boldsymbol{q}^2 \, \mathrm{d}\omega \, \mathrm{d}E_l} \right]}{\int \mathrm{d}\boldsymbol{q}^2 \mathrm{d}\omega \mathrm{d}E_l \left[\frac{\mathrm{d}\Gamma}{\mathrm{d}\boldsymbol{q}^2 \, \mathrm{d}\omega \, \mathrm{d}E_l} \right]} \,, \tag{3.113}$$

$$\Gamma_{H_n} \equiv \int \mathrm{d}\boldsymbol{q}^2 \mathrm{d}\omega \mathrm{d}E_l \, \left(\omega^2 - \boldsymbol{q}^2 \right)^n \left[\frac{\mathrm{d}\Gamma}{\mathrm{d}\boldsymbol{q}^2 \, \mathrm{d}\omega \, \mathrm{d}E_l} \right] \,, \tag{3.114}$$

as well as the lepton energy moments $\langle E_l^n \rangle$

$$\langle E_l^n \rangle = \frac{\Gamma_{L_n}}{\Gamma} = \frac{\int \mathrm{d}\boldsymbol{q}^2 \mathrm{d}\omega \mathrm{d}E_l \, E_l^n \left[\frac{\mathrm{d}\Gamma}{\mathrm{d}\boldsymbol{q}^2 \, \mathrm{d}\omega \, \mathrm{d}E_l} \right]}{\int \mathrm{d}\boldsymbol{q}^2 \mathrm{d}\omega \mathrm{d}E_l \left[\frac{\mathrm{d}\Gamma}{\mathrm{d}\boldsymbol{q}^2 \, \mathrm{d}\omega \, \mathrm{d}E_l} \right]} \,, \tag{3.115}$$

$$\Gamma_{L_n} \equiv \int \mathrm{d}\boldsymbol{q}^2 \mathrm{d}\omega \mathrm{d}E_l \, E_l^n \left[\frac{\mathrm{d}\Gamma}{\mathrm{d}\boldsymbol{q}^2 \, \mathrm{d}\omega \, \mathrm{d}E_l} \right] \,. \tag{3.116}$$

We also consider the corresponding *differential moments*

$$H_n(\boldsymbol{q}^2) \equiv \langle (M_{X_c}^2)^n \rangle_{\boldsymbol{q}^2} = \frac{\int \mathrm{d}\omega \mathrm{d}E_l \, (\omega^2 - \boldsymbol{q}^2)^n \left[\frac{\mathrm{d}\Gamma}{\mathrm{d}\boldsymbol{q}^2 \, \mathrm{d}\omega \, \mathrm{d}E_l} \right]}{\int \mathrm{d}\omega \mathrm{d}E_l \left[\frac{\mathrm{d}\Gamma}{\mathrm{d}\boldsymbol{q}^2 \, \mathrm{d}\omega \, \mathrm{d}E_l} \right]} \,, \tag{3.117}$$

$$L_n(\boldsymbol{q}^2) \equiv \langle E_l^n \rangle_{\boldsymbol{q}^2} = \frac{\int \mathrm{d}\omega \mathrm{d}E_l \, E_l^n \left[\frac{\mathrm{d}\Gamma}{\mathrm{d}\boldsymbol{q}^2 \, \mathrm{d}\omega \, \mathrm{d}E_l} \right]}{\int \mathrm{d}\omega \mathrm{d}E_l \left[\frac{\mathrm{d}\Gamma}{\mathrm{d}\boldsymbol{q}^2 \, \mathrm{d}\omega \, \mathrm{d}E_l} \right]} \,. \tag{3.118}$$

We can address the numerator of these moments in a similar way with respect to what we discussed in the previous sections. We define

$$\begin{aligned} X_H^{(n)}(\boldsymbol{q}^2, \omega) &= \frac{24\pi^3}{G_F^2 |V_{cb}|^2} \frac{1}{\sqrt{\boldsymbol{q}^2}} \int \mathrm{d}E_l \, (\omega^2 - \boldsymbol{q}^2)^n \left[\frac{\mathrm{d}\Gamma}{\mathrm{d}\boldsymbol{q}^2 \, \mathrm{d}\omega \, \mathrm{d}E_l} \right] \\ &= \frac{3}{\sqrt{\boldsymbol{q}^2}} \int \mathrm{d}E_l \, (\omega^2 - \boldsymbol{q}^2)^n L_{\mu\nu} W^{\mu\nu} \,, \end{aligned} \tag{3.119}$$

$$\begin{aligned} X_L^{(n)}(\boldsymbol{q}^2, \omega) &= \frac{24\pi^3}{G_F^2 |V_{cb}|^2} \frac{1}{\sqrt{\boldsymbol{q}^2}} \int \mathrm{d}E_l \, E_l^n \left[\frac{\mathrm{d}\Gamma}{\mathrm{d}\boldsymbol{q}^2 \, \mathrm{d}\omega \, \mathrm{d}E_l} \right] \\ &= \frac{3}{\sqrt{\boldsymbol{q}^2}} \int \mathrm{d}E_l \, E_l^n L_{\mu\nu} W^{\mu\nu} \,, \end{aligned} \tag{3.120}$$

where the prefactor $\frac{24\pi^3}{G_F^2 |V_{cb}|^2} \frac{1}{\sqrt{\boldsymbol{q}^2}}$ has been introduced for convenience to match the conventions in Eq. (3.74). We also define the corresponding versions integrated over ω, i.e. $\bar{X}_H^{(n)}(\boldsymbol{q}^2) = \int \mathrm{d}\omega X_H^{(n)}(\boldsymbol{q}^2, \omega)$ and $\bar{X}_L^{(n)}(\boldsymbol{q}^2) = \int \mathrm{d}\omega X_L^{(n)}(\boldsymbol{q}^2, \omega)$, such that

$$\Gamma_{H_n} = \frac{G_F^2 |V_{cb}|^2}{24\pi^3} \int \mathrm{d}\boldsymbol{q}^2 \sqrt{\boldsymbol{q}^2} \bar{X}_H^{(n)}(\boldsymbol{q}^2) \,, \tag{3.121}$$

$$\Gamma_{L_n} = \frac{G_F^2 |V_{cb}|^2}{24\pi^3} \int \mathrm{d}\boldsymbol{q}^2 \sqrt{\boldsymbol{q}^2} \bar{X}_L^{(n)}(\boldsymbol{q}^2) \,. \tag{3.122}$$

The moments can then be computed as

$$\langle (M_{X_c}^2)^n \rangle = \frac{\Gamma_{H_n}}{\Gamma} = \frac{\int \mathrm{d}\boldsymbol{q}^2 \sqrt{\boldsymbol{q}^2} \bar{X}_H^{(n)}(\boldsymbol{q}^2)}{\int \mathrm{d}\boldsymbol{q}^2 \sqrt{\boldsymbol{q}^2} \bar{X}(\boldsymbol{q}^2)}\,, \tag{3.123}$$

$$\langle E_l^n \rangle = \frac{\Gamma_{L_n}}{\Gamma} = \frac{\int \mathrm{d}\boldsymbol{q}^2 \sqrt{\boldsymbol{q}^2} \bar{X}_L^{(n)}(\boldsymbol{q}^2)}{\int \mathrm{d}\boldsymbol{q}^2 \sqrt{\boldsymbol{q}^2} \bar{X}(\boldsymbol{q}^2)}\,, \tag{3.124}$$

together with their differential versions

$$H_n(\boldsymbol{q}^2) = \frac{\bar{X}_H^{(n)}(\boldsymbol{q}^2)}{\bar{X}(\boldsymbol{q}^2)}\,, \tag{3.125}$$

$$L_n(\boldsymbol{q}^2) = \frac{\bar{X}_L^{(n)}(\boldsymbol{q}^2)}{\bar{X}(\boldsymbol{q}^2)}\,. \tag{3.126}$$

Let us now calculate explicitly the central quantities $X_H^{(n)}(\boldsymbol{q}^2,\omega)$ and $X_L^{(n)}(\boldsymbol{q}^2,\omega)$. For the leptonic moments, the calculation is quite involved as the factor E_l^n adds power of the lepton energy in the integral. In the massless limit, using Eq. (3.47) we get

$$\begin{aligned}\int \mathrm{d}E_l\, E_l^n L_{\mu\nu} W^{\mu\nu}\Big|_{m_l=0} =& q^2 \left(W_1 - \frac{1}{2}W_2 - q_0 W_3\right)\frac{\Delta E_l^{n+1}}{n+1} \\ &+ 2(q_0 W_2 + q^2 W_3)\frac{\Delta E_l^{n+2}}{n+2} - 2W_2 \frac{\Delta E_l^{n+3}}{n+3}\,.\end{aligned} \tag{3.127}$$

Recalling the definition in Eq. (3.120), we can substitute the structure functions in Eqs. (3.66), (3.67) and (3.68) to obtain

$$\begin{aligned}X_L^{(n)}(\boldsymbol{q}^2,\omega) =& \frac{3}{\sqrt{\boldsymbol{q}^2}}\Bigg\{ W_{00}\left[-\frac{1}{2}(q_0^2-\boldsymbol{q}^2)\frac{\Delta E_l^{n+1}}{n+1} + 2q_0\frac{\Delta E_l^{n+2}}{n+2} - 2\frac{\Delta E_l^{n+3}}{n+3}\right] \\ &+ \frac{q_0^2-\boldsymbol{q}^2}{\boldsymbol{q}^2}\sum_i W_{ii}\left[\frac{1}{4}\frac{\Delta E_l^{n+1}}{n+1}\left(\boldsymbol{q}^2+q_0^2\right) - q_0\frac{\Delta E_l^{n+2}}{n+2} + \frac{\Delta E_l^{n+3}}{n+3}\right] \\ &+ \sum_i q^i (W_{0i}+W_{i0})\frac{q_0}{\boldsymbol{q}^2}\left[\frac{1}{2}(q_0^2-\boldsymbol{q}^2)\frac{\Delta E_l^{n+1}}{n+1} - 2q_0\frac{\Delta E_l^{n+2}}{n+2} + 2\frac{\Delta E_l^{n+3}}{n+3}\right] \\ &+ \sum_{i,j} q^i W_{ij} q^j \frac{1}{|\boldsymbol{q}|^4}\Bigg[-\frac{1}{4}(\boldsymbol{q}^2+3q_0^2)(q_0^2-\boldsymbol{q}^2)\frac{\Delta E_l^{n+1}}{n+1} + \\ &\qquad (\boldsymbol{q}^2-3q_0^2)\left(-q_0\frac{\Delta E_l^{n+2}}{n+2} + \frac{\Delta E_l^{n+3}}{n+3}\right)\Bigg] \\ &+ i\frac{q_0^2-\boldsymbol{q}^2}{\boldsymbol{q}^2}\sum_{i,j,k} W_{ij}\varepsilon^{ijk} q_k\left[-q_0\frac{\Delta E_l^{n+1}}{n+1} + 2\frac{\Delta E_l^{n+2}}{n+2}\right]\Bigg\}\,,\end{aligned} \tag{3.128}$$

which provides a full and complete expression for all orders n in terms of the hadronic tensor. We can then make use of the general formula in Eq. (3.52) to determine explicitly all values of n. In particular, for $n=1$ we can substitute the expressions in Eq. (3.53)

to obtain the final result

$$X_L^{(1)}(\boldsymbol{q}^2,\omega) = \frac{1}{2}q_0|\boldsymbol{q}|^2 W_{00} + \frac{1}{2}q_0(q_0^2-|\boldsymbol{q}|^2)\sum_i W_{ii} + \frac{1}{2}q_0\sum_{i,j} q^i W_{ij} q^j \\ - \frac{1}{2}q_0^2\sum_i q_i(W_{0i}+W_{i0}) + \frac{i}{2}(q_0^2-|\boldsymbol{q}|^2)\sum_{i,j,k} W_{ij}\varepsilon^{ijk}q_k\,. \tag{3.129}$$

Finally, the case involving the hadronic moments is trivial, as ω and $\boldsymbol{q}^2$ are independent and do not contribute to the E_l integral, i.e.

$$X_H^{(n)}(\boldsymbol{q}^2,\omega) = (\omega-\boldsymbol{q}^2)^n X(\boldsymbol{q}^2,\omega)\,. \tag{3.130}$$

We will explicitly consider the moments at order $n=1$ for the numerical investigations in this work.

CHAPTER 4

INCLUSIVE DECAYS ON THE LATTICE

In this chapter we discuss the strategy for computing the inclusive-decay observables we defined in Chap. 3 in Lattice QCD. We start off in Sec. 4.1 by defining a set of Euclidean correlation functions, in terms of which we express a number of target observables in Sec. 4.2. In Sec. 4.3 we then address the underlying data-analysis problem.

4.1 Operators and correlation functions

The interpolating operators for the $B_s \to X_c\, l\nu_l$ semileptonic processes (exclusive and inclusive) are given by

$$\mathcal{O}_{B_s}(x) = \bar{b}(x)\,\gamma_5\, s(x)\,, \tag{4.1}$$

$$\mathcal{O}_{D_s}(x) = \bar{c}(x)\,\gamma_5 s(x), \tag{4.2}$$

$$J_\nu(x) = \bar{b}(x)\,\Gamma^J_\nu\, c(x)\,, \tag{4.3}$$

where $\Gamma^V_\nu = \gamma_\nu$ and $\Gamma^A_\nu = \gamma_\nu\gamma_5$ (see App. A.1), and where the fermion fields $b(x), c(x)$ and $s(x)$ correspond to the b, c and s quark (Euclidean) fields, respectively.

We start considering the B_s two-point functions. Following the conventions of Sec. 2.3.3, we rewrite the operator at source and sink in a more general way as

$$\mathcal{O}^X_{B_s}(x_{\rm src}) = \bar{b}^X(x_{\rm src})\Gamma_{\rm src}\, s^X(x_{\rm src})\,, \qquad \mathcal{O}^X_{B_s}(x_{\rm snk}) = \bar{b}^X(x_{\rm snk})\Gamma_{\rm snk}\, s^X(x_{\rm snk})\,, \tag{4.4}$$

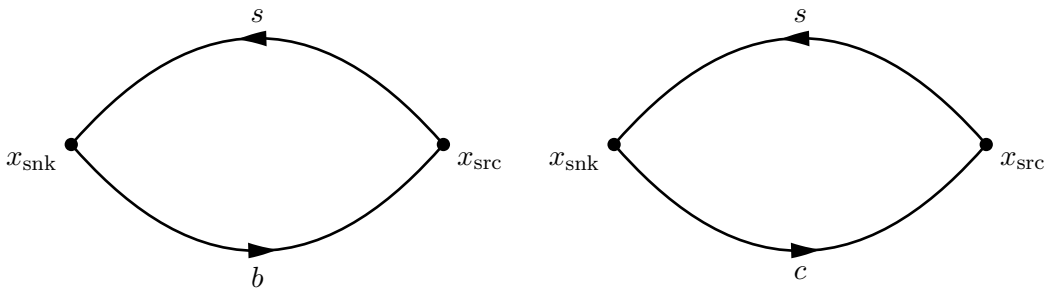

FIGURE 4.1: Illustration of valence quarks in two-point correlation functions for the B_s (left) and D_s (right) mesons.

where $\Gamma_{\rm src} = \Gamma_{\rm snk} = \gamma_5$ and the superscript $X, Y \in \{S, L\}$, indicate smearing (S) or no smearing (L). The correlator reads

$$C_{B_s}^{YX}(\boldsymbol{p}_{\rm snk}, t_{\rm snk}, t_{\rm src}) = \sum_{\boldsymbol{x}_{\rm snk}} e^{-i\boldsymbol{p}_{\rm snk}\cdot(\boldsymbol{x}_{\rm snk}-\boldsymbol{x}_{\rm src})} \times \left\langle \mathrm{Tr}\Big[\gamma_5\Gamma_{\rm snk} G_s^{YX}(x_{\rm snk}, x_{\rm src})\Gamma_{\rm src}^\dagger\gamma_5 G_b^{YX\,\dagger}(x_{\rm snk}, x_{\rm src})\Big]\right\rangle_G , \tag{4.5}$$

where G_q^{YX} indicates the propagator of the quark q with smearing X at the source and Y at the sink. In particular, we compute zero-momentum projected two-point correlators with all possible combinations of smearing at source and sink, i.e. $C_{B_s}^{LS}(t_{\rm snk}, t_{\rm src})$, $C_{B_s}^{SL}(t_{\rm snk}, t_{\rm src})$ and $C_{B_s}^{SS}(t_{\rm snk}, t_{\rm src})$, where we suppressed the momentum dependence to indicate that $\boldsymbol{p}_{\rm snk} = \boldsymbol{0}$. We will use the same convention in the rest of the manuscript. In a similar way, we compute the smeared-smeared and local-smeared two-point functions for the D_s correlation function $C_{D_s}^{LS}(\boldsymbol{p}_{\rm snk}, t_{\rm snk}, t_{\rm src})$ and $C_{D_s}^{SS}(\boldsymbol{p}_{\rm snk}, t_{\rm snk}, t_{\rm src})$. Both two-point correlators are depicted in Fig. 4.1.

We also compute three-point correlators for the $B_s \to D_s\, l\nu_l$ process in Fig. 4.2, which, together with the D_s two-point functions, will be used to investigate the corresponding exclusive process and compare it with our inclusive study. The smeared-smeared correlator is

$$C_{D_sB_s,\mu}^{SS}(\boldsymbol{q}, \boldsymbol{p}_{\rm snk}, t_{\rm snk}, t, t_{\rm src}) = \sum_{\boldsymbol{x}_{\rm snk}, \boldsymbol{x}} e^{-i\boldsymbol{p}_{\rm snk}\cdot(\boldsymbol{x}_{\rm snk}-\boldsymbol{x}_{\rm src})} e^{-i\boldsymbol{q}\cdot(\boldsymbol{x}-\boldsymbol{x}_{\rm src})} \times \langle T\{\mathcal{O}_{D_s}^S(\boldsymbol{x}_{\rm snk}, t_{\rm snk}) V_\mu(\boldsymbol{x}, t) \mathcal{O}_{B_s}^{S\dagger}(\boldsymbol{x}_{\rm src}, t_{\rm src})\}\rangle , \tag{4.6}$$

which after Wick contraction reads

$$C_{D_sB_s,\mu}^{SS}(\boldsymbol{q}, \boldsymbol{p}_{\rm snk}, t_{\rm snk}, t, t_{\rm src}) = \sum_{\boldsymbol{x}} e^{-i\boldsymbol{q}\cdot(\boldsymbol{x}-\boldsymbol{x}_{\rm src})} \left\langle \mathrm{Tr}\Big[\gamma_5\Gamma_\mu^V \Sigma_{cs}(x, x_{\rm src})\Gamma_{\rm src}^\dagger\gamma_5 G_b^\dagger(x, x_{\rm src})\Big]\right\rangle_G , \tag{4.7}$$

where the sequential propagator is given by

$$\Sigma_{cs}(x, x_{\rm src}) = \sum_{\boldsymbol{x}_{\rm snk}} e^{-i\boldsymbol{p}_{\rm snk}\cdot(\boldsymbol{x}_{\rm snk}-\boldsymbol{x}_{\rm src})} G_c(x, x_{\rm snk})\Gamma_{\rm snk}\, G_s(x_{\rm snk}, x_{\rm src}) \tag{4.8}$$

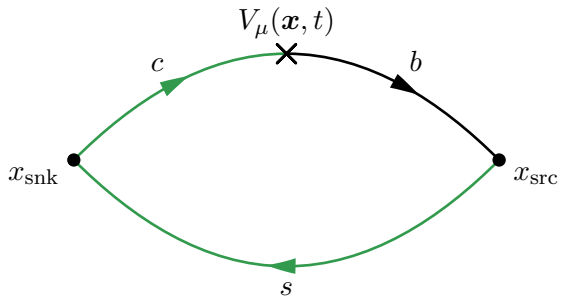

FIGURE 4.2: Three-point correlator diagram for the exclusive channel $B_s \to D_s\, l\nu_l$.

where $G_s(x_{\text{snk}}, x_{\text{src}})$ propagates the s quark from x_{src} to x_{snk} and $G_c(x, x_{\text{snk}})$ propagates the c quark from x_{snk} to x.

The core of the inclusive computation relies on the construction of the four-point correlator in Fig. 4.3, which addresses the matrix element in the hadronic tensor in Eq. (3.33)

$$W^{\mu\nu} \sim \langle B_s |\, \tilde{J}^{\mu\dagger} \tilde{J}^{\nu}\, | B_s \rangle \ . \tag{4.9}$$

In particular, with $t_{\text{snk}} \geq t_2 \geq t_1 \geq t_{\text{src}}$,

$$\begin{aligned} C_{\mu\nu}^{SJJS}\left(\boldsymbol{q}, \boldsymbol{p}_{\text{snk}}, t_{\text{snk}}, t_2, t_1, t_{\text{src}}\right) = & \sum_{\boldsymbol{x}_{\text{snk}}} e^{-i\boldsymbol{p}_{\text{snk}}\cdot(\boldsymbol{x}_{\text{snk}}-\boldsymbol{x}_{\text{src}})} \times \\ & \left\langle \mathcal{O}_{B_s}^{S}\left(\boldsymbol{x}_{\text{snk}}, t_{\text{snk}}\right) \tilde{J}_{\mu}^{\dagger}\left(\boldsymbol{q}, t_2\right) \tilde{J}_{\nu}\left(\boldsymbol{q}, t_1\right) \mathcal{O}_{B_s}^{S\dagger}\left(\boldsymbol{x}_{\text{src}}, t_{\text{src}}\right) \right\rangle \\ = & \sum_{\boldsymbol{x}_{\text{snk}}, \boldsymbol{x}_1, \boldsymbol{x}_2} e^{-i\boldsymbol{p}_{\text{snk}}\cdot(\boldsymbol{x}_{\text{snk}}-\boldsymbol{x}_{\text{src}})} e^{i\boldsymbol{q}\cdot\boldsymbol{x}_2} e^{-i\boldsymbol{q}\cdot\boldsymbol{x}_1} \times \\ & \left\langle \mathcal{O}_{B_s}^{S}\left(\boldsymbol{x}_{\text{snk}}, t_{\text{snk}}\right) J_{\mu}^{\dagger}\left(\boldsymbol{x}_2, t_2\right) J_{\nu}\left(\boldsymbol{x}_1, t_1\right) \mathcal{O}_{B_s}^{S\dagger}\left(\boldsymbol{x}_{\text{src}}, t_{\text{src}}\right) \right\rangle \ , \end{aligned} \tag{4.10}$$

where the currents are projected onto three-momentum by a discrete Fourier transform $\tilde{J}_\nu(\boldsymbol{q}, t) = \sum_{\boldsymbol{x}} e^{-i\boldsymbol{q}\cdot\boldsymbol{x}} J_\nu(\boldsymbol{x}, t)$. We can now use Wick's theorem to get an expression for the four-point correlator in terms of propagators (cf. with Sec. 2.4), i.e.

$$\begin{aligned} & \left\langle \mathcal{O}_{B_s}^{S}\left(\boldsymbol{x}_{\text{snk}}, t_{\text{snk}}\right) J_{\mu}^{\dagger}\left(\boldsymbol{x}_1, t_1\right) J_{\nu}\left(\boldsymbol{x}_2, t_2\right) O_{B_s}^{S\dagger}\left(\boldsymbol{x}, t_{\text{src}}\right) \right\rangle = \\ & = \left\langle \bar{b}(x_{\text{snk}}) \Gamma_{\text{snk}} s(x_{\text{snk}})\, \bar{c}(x_2) \Gamma_{\mu}^{J\dagger} b(x_2)\, \bar{b}(x_1) \Gamma_{\nu}^{J} c(x_1)\, \bar{s}(x_{\text{src}}) \Gamma_{\text{src}}^{\dagger} b(x_{\text{src}}) \right\rangle \\ & = \left\langle \text{Tr}\left[G_b(x_2, x_{\text{snk}}) \Gamma_{\text{snk}} G_s(x_{\text{snk}}, x_{\text{src}}) \Gamma_{\text{src}}^{\dagger} G_b(x_{\text{src}}, x_1) \Gamma_{\nu}^{J} G_c(x_1, x_2) \Gamma_{\mu}^{J\dagger} \right] \right\rangle_G + \\ & \quad \left\langle \text{Tr}\left[G_b(x_{\text{src}}, x_{\text{snk}}) \Gamma_{\text{snk}} G_s(x_{\text{snk}}, x_{\text{src}}) \Gamma_{\text{src}}^{\dagger} \right] \right\rangle_G \left\langle \text{Tr}\left[G_b(x_2, x_1) \Gamma_{\nu}^{J} G_c(x_1, x_2) \Gamma_{\mu}^{J\dagger} \right] \right\rangle_G \end{aligned} \tag{4.11}$$

$=$ 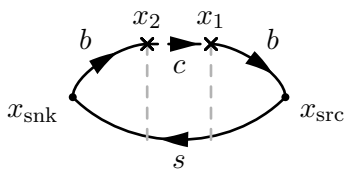 $+$ 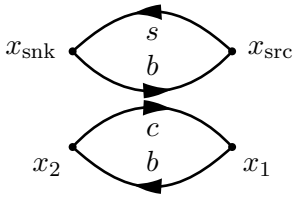 .

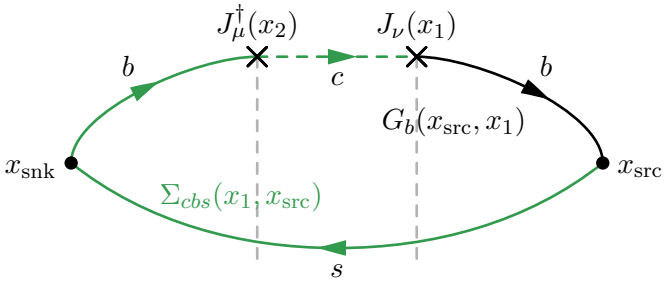

FIGURE 4.3: Diagram of the four-point correlator. The black line, $G_b(x_{\rm src}, x_1)$, is a propagator for the b quark from x_1 to $x_{\rm src}$; the green one, $\Sigma_{cbs}(x_1, x_{\rm src})$, is a sequential propagator that propagates the s quark from $x_{\rm src}$ to $x_{\rm snk}$, the b quark from $x_{\rm snk}$ to x_2 and the c quark from x_2 to x_1.

The disconnected diagrams are suppressed in the semileptonic region because of energy conservation, as the $\bar{b}c$ state is more massive than the B_s meson, and will therefore be ignored in the remaining of this work. The only contribution is then given by

$$C^{SJJS}_{\mu\nu}(\boldsymbol{q}, \boldsymbol{p}_{\rm snk}, t_{\rm snk}, t_2, t_1, t_{\rm src}) = \sum_{\boldsymbol{x}_{\rm snk}, \boldsymbol{x}_1, \boldsymbol{x}_2} e^{-i\boldsymbol{p}_{\rm snk}\cdot(\boldsymbol{x}_{\rm snk}-\boldsymbol{x}_{\rm src})} e^{i\boldsymbol{q}\cdot\boldsymbol{x}_2} e^{-i\boldsymbol{q}\cdot\boldsymbol{x}_1} \times \tag{4.12}$$
$$\left\langle \mathrm{Tr}\Big[G_b(x_2, x_{\rm snk}) \Gamma_{\rm snk} G_s(x_{\rm snk}, x_{\rm src}) \Gamma^\dagger_{\rm src} G_b(x_{\rm src}, x_1) \Gamma^J_\nu G_c(x_1, x_2) \Gamma^{J\dagger}_\mu \Big] \right\rangle_G .$$

The above expression can be evaluated with the sequential-propagator method as depicted in Fig. 4.3, for which the correlator reads

$$C^{SJJS}_{\mu\nu}(\boldsymbol{q}, \boldsymbol{p}_{\rm snk}, t_{\rm snk}, t_2, t_1, t_{\rm src}) = \sum_{\boldsymbol{x}_1} e^{-i\boldsymbol{q}\cdot\boldsymbol{x}_1} \times \tag{4.13}$$
$$\left\langle \mathrm{Tr}\Big[\gamma_5 \Gamma^J_\nu \Sigma_{cbs}(x_1, x_{\rm src}) \Gamma^\dagger_{\rm src} \gamma_5 G^\dagger_b(x_1, x_{\rm src}) \Big] \right\rangle_G .$$

where

$$\Sigma_{cbs}(x_1, x_{\rm src}) = \sum_{\boldsymbol{x_2}} e^{i\boldsymbol{q}\cdot\boldsymbol{x}_2} G_c(x_1, x_2) \Gamma^{J\dagger}_\mu \Sigma_{bs}(x_2, x_{\rm src}) , \tag{4.14}$$

$$\Sigma_{bs}(x_2, x_{\rm src}) = \sum_{\boldsymbol{x}_{\rm snk}} e^{-i\boldsymbol{p}_{\rm snk}\cdot(\boldsymbol{x}_{\rm snk}-\boldsymbol{x}_{\rm src})} G_b(x_2, x_{\rm snk}) \Gamma_{\rm snk} G_s(x_{\rm snk}, x_{\rm src}) . \tag{4.15}$$

In particular, $\Sigma_{cbs}(x_1, x_{\rm src})$ is a sequential propagator whose source $S_{\rm seq}$ (cf. Eq. (2.103)) is built on a sequential propagator $\Sigma_{bs}(x_2, x_{\rm src})$.

Let us now work out the full Euclidean-time dependence for the four-point correlator by inserting a complete set of states, $I = \sum_{X_c} |X_c(\boldsymbol{p}_{X_c})\rangle \langle X_c(\boldsymbol{p}_{X_c})|$, which is understood to

include an integration over all possible momenta $\boldsymbol{p}_{X_c}$ under a Lorentz invariant phase-space integral. Considering that $\boldsymbol{q} = \boldsymbol{p}_{B_s} - \boldsymbol{p}_{X_c}$, with $\boldsymbol{p}_{B_s} = \boldsymbol{p}_{\text{snk}} = \boldsymbol{p}_{\text{src}}$, we get

$$\begin{aligned} C_{\mu\nu}^{SJJS}(\boldsymbol{q}, \boldsymbol{p}_{B_s}, t_{\text{snk}}, t_2, t_1, t_{\text{src}}) = & \qquad (4.16) \\ = & \sum_{\boldsymbol{x}_{\text{snk}}} e^{-i\boldsymbol{p}_{B_s}(\boldsymbol{x}_{\text{snk}} - \boldsymbol{x}_{\text{src}})} \langle \mathcal{O}_{B_s}^{S}(\boldsymbol{x}_{\text{snk}}, t_{\text{snk}}) \tilde{J}_{\mu}^{\dagger}(\boldsymbol{q}, t_2) \tilde{J}_{\nu}(\boldsymbol{q}, t_1) \mathcal{O}_{B_s}^{S\dagger}(\boldsymbol{x}_{\text{src}}, t_{\text{src}}) \rangle \\ = & \sum_{\boldsymbol{x}_{\text{snk}}} e^{-i\boldsymbol{p}_{B_s}(\boldsymbol{x}_{\text{snk}} - \boldsymbol{x}_{\text{src}})} \langle 0 | e^{-(T - t_{\text{snk}})\hat{H}} \mathcal{O}_{B_s}^{S}(\boldsymbol{x}_{\text{snk}}, 0) e^{-(t_{\text{snk}} - t_2)\hat{H}} \times \\ & \tilde{J}_{\mu}^{\dagger}(\boldsymbol{q}, 0) e^{-t_2\hat{H}} e^{t_1\hat{H}} \tilde{J}_{\nu}(\boldsymbol{q}, 0) e^{-(t_1 - t_{\text{src}})\hat{H}} \mathcal{O}_{B_s}^{\dagger S}(\boldsymbol{x}_{\text{src}}, 0) e^{-t_{\text{src}}\hat{H}} | 0 \rangle \\ = & \frac{e^{-(t_{\text{snk}} - t_2)E_{B_s}} \; e^{-(t_1 - t_{\text{src}})E_{B_s}}}{(2E_{B_s})^2} \langle 0 | \mathcal{O}_{B_s}^{S} | B_s(\boldsymbol{p}_{B_s}) \rangle \langle B_s(\boldsymbol{p}_{B_s}) | \mathcal{O}_{B_s}^{S\dagger} | 0 \rangle \times \\ & \langle B_s(\boldsymbol{p}_{B_s}) | \tilde{J}_{\mu}^{\dagger}(\boldsymbol{q}, 0) e^{-(t_2 - t_1)\hat{H}} \tilde{J}_{\nu}(\boldsymbol{q}, 0) | B_s(\boldsymbol{p}_{B_s}) \rangle \; , \end{aligned}$$

where we assumed $t_{\text{snk}} - t_2 \gg 0$ and $t_1 - t_{\text{src}} \gg 0$ such that the excited states of the $\mathcal{O}_{B_s}$ operator are suppressed and the B_s ground state dominates. In order to obtain the matrix element

$$\langle B_s(\boldsymbol{p}_{B_s}) | \tilde{J}_{\mu}^{\dagger}(\boldsymbol{q}, 0) e^{-t\hat{H}} \tilde{J}_{\nu}(\boldsymbol{q}, 0) | B_s(\boldsymbol{p}_{B_s}) \rangle \; , \tag{4.17}$$

which will be used to address the computation of the hadronic tensor, we can remove the exponential factors that do not depend on E_{X_c} using the two-point correlators

$$\begin{cases} C_{B_s}^{SL}(\boldsymbol{p}_{B_s}, t_{\text{snk}}, t_2) & \overset{t_{\text{snk}} - t_2 \gg 0}{=} \frac{1}{2E_{B_s}} \langle 0 | \mathcal{O}_{B_s}^{S} | B_s(\boldsymbol{p}_{B_s}) \rangle \langle B_s(\boldsymbol{p}_{B_s}) | \mathcal{O}_{B_s}^{\dagger L} | 0 \rangle \; e^{-(t_{\text{snk}} - t_2)E_{B_s}} \\ C_{B_s}^{LS}(\boldsymbol{p}_{B_s}, t_1, t_{\text{src}}) & \overset{t_1 - t_{\text{src}} \gg 0}{=} \frac{1}{2E_{B_s}} \langle 0 | \mathcal{O}_{B_s}^{L} | B_s(\boldsymbol{p}_{B_s}) \rangle \langle B_s(\boldsymbol{p}_{B_s}) | \mathcal{O}_{B_s}^{\dagger S} | 0 \rangle \; e^{-(t_1 - t_{\text{src}})E_{B_s}} \end{cases} . \tag{4.18}$$

We can indeed build the ratio

$$R_{\mu\nu}(\boldsymbol{q}, \boldsymbol{p}_{B_s}, t_2, t_1) = \frac{C^{SJJS}(\boldsymbol{q}, \boldsymbol{p}_{B_s}, t_{\text{snk}}, t_2, t_1, t_{\text{src}})}{C_{B_s}^{SL}(\boldsymbol{p}_{B_s}, t_{\text{snk}}, t_2) C_{B_s}^{LS}(\boldsymbol{p}_{B_s}, t_1, t_{\text{src}})} \, , \tag{4.19}$$

which in the limits $t_{\text{snk}} - t_2 \gg 0$ and $t_1 - t_{\text{src}} \gg 0$ gives

$$R_{\mu\nu}(\boldsymbol{q}, \boldsymbol{p}_{B_s}, t_2, t_1) \longrightarrow \frac{\frac{1}{2E_{B_s}} \langle B_s(\boldsymbol{p}_{B_s}) | \tilde{J}_{\mu}^{\dagger}(\boldsymbol{q}, 0) e^{-(t_2 - t_1)\hat{H}} \tilde{J}_{\nu}(\boldsymbol{q}, 0) | B_s(\boldsymbol{p}_{B_s}) \rangle}{\frac{1}{2E_{B_s}} | \langle 0 | \mathcal{O}_{B_s}^{L} | B_s(\boldsymbol{p}_{B_s}) \rangle |^2} \, . \tag{4.20}$$

Inserting a complete set of states we get

$$\begin{aligned} R_{\mu\nu}(\boldsymbol{q}, \boldsymbol{p}_{B_s}, t_2, t_1) = & \frac{1}{| \langle 0 | \mathcal{O}_{B_s}^{L} | B_s(\boldsymbol{p}_{B_s}) \rangle |^2} \sum_{X_c} \langle B(\boldsymbol{p}_{B_s}) | \tilde{J}_{\mu}^{\dagger}(\boldsymbol{q}, 0) | X_c(\boldsymbol{p}_{X_c}) \rangle \times \qquad (4.21) \\ & e^{-(t_2 - t_1)E_{X_c}} \langle X_c(\boldsymbol{p}_{X_c}) | \tilde{J}_{\nu}(\boldsymbol{q}, 0) | B_s(\boldsymbol{p}_{B_s}) \rangle \; . \end{aligned}$$

From the ratio $R_{\mu\nu}(\boldsymbol{q}, \boldsymbol{p}_{B_s}, t_2, t_1)$ we can finally construct the key correlator $C_{\mu\nu}(\boldsymbol{q}, \boldsymbol{p}_{B_s}, t)$ to address the inclusive analysis: using in particular translational invariance, $t = t_2 - t_1$,

we obtain

$$
\begin{aligned}
C_{\mu\nu}(\boldsymbol{q}, \boldsymbol{p}_{B_s}, t) &= \frac{1}{2E_{B_s}} |\langle 0| \mathcal{O}^L_{B_s} |B_s(\boldsymbol{p}_{B_s})\rangle|^2 R_{\mu\nu}(\boldsymbol{q}, \boldsymbol{p}_{B_s}, t, 0) \qquad (4.22)\\
&= \frac{1}{2E_{B_s}} \sum_X \langle B_s(\boldsymbol{p}_{B_s})| \tilde{J}^\dagger_\mu(\boldsymbol{q}, 0) |X_c(\boldsymbol{p}_{X_c})\rangle e^{-tE_{X_c}} \langle X_c(\boldsymbol{p}_{X_c})| \tilde{J}_\nu(\boldsymbol{q}, 0) |B_s(\boldsymbol{p}_{B_s})\rangle \\
&= \frac{1}{2E_{B_s}} \langle B_s(\boldsymbol{p}_{B_s})| \tilde{J}^\dagger_\mu(\boldsymbol{q}, 0) e^{-t\hat{H}} \tilde{J}_\nu(\boldsymbol{q}, 0) |B_s(\boldsymbol{p}_{B_s})\rangle \ ,
\end{aligned}
$$

where the factor $|\langle 0| \mathcal{O}^L_{B_s} |B_s(\boldsymbol{p}_{B_s})\rangle|^2/(2E_{B_s})$ can be extracted from fits of B_s the two-point functions. This correlator is now directly related to the matrix element relevant to address the evaluation of the hadronic tensor, as we will discuss in the next section. Since we assume to be in the rest frame of the B_s meson, we set $\boldsymbol{p}_{B_s} = \boldsymbol{0}$ and $E_{B_s} = M_{B_s}$. For simplicity we suppress the B_s and X_c momentum label in the rest of the chapter.

4.2 Decay rate and moments

The previous expression Eq. (4.22) is related to the hadronic tensor in Eq. (3.33) through a Laplace transform

$$
\begin{aligned}
C_{\mu\nu}(\boldsymbol{q}, t) &= \int_0^\infty \mathrm{d}\omega \, \frac{1}{2M_{B_s}} \langle B_s| \tilde{J}^\dagger_\mu(\boldsymbol{q}, 0) \delta(\hat{H} - \omega) \tilde{J}_\nu(\boldsymbol{q}, 0) |B_s\rangle \, e^{-\omega t} \\
&= \int_0^\infty \mathrm{d}\omega \, W_{\mu\nu}(\boldsymbol{q}, \omega) e^{-\omega t} \ ,
\end{aligned} \qquad (4.23)
$$

where we dropped the label $\boldsymbol{p}_{B_s}$ for simplicity, and where

$$
W_{\mu\nu}(\boldsymbol{q}, \omega) = \frac{1}{2M_{B_s}} \sum_{X_c} \delta(\omega - E_{X_c}) \langle B_s| \tilde{J}^\dagger_\mu(\boldsymbol{q}, 0) |X_c\rangle \langle X_c| \tilde{J}_\nu(\boldsymbol{q}, 0) |B_s\rangle \ . \qquad (4.24)
$$

Determining the hadronic tensor through the inversion of Eq. (4.23) presents an ill-posed inverse problem, similar to extracting hadronic spectral densities from Euclidean correlators. While it is relatively straightforward to reconstruct $C_{\mu\nu}$ from $W_{\mu\nu}$, the reverse process is highly challenging. There is no universal prescription to address the inverse-Laplace transform: common approaches rely on the maximum entropy method [167–169], the Bayesian approach [170], the sparse modelling approach [171], the Backus-Gilbert method [24, 28] and the Chebyshev-polynomial technique [26, 27].

Fortunately, for computing the inclusive decay rate and the moments, it is not necessary to directly calculate the hadronic tensor itself. Instead, we only need to compute integrals $\bar{X}^{(l)}(\boldsymbol{q}^2)$ in Eq. (3.80), which involve smearing the hadronic tensor with the leptonic tensor integrated over the lepton energy. Note that, without loss of generality, $\bar{X}^{(l)}(\boldsymbol{q}^2)$ can refer to the decay rate, as in Eq. (3.80), or to one of the moments $\bar{X}^{(l)}_H$ and $\bar{X}^{(l)}_L$ in Eqs. (3.119) and (3.120), respectively, where l refers to the order of the given

moment. Indeed, in general we can write

$$\bar{X}^{(l)}(\boldsymbol{q}^2) = \int_{\omega_{\min}}^{\omega_{\max}} \mathrm{d}\omega\, W^{\mu\nu}(\boldsymbol{q},\omega) k^{(l)}_{\mu\nu}(\boldsymbol{q},\omega)\,, \tag{4.25}$$

where $k^{(l)}_{\mu\nu}(\boldsymbol{q},\omega)$ represents a known kinematic factor dependent solely on energy and three-momentum. We can modify this expression by introducing a Heaviside step function $\theta(\omega_{\max}-\omega)$ and extending the integration limits to $\omega_{\max}\to\infty$ and $\omega_{\min}\to\omega_0$, where $\omega_0 \le \omega_{\min}$. This allows us to rewrite it as

$$\begin{aligned}\bar{X}^{(l)}(\boldsymbol{q}^2) &= \int_{\omega_0}^{\infty} \mathrm{d}\omega W^{\mu\nu}(\boldsymbol{q},\omega) k^{(l)}_{\mu\nu}(\boldsymbol{q},\omega)\theta(\omega_{\max}-\omega) \\ &= \int_{\omega_0}^{\infty} \mathrm{d}\omega W^{\mu\nu}(\boldsymbol{q},\omega) K^{(l)}_{\mu\nu}(\boldsymbol{q},\omega)\,,\end{aligned} \tag{4.26}$$

where we defined the *kernel function* $K^{(l)}_{\mu\nu}(\boldsymbol{q},\omega) = k^{(l)}_{\mu\nu}(\boldsymbol{q},\omega)\theta(\omega_{\max}-\omega)$. It is important to note that the value of ω_0 can be freely chosen within the range $0 \le \omega_0 \le \omega_{\min}$. This freedom exists because there are no states below the ground state energy $\omega_{\min}$, as indicated by Eq. (4.24). For example, in the case of $B_s \to X_c\, l\nu_l$ we have $\omega_{\min} = M_{D_s}$ for the contribution from the vector channel when the transferred momentum $\boldsymbol{q}$ approaches zero. We will later take advantage of this flexibility in selecting the value of ω_0.

Let us now discuss the process of obtaining $\bar{X}^{(l)}(\boldsymbol{q}^2)$ from lattice data for $C_{\mu\nu}(\boldsymbol{q},t)$. To begin with, we introduce a smoothing technique for the kernel $K^{(l)}_{\mu\nu}(\boldsymbol{q},\omega)$ by replacing the step function with a sigmoid function given by

$$\theta_\sigma(x) = \frac{1}{1+e^{-x/\sigma}}\,. \tag{4.27}$$

While it is necessary to eventually take the limit $\sigma \to 0$ to obtain the physical observables, smoothing is valuable for controlling and understanding the systematic effects involved in computation strategy. Following the approach in [25], we expand the smoothed kernel $K^{(l)}_{\sigma,\mu\nu}(\boldsymbol{q},\omega)$ as a polynomial of $e^{-a\omega}$ (setting $a=1$ for simplicity) up to a certain order N. This expansion [26] can be written as

$$K^{(l)}_{\sigma,\mu\nu}(\boldsymbol{q},\omega) \simeq c^{(l)}_{\mu\nu,0}(\boldsymbol{q},\sigma) + c^{(l)}_{\mu\nu,1}(\boldsymbol{q},\sigma)e^{-\omega} \cdots + c^{(l)}_{\mu\nu,N}(\boldsymbol{q},\sigma)e^{-\omega N}\,, \tag{4.28}$$

where we have $N+1$ coefficients $c^{(l)}_{\mu\nu,k}(\boldsymbol{q},\sigma)$. Consequently, the target quantity $\bar{X}^{(l)}_\sigma(\boldsymbol{q}^2)$, which now depends on the smearing parameter σ, can be computed as

$$\begin{aligned}\bar{X}^{(l)}_\sigma(\boldsymbol{q}^2) &= \int_{\omega_0}^{\infty} \mathrm{d}\omega\, W^{\mu\nu}(\boldsymbol{q},\omega) e^{-2\omega t_0} K^{(l)}_{\sigma,\mu\nu}(\boldsymbol{q},\omega;t_0) \\ &\simeq c^{(l)}_{\mu\nu,0}\int_{\omega_0}^{\infty} \mathrm{d}\omega\, W^{\mu\nu}(\boldsymbol{q},\omega) e^{-2\omega t_0} + c^{(l)}_{\mu\nu,1}\int_{\omega_0}^{\infty} \mathrm{d}\omega\, W^{\mu\nu}(\boldsymbol{q},\omega) e^{-2\omega t_0} e^{-\omega} + \dots \\ &\quad + c^{(l)}_{\mu\nu,N}\int_{\omega_0}^{\infty} \mathrm{d}\omega\, W^{\mu\nu}(\boldsymbol{q},\omega) e^{-2\omega t_0} e^{-\omega N}\,,\end{aligned} \tag{4.29}$$

where now $c^{(l)}_{\mu\nu,k} \equiv c^{(l)}_{\mu\nu,k}(\boldsymbol{q},\sigma;t_0)$. The factor $e^{-2\omega t_0}$ has been introduced, and compensated for in the new kernel $K^{(l)}_{\sigma,\mu\nu}(\boldsymbol{q},\omega;t_0) = e^{2\omega t_0}K^{(l)}_{\sigma,\mu\nu}(\boldsymbol{q},\omega)$, in order to avoid the equal-time matrix element $t_1 = t_2$, see Eq. (4.10), which contains contributions from the opposite time ordering corresponding to the unphysical $\bar{b}sc\bar{b}$ final states. Inserting now Eq. (4.23) we arrive at the compact expression

$$\bar{X}^{(l)}_{\sigma}(\boldsymbol{q}^2) = \sum_{k=0}^{N} c^{(l)}_{\mu\nu,k} C^{\mu\nu}(\boldsymbol{q}, k + 2t_0)\,, \tag{4.30}$$

which relates $C^{\mu\nu}(\boldsymbol{q},t)$, which can be computed on the lattice, to $\bar{X}^{(l)}_{\sigma}(\boldsymbol{q}^2)$. It is important to note that the expression provided is an approximation of $\bar{X}^{(l)}_{\sigma}(\boldsymbol{q}^2)$ due to the truncation at a finite value N. We follow the same convention for all similar quantities discussed in the subsequent sections. Furthermore, the order N of the polynomial approximation is directly linked to the temporal separation $t = t_2 - t_1$ of the two charged currents in the four-point function in Eq. (4.10). To complete the computation of the observables for a specific σ value, the next step involves performing the phase-space integration over the energy ω, as for example in Eq. (3.80) for the decay rate.

The most general expressions for the kernels related to the decay rate are

$$K^{(0)}_{\sigma,00}(\boldsymbol{q},\omega;t_0) = e^{2\omega t_0}\boldsymbol{q}^2\,\theta_\sigma\left(\omega_{\max}-\omega\right)\,, \tag{4.31}$$

$$K^{(0)}_{\sigma,ii}(\boldsymbol{q},\omega;t_0) = e^{2\omega t_0}(q_i^2-\boldsymbol{q}^2)\,\theta_\sigma\left(\omega_{\max}-\omega\right)\,, \tag{4.32}$$

$$K^{(0)}_{\sigma,ij}(\boldsymbol{q},\omega;t_0) \overset{i\neq j}{=} e^{2\omega t_0}q_iq_j\,\theta_\sigma\left(\omega_{\max}-\omega\right)\,, \tag{4.33}$$

$$K^{(1)}_{\sigma,0i}(\boldsymbol{q},\omega;t_0) = -e^{2\omega t_0}q_iq_0\,\theta_\sigma\left(\omega_{\max}-\omega\right)\,, \tag{4.34}$$

$$K^{(2)}_{\sigma,ii}(\boldsymbol{q},\omega;t_0) = e^{2\omega t_0}q_0^2\,\theta_\sigma\left(\omega_{\max}-\omega\right)\,, \tag{4.35}$$

where $\omega_{\max} \equiv \omega_{\max}(\boldsymbol{q}^2) = M_{B_s} - \sqrt{\boldsymbol{q}^2}$. For the transverse components we have

$$K^{\perp}_{\sigma,ii}(\boldsymbol{q},\omega;t_0) = e^{2\omega t_0}(q_i^2-\boldsymbol{q}^2)\left(1-\frac{q_0^2}{\boldsymbol{q}^2}\right)\,\theta_\sigma\left(\omega_{\max}-\omega\right)\,, \tag{4.36}$$

$$K^{\perp}_{\sigma,ij}(\boldsymbol{q},\omega;t_0) \overset{i\neq j}{=} e^{2\omega t_0}q_iq_j\left(1-\frac{q_0^2}{\boldsymbol{q}^2}\right)\,\theta_\sigma\left(\omega_{\max}-\omega\right)\,, \tag{4.37}$$

and for the longitudinal ones

$$K^{\parallel}_{\sigma,00}(\boldsymbol{q},\omega;t_0) = e^{2\omega t_0}\boldsymbol{q}^2\,\theta_\sigma\left(\omega_{\max}-\omega\right)\,, \tag{4.38}$$

$$K^{\parallel}_{\sigma,0i}(\boldsymbol{q},\omega;t_0) = -e^{2\omega t_0}q_0q_i\,\theta_\sigma\left(\omega_{\max}-\omega\right)\,, \tag{4.39}$$

$$K^{\parallel}_{\sigma,ij}(\boldsymbol{q},\omega;t_0) = e^{2\omega t_0}\frac{q_0^2}{\boldsymbol{q}^2}q_iq_j\,\theta_\sigma\left(\omega_{\max}-\omega\right)\,. \tag{4.40}$$

All the other combinations vanish. Note that the kernels $K^{(n)}_{H,\sigma,\mu\nu}(\boldsymbol{q},\omega;t_0)$ for the hadronic mass moment are proportional to the ones for the decay rate up to a factor $(M_X^2)^n = (\omega^2-\boldsymbol{q}^2)^n$.

For the lepton moments with $n = 1$ as in Eq. (3.129), which we will take as a case study later, we obtain explicitly the kernels

$$K^{(1)}_{L,\sigma,00}(\boldsymbol{q},\omega;t_0) = e^{2\omega t_0}\frac{1}{2}q_0\boldsymbol{q}^2\,\theta_\sigma\left(\omega_{\max}-\omega\right)\,, \tag{4.41}$$

$$K^{(1)}_{L,\sigma,0i}(\boldsymbol{q},\omega;t_0) = -e^{2\omega t_0}\frac{1}{2}q_0^2 q_i\,\theta_\sigma\left(\omega_{\max}-\omega\right)\,, \tag{4.42}$$

$$K^{(1)}_{L,\sigma,ij}(\boldsymbol{q},\omega;t_0) \overset{i\neq j}{=} e^{2\omega t_0}\frac{1}{2}q_0 q^i q^j\,\theta_\sigma\left(\omega_{\max}-\omega\right)\,, \tag{4.43}$$

$$K^{(1)}_{L,\sigma,ii}(\boldsymbol{q},\omega;t_0) = e^{2\omega t_0}\frac{1}{2}\left(q_0^2-\boldsymbol{q}^2-(q^i)^2\right)\,\theta_\sigma\left(\omega_{\max}-\omega\right)\,, \tag{4.44}$$

together with the antisymmetric kernel (indicated with "tilde")

$$\tilde{K}^{(1)}_{L,\sigma,ij}(\boldsymbol{q},\omega;t_0) = e^{2\omega t_0}\frac{1}{2}(q_0^2-\boldsymbol{q}^2)\sum_k \varepsilon^{ijk}q_k\,\theta_\sigma\left(\omega_{\max}-\omega\right)\,. \tag{4.45}$$

We have now presented the main idea of how to address the calculation of the quantities $\bar{X}^{(l)}(\boldsymbol{q}^2)$ and provided the explicit form of the kernels relevant for our study. In the remaining of this chapter we describe in practice the strategies adopted to perform the analysis of the lattice data for extracting the inclusive-decay observables.

4.3 Data analysis

In the previous section we discussed the problem of computing the inclusive decay rate and moments and how it can be translated into finding a suitable polynomial approximation for the kernel $K^{(l)}_{\sigma,\mu\nu}(\boldsymbol{q},\omega;t_0)$. Here we present two distinct approaches that we use to determine the expansion coefficients $c^{(l)}_{\mu\nu,k}$ given the lattice data for the ratio of correlation functions in Eq. (4.19). The aim is to compare how the two methods perform and determine if there is any advantage in using one instead of the other.

In principle, one could directly compute $\bar{X}^{(l)}_\sigma(\boldsymbol{q}^2)$ as defined in Eq. (4.30) from the lattice data for $C_{\mu\nu}(\boldsymbol{q},t)$. For example, for a given order N, the coefficients $c^{(l)}_{\mu\nu,k}$ in the power series for the analytically known kernel $K^{(l)}_{\sigma,\mu\nu}(\boldsymbol{q},\omega;t_0)$ could be determined via linear regression: this would allow to construct $\bar{X}^{(l)}_\sigma(\boldsymbol{q}^2)$ from the data for $C_{\mu\nu}(\boldsymbol{q},t)$. However, the number of available time slices in the window where $C_{\mu\nu}(\boldsymbol{q},t)$ can be extracted from the lattice data limits the order of the expansion. Moreover, extracting a significant signal for the observables becomes challenging due to the exponential decay of the signal-to-noise ratio [172, 173] as the Euclidean time separation $t_1 - t_{\text{src}}$ increases. Note that, given the structure of the four-point functions, this corresponds to small values of t for the correlator $C_{\mu\nu}(t)$. To address this issue, we need a *regulator* that balances the truncation-induced systematic errors and the statistical noise. Therefore, we outline two *regularisation approaches* that achieve this balance, one based on Chebyshev polynomials and the other based on the modified Backus-Gilbert method.

For completeness and more flexibility we introduce the following notation

$$\begin{aligned}\bar{X}^{(l)}_{\sigma}(\boldsymbol{q}^2) &= \int_{\omega_0}^{\infty} \mathrm{d}\omega\, W^{\mu\nu}(\boldsymbol{q},\omega) e^{-2\omega t_0} K^{(l)}_{\sigma,\mu\nu}(\boldsymbol{q},\omega;t_0) \\ &= \frac{1}{2M_{B_s}} \int_{\omega_0}^{\infty} \mathrm{d}\omega\, K^{(l)}_{\sigma,\mu\nu}(\boldsymbol{q},\omega;t_0) \langle B_s| \tilde{J}^{\mu\dagger}(\boldsymbol{q},0) e^{-\omega t_0} \delta(\hat{H}-\omega) e^{-\omega t_0} \tilde{J}^{\nu}(\boldsymbol{q},0) |B_s\rangle \\ &\equiv \langle \psi^{\mu}(\boldsymbol{q})| K^{(l)}_{\sigma,\mu\nu}(\boldsymbol{q},\hat{H};t_0) |\psi^{\nu}(\boldsymbol{q})\rangle \ ,\end{aligned} \tag{4.46}$$

where we made use of Eq. (4.24) and defined $|\psi^{\nu}(\boldsymbol{q})\rangle = e^{-\hat{H}t_0}\tilde{J}^{\nu}(\boldsymbol{q},0)|B_s\rangle / \sqrt{2M_{B_s}}$. Note that the Dirac delta $\delta(\hat{H}-\omega)$ has been introduced in order to restrict the integral over the physical states and that the kernel has been promoted to an operator, $K^{(l)}_{\sigma,\mu\nu}(\boldsymbol{q},\hat{H};t_0)$.

4.3.1 Chebyshev-polynomial approach

Chebyshev polynomials $T_k(\omega)$, defined on $-1 \leq \omega \leq 1$, provide an optimal approximation of functions under the L_∞-norm. For the case at hand we define *shifted Chebyshev polynomials* $\tilde{T}_k(\omega)$, which represent a family of polynomials in $e^{-\omega}$ defined on an arbitrary interval: we provide a summary of basic properties in App. C. Through the use of these shifted polynomials, the generic kernel function can be expanded up to order N as

$$K^{(l)}_{\sigma,\mu\nu}(\boldsymbol{q},\omega;t_0) = \frac{1}{2}\tilde{c}^{(l)}_{\mu\nu,0}\tilde{T}_0(\omega) + \sum_{k=1}^{N} \tilde{c}^{(l)}_{\mu\nu,k}\tilde{T}_k(\omega)\,, \tag{4.47}$$

where

$$\tilde{T}_k(x) = T_k(h(x)) = \sum_{j=0}^{k} \tilde{t}^{(k)}_j e^{-j\omega}\,, \tag{4.48}$$

and $h(x) = Ae^{-x} + B$ is a map $h : [\omega_0, \infty] \to [-1, 1]$, with A and B given in Eq. (C.28) and the coefficients $\tilde{t}^{(k)}_j$ given in Eq. (C.33). Thanks to the polynomials' orthogonality properties, the coefficients of the approximation can be computed by projecting the kernel function into the Chebyshev-polynomial basis as

$$\tilde{c}^{(l)}_{\mu\nu,k} = \int_{\omega_0}^{\infty} \mathrm{d}\omega\, K^{(l)}_{\sigma,\mu\nu}(\boldsymbol{q},\omega;t_0)\tilde{T}_k(\omega)\Omega_h(\omega)\,, \tag{4.49}$$

where the weight function $\Omega_h(x)$ is defined in Eq. (C.18). In this way, the expectation value of the kernel operator is

$$\langle \psi_\mu| K^{(l)}_{\sigma,\mu\nu}(\boldsymbol{q},\hat{H};t_0)|\psi_\nu\rangle = \frac{1}{2}\tilde{c}^{(l)}_{\mu\nu,0}\langle\psi_\mu|\tilde{T}_0(\hat{H})|\psi_\nu\rangle + \sum_{k=1}^{N}\tilde{c}^{(l)}_{\mu\nu,k}\langle\psi_\mu|\tilde{T}_k(\hat{H})|\psi_\nu\rangle \ , \tag{4.50}$$

where there is no summation over pairs of indices μ and ν. In order to exploit the bound on the Chebyshev polynomials in $|\tilde{T}_k(\omega)| \leq 1$, we divide the terms in the previous expression by the normalising factor $\langle\psi_\mu|\psi_\nu\rangle = C_{\mu\nu}(2t_0)$. For a more compact notation we define

$$\langle K_\sigma^{(l)}\rangle_{\mu\nu} \equiv \frac{\langle\psi_\mu|\, K_{\mu\nu}^{(l)}(\boldsymbol{q},\hat{H};t_0)\,|\psi_\nu\rangle}{\langle\psi_\mu|\psi_\nu\rangle}\,, \qquad \langle\tilde{T}_k\rangle_{\mu\nu} \equiv \frac{\langle\psi_\mu|\,\tilde{T}_k(\hat{H})\,|\psi_\nu\rangle}{\langle\psi_\mu|\psi_\nu\rangle}\,, \tag{4.51}$$

with $\langle\tilde{T}_k\rangle_{\mu\nu}$ being the *Chebyshev matrix elements*, for which $|\langle\tilde{T}_k\rangle_{\mu\nu}| \leq 1$, such that

$$\langle K_\sigma^{(l)}\rangle_{\mu\nu} = \frac{1}{2}\tilde{c}_{\mu\nu,0}^{(l)}\langle\tilde{T}_0\rangle_{\mu\nu} + \sum_{k=1}^{N}\tilde{c}_{\mu\nu,k}^{(l)}\langle\tilde{T}_k\rangle_{\mu\nu}\,. \tag{4.52}$$

The generic state $\bar{X}_\sigma(\boldsymbol{q}^2)$ now reads

$$\bar{X}_\sigma^{(l)}(\boldsymbol{q}^2) = \sum_{\{\mu,\nu\}}\langle\psi_\mu|\psi_\nu\rangle\,\langle K_\sigma^{(l)}\rangle_{\mu\nu}\,, \tag{4.53}$$

and in particular for the decay rate,

$$\bar{X}_\sigma^{(0)}(\boldsymbol{q}^2) = C_{00}(2t_0)\langle K_\sigma^{(0)}\rangle_{00} + \sum_i C_{ii}(2t_0)\langle K_\sigma^{(0)}\rangle_{ii} + \sum_{i\neq j} C_{ij}(2t_0)\langle K_\sigma^{(0)}\rangle_{ij}\,, \tag{4.54}$$

$$\bar{X}_\sigma^{(1)}(\boldsymbol{q}^2) = \sum_i\Big(C_{0i}(2t_0)\langle K_\sigma^{(1)}\rangle_{0i} + C_{i0}(2t_0)\langle K_\sigma^{(1)}\rangle_{i0}\Big)\,, \tag{4.55}$$

$$\bar{X}_\sigma^{(2)}(\boldsymbol{q}^2) = \sum_i C_{ii}(2t_0)\langle K_\sigma^{(2)}\rangle_{ii}\,. \tag{4.56}$$

The transverse component in Eq. (3.85) is given by

$$\bar{X}_\sigma^{\perp}(\boldsymbol{q}^2) = \sum_i C_{ii}(2t_0)\langle K_\sigma^{\perp}\rangle_{ii} + \sum_{i\neq j} C_{ij}(2t_0)\langle K_\sigma^{\perp}\rangle_{ij}\,, \tag{4.57}$$

together with the longitudinal one in Eq. (3.84)

$$\begin{aligned}\bar{X}_\sigma^{\parallel}(\boldsymbol{q}^2) = C_{00}(2t_0)\;\langle K_\sigma^{\parallel}\rangle_{00} + \sum_{i,j} C_{ij}(2t_0)\langle K_\sigma^{\parallel}\rangle_{ij} \\ + \sum_i\Big(C_{0i}(2t_0)\langle K_\sigma^{\parallel}\rangle_{0i} + C_{i0}(2t_0)\langle K_\sigma^{\parallel}\rangle_{i0}\Big)\,.\end{aligned} \tag{4.58}$$

The Chebyshev matrix elements can be constructed directly from the lattice data using

$$\frac{\langle\psi_\mu|\,e^{-\hat{H}t}\,|\psi_\nu\rangle}{\langle\psi_\mu|\psi_\nu\rangle} = \frac{C_{\mu\nu}(t+2t_0)}{C_{\mu\nu}(2t_0)} \equiv \bar{C}_{\mu\nu}(t)\,, \tag{4.59}$$

such that we can relate $\langle\tilde{T}_k\rangle_{\mu\nu}$ to the correlator $\bar{C}_{\mu\nu}$. Recalling that a generic function of an operator can be written in terms of its eigenvalues, $f(\hat{H}) = \sum_X f(E_X)P_X$, where $P_X = |X\rangle\langle X|$ is a projector on the state $|X\rangle$, which is part of a complete set of states,

$I = \sum_X |X\rangle \langle X|$, we get

$$\begin{aligned}
\langle \tilde{T}_k \rangle_{\mu\nu} &= \frac{\langle \psi_\mu | \tilde{T}_k(\hat{H}) | \psi_\nu \rangle}{\langle \psi_\mu | \psi_\nu \rangle} = \sum_X \frac{\langle \psi_\mu | \tilde{T}_k(\hat{H}) | X \rangle \langle X | \psi_\nu \rangle}{\langle \psi_\mu | \psi_\nu \rangle} \\
&= \sum_X \tilde{T}_k(E_X) \frac{\langle \psi_\mu | X \rangle \langle X | \psi_\nu \rangle}{\langle \psi_\mu | \psi_\nu \rangle} = \sum_X \sum_{j=0}^{k} \tilde{t}_j^{(k)} e^{-jE_X} \frac{\langle \psi_\mu | X \rangle \langle X | \psi_\nu \rangle}{\langle \psi_\mu | \psi_\nu \rangle} \\
&= \tilde{t}_0^{(k)} \sum_X \frac{\langle \psi_\mu | X \rangle \langle X | \psi_\nu \rangle}{\langle \psi_\mu | \psi_\nu \rangle} + \tilde{t}_1^{(k)} \sum_X e^{-E_X} \frac{\langle \psi_\mu | X \rangle \langle X | \psi_\nu \rangle}{\langle \psi_\mu | \psi_\nu \rangle} \\
&\quad + \cdots + \tilde{t}_k^{(k)} \sum_X e^{-kE_X} \frac{\langle \psi_\mu | X \rangle \langle X | \psi_\nu \rangle}{\langle \psi_\mu | \psi_\nu \rangle} \\
&= \tilde{t}_0^{(k)} \bar{C}_{\mu\nu}(0) + \tilde{t}_1^{(k)} \bar{C}_{\mu\nu}(1) + \cdots + \tilde{t}_k^{(k)} \bar{C}_{\mu\nu}(k) \,,
\end{aligned} \tag{4.60}$$

such that

$$\langle \tilde{T}_k \rangle_{\mu\nu} = \sum_{j=0}^{k} \tilde{t}_j^{(k)} \bar{C}_{\mu\nu}(j) \,. \tag{4.61}$$

Overall the full Chebyshev expansion of the kernel reads

$$\begin{aligned}
\langle K_\sigma^{(l)} \rangle_{\mu\nu} &= \frac{1}{2} \tilde{c}_{\mu\nu,0}^{(l)} \langle \tilde{T}_0 \rangle_{\mu\nu} + \sum_{k=1}^{N} \tilde{c}_{\mu\nu,k}^{(l)} \langle \tilde{T}_k \rangle_{\mu\nu} = \frac{1}{2} \tilde{c}_{\mu\nu,0}^{(l)} + \sum_{k=1}^{N} \tilde{c}_{\mu\nu,k}^{(l)} \sum_{j=0}^{k} \tilde{t}_j^{(k)} \bar{C}_{\mu\nu}(j) \\
&= \bar{C}_{\mu\nu}(0) \left(\frac{1}{2} \tilde{c}_{\mu\nu,0}^{(l)} \tilde{t}_0^{(0)} + \tilde{c}_{\mu\nu,1}^{(l)} \tilde{t}_0^{(1)} + \cdots + \tilde{c}_{\mu\nu,N}^{(l)} \tilde{t}_0^{(N)} \right) \\
&\quad + \bar{C}_{\mu\nu}(1) \left(\tilde{c}_{\mu\nu,1}^{(l)} \tilde{t}_1^{(1)} + \tilde{c}_{\mu\nu,2}^{(l)} \tilde{t}_1^{(2)} + \cdots + \tilde{c}_{\mu\nu,N}^{(l)} \tilde{t}_1^{(N)} \right) + \cdots \\
&\quad + \bar{C}_{\mu\nu}(N) \left(\tilde{c}_{\mu\nu,N}^{(l)} \tilde{t}_N^{(N)} \right) \\
&= \sum_{k=0}^{N} \bar{C}_{\mu\nu}(k) \sum_{j=k}^{N} \tilde{c}_{\mu\nu,j}^{(l)} \left(1 - \frac{1}{2} \delta_{0j} \right) \tilde{t}_k^{(j)} \,,
\end{aligned} \tag{4.62}$$

where we recall that $\langle \tilde{T}_0 \rangle_{\mu\nu} = 1$ by definition. Collecting the coefficients into

$$\bar{c}_{\mu\nu,k}^{(l)} \equiv \sum_{j=k}^{N} \tilde{c}_{\mu\nu,j}^{(l)} \tilde{t}_k^{(j)} \left(1 - \frac{1}{2} \delta_{0j} \right) \,, \tag{4.63}$$

we arrive at the compact expression

$$\langle K_\sigma^{(l)} \rangle_{\mu\nu} = \sum_{k=0}^{N} \bar{c}_{\mu\nu,k}^{(l)} \bar{C}_{\mu\nu}(k) \,. \tag{4.64}$$

This expression has now the advantage of relating directly the approximation of the kernel operator to the lattice data $\bar{C}_{\mu\nu}$ instead of the Chebyshev matrix elements $\langle \tilde{T}_k \rangle_{\mu\nu}$. Furthermore, this expression may be quite convenient to assess the effect of the excited

states, particularly those above $\omega_{\max}$. In particular, we may think of the data as a spectral sum over lower- and higher-energy states $X = \{X_L, X_H\}$, as

$$\begin{aligned}\bar{C}_{\mu\nu}(t) &= \sum_X e^{-tE_X} \frac{\langle\psi_\mu|X\rangle\langle X|\psi_\nu\rangle}{\langle\psi_\mu|\psi_\nu\rangle} \\ &= \sum_{X_L} e^{-tE_{X_L}} \frac{\langle\psi_\mu|X_L\rangle\langle X_L|\psi_\nu\rangle}{\langle\psi_\mu|\psi_\nu\rangle} + \sum_{X_H} e^{-tE_{X_H}} \frac{\langle\psi_\mu|X_H\rangle\langle X_H|\psi_\nu\rangle}{\langle\psi_\mu|\psi_\nu\rangle} \\ &\equiv \bar{C}^L_{\mu\nu}(t) + \bar{C}^H_{\mu\nu}(t)\,.\end{aligned} \tag{4.65}$$

Considering that the kernel $K^{(l)}_{\sigma,\mu\nu}$ contains a (smooth) step function to cut the high energy modes $E_{X_H} > \omega_{\max}$ (in the limit $\sigma \to 0$), this implies that, assuming the polynomial approximation to be good enough, the coefficients $\bar{c}^{(l)}_{\mu\nu,k}$ are such that

$$\sum_{k=0}^{N} \bar{c}^{(l)}_{\mu\nu,k} \bar{C}^H_{\mu\nu}(k) \approx 0\,, \quad min(E_{X_H}) > \omega_{\max}\,. \tag{4.66}$$

This shows the role of the polynomial approximation above $\omega_{\max}$ and in particular the role of the step function, whose effect is now encoded in the coefficients $\bar{c}^{(l)}_{\mu\nu,k}$.

While the coefficients $\tilde{c}^{(l)}_{\mu\nu,k}$ and $\bar{c}^{(l)}_{\mu\nu,k}$ are known analyticaly, $\bar{C}_{\mu\nu}(k)$ needs to be computed on the lattice using Monte-Carlo methods. The resulting statistical error on $\bar{C}_{\mu\nu}(k)$ can lead to violations of the bound $|\langle\tilde{T}_k\rangle_{\mu\nu}| \leq 1$ despite the above normalisation when solving the linear system (as in Eq. (C.39))

$$\begin{pmatrix} \bar{C}_{\mu\nu}(0) \\ \bar{C}_{\mu\nu}(1) \\ \vdots \\ \vdots \\ \bar{C}_{\mu\nu}(n) \end{pmatrix} = \begin{pmatrix} \tilde{a}^{(0)}_0 & 0 & \cdots & \cdots & 0 \\ \tilde{a}^{(1)}_0 & \tilde{a}^{(1)}_1 & 0 & \cdots & 0 \\ \vdots & \vdots & \ddots & \ddots & \vdots \\ \vdots & \vdots & & \ddots & 0 \\ \tilde{a}^{(n)}_0 & \tilde{a}^{(n)}_1 & \cdots & \cdots & \tilde{a}^{(n)}_n \end{pmatrix} \begin{pmatrix} \langle\tilde{T}_0\rangle_{\mu\nu} \\ \langle\tilde{T}_1\rangle_{\mu\nu} \\ \vdots \\ \vdots \\ \langle\tilde{T}_n\rangle_{\mu\nu} \end{pmatrix}. \tag{4.67}$$

This can however be avoided in a Bayesian analysis of the correlator data, imposing the bound in terms of priors. In particular, this bound has the effect of reducing the variance of Eq. (4.52), as we will show in Sec. 6.2.3. One way to impose the constraint is to use a Gaussian prior on some internal normally-distributed parameters $\langle\tilde{\tau}_k\rangle_{\mu\nu} \sim \mathcal{N}(0,1)$ and convert it to a flat prior on the interval $[-1,1]$ using the map $f(x) = \mathrm{erf}(x/\sqrt{2})$ such that $\langle\tilde{T}_k\rangle_{\mu\nu} = f(\langle\tilde{\tau}_k\rangle_{\mu\nu})$. We refer to App. E.3 for a discussion on the fitting procedure that we adopt.

4.3.2 Backus-Gilbert method

A different way to approach the polynomial approximation of the kernel is given by a variant of the Backus-Gilbert method [174] proposed in [28, 175]. In this work we introduce a generalisation of this method in order to consider a more flexible scenario which allows us to choose polynomial bases that simplify the numerical treatment. Although what we propose is mathematically equivalent to the approach in [176], our formulation may have the advantage of avoiding some of the numerical technicalities that arise in the original version. Note that we adopt a different notation with respect to the original works (we use F instead of W for the final functional to avoid confusion with the hadronic tensor).

The Backus-Gilbert method with our generalisation is presented in detail in App. D. Here we briefly present the central idea in order to highlight the main features relevant for the data analysis performed in this work. The strategy consists in addressing the reconstruction of a given kernel $K^{(l)}_{\sigma,\mu\nu}$ of the form

$$K^{(l)}_{\sigma,\mu\nu}(\boldsymbol{q},\omega;t_0) = \sum_{k=0}^{N} g^{(l)}_{\mu\nu,k}\tilde{P}_k(\omega)\,, \tag{4.68}$$

where $\tilde{P}_k(\omega) = \sum_{j=0}^{k}\tilde{p}_j^{(k)}e^{-j\omega}$ are a basis of functions with domain in $[\omega_0,\infty)$, and $g^{(l)}_{\mu\nu,k} \equiv g^{(l)}_{\mu\nu,k}(\boldsymbol{q},\sigma;t_0)$ is a set of coefficients. In order to determine them, the strategy is to minimise the functional [28, 175]

$$F^{(l)}_{\mu\nu,\lambda}[g] = (1-\lambda)\frac{A^{(l)}_{\mu\nu}[g]}{A^{(l)}_{\mu\nu}[0]} + \lambda B^{(l)}_{\mu\nu}[g]\,, \tag{4.69}$$

where

$$A^{(l)}_{\mu\nu}[g] = \int_{\omega_0}^{\infty}\mathrm{d}\omega\,\Omega(\omega)\left[K^{(l)}_{\sigma,\mu\nu}(\boldsymbol{q},\omega;t_0) - \sum_{k=0}^{N} g^{(l)}_{\mu\nu,k}\tilde{P}_k(\omega)\right]^2 \tag{4.70}$$

is the L_2-norm of the difference between the target kernel function and its reconstruction, weighted with a smooth function $\Omega(\omega)$, and

$$B^{(l)}_{\mu\nu}[g] = \sum_{j,k=0}^{N} g^{(l)}_{\mu\nu,j}\mathrm{Cov}(\bar{C}^{P}_{\mu\nu}(j),\bar{C}^{P}_{\mu\nu}(k))g^{(l)}_{\mu\nu,k} \tag{4.71}$$

is the variance of the corresponding channel $\bar{X}^{(l)}_{\mu\nu}$, with $\bar{C}^{P}_{\mu\nu}(k) = \sum_{j=0}^{k}\tilde{p}_j^{(k)}\bar{C}_{\mu\nu}(j)$. The functional $F^{(l)}_{\mu\nu,\lambda}$ encodes the information about both systematic and statistical errors, whose interplay is controlled by the parameter $\lambda \in [0,1)$, which in principle can be chosen by hand. The values of the coefficients $g^{(l)}_{\mu\nu,k}(\lambda)$ for each λ are given by the

variational principle, i.e.

$$g^{(l)}_{\mu\nu,k}(\lambda) \quad \leftrightarrow \quad \frac{\partial F^{(l)}_{\mu\nu,\lambda}}{\partial g^{(l)}_{\mu\nu,k}} = 0\,. \tag{4.72}$$

We can now devise a method to find the optimal λ^*, which balance systematic and statistical errors. Following [175], we can evaluate the functional $F^{(l)}_{\mu\nu,\lambda}$ at its minimum i.e. $F^{(l)}_{\mu\nu}(\lambda) = F^{(l)}_{\mu\nu,\lambda}[g(\lambda)]$, which then becomes a function of λ, and require that λ^* maximises $F^{(l)}_{\mu\nu}(\lambda)$, $\frac{\mathrm{d}F^{(l)}_{\mu\nu}(\lambda)}{\mathrm{d}\lambda}\Big|_{\lambda^*} = 0$. This choice corresponds to $A^{(l)}_{\mu\nu}[g^*]/A^{(l)}_{\mu\nu}[0] = B^{(l)}_{\mu\nu}[g^*]$, i.e. an optimal balance between statistical and systematic errors. This is the prescription we follow and take $g^{*(l)}_{\mu\nu,k} \equiv g^{(l)}_{\mu\nu,k}(\lambda^*)$.

Following the steps for the Chebyshev approach we get for the kernel

$$\langle K^{(l)}_\sigma \rangle_{\mu\nu} = \sum_{k=0}^{N} g^{*(l)}_{\mu\nu,k} \langle \tilde{P}_k \rangle_{\mu\nu}\,, \tag{4.73}$$

$$\langle \tilde{P}_k \rangle_{\mu\nu} = \frac{\langle \psi_\mu |\, \tilde{P}_k(\hat{H})\, | \psi_\nu \rangle}{\langle \psi_\mu | \psi_\nu \rangle} = \sum_{j=0}^{k} \tilde{p}^{(k)}_j \frac{\langle \psi_\mu |\, e^{-j\hat{H}}\, | \psi_\nu \rangle}{\langle \psi_\mu | \psi_\nu \rangle} = \bar{C}^P_{\mu\nu}(k)\,. \tag{4.74}$$

In particular, considering the domain $\omega \in [\omega_0, \infty)$ of the kernel functions and the polynomials, we focus on two choices:

- *exponential Backus-Gilbert:* $\tilde{P}_k(\omega) = e^{-k\omega}$ and $\Omega(\omega) = 1$ (and set $g^{(l)}_{\mu\nu,0} = 0$ by hand, as in the original proposal [28]);
- *Chebyshev Backus-Gilbert:* $\tilde{P}_k(\omega) = \tilde{T}_k(\omega)$, i.e. the shifted Chebyshev polynomials with $\Omega(\omega) = 1/\sqrt{e^{(\omega-\omega_0)} - 1}$ being the weight in Eq. (C.18) that enters in the definition of the scalar product.

CHAPTER 5

SIMULATION AND DATA ANALYSIS DETAILS

After outlining the theoretical framework for treating inclusive B_s-meson decays on the lattice in Chap. 4, we now turn to the details of the simulation. The focus of this work is a purely qualitative understanding of the method and we therefore perform a pilot study using a single ensemble for a $24^3 \times 64$ lattice. We make no attempt to determine a proper error budget to extract any sort of phenomenological prediction. In particular, the goal is to test the methods developed and discussed in Chap. 4 and to build a solid strategy to reliably study inclusive decays on the lattice, which in the future can be extended by comprehensive studies of systematic effects.

In Sec. 5.1 we discuss the details of the simulation and the lattice setup. In Sec. 5.2 we discuss the fundamentals of the data analysis and show some of the basic properties of the two-, three- and four-point correlation functions obtained from the gauge ensemble used, together with the details of the renormalisation procedure adopted.

5.1 Lattice setup

Our calculation is based on a $24^3 \times 64$ lattice with 2+1-flavour domain-wall fermion (DWF) [111, 114] gauge-field ensembles with the Iwasaki gauge action [101] taken from the RBC/UKQCD Collaboration [177] at lattice spacing $a^{-1} = 1.785(5)\,\text{GeV}$ (corresponding to $a \simeq 0.11\,\text{fm}$), pion mass $M_\pi \simeq 340\,\text{MeV}$ and close-to-physical strange-quark mass. The computations have been performed with the Grid [178–180] and Hadrons [181] software packages.

We use the same simulation parameters RBC/UKQCD is using in the heavy-light meson projects on exclusive semileptonic $B_{(s)}$ meson decays [150, 182–184]. In particular, the valence-strange quark is simulated using DWF, whereas the valence-charm quark is

simulated by using the Möbius DWF action [185,186]. Their masses are tuned such that mesons containing bottom, charm and strange valence quarks have masses close to the physical ones. The bottom quark cannot currently be simulated with DWF and some EFT-based action is required; this will likely be overcome in the future. The b quark has then been simulated at its physical mass using the Columbia formulation of the relativistic-heavy-quark (RHQ) action [104,105], which is based on the Fermilab heavy quark action [106].

For the computation we average over 120 statistically independent gauge configurations, and on each configuration the measurements are performed on 8 different linearly spaced source time planes. We use $\mathbb{Z}_2$ wall sources [131,132,187] to improve the signal. We induce 10 different momenta using partially twisted boundary conditions [98,99] for the charm quark with the same momentum in all three spatial directions. All other momenta in the Fourier sums in the expressions of two-, three- and four-point functions are set to zero. Considering $\boldsymbol{q} = 2\pi\boldsymbol{\theta}/L$ in lattice units we have $\boldsymbol{\theta} \equiv (\theta, \theta, \theta)$, where θ indicates the twist. We choose them such that all the momenta are linearly spaced in $\boldsymbol{q}^2$, i.e. $\theta_k = 1.90\sqrt{\frac{k}{3}}$ for $k = 0, 1, \ldots, 7$, where the factor 1.90 is determined by the value of $\boldsymbol{q}^2_{\text{max}} = 1.83$ in lattice units. We also take $\theta = 1.90\sqrt{\frac{1}{9}}$ and $\theta = 1.90\sqrt{\frac{2}{9}}$ to increase the resolution in $\boldsymbol{q}^2$ for small momenta. The large momenta induced may present non-negligible cutoff effects: since our work is purely qualitative, we do not address them at this stage and leave their treatment for future studies.

We compute two-point functions for both B_s and D_s. As discussed in Sec. 4.1, for B_s we consider three cases at zero momentum $C^{LS}_{B_s}(t, t_{\text{src}})$, $C^{SL}_{B_s}(t, t_{\text{src}})$ and $C^{SS}_{B_s}(t, t_{\text{src}})$ with different smearing combinations, as indicated by the superscripts "L" (local) and "S" (smeared). The smeared-smeared $C^{SS}_{B_s}(t, t_{\text{src}})$ is also used to determine the renormalisation constant together with the three-point function. The sources are smeared gauge-invariantly using Jacobi iteration [188, 189] using the same parameters as in RBC/UKQCD's study of exclusive semileptonic decays in [184,190,191].

The D_s correlators are relevant mainly for the analysis of the ground-state limit. We compute the smeared-smeared correlator $C^{SS}_{D_s}(\boldsymbol{q}, t, t_{\text{src}})$ and the local-smeared correlator $C^{LS}_{D_s}(\boldsymbol{q}, t, t_{\text{src}})$: the first one is used directly in combination with the three-point functions for the exclusive-decay analysis, whereas the second one is used to extract the D_s-meson energies at different momenta.

We also compute three-point correlators for the $B_s \to D_s\, l\nu_l$ process

$$C^{SS}_{D_s B_s,\mu}(\boldsymbol{q}, t_{\text{snk}}, t, t_{\text{src}}) = \sum_{\boldsymbol{x}_{\text{snk}}, \boldsymbol{x}} \langle \mathcal{O}^S_{D_s}(x_{\text{snk}}) V_\mu(\boldsymbol{x}, t) \mathcal{O}^{S\dagger}_{B_s}(x_{\text{src}}) \rangle \,. \tag{5.1}$$

Following the analysis of [150, 182, 183], we extract its form factors and compare with our inclusive results. The momentum is carried by the charm quark through twisted boundary conditions, $\boldsymbol{q} = 2\pi\boldsymbol{\theta}/L$. We use a source-sink separation of $t_{\text{snk}} - t_{\text{src}} = 20$ in

lattice units. The latter has been taken from other works [184] as initial guidance, but it is certainly to be studied more carefully in future calculations.

We now move to the four-point correlators defined in Eq. (4.10), which are the building blocks in the computation of inclusive processes. We use the same source-sink separation as for the three-point functions, i.e., $t_{\rm snk} - t_{\rm src} = 20$ in lattice units. The current $J_\mu^\dagger$ is fixed at the time slice $t_2 = t_{\rm src} + 14$, such that the time dependence is enclosed in $0 \leq t \leq 14$ with $t = t_2 - t_1$. For this choice we find ground state saturation at the points where we insert the currents. In practice, referring to Fig. 4.3, the contractions are performed between a b-quark propagator $G_b(x_1, x_{\rm src})$ and a sequential propagator $\Sigma_{cbs}(x_1, x_{\rm src})$. For the latter, we first propagate the s quark to point $x_{\rm snk}$, starting from a $\mathbb{Z}_2$ wall source at $t_{\rm src}$; we then use it as a sequential source at fixed $t_{\rm snk}$ with zero momentum to propagate the b quark. The b quark is propagated to point x_2, and it is then used again as a source with a specific choice of gamma matrix corresponding to the current $J_\mu^\dagger(x_2)$ and the momentum insertion to propagate the c quark.

As before, the momentum $\boldsymbol{q}$ induced through partially twisted boundary conditions is carried by the c quark. Given that we are dealing with $(V-A)$ currents, we consider all possible combinations of $J_\mu^\dagger(x_2)$ and $J_\nu(x_1)$, i.e. $V_\mu^\dagger V_\nu, V_\mu^\dagger A_\nu, A_\mu^\dagger V_\nu, A_\mu^\dagger A_\nu$. However, in the limit of massless leptons the combinations $A_\mu^\dagger V_\nu$ and $V_\mu^\dagger A_\nu$ do no contribute to the total decay rate. Indeed, these terms are related to the structure function W_3 as $W_{ij}^{AV} + W_{ij}^{VA} = i\epsilon_{ij0k} q^k W_3$, as can be seen analysing parity in Eq. (3.56), which does not contribute to the total decay rate for $m_l = 0$.

For all the three-point and four-point functions we always average over the spatial directions given that the momentum is the same in all three directions. Note in particular that for the four-point correlators we have to average separately over $J_i^\dagger J_i$ and $J_i^\dagger J_k$ with $i \neq k$, as can be seen from Eq. (3.56).

5.2 Statistical analysis

We now briefly discuss the details of the data analysis, recalling first the very basics of error propagation and refer to other sources for a more extensive discussion (see for example [192, 193]).

Considering a primary observable x, i.e. an observable that is directly measured through lattice simulations, the mean $\langle x \rangle$ and variance $\sigma_x^2 = \langle (x - \langle x \rangle)^2 \rangle$ can be estimated straightforwardly through the *sample mean* $\bar{x}$ and the *sample variance* s_x^2 as

$$\bar{x} = \frac{1}{N_{\rm config}} \sum_{i=1}^{N_{\rm config}} x_i \,, \quad s_x^2 = \frac{1}{N_{\rm config}} \sum_{i=1}^{N_{\rm config}} (x_i - \bar{x})^2 \,, \tag{5.2}$$

where N_{config} is the number of independent measurements and x_i the actual measurement on a given gauge configuration. We assume in general that the sample variance is a good estimator and therefore simply refer to it as σ_x^2 in the rest of the manuscript. For a secondary observable $y = f(\boldsymbol{x})$ that depends on a set of primary observables $\boldsymbol{x} = (x^{(1)}, x^{(2)}, \dots)$ through a generic function f, the mean and the variance are estimated as

$$\bar{y} = f(\bar{\boldsymbol{x}}) \,, \quad s_y^2 = \boldsymbol{\nabla} f^T \cdot \boldsymbol{\sigma} \cdot \boldsymbol{\nabla} f \,, \tag{5.3}$$

where $\boldsymbol{\nabla} f \equiv (\partial f/\partial x^{(1)}, \partial f/\partial x^{(2)}, \dots)$ is the gradient of the funcion f and $\boldsymbol{\sigma}$ is the estimator of the covariance matrix $\text{Cov}(x^{(i)}, x^{(j)}) = \langle (x^{(i)} - \langle x^{(i)} \rangle)(x^{(j)} - \langle x^{(j)} \rangle) \rangle$, computed as

$$\boldsymbol{\sigma}_{ij} = \frac{1}{N_{\text{config}}} \sum_{k,l=1}^{N_{\text{config}}} (x_k^{(i)} - \bar{x}^{(i)})(x_l^{(j)} - \bar{x}^{(j)}) \,. \tag{5.4}$$

The error propagation for secondary observables requires the computation of the gradient of the given function f, whose calculation may be rather involved. To overcome this, we can rely on methods that automatically account for the correct error propagation without requiring the knowledge of the function derivatives.

In particular, in this work we make use of the bootstrap resampling method [194]. Given a number N_{config} independent measurements $\mathcal{D} = \{x_1, x_2, \dots, x_{N_{\text{config}}}\}$ of the primary observable x, we create N_{b} bootstrap samples $\{x_1^{\text{b}}, x_2^{\text{b}}, \dots, x_{N_b}^{\text{b}}\}$, where

$$x_i^{\text{b}} = \frac{1}{N_{\text{config}}} \sum_{j=1}^{N_{\text{config}}} x_{i,j}^{\text{b}} \,. \tag{5.5}$$

where $\mathcal{D}_i^b = \{x_{i,1}^{\text{b}}, x_{i,2}^{\text{b}}, \dots, x_{i,N_{\text{config}}}^{\text{b}}\}$ is a set of N_{config} measurements randomly sampled from the original dataset $\mathcal{D}$. The mean and variance can then be computed as

$$\bar{x}^b = \frac{1}{N_{\text{b}}} \sum_{i=1}^{N_{\text{b}}} x_i^b \,, \quad (s_x^b)^2 = \frac{1}{N_{\text{b}}} \sum_{i=1}^{N_{\text{b}}} (x_i^b - \bar{x}^b)^2 \,, \tag{5.6}$$

Note that these estimators are not unbiased and therefore $\bar{x}^b \neq \bar{x}$. The difference $\bar{x}^b - \bar{x}$ is typically negligible, but it gives an idea of how far the result may be from the mean $\langle x \rangle$. The final measurement is quoted as $\bar{x}^b \pm s_x^b$.

A secondary observable $y = f(\boldsymbol{x}) = f(x^{(1)}, x^{(2)}, \dots)$ can now be computed in the same way as

$$\bar{y}^b = f(\bar{\boldsymbol{x}}^b) \,, \quad (s_y^b)^2 = \frac{1}{N_{\text{b}}} \sum_{i=1}^{N_{\text{b}}} (y_i^b - \bar{y}^b)^2 \,. \tag{5.7}$$

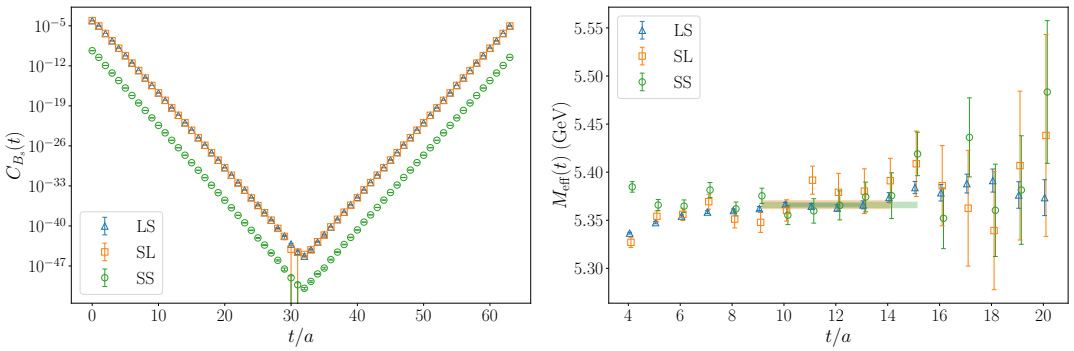

FIGURE 5.1: B_s two-point correlators at zero momentum (left) and corresponding effective mass (right) for all the combinations of smearing. The horizontal lines correspond to the fitted values of the mass determined through a fit to the correlation functions with the ansatz $C^{XY}_{B_s}(t) = 2A^{XY}e^{-T/2}\cosh(E(T/2-t))$.

where $y^b_i = f(x^{(1)b}_i, x^{(2)b}_i, \dots)$. It can be shown explicitly that this variance estimator agrees with the previous one obtained with standard error propagation. The bootstrap approach can then be easily implemented numerically without any specific knowledge of the function f. For the analysis in this work we use $N_b = 1000$.

The fits are performed through a maximum likelihood method with a frequentist approach, as detailed in App. E.1. The only exception is given by the fits to extract the Chebyshev matrix elements as described in Sec. 6.2.1 and in Apps. E.2 and E.3. The latter have been performed partially using the library *lsqfit* [195, 196]. The data analysis has been performed using the lattice data analysis package *labc* [197] (under construction).

5.2.1 Two-point correlators

Let us give some details of the correlation functions from the gauge ensemble under study. The B_s two-point functions for all the three combination of smearing "*LS*", "*SL*" and "*SS*" are plotted in Fig. 5.1 together with the effective mass defined as

$$M^{XY}_{\text{eff},B_s}(t) = -\ln\left(\frac{C^{XY}_{B_s}(t+1)}{C^{XY}_{B_s}(t)}\right). \tag{5.8}$$

The masses are determined through a fit to the correlator using the ansatz in Eq. (2.93). The details of the fits are reported in Tab. 5.1.

The final value we use for the B_s mass is taken from the LS correlator and is given by

$$M_{B_s} = 5.3659(19)\,\text{GeV}\,, \tag{5.9}$$

which is fully compatible with the PDG value $M^{\text{PDG}}_{B_s} = 5366.92(10)\,\text{MeV}$, as expected thanks to the RHQ tuning in [184, 190]. The amplitude $A^{LL} = |\langle 0|\mathcal{O}^L_{B_S}|B_s(\boldsymbol{p}_{B_s})\rangle|^2$,

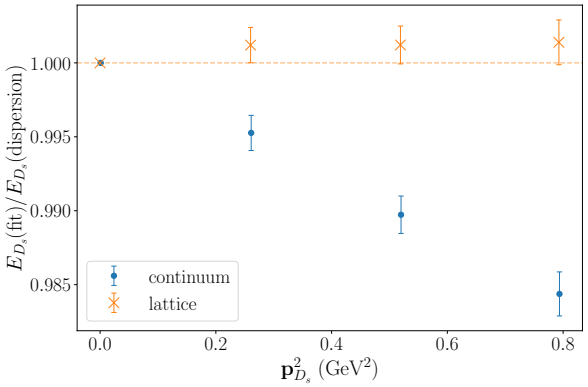

FIGURE 5.2: Speed-of-light plot for the D_s meson. The numerator is the ground-state energy for a given momentum as extracted from a fit to the data. The denominator is given by either the lattice dispersion relation or the continuum one, where the D_s-meson mass has been determined from a fit to the data at zero momentum.

necessary to build the correlator in Eq. (4.22), is obtained from the combination

$$A^{LL} = \frac{A^{LS}A^{SL}}{A^{SS}} = 1.002(28) \times 10^2 \tag{5.10}$$

in lattice units.

Smearing XY	A (lattice units)	M_{eff} (GeV)	fit range	χ^2/dof	p-value
LS	$2.106(22) \times 10^{-4}$	5.3659(19)	$[10, 13]$	0.69	0.50
SL	$2.112(55) \times 10^{-4}$	5.3663(48)	$[9, 14]$	2.22	0.07
SS	$4.436(87) \times 10^{-10}$	5.3659(34)	$[9, 15]$	0.56	0.73

TABLE 5.1: Summary of the two-point correlator fits (correlated) for the B_s meson at zero momentum.

Concerning the D_s meson, we are mainly interested in the E_{D_s} energy for the smaller twists, as this will be used in the determination of the form factors from the exclusive channels. We fit the ground-state energy to the correlator $C^{LS}_{D_s}$ following the same strategy we used for the B_s meson and report the results in Tab. 5.2.

$\boldsymbol{q}^2$ (GeV^2)	E_{D_s} (GeV)	fit range	χ^2/dof	p-value
0.00	1.6965(17)	$[16, 22]$	0.36	0.88
0.26	1.7631(18)	$[10, 17]$	0.99	0.43
0.52	1.8241(19)	$[8, 13]$	0.84	0.50
0.79	1.8860(25)	$[8, 13]$	0.67	0.61

TABLE 5.2: Summary of the two-point correlator fits (correlated) for the D_s-meson correlator $C^{LS}_{D_s}$ for the smallest momenta.

We also show the speed of light from the fitted masses of the D_s for the smallest momenta, comparing with the continuum dispersion relation $E = \sqrt{M^2 + \boldsymbol{p}^2}$ and the

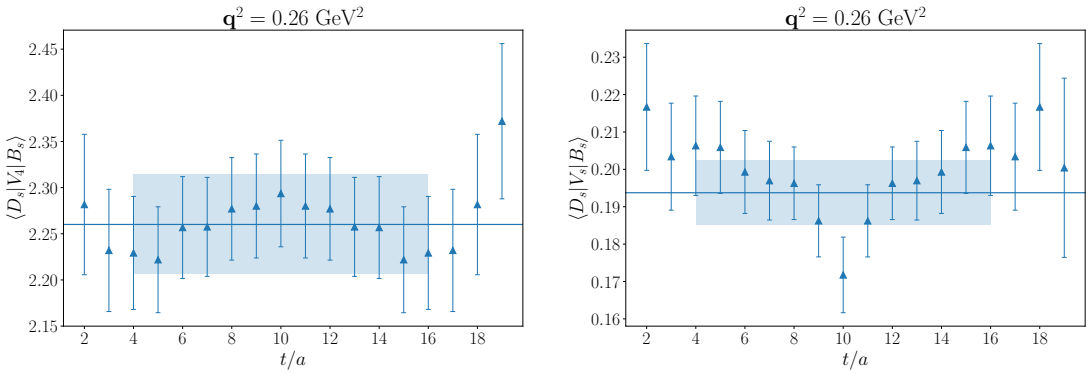

FIGURE 5.3: Ratio $R_{B_sD_s,4}(\boldsymbol{q},t)$ (left) and $R_{B_sD_s,s}(\boldsymbol{q},t)$ (right) built from the three-point functions $C_{B_sD_s,\mu}$ at $\boldsymbol{q}^2 = 0.26\,\text{GeV}^2$, where "$s$" stands for the average of the spatial components 1,2,3. The horizontal bands correspond to the final values for $\langle D_s|V_4|B_s\rangle$ (left) and $\langle D_s|V_s|B_s\rangle$ (right) extracted from a constant fit to the data.

lattice dispersion relation (in lattice units) $E = \cosh^{-1}(\cosh(M) + \sum_{k=1}^{3}(1-\cos(p_k)))$ in Fig. 5.2. The plot shows excellent agreement with the fitted energies.

5.2.2 Three-point correlators

The three-point functions generated in this work are used for determining some of the form factors from exclusive decays to study the ground-state limit of the inclusive process. In particular, the extraction of the form factors is addressed in Sec. 6.4. Here we show explicitly some example of the extraction of the matrix element $\langle D_s|V_\mu|B_s\rangle$ that appears in the three-point function $C_{B_sD_s,\mu}$, as in Eq. (2.105), through the ratio [198]

$$R_{D_sB_s,\mu}(\boldsymbol{q},t) = \sqrt{4M_{B_s}E_{D_s}}\sqrt{\frac{C^{SS}_{D_sB_s,\mu}(\boldsymbol{q},t_{\text{snk}},t,t_{\text{src}})C^{SS}_{B_sD_s,\mu}(\boldsymbol{q},t_{\text{snk}},t,t_{\text{src}})}{C^{SS}_{B_s}(t_{\text{snk}},t_{\text{src}})C^{SS}_{D_s}(\boldsymbol{q},t_{\text{snk}},t_{\text{src}})}}\,, \tag{5.11}$$

which converges to $\langle D_s|V_\mu|B_s\rangle$ for $t \gg t_{\text{src}}$ and $t \ll t_{\text{snk}}$. Note that for the second three-point correlator we have $C^{SS}_{B_sD_s,\mu}(\boldsymbol{q},t_{\text{snk}},t,t_{\text{src}}) = C^{SS}_{D_sB_s,\mu}(\boldsymbol{q},T-t_{\text{src}},T-t,T-t_{\text{snk}})$ in the region $t_{\text{src}} \le t \le t_{\text{snk}}$. We show an explicit example for the case $\boldsymbol{q}^2 = 0.26\,\text{GeV}^2$ in Fig. 5.3 for the average of the spatial components $R_{D_sB_s,s}(\boldsymbol{q},t) = 1/3\sum_{k=1}^{3} R_{D_sB_s,k}(\boldsymbol{q},t)$ and the time component $R_{D_sB_s,4}(\boldsymbol{q},t)$.

5.2.3 Four-point correlators

The four-point correlators are central to the computation of the inclusive decay rate and moments. Let us show an explicit example of the correlators we build for the average of the spatial axial currents (denoted by "ss" to indicate the average over the directions 11, 22 and 33) in Fig. 5.4, where we show the zero-momentum and the $\boldsymbol{q}^2 = 4.74\,\text{GeV}$ cases. Note that the signal-to-noise ratio problem appears in the early time-slices: indeed,

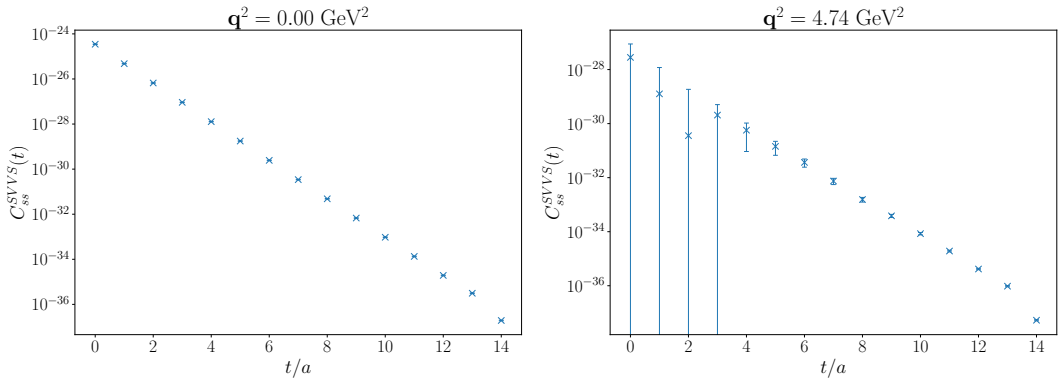

FIGURE 5.4: Four-point correlators with currents A_sA_s, which correspond to the average over the spatial channels A_1A_1, A_2A_2 and A_3A_3 at zero momentum (left) and $\boldsymbol{q}^2 = 4.74\,\mathrm{GeV}^2$ (right).

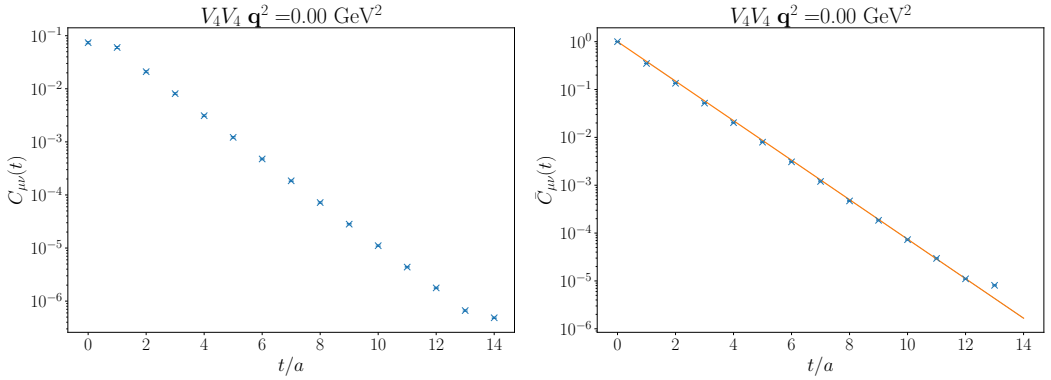

FIGURE 5.5: Correlator $C_{\mu\nu}(t)$ (left) and $\bar{C}_{\mu\nu}(t) = C_{\mu\nu}(t+1)/C_{\mu\nu}(1)$ (right) for the channel V_4V_4 at zero momentum. The orange line on the right plot is the exponential functional $e^{-tM_{D_s}}$, where the D_s-meson mass M_{D_s} has been extracted from a fit to the local-smeared two-point correlation function.

$t = 0$ corresponds to the case $t_1 = t_2$ (cf. Eq. (4.10)), hence the case where t_1 is as far as possible from the source in t_{src}.

We also show an example of the correlator $C_{\mu\nu}(\boldsymbol{q}, t)$ of Eq. (4.22) for the channel V_4V_4 at zero momentum in Fig. 5.5 (left). In particular, the ground state is represented by the pseudoscalar D_s: to show the exponential dependence as in Eq. (4.22), we consider the normalised correlator $\bar{C}_{\mu\nu}(t) = C_{\mu\nu}(t+1)/C_{\mu\nu}(1)$ in Eq. (4.59) and simply plot the single exponential $e^{-tM_{D_s}}$ on top of it, see Fig. 5.5 (right), where the M_{D_s} has been extracted from the two-point correlator fit. While this is a rough operation, it shows by visual inspection that the correlator reproduces the expected exponential behaviour. In this particular case, it also suggests that the effect of the excited states is mild.

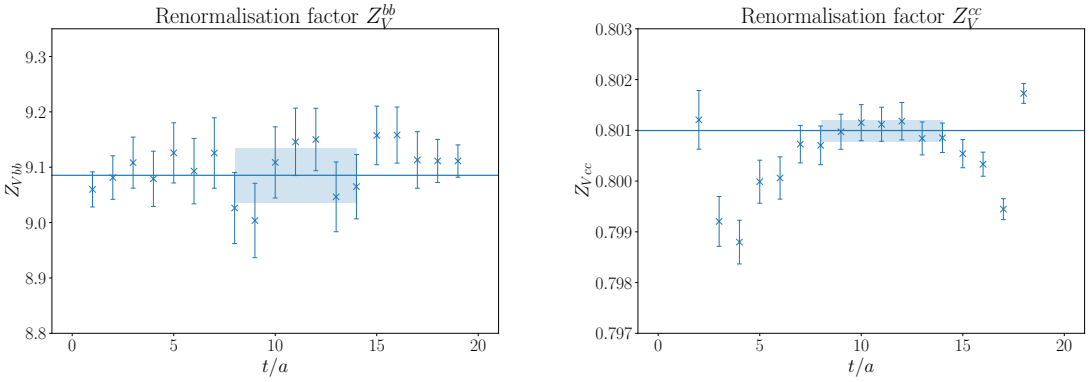

FIGURE 5.6: Determination of renormalisation Z_V^{bb} (left) and Z_V^{cc} (right) from the ratio of two- and three-point functions defined in Eq. (5.13).

5.2.4 Renormalisation

The local vector and axial-vector currents used in our lattice calculation receive a finite renormalisation. We use the *almost nonperturbative* prescription of [199], whereby

$$V_\mu = \rho_V^{bc}\sqrt{Z_V^{cc}Z_V^{bb}}\,(V_\mu)_{\text{bare}} \qquad \text{and} \qquad A_\mu = \rho_A^{bc}\sqrt{Z_V^{cc}Z_V^{bb}}\,(A_\mu)_{\text{bare}}\,. \tag{5.12}$$

The subscript "bare" indicates the bare, unrenormalised heavy-light vector or axial-vector current. Z_V^{cc} is the vector-current renormalisation constant for domain-wall fermions. Due to the approximate chiral symmetry of domain-wall fermions, $Z_V^{cc} = Z_A^{cc}$ up to residual chiral-symmetry-breaking effects. The renormalisation constants Z_V^{bb} and Z_V^{cc} are computed from the *charge* of the heavy-light mesons, and are defined as

$$Z_V^{bb} = \frac{C_{B_s}^{SS}(t_{\text{snk}}, t_{\text{src}})}{C_{B_sB_s,0}^{SS}(t_{\text{snk}}, t, t_{\text{src}})} \quad \text{and} \quad Z_V^{cc} = \frac{C_{D_s}^{LL}(t_{\text{snk}}, t_{\text{src}})}{C_{D_sD_s,0}^{LL}(t_{\text{snk}}, t, t_{\text{src}})}\,, \tag{5.13}$$

where both the two- and three-point functions are zero-momentum projected. The results

$$Z_V^{bb} = 9.085(50) \quad \text{and} \quad Z_V^{cc} = 0.80099(21) \tag{5.14}$$

are illustrated in Fig. 5.6. The coefficient $\rho_{V/A}^{bc}$ is expected to be close to unity and can be computed in perturbation theory. Here we set it to its tree-level value, i.e. $\rho_{V/A}^{bc} = 1$. This is sufficient for the qualitative study aimed at here, where no attempt is made at taking the continuum limit.

CHAPTER 6

RESULTS

In this chapter we present and discuss the main results of this work. In Sec. 6.1 we discuss how well the kernels $K^{(l)}_{\sigma,\mu\nu}$ are approximated, for a given truncation, by the polynomials through the reconstruction via Chebyshev and Backus-Gilbert methods. In Sec. 6.2 we show the application of the data analysis strategies described in Sec. 4.3. Eventually, we combine various analysis steps for a prediction of the inclusive decay rate quantities in Sec. 6.3 and compare our results with the ground-state contribution in Sec. 6.4. We report some first results for the moments in Sec. 6.5.

We emphasise once again that the work presented here focuses on a qualitative understanding of the methods aiming at developing reliable techniques, which in future work can be used to make phenomenologically relevant predictions.

6.1 Polynomial approximation of the kernels

In this section we discuss the central aspects of the polynomial approximation. The two ingredients to optimise the approximation are the choice of the lower end of the integral in ω of the approximation ω_0, and the value of t_0 in Eq. (4.59). In particular, we choose $t_0 = 1/2$ in lattice units, such that the exponential growth of the term $e^{2\omega t_0}$ in the kernels in Eqs. (4.31)-(4.45) is minimal, and the number of data points we can use is maximised. We study two values of ω_0, i.e. $\omega_0 = 0$ and $\omega_0 = 0.9\,\omega_{\text{min}}$ for each momentum $\boldsymbol{q}^2$. We will present plots for the smallest $\boldsymbol{q}^2 = 0.26\,\text{GeV}^2$ and one of the largest $\boldsymbol{q}^2 = 4.74\,\text{GeV}^2$ computed, and illustrate the case of $\sigma = 0.02$, which smoothes the step function only mildly. Later we will also discuss the case of larger values of σ to show how the limit $\sigma \to 0$ is approached. Note that this section deals purely with the approximation of the kernel with no connection to the data; for the Backus-Gilbert method this means that we set $\lambda = 0$.

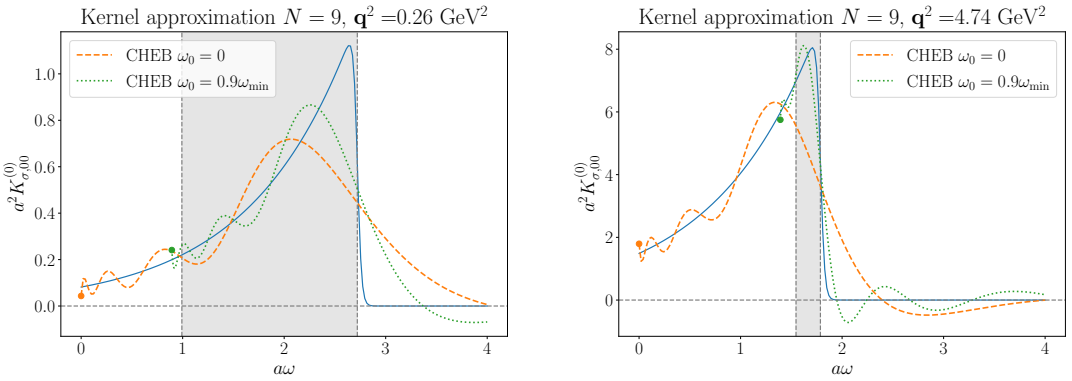

FIGURE 6.1: Chebyshev-polynomial approximation of the kernel $K^{(0)}_{\sigma,00}$ with $N = 9$ at $\boldsymbol{q}^2 = 0.26\,\text{GeV}^2$ (left) and $\boldsymbol{q}^2 = 4.74\,\text{GeV}^2$ (right) with different values of $\omega_0 = 0$ and $\omega_0 = 0.9\omega_{\min}$. The solid blue line shows the target kernel function with a smearing $\sigma = 0.02$.

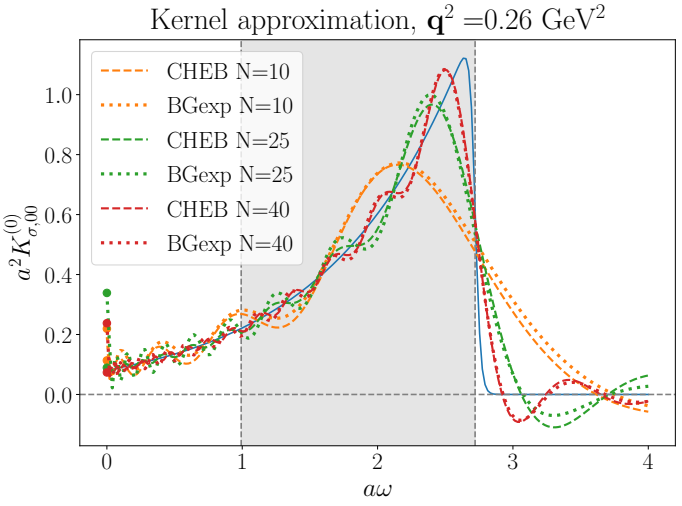

FIGURE 6.2: Polynomial approximation with Chebyshev and Backus-Gilbert (with exponential basis) at different values of N for kernel $K^{(0)}_{\sigma,00}$ at $\boldsymbol{q}^2 = 0.26\,\text{GeV}^2$ and $\omega_0 = 0$.

We first highlight some of the main features of our approach. As shown in Fig. 6.1, the quality of the approximation varies with ω_0: starting the approximation as close as possible to $\omega_{\min}$ gives the best result, as the nodes of the interpolation (the points where the target function and its polynomial reconstruction meet) are denser in the allowed phase space in energy (the grey shaded area). This is most evident in the case of large $\boldsymbol{q}^2$, as $\omega_{\min}$ is further away from 0. This is then the region where we expect larger deviations for the values of $\bar{X}^{(l)}(\boldsymbol{q}^2)$ between the two choices of ω_0. Note also that a value slightly below $\omega_{\min}$ (e.g. $0.9\omega_{\min}$) safeguards against statistical fluctuations in the D_s-meson mass.

Furthermore, we can see by visual inspection that the quality of the two polynomial approximation strategies is comparable. This difference shrinks further as we increase

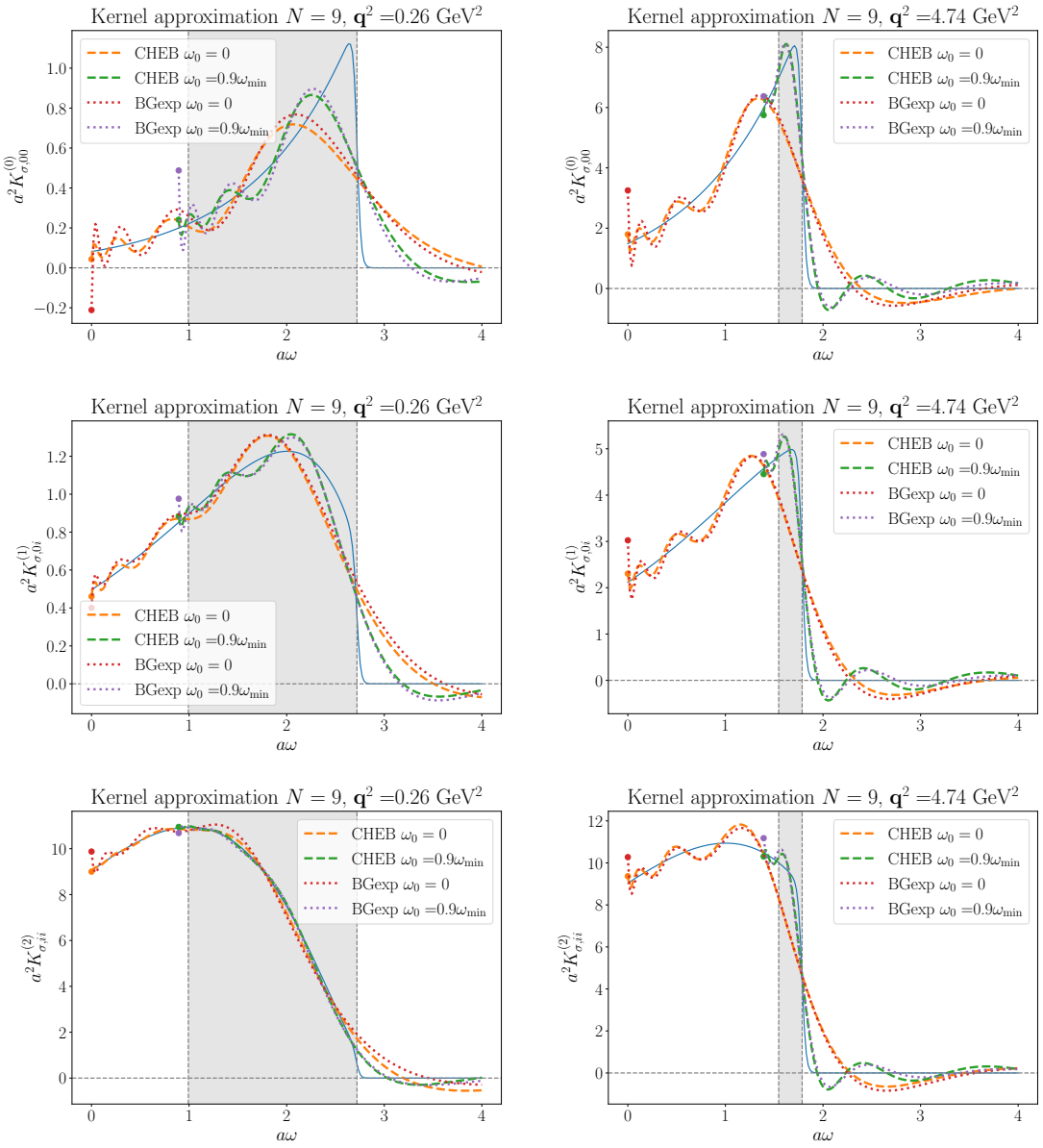

FIGURE 6.3: Polynomial approximation at order $N = 9$ of the kernel $K^{(l)}_{\sigma,\mu\nu}(\boldsymbol{q}, \omega; 2t_0)$, for $l = 0$ (first row), $l = 1$ (second row) and $l = 2$ (third row) with $t_0 = 1/2$ and $\sigma = 0.02$. The left column shows the case of the smallest $\boldsymbol{q}^2 = 0.26\,\text{GeV}^2$, whereas the right column shows one of the largest momentum $\boldsymbol{q}^2 = 4.74\,\text{GeV}^2$. The grey area corresponds to the kinematically allowed range $\omega_{\min} \leq \omega \leq \omega_{\max}$ for the given $\boldsymbol{q}^2$. The solid lines show the target function; the dashed lines show the approximation with the Chebyshev approach, whereas the dotted ones show the approximation with Backus-Gilbert with an exponential basis and $\lambda = 0$.

the value of N, as we show exemplary in Fig. 6.2, where the polynomial approximation is performed for degree $N = 10, 25, 40$.

In Fig. 6.3 we show the approximation for different components of the kernels $K^{(l)}_{\sigma,\mu\nu}$ for the decay rate with $l = 0, 1, 2$ and in Figs. 6.4 and 6.5 we show the total ones for the leptonic kernel $K^{(n)}_{L,\sigma,\mu\nu}(\omega, \boldsymbol{q}; t_0)$ and $\tilde{K}^{(n)}_{L,\sigma,ij}(\omega, \boldsymbol{q}; t_0)$ at order $n = 1$, respectively.

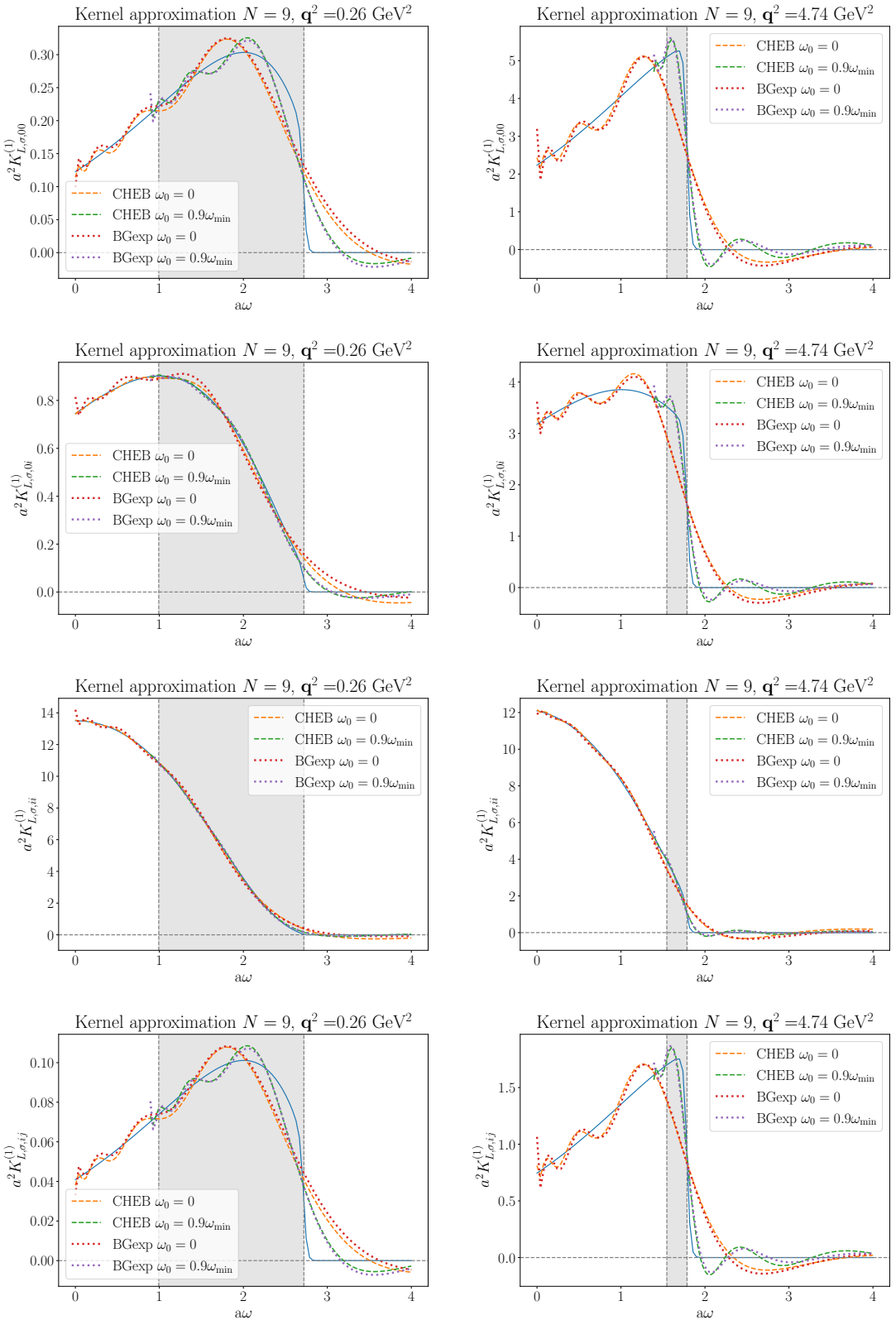

FIGURE 6.4: Polynomial approximation at order $N = 9$ of the leptonic kernel $K^{(n)}_{L,\sigma,\mu\nu}(\boldsymbol{q},\omega;2t_0)$ at order $n = 1$ with $t_0 = 1/2$ and $\sigma = 0.02$ for the $\mu\nu$ components 00 (first row), $0i$ (second row), ii (third row) and ij with $i \neq j$ (fourth row).

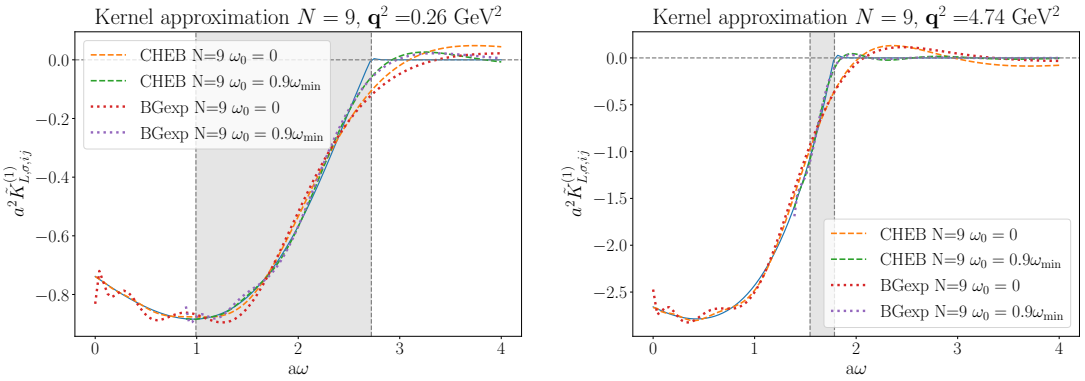

FIGURE 6.5: Polynomial approximation at order $N = 9$ of the leptonic kernel $\tilde{K}^{(n)}_{L,\sigma,ij}(\boldsymbol{q},\omega;2t_0)$ with $i \neq j$ at order $n = 1$ with $t_0 = 1/2$ and $\sigma = 0.02$.

Some comments are in order. While we recall once again that the plots presented in this section are independent from the data, we need to take into account the available dataset for the choice of the value of N. Indeed, due to the parameters of our simulations the polynomial order $N = 9$ is the maximum value available. This depends on the size of the lattice and the choice of t_{src}, t_2 and t_{snk} in the four-point correlator. In particular, setting $a = 1$, the available time slices are $2t_0 \leq t < t_2 - t_{\text{src}}$, which in our case correspond to $1 \leq t < 14$. Moreover, we need to make sure that $t \ll t_2 - t_{\text{src}}$, i.e. $t_1 - t_{\text{src}} \gg 0$: the choice $N = 9$ corresponds to a separation $t_1 - t_{\text{src}} = 4$. Of course, with an improved dataset N could be chosen larger and the differences between the two approaches would reduce further.

We also notice that the kernel for the decay rate with $l = 0$ is the most delicate to treat, as it is the one that shows the sharpest drop to zero at the threshold. Note also that for the case $l = 0$ we plotted only $K^{(0)}_{\sigma,00}$ as all the other kernels are the same up to a constant factor. Furthermore, as shown in Fig. 6.2 the results for Chebyshev and Backus-Gilbert agree very well and the quality of the approximation seems comparable.

To conclude, we point out that the approximation for the leptonic kernel $K^{(1)}_{L,\sigma,\mu\nu}$ turns out to be very smooth: this suggests that the systematic effect associated with the polynomial approximation may be less significant than in other cases. However, the impact of the systematics also depends on the magnitude of the contribution of each channel. Finally, we recall that the kernels for the hadronic mass moments $K^{(n)}_{H,\sigma,\mu\nu}(\omega,\boldsymbol{q};t_0)$ are related to the decay rate kernels $K_{\sigma,\mu\nu}(\omega,\boldsymbol{q};t_0) = K^{(0)}_{\sigma,\mu\nu}(\omega,\boldsymbol{q};t_0) + K^{(1)}_{\sigma,\mu\nu}(\omega,\boldsymbol{q};t_0) + K^{(2)}_{\sigma,\mu\nu}(\omega,\boldsymbol{q};t_0)$ by a multiplicative factor $(\omega^2 - \boldsymbol{q}^2)^n$.

6.2 Regularisation approaches in practice

We now include the data to complete the discussion of Sec. 6.1 and address the quality of the regularisation approaches of Sec. 4.3 adopted for the data analysis. In this case,

the term "regularisation" refers to the fact that the analysis techniques employed have the effect of reducing the variance of the final observables by balancing systematic and statistical noise. In this way, the computation of these quantities is well-defined and feasible through numerical simulations. We focus separately on the Chebyshev-polynomial approach in Sec. 6.2.1 and the modified Backus-Gilbert approach in Sec. 6.2.2. We outline the effect on the variance and the main differences between the two in Sec. 6.2.3.

6.2.1 Chebyshev polynomials

Concerning the Chebyshev-polynomial approach, the correlator data $\bar{C}_{\mu\nu}(t)$ are traded with the fitted Chebyshev matrix elements as

$$\bar{C}^{\text{fit}}_{\mu\nu}(k) = \sum_{j=0}^{k} \tilde{a}_j^{(k)} \langle \tilde{T}_j \rangle_{\mu\nu} \,, \tag{6.1}$$

where the Chebyshev matrix elements satisfy $|\langle \tilde{T}_j \rangle_{\mu\nu}| \leq 1$ by construction and the coefficients $\tilde{a}_j^{(k)}$ are known and given by the power representation of the Chebyshev polynomials, see App. C.2.4. Indeed, while the above equation implies a linear relation between correlator and Chebyshev matrix elements as in Eq. (4.67), $\bar{C}_{\mu\nu}(k)$ needs to be computed on the lattice using Monte-Carlo methods and the resulting statistical error can lead to violations of the bound $|\langle \tilde{T}_k \rangle_{\mu\nu}| \leq 1$ when solving the linear system. This can, however, be avoided with the help of a Bayesian analysis of the correlator data. In practice, we adopt a MAP procedure with bootstrap as detailed in App. E and in particular in App. E.3. This allows us to impose the constraints using a Gaussian prior on some internal parameters $\langle \tilde{\tau}_k \rangle_{\mu\nu} \sim \mathcal{N}(0,1)$ and convert it to a flat prior on the interval $[-1,1]$ for $\langle \tilde{T}_k \rangle_{\mu\nu}$ using the map $f(x) = \text{erf}(x/\sqrt{2})$, for which $\langle \tilde{T}_k \rangle_{\mu\nu} = f(\langle \tilde{\tau}_k \rangle_{\mu\nu})$. The augmented χ^2 to minimise for each bootstrap bin b reads

$$\begin{aligned} \chi^2_{\text{aug}}\Big|_b = &\sum_{i,j=1}^{N} \left(\bar{C}^b_{\mu\nu}(i) - \sum_{k=0}^{i} \tilde{a}_k^{(i)} f(\langle \tilde{\tau}_k \rangle_{\mu\nu}) \right) \sigma_{ij}^{-1} \left(\bar{C}^b_{\mu\nu}(j) - \sum_{k=0}^{j} \tilde{a}_k^{(j)} f(\langle \tilde{\tau}_k \rangle_{\mu\nu}) \right) \\ &+ \sum_{k=1}^{N} (\langle \tilde{\tau}_k \rangle_{\mu\nu} - \langle \tilde{\tau}^b_k \rangle_{\mu\nu})^2 \,, \end{aligned} \tag{6.2}$$

where $\bar{C}^b_{\mu\nu}(i)$ is the b-th bootstrap bin for the correlator, $\sigma_{ij} = \text{Cov}(\bar{C}(i), \bar{C}(j))$ and $\langle \tilde{\tau}^b_k \rangle_{\mu\nu}$ is randomly sampled from the normal distribution $\mathcal{N}(0,1)$, as described in more detail App. E.3. Note that the first Chebyshev matrix element $\langle \tilde{T}_0 \rangle_{\mu\nu} = f(\langle \tilde{\tau}_0 \rangle_{\mu\nu}) = 1$ by definition. It is therefore not treated as a fit parameter.

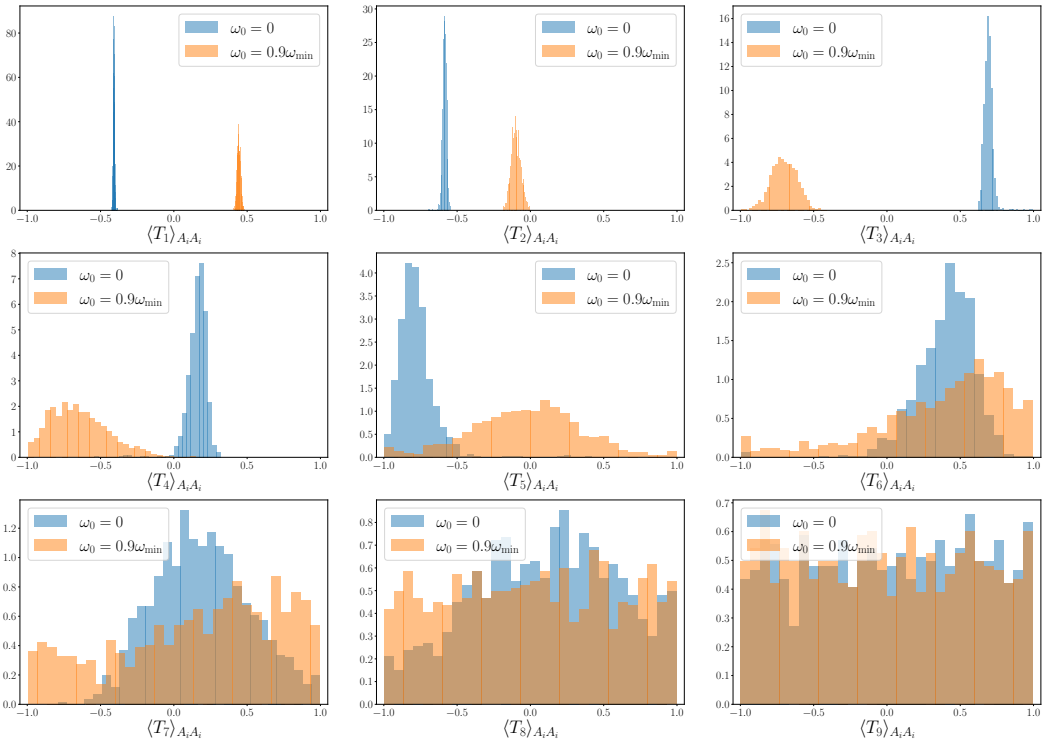

FIGURE 6.6: Histogram of the Chebyshev matrix elements $\langle \tilde{T}_k \rangle_{A_i A_i}$ for $k = 1, 2, \ldots, N$ with $N = 9$ for two values $\omega_0 = 0$ (blue) and $\omega_0 = 0.9\omega_{\min}$ (orange) at $\boldsymbol{q}^2 = 0.26\,\text{GeV}^2$. The matrix element $\langle \tilde{T}_0 \rangle_{A_i A_i} = 1$ by definition and is therefore not shown. This channel is one of the most precise: we find that in both cases the fitting procedure is able to determine the matrix elements up to order $N \simeq 7$, after which the distribution of the bootstrap bins remains flat.

Following Eqs. (4.52) and (4.64), the kernel with fitted Chebyshev matrix elements can be written as

$$\langle K_\sigma^{(l)} \rangle_{\mu\nu} = \frac{\tilde{c}^{(l)}_{\mu\nu,0}}{2} \langle \tilde{T}_0 \rangle_{\mu\nu} + \sum_{k=1}^{N} \tilde{c}^{(l)}_{\mu\nu,k} \langle \tilde{T}_k \rangle_{\mu\nu} = \sum_{k=0}^{N} \bar{c}^{(l)}_{\mu\nu,k} \bar{C}^{\text{fit}}_{\mu\nu}(k)\,. \tag{6.3}$$

An example of the Chebyshev matrix elements obtained from the fits can be seen in Fig. 6.6, where we compare two different extractions according to the starting point of the approximation ω_0. The plots show the distribution of each order of the Chebyshev matrix elements obtained through the fitting procedure, where each histogram reports values obtained for all the 1000 bootstrap bins. We show the axial channel $A_i A_i$, as its signal turns out to be particularly clean. In Fig. 6.7 we show results for the $A_i A_j$ channel, with $i \neq j$, which is found to be the noisiest channel. Here, only few terms can be determined meaningfully by the lattice data and higher-order terms just follow the flat prior distribution in $[-1, 1]$.

In both cases we observe that a larger number of Chebyshev matrix elements can be determined meaningfully for $\omega_0 = 0$ than for $\omega_0 = 0.9\,\omega_{\min}$. For example, in the $A_i A_i$ channel the distribution of the former is close to the prior distribution, which is flat

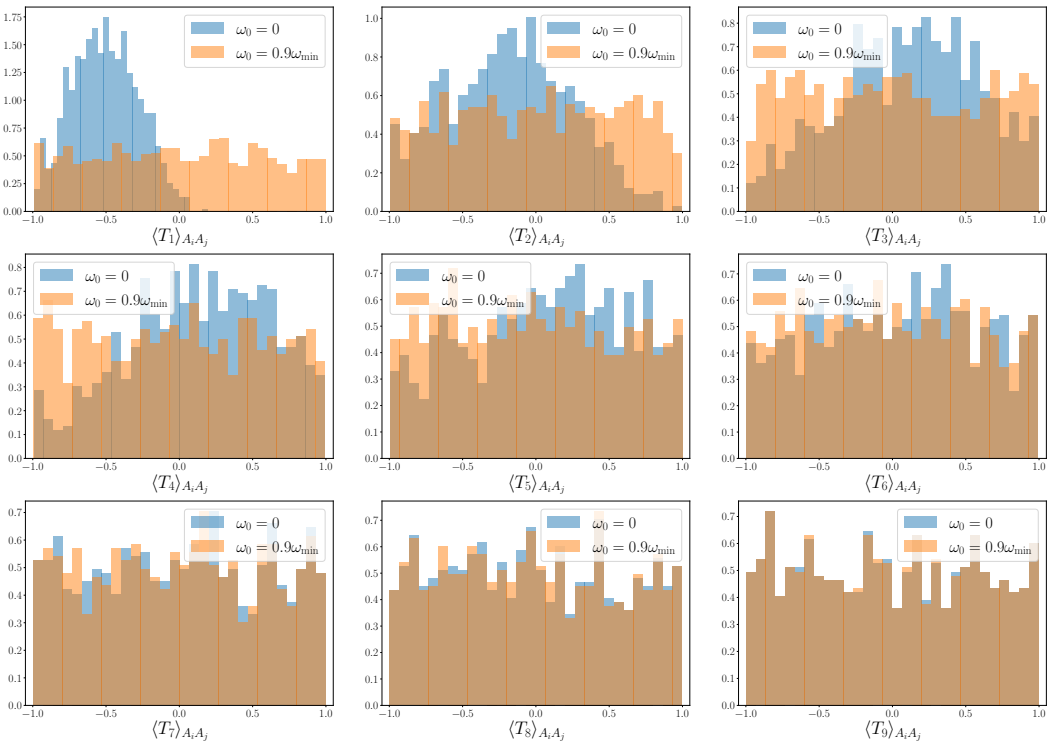

FIGURE 6.7: Histogram of the Chebyshev matrix elements $\langle \tilde{T}_k \rangle_{A_i A_j}$ with $i \neq j$ for $k = 1, 2, \ldots, N$ with $N = 9$ for two values $\omega_0 = 0$ (blue) and $\omega_0 = 0.9\omega_{\text{min}}$ (orange) at $\boldsymbol{q}^2 = 0.26\,\text{GeV}^2$. The results for $\langle \tilde{T}_k \rangle_{A_i A_j}$ are less well constrained than the ones for $A_i A_i$ shown in Fig. 6.6. The minimum of the χ^2 is determined almost entirely by the uniform priors.

between -1 and $+1$, for $N = 9$, whereas the latter starts flattening at $N \gtrsim 7$. A possible explanation follows from the properties of the polynomial representation and the power representation of the shifted Chebyshev polynomials (discussed in App. C) for the choice of domains $[0, \infty)$ and $[0.9\omega_{\text{min}}, \infty)$. Indeed, the matrix $\tilde{\boldsymbol{t}}$ from Eq. (C.34), which in our case relates the Chebyshev polynomials to the power of the exponential $e^{-\omega}$, can be further decomposed as

$$\tilde{\boldsymbol{t}} = \boldsymbol{A}\boldsymbol{P}\boldsymbol{t}\,, \tag{6.4}$$

where $\boldsymbol{A}_{kk} = (-2e^{\omega_0})^k$ is a diagonal matrix, $\boldsymbol{P}_{jk} = \binom{j}{k}$ is the lower triangular Pascal matrix and the matrix $\boldsymbol{t}$ is related to the power representation of the standard Chebyshev polynomials $T_k(\omega)$ as in Eq. (C.10). This exposes the effect the choice of ω_0 has: considering $\boldsymbol{A}_{kk}\Big|_{\omega_0 \neq 0} = e^{\omega_0 k} \boldsymbol{A}_{kk}\Big|_{\omega_0 = 0}$ it follows that

$$(\tilde{\boldsymbol{t}})_{nk}\Big|_{\omega_0 \neq 0} = \tilde{t}_k^{(n)}\Big|_{\omega_0 \neq 0} = e^{\omega_0 n}\, \tilde{t}_k^{(n)}\Big|_{\omega_0 = 0}\,, \qquad (\tilde{\boldsymbol{a}})_{nk}\Big|_{\omega_0 \neq 0} = \tilde{a}_k^{(n)}\Big|_{\omega_0 \neq 0} = e^{-\omega_0 n}\, \tilde{a}_k^{(n)}\Big|_{\omega_0 = 0}\,. \tag{6.5}$$

In our case, this implies that $\tilde{a}_j^{(k)}|_{\omega_0=0.9\omega_{\min}} = e^{-0.9\omega_{\min}k}\,\tilde{a}_j^{(k)}|_{\omega_0=0}$. The additional exponential factor largely cancels the ground-state exponential decay in the correlation function in Eq. (6.1). Hence, the polynomial approximation has less structure to describe and higher-order terms become less relevant. Nevertheless, in both cases the correlated χ^2/dof of the fits are acceptable and the reconstruction of the data as in Eq. (6.1) gives comparable results.

6.2.2 Backus-Gilbert

We now move to the modified Backus-Gilbert approach in the general case $\lambda \neq 0$, for which the coefficients are determined with reference to the data, in contrast with the $\lambda = 0$ case. We consider the case $\lambda = \lambda^*$, which corresponds to the choice of optimal balance between systematic and statistical error, as explained in Sec. 4.3.2. By visual inspection of Fig. 6.8, which shows exemplarily the case of the decay rate, we find that the polynomial approximation of the kernel functions gets worse. The effect of non-zero λ can be understood as a correction to the optimal coefficients at $\lambda = 0$, see App. D.2. In particular, if we rewrite the coefficients as $g^{*(l)}_{\mu\nu,k} = \gamma^{(l)}_{\mu\nu,k} + \epsilon^{*(l)}_{\mu\nu,k}$ we have

$$\langle K_\sigma^{(l)}\rangle_{\mu\nu} = \sum_{k=0}^{N} g^{*(l)}_{\mu\nu,k}\bar{C}_{\mu\nu}(k) = \sum_{k=0}^{N}\gamma^{(l)}_{\mu\nu,k}\bar{C}_{\mu\nu}(k) + \sum_{k=0}^{N}\epsilon^{*(l)}_{\mu\nu,k}\bar{C}_{\mu\nu}(k)\,, \tag{6.6}$$

where $\gamma^{(l)}_{\mu\nu}$ are the coefficients for $\lambda = 0$ and $\epsilon^{*(l)}_{\mu\nu,k}$ is a correction that takes care of the reduction of the noise originating from the statistical error, as further discussed in the following section.

6.2.3 Comparison between Chebyshev and Backus-Gilbert approach

We now point out similarities and differences between the two approaches. The calculation of $\langle K_\sigma^{(l)}\rangle_{\mu\nu}$ aims to improve accuracy by combining the naive polynomial approximation with a correction term $\delta\langle K_\sigma^{(l)}\rangle_{\mu\nu}$ that accounts for variance reduction, i.e.

$$\langle K_\sigma^{(l)}\rangle_{\mu\nu} = \langle K_\sigma^{(l)}\rangle^{\text{naive}}_{\mu\nu} + \delta\langle K_\sigma^{(l)}\rangle_{\mu\nu}\,, \tag{6.7}$$

where $\langle K_\sigma^{(l)}\rangle^{\text{naive}}_{\mu\nu}$ corresponds to Eq. (4.64). The correction term is specific to the adopted strategy and is given by:

- $\delta\langle K_\sigma^{(l)}\rangle^{\text{CHEB}}_{\mu\nu} = \sum_{k=0}^{N}\bar{c}_{\mu\nu,k}\delta\bar{C}_{\mu\nu}(k)$, for the Chebyshev polynomials technique, where $\delta\bar{C}_{\mu\nu}(k) = \bar{C}^{\text{fit}}_{\mu\nu}(k) - \bar{C}_{\mu\nu}(k)$;
- $\delta\langle K_\sigma^{(l)}\rangle^{\text{BG}}_{\mu\nu} = \sum_{k=0}^{N}\epsilon^{*}_{\mu\nu,k}\bar{C}_{\mu\nu}(k)$, for the Backus-Gilbert method, which corrects the coefficients of the polynomial approximation as in Eq. (6.6).

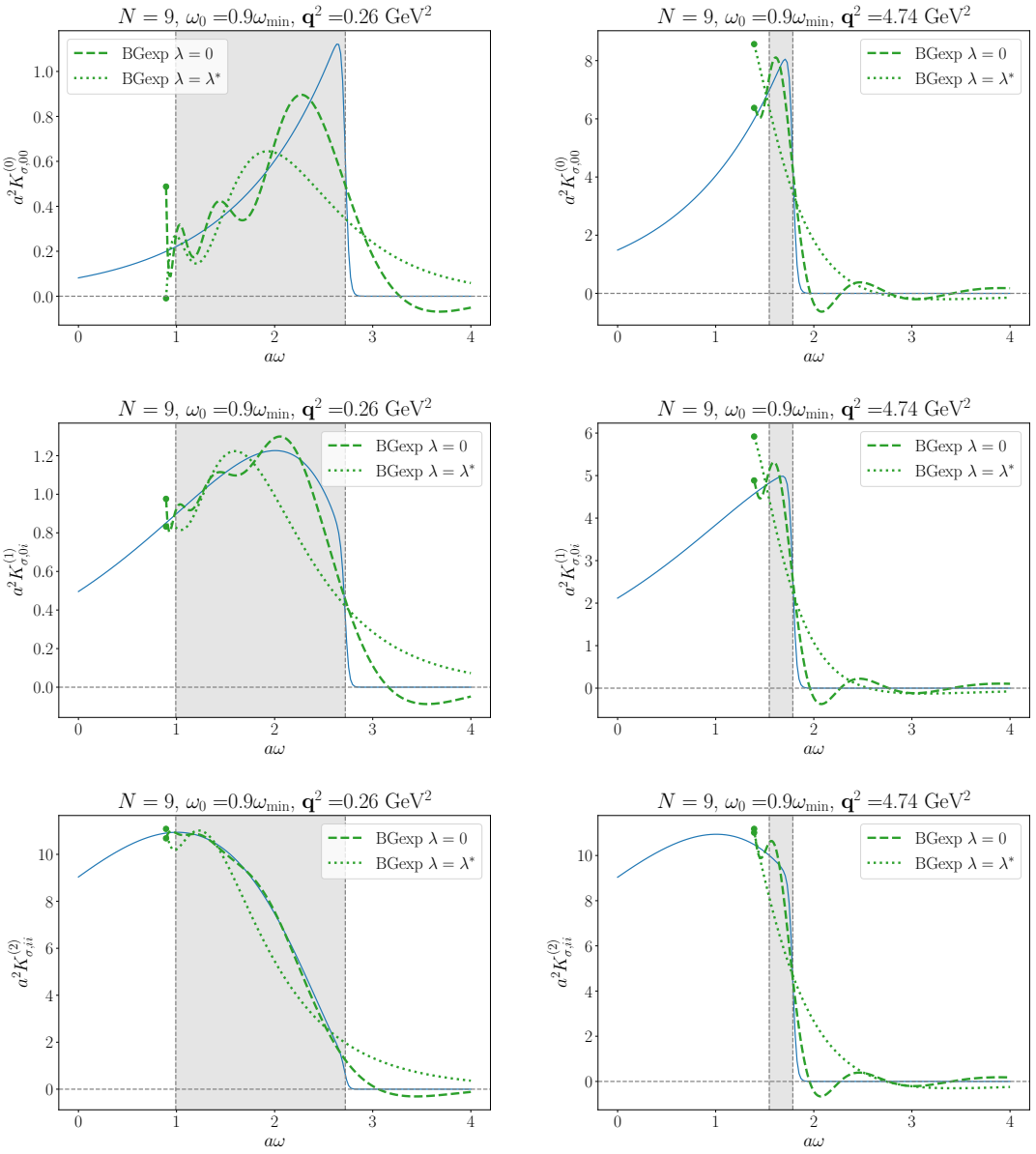

FIGURE 6.8: Polynomial approximation of the kernel $K^{(l)}_{\sigma,\mu\nu}(\boldsymbol{q}, \omega; 2t_0)$, for $l = 0$ (first row), $l = 1$ (second row) and $l = 2$ (third row) with $t_0 = 1/2$ and $\sigma = 0.02$ in the case of Backus-Gilbert with exponential basis and $\lambda \neq 0$. The value of λ has been chosen to be λ^* for each plot, which gives equal weight to the statistical and systematic errors.

This exposes that the Chebyshev-polynomial approach addresses the variance reduction acting on the data, imposing rigorous mathematical bounds, whereas the Backus-Gilbert method deals with it by modifying the coefficients of the polynomial approximation such that they take into account information about the statistical error of the data. In both cases, $\delta\langle K^{(l)}_{\sigma}\rangle_{\mu\nu}$ can be interpreted as a noisy zero that does not impact the naive calculation but helps with variance reduction.

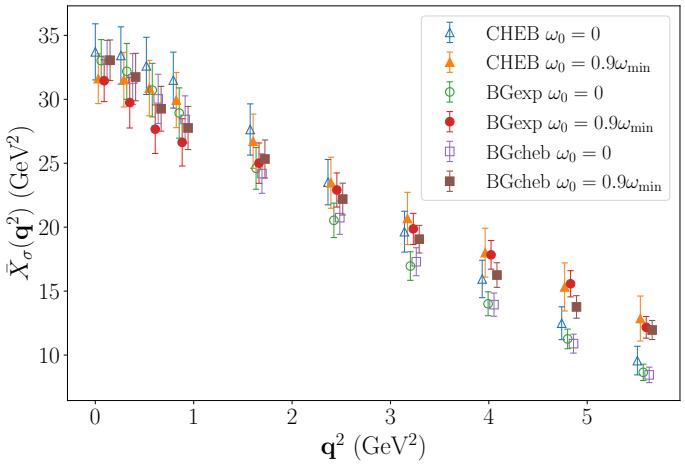

FIGURE 6.9: Estimate of $\bar{X}_\sigma(\boldsymbol{q}^2)$ with the two different strategies for 10 different $\boldsymbol{q}^2$ with $N = 9$ and $\boldsymbol{q}^2_{\text{max}} = 5.83\,\text{GeV}^2$.

6.3 Decay rate

In this section we present the main results of our work. In Fig. 6.9 we show the results of $\bar{X}_\sigma(\boldsymbol{q}^2)$ for the decay rate for all the simulated values of $\boldsymbol{q}^2$ with a value $\sigma = 0.02$ for the smearing parameter of the kernel (cf. Eq. (4.27)). For each simulation point we show the results of three studied approaches, i.e., Chebyshev polynomials, exponential Backus-Gilbert and Chebyshev Backus-Gilbert, all of them for both $\omega_0 = 0$ and $\omega_0 = 0.9\,\omega_{\text{min}}$. We find that all sets of three points for a given value of ω_0 agree very well. However, sets with different ω_0 start deviating as we increase the value of $\boldsymbol{q}^2$. This can be understood in terms of the polynomial approximation of the kernel: as $\boldsymbol{q}^2$ increases, the phase space in ω shrinks, and the two approximations start differing increasingly. Our data indicate that the approximation improves as $\omega_0 \to \omega_{\text{min}}$, as discussed in Sec. 6.1. In order for the approximations for different ω_0 to be comparable the order of the polynomial needs to be increased for lower ω_0. This is due to the fact for $\omega_0 = 0$ the nodes of the approximation are not dense enough in the region of interest $[\omega_{\text{min}}, \omega_{\text{max}}]$ with respect to the case $\omega_0 = 0.9\omega_{\text{min}}$, as shown for example in Fig. 6.1. It is also conceivable that other systematics like finite-volume or cutoff effects may play a role here: indeed, different values of ω_0 result in different sets of coefficients of the polynomial approximation, which give different weights to the the time-slices of the correlator $\bar{C}_{\mu\nu}(t)$, as from Eq. (4.64). These effects are beyond the scope of this work but will have to be addressed in future studies.

In the previous section we have seen that the shape of the kernel, and hence, the quality of approximation, varies substantially for different l and $\boldsymbol{q}^2$. The degree to which this impacts the combined result $\bar{X}_\sigma(\boldsymbol{q}^2) = \bar{X}^{(0)}_\sigma(\boldsymbol{q}^2) + \bar{X}^{(1)}_\sigma(\boldsymbol{q}^2) + \bar{X}^{(2)}_\sigma(\boldsymbol{q}^2)$ depends on the magnitude of each contribution, as illustrated in Fig. 6.10. The plots indicate that the

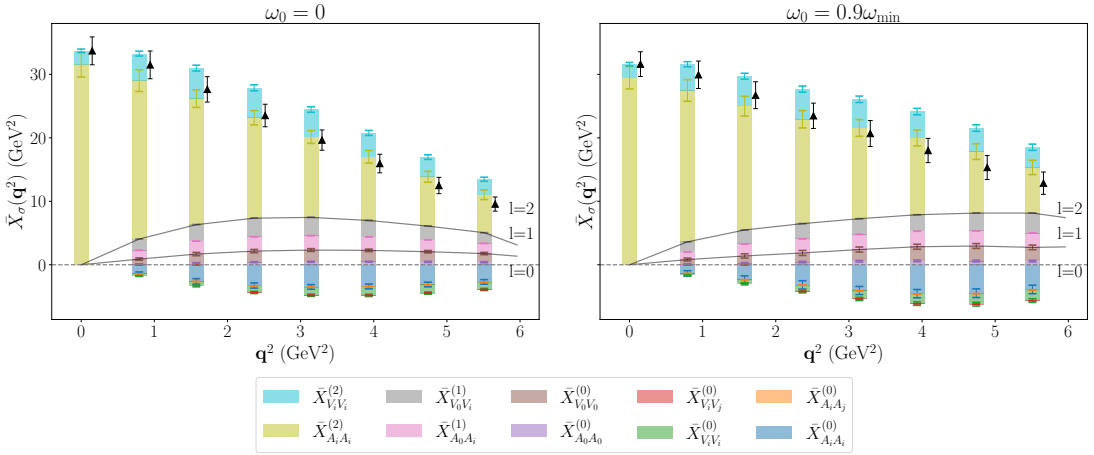

FIGURE 6.10: Contributions to $\bar{X}_\sigma(\boldsymbol{q})$ from the Chebyshev-polynomial approach at $N = 9$ and $\omega_0 = 0$ (left) and $\omega_0 = 0.9\omega_{\min}$ (right) with associated error bars. The black triangles correspond to the final value $\bar{X}_\sigma(\boldsymbol{q}^2) = \sum_{l=0}^{2} \sum_{\{\mu,\nu\}} \bar{X}^{(l)}_{\sigma,\mu\nu}(\boldsymbol{q}^2)$. The solid black lines separate the contributions from $l = 0$ (bottom), $l = 1$ (middle) and $l = 2$ (top).

largest contribution originates from the channel with $l = 2$. The underlying kernel is, at least for smaller values of $\boldsymbol{q}^2$, relatively smooth (Fig. 6.3). We therefore expect less sensitivity to the systematics of the polynomial approximation in this kinematical region, but more care is needed for larger $\boldsymbol{q}^2$.

We now address the stability under a change of the order N of the polynomial. Starting from the Chebyshev approach, we study the saturation in Fig. 6.11. We start from the fit with $N = 9$ (left). The plot shows the result where the first k Chebyshev matrix elements (cf. legend) are taken from the fit, and the remaining $N - k$ are replaced by a flat distribution $-1 \leq \langle \tilde{T}_j \rangle_{\mu\nu} \leq 1$ with $j = k + 1, \ldots, N$. Comparing with the right plot, we can see that the signal is dominated by small orders; for $\omega_0 = 0$, the signal is saturated at around $N \simeq 5$, whereas for $\omega_0 = 0.9\,\omega_{\min}$ saturation starts at $N \simeq 3$. This is also compatible with the previous discussion on the fit of the Chebyshev matrix elements, cf. with Figs. 6.6 and 6.7.

In order to estimate higher-order contributions, which are not constrained by our data, we study how the results change after adding more terms in the Chebyshev distributions on top of the $N = 9$ available. In this way we obtain an estimate of the approximation up to $N = 50$, as in Fig. 6.12. We show in particular the case of distributions with random values in $\mathbb{Z}_2 = \{-1, 1\}$ (left) for $\langle \tilde{T}_k \rangle_{\mu\nu}$ beyond $k = 9$: these correspond to the minimum and maximum value that the Chebyshev matrix elements can have. The case with uniform distribution with values in $[-1, +1]$ (right) gives similar results with slightly smaller errors. In both cases, the extra terms contribute to the final error only mildly: these observations suggest that the results obtained do not suffer from huge systematic error from the polynomial approximation and represent a possible way to estimate the

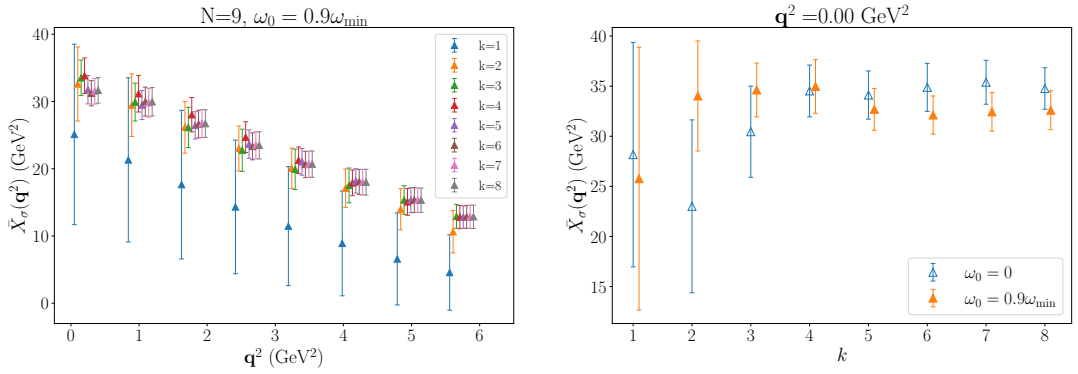

FIGURE 6.11: Saturation of the Chebyshev polynomial approach for different $\boldsymbol{q}^2$ and $\omega_0 = 0.9\omega_{\min}$ (left) and for case $\boldsymbol{q}^2 = 0$ for both values of ω_0 as a function of k (right), where k is the number of Chebyshev matrix elements taken from the fit.

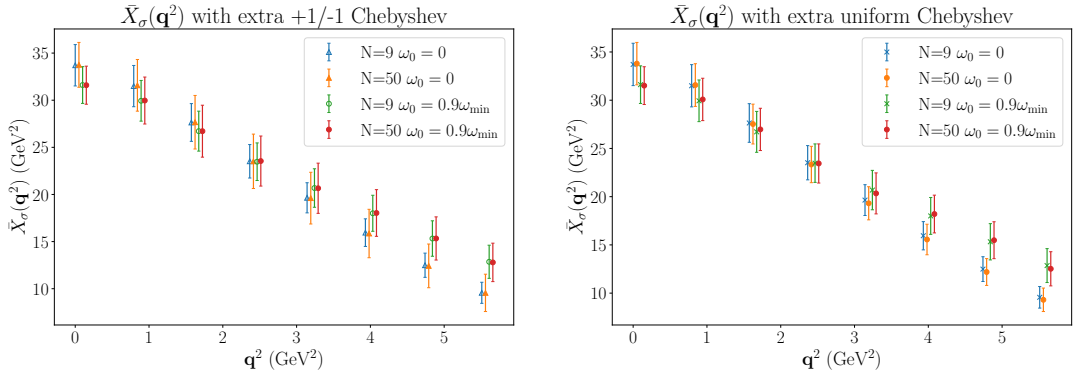

FIGURE 6.12: Truncation dependence of the Chebyshev polynomial approach, where $N = 9$ is the reference case, and for $N = 50$ higher-order terms are sampled from a $\mathbb{Z}_2$ distribution (left) or a uniform flat distribution in $[-1, 1]$ (right).

corresponding truncation error. A more complete study is however required for a reliable estimate of the underlying systematic effects.

Concerning the Backus-Gilbert method, we investigate the stability around the chosen value of λ^*, obtained with the prescription of Sec. 4.3.2. We focus in particular on the channel $\bar{X}^{(2)}_{\sigma,A_iA_i}(\boldsymbol{q}^2)$ as it is the one responsible for the largest contribution. The plot is shown in Fig. 6.13. We can see that for small $\boldsymbol{q}^2$ the value of $\bar{X}^{(2)}_{\sigma}(\boldsymbol{q})$ is stable, which implies that statistical and systematic errors are well balanced. For larger $\boldsymbol{q}^2$ the situation is more delicate: this can be understood in terms of the reduced phase space in ω, as shown for example in Fig. 6.8. A first attempt at mitigating the induced systematic effect could be to identify the region where the two Backus-Gilbert approaches with different bases are consistent, to identify (where possible) a plateau, and to estimate a value inside such a region. In Fig. 6.13 (right) we see, however, that this is not always the case: there is no clear plateau region for λ. Interestingly, the statistical error of the Chebyshev approach turns out more conservative in this case, and compatible with the result one would obtain from Backus-Gilbert. More generally, apart from the absence of

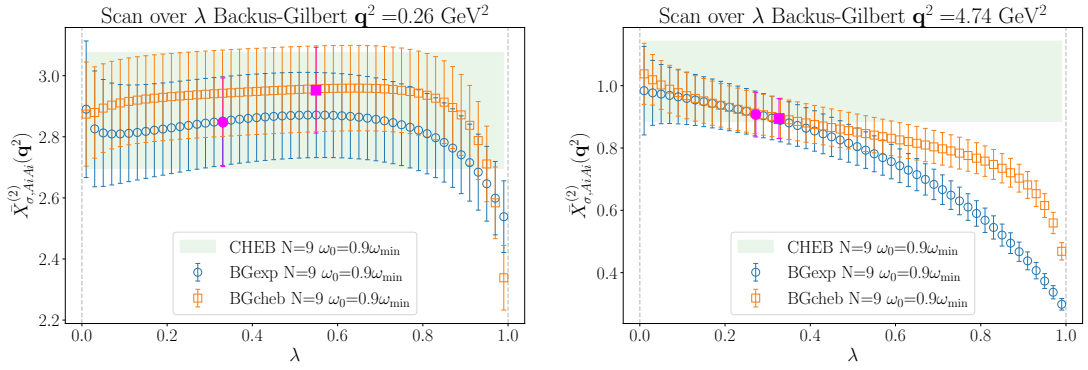

FIGURE 6.13: Scan over λ for $\boldsymbol{q}^2 = 0.26\,\mathrm{GeV}^2$ (left) and $\boldsymbol{q}^2 = 4.74\,\mathrm{GeV}^2$ (right) for the Backus-Gilbert method with exponential and Chebyshev basis for $\bar{X}^{(2)}_{\sigma,A_iA_i}$ with $\omega_0 = 0.9\,\omega_{\mathrm{min}}$. The green shaded band is the reference from the Chebyshev approach; the magenta points correspond to the choice of λ^*. Note that the points $\lambda = 0$ and $\lambda = 1$ (vertical grey dashed lines) are not included in this plot.

a plateau region in some cases, both choices of polynomial basis are consistent between themselves and with the Chebyshev-polynomial approach.

Coming back to the decay rate, to extract the final result we perform a polynomial fit of degree two on $\bar{X}^{(l)}_{\sigma}(\boldsymbol{q}^2)/(\sqrt{\boldsymbol{q}^2})^{2-l}$. The final decay rate is then obtained integrating these results in the physical range in $\boldsymbol{q}$. Since this is a qualitative study, we do not report any final number. However, we report that the result obtained here seems to be in the right ballpark if compared with the inclusive B_s-meson decay rate. Furthermore, all the approaches give compatible results, and the final statistical error is of order 5%.

We now address similarities and differences between the two approaches. As in Sec. 6.2.3, the calculation of $\bar{X}_\sigma(\boldsymbol{q}^2)$ aims to improve the accuracy by combining the naive polynomial approximation with a correction term $\delta\bar{X}_\sigma(\boldsymbol{q}^2)$ that accounts for variance reduction, i.e.,

$$\bar{X}_\sigma(\boldsymbol{q}^2) = \bar{X}^{\mathrm{naive}}_\sigma(\boldsymbol{q}^2) + \delta\bar{X}_\sigma(\boldsymbol{q}^2)\,, \tag{6.8}$$

where $\bar{X}^{\mathrm{naive}}_\sigma(\boldsymbol{q}^2)$ would correspond to Eq. (4.30). The correction terms are

$$\delta\bar{X}^{\mathrm{CHEB}}_\sigma(\boldsymbol{q}^2) = C_{\mu\nu}(2t_0)\sum_{k=0}^{N}\bar{c}_{\mu\nu,k}\delta\bar{C}_{\mu\nu}(k)\,, \quad \delta\bar{C}_{\mu\nu}(k) = \bar{C}^{\mathrm{fit}}_{\mu\nu}(k) - \bar{C}_{\mu\nu}(k) \tag{6.9}$$

for the Chebyshev-polynomial approach, and

$$\delta\bar{X}^{\mathrm{BG}}_\sigma(\boldsymbol{q}^2) = C_{\mu\nu}(2t_0)\sum_{k=0}^{N}\epsilon^*_{\mu\nu,k}\bar{C}_{\mu\nu}(k) \tag{6.10}$$

for the Backus-Gilbert method. The effect of the variance reduction is illustrated in Fig. 6.14, which shows the statistical error on $\bar{X}_\sigma(\boldsymbol{q}^2)$ with and without the correction

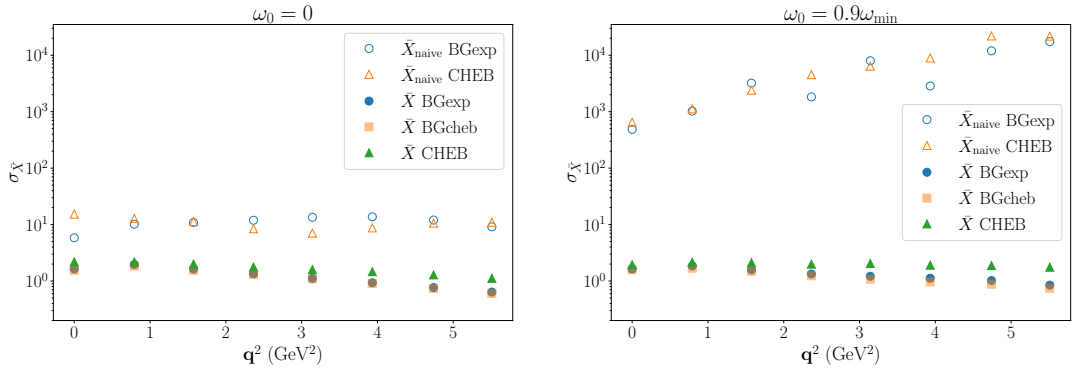

FIGURE 6.14: Effect of the variance reduction to $\bar{X}_\sigma^{\text{naive}}(\boldsymbol{q}^2)$ from the correction $\delta\bar{X}_\sigma(\boldsymbol{q}^2)$ as in Eq. (6.8) for $\omega_0 = 0$ (left) and $\omega_0 = 0.9\omega_{\min}$ (right) at $N = 9$. The y axis shows the standard deviation $\sigma_{\bar{X}}$ for $\bar{X}_\sigma^{\text{naive}}(\boldsymbol{q}^2)$ (empty symbols) and $\bar{X}_\sigma(\boldsymbol{q}^2) = \bar{X}_\sigma^{\text{naive}}(\boldsymbol{q}^2) + \delta\bar{X}_\sigma(\boldsymbol{q}^2)$ (filled symbols).

term. The reduction in statistical error is substantial, in particular for the $\omega_0 = 0.9\omega_{\min}$ case, where the error is reduced by roughly 3–4 orders of magnitude. Additionally, the magnitude of the correction varies depending on ω_0, where larger values result in a greater increase in $|\delta\bar{X}_\sigma(\boldsymbol{q}^2)|$ as $\boldsymbol{q}^2$ increases. As outlined before through Eq. (6.5), the higher-order terms of the polynomial approximation for larger values of ω_0 are less relevant, and therefore the expansion gives more weight to the earlier time-slices, where the signal-to-noise ratio is more pronounced.

To conclude this section we discuss some of the aspects we neglected for the purpose of this study. In particular, all the results presented here have been obtained with kernels smeared by a sigmoid with a fixed $\sigma = 0.02$. Eventually, however, one will have to first take the infinite-volume and continuum limits, followed by an extrapolation to $\sigma \to 0$. The smearing of the step function is required to perform the polynomial approximation and the numerical calculation. Note that the smearing is closely related to the inverse problem associated with the extraction of the spectral function as in [24].

Exemplarily, we show the σ dependence at finite lattice spacing and volume in Fig. 6.15. There, one sees that for our setup and statistical precision the dependence on σ is mild. There is an indication that it might be more pronounced for larger $\boldsymbol{q}^2$. We argue that here the extrapolation in σ is quite delicate and could lead to misleading results. Indeed, increasing values of sigma would result in kernel functions quite different from the target ones; on the other side, differences in small values of σ will not be captured by a polynomial approximation with small value of N, as small deviations would be noticeable only for higher degrees of approximations.

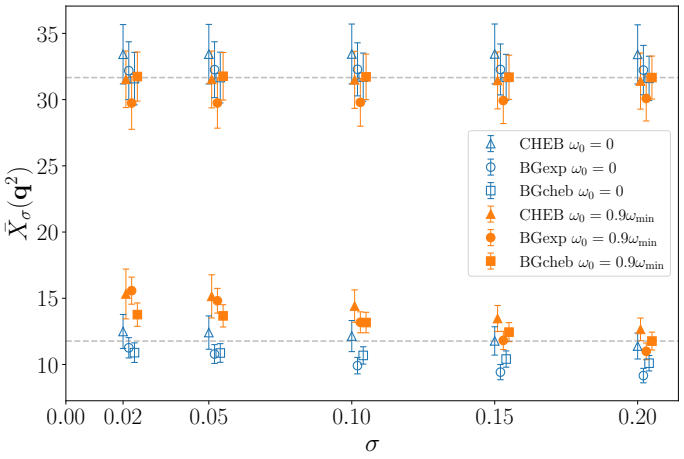

FIGURE 6.15: Dependence on the smearing parameter σ of $\bar{X}_\sigma(\boldsymbol{q}^2)$ for all the approaches at $N = 9$ in the case $\boldsymbol{q}^2 = 0.26\,\mathrm{GeV}^2$ (top) and $\boldsymbol{q}^2 = 4.74\,\mathrm{GeV}^2$ (bottom). The horizontal dashed lines correspond to the central values from the Chebyshev Backus-Gilbert with $\sigma = 0.02$ and $\omega_0 = 0.9\omega_{\min}$.

6.4 Decay rate in the ground-state limit

We now study the ground-state limit of the inclusive approach as discussed in Sec. 3.3.3, which provides a qualitative insight on the contribution of the excited states compared to the exclusive process. Furthermore, it also serves as a useful cross-check of the inclusive-decay analysis strategies.

The four-point function representing the ground state can be constructed with input from lattice data for the exclusive decay $B_s \to D_s\, l\nu_l$. In particular, restricting the discussion to the vector channel VV, the ground-state correlator

$$C^G_{\mu\nu}(t) = \frac{1}{4M_{B_s}E_{D_s}}\langle B_s|V^\dagger_\mu|D_s\rangle\langle D_s|V_\nu|B_s\rangle e^{-E_{D_s}t}\,, \tag{6.11}$$

can be constructed from lattice data for the ratio in Eq. (5.11) of three-point and two-point functions

$$R_{D_sB_s,\mu}(t;\boldsymbol{q}) = \sqrt{4M_{B_s}E_{D_s}}\sqrt{\frac{C^{SS}_{D_sB_s,\mu}(\boldsymbol{q},t_{\mathrm{snk}},t,t_{\mathrm{src}})C^{SS}_{B_sD_s,\mu}(\boldsymbol{q},t_{\mathrm{snk}},t,t_{\mathrm{src}})}{C^{SS}_{B_s}(t_{\mathrm{snk}},t_{\mathrm{src}})C^{SS}_{D_s}(\boldsymbol{q},t_{\mathrm{snk}},t_{\mathrm{src}})}}\,, \tag{6.12}$$

which converges to $\mathcal{M}_\mu \equiv \langle D_s|V_\mu|B_s\rangle$ for $t \gg t_{\mathrm{src}}$ and $t \ll t_{\mathrm{snk}}$. As in Eq. (3.18), the matrix element can be decomposed into form factors

$$\mathcal{M}_\mu = f^+(q^2)(p_{B_s} + p_{D_s})_\mu + f^-(q^2)(p_{B_s} - p_{D_s})_\mu\,. \tag{6.13}$$

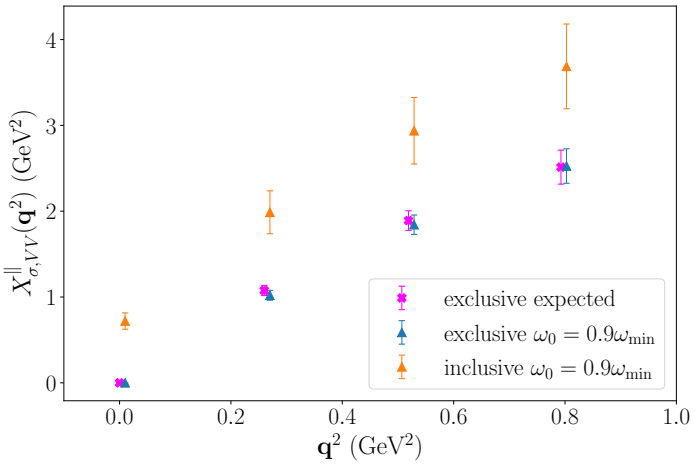

FIGURE 6.16: Ground-state limit. The "exclusive" labels refer to the data built from the three-point correlators as in Eq. (6.11), whereas the "inclusive" label refers to the full inclusive data analysis starting from the four-point correlation functions. The analysis has been performed using the Chebyshev approach.

Recalling that we assume $\boldsymbol{p}_{B_s} = \mathbf{0}$, we then extract $f^+(q^2)$ from a constant fit to the combination (cf. Eq. (3.19))

$$R_{f^+}(t;\boldsymbol{q}) \overset{\boldsymbol{q}\neq\mathbf{0}}{=} \frac{1}{2M_{B_s}} \left(R_{B_s D_s,0}(t;\boldsymbol{q}) + (M_{B_s} - E_{D_s}) \frac{\sum_{i=1}^{3} R_{D_s B_s,i}(t;\boldsymbol{q})}{\sum_{i=1}^{3} q_i} \right) , \tag{6.14}$$

which converges to $f^+(q^2)$ as $R_{D_s B_s,\mu}(t;\boldsymbol{q}) \to \mathcal{M}_\mu$. We consider only the three smaller momenta to test the approach, as the signal-to-noise deteriorates rapidly with larger $\boldsymbol{q}^2$.

The result of the inclusive analysis for the channel $\bar{X}^{\parallel}_{\sigma,VV}(\boldsymbol{q}^2)$ is reported in Fig. 6.16. In particular, we compare the expected value of $\bar{X}^{\parallel}_{\sigma,VV}(\boldsymbol{q}^2)$ in Eq. (3.112) from the extracted values of $f^+(q^2)$ with the inclusive analysis performed using the mock data $C^G_{\mu\nu}$ and the real data $C_{\mu\nu}$. Note that for the mock data the normalised correlator corresponds simply to $\bar{C}^G_{\mu\nu}(t) = e^{-E_{D_s} t}$ by construction.

We find excellent agreement between the results from the conventional analysis for exclusive decay on the one side, and the one based on ground-state saturation, but using the full analysis chain adopted for the inclusive decay, on the other side. This provides a strong test of the analysis method for inclusive decay discussed in this work. The results for the full inclusive decay, on the other hand, differ significantly from the exclusive case: while future studies will have to establish to which extend this could be down to systematics like finite-volume or cutoff effects, the magnitude of the effect makes appear likely to be to in large part due to contributions from the tower of finite states contributing to the inclusive decay. In particular, the deviation is expected to be larger for smaller $\boldsymbol{q}^2$, as the available phase space in ω is larger and may include more excited states.

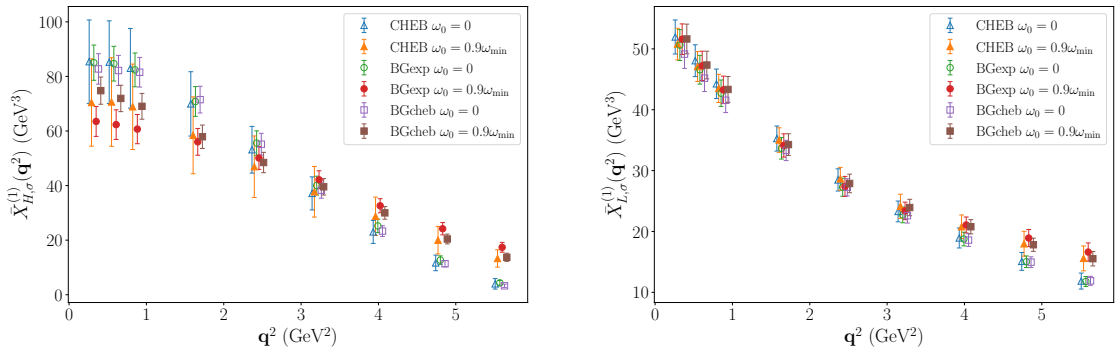

FIGURE 6.17: Evaluation of the numerators $X^{(1)}_{H,\sigma}(\boldsymbol{q}^2)$ (left) and $X^{(1)}_{L,\sigma}(\boldsymbol{q}^2)$ (right) of the hadronic mass and lepton differential moments at $n = 1$, respectively.

6.5 Moments

Let us conclude this chapter by showing some results for the kinematic moments discussed in Sec. 3.3.4. In particular, at this stage we focus on the numerators $\bar{X}^{(n)}_{H,\sigma}(\boldsymbol{q}^2)$ and $\bar{X}^{(n)}_{L,\sigma}(\boldsymbol{q}^2)$ of the differential hadronic mass and lepton moments as defined in Eqs. (3.125) and (3.126), which refer to the distribution of the invariant mass $(M^2_{X_c})^n$ and the lepton energy E^n_l, respectively. The ratio in the moments $\langle (M^2_{X_c})^n \rangle$ and $\langle E^n_l \rangle$ requires a deeper understanding of the systematics involved. Indeed, apart from the systematics of the polynomial approximation, both the numerator and denominator of these moments involve a fit of $\sqrt{\boldsymbol{q}^2}\bar{X}_\sigma(\boldsymbol{q}^2)$, which has to be taken into account properly.

In Fig. 6.17 we show the hadronic mass (left) and lepton energy (right) moments at order $n = 1$. As for the case of the decay rate, we see excellent agreement among the different methods. The only tension is again the one appearing for different values of ω_0 at higher $\boldsymbol{q}^2$, as discussed in Sec. 6.3. Note that, compared to the decay rate, the errors are larger for $\bar{X}^{(1)}_{H,\sigma}(\boldsymbol{q}^2)$ and smaller (or comparable) for $\bar{X}^{(1)}_{L,\sigma}(\boldsymbol{q}^2)$. This can be understood in terms of the differences of the kernels: indeed, the hadronic mass moments introduce extra factors that depend on ω in the kernels, whereas the behaviour of the leptonic kernels is smooth as shown in Figs. 6.4 and 6.5. We therefore expect the polynomial approximation to be more efficient in this second case.

A full treatment of (differential) moments on the lattice will allow to compare with analytical OPE approaches [29] to further test their validity. Moreover, lattice calculations may allow to extract some of the parameters that appear in the perturbative expansion.

CONCLUSIONS

In this work we have extended and improved the theoretical and computational framework for addressing inclusive semileptonic decays in Lattice QCD first introduced in [25], with specific focus on $B_{(s)}$ mesons. The discussion focused on the comparison of the Chebyshev-polynomial approach [27] and the modified Backus-Gilbert method [28], which both provide a promising way to address the calculations of physically relevant observables, such as decay rate and moments, specifically lepton energy and hadronic mass moments. In particular, we improved the Chebyshev-polynomial technique through the use of a generic set of shifted polynomials in $e^{-\omega}$, and we refined the statistical analysis with a bootstrap method, that accounts for the bounds $[-1, 1]$ in a consistent and theoretical clean way. We also investigated how the results depend on the order N of Chebyshev matrix elements, and we proposed a way to estimate the truncation error, that will allow to address the systematics associated with the polynomial approximation. Regarding the Backus-Gilbert approach, we introduced a generalisation of the method of [28] similar to [176] to allow for the use of arbitrary bases of polynomials.

The two analysis methods have been shown to be compatible, and the final results for the decay rate and the moments are in excellent agreement within the present statistical resolution. We compared how the two techniques deal with the variance reduction of the final observables: the Chebyshev-polynomial technique relies on trading the data with Chebyshev matrix elements that fully account for the bounds, whereas the Backus-Gilbert approach achieves the same objective by adjusting the coefficients of the polynomial approximation to reduce the statistical error.

In addition, we studied the ground-state limit, which offered a cross-check of the inclusive analysis technique. At the same time, the data on the ground-state provide for a quantitative measure for its contribution to the inclusive process.

Overall, this work provides a robust foundation for studies employing these techniques. However, several areas are still rather unexplored, as for instance systematic errors associated with the polynomial approximation, finite-volume effects, discretisation errors, and the continuum limit, to name a few. These can be addressed in future work, in particular through the study of processes such as $B_{(s)} \to X\, l\nu_l$ and $D_{(s)} \to X\, l\nu_l$ (and their corresponding exclusive version) performing more extended simulations with a comprehensive set of simulation parameters.

The long-term goal consists in obtaining precise and accurate predictions for the total decay rate in the continuum and finite-volume limit of Lattice QCD with physical quark masses. This long-term goal will play a crucial role in addressing the long-standing tension of the CKM-matrix elements $|V_{cb}|$ and $|V_{ub}|$, contributing in this way to a wide array of New Physics searches. However, many steps still have to be taken in order to move towards a relevant phenomenological prediction. In particular, one of the first tasks is to reiterate similar studies with new simulations on multiple ensembles, in order to address finite-volume effects and to explore the continuum limit, as well as to develop a solid strategy to perform the limit of the smearing parameter $\sigma \to 0$. Such studies will have to be supplemented by improved analytical understanding that guides the mentioned extrapolations. Furthermore, a deeper understanding of the systematics involved is required, which can be achieved, e.g., with the help of dedicated studies with toy models, which offer a controlled environment to develop the required analysis techniques. While the road ahead is long and the lattice precision is unlikely to deliver a competitive prediction for the decay rate in the near future, these calculations also provide an interesting framework to test other theoretical techniques. In particular, the study of moments, which do not depend on the CKM-matrix elements, provide a common ground to compare with OPE approaches and cross-validate their results.

APPENDIX A

EUCLIDEAN FORMULATION

In this appendix we report some of the conventions and relations between the Euclidean (E) and Minkowski (M) formulations used in this work. For Minkowski space-time we use the metric

$$g = \begin{pmatrix} 1 & 0 & 0 & 0 \\ 0 & -1 & 0 & 0 \\ 0 & 0 & -1 & 0 \\ 0 & 0 & 0 & -1 \end{pmatrix} . \tag{A.1}$$

A.1 Gamma matrices

Let us first introduce the general notation we use for the gamma matrices. In order to describe in a compact way all the relevant operators used in this work (i.e. scalar, pseudoscalar, vector and axial operators) and their properties (such as, e.g., transformation under hermitian conjugation, transposition,...etc.), we indicate all possible gammas with $\Gamma \in \{\Gamma^J, \Gamma^J_\mu\}$ with $J = V, A$, and introduce the sign s^J as

$$\begin{cases} \Gamma^V = \mathrm{I} \\ \Gamma^A = \gamma_5 \end{cases} , \qquad \begin{cases} \Gamma^V_\mu = \gamma_\mu \\ \Gamma^A_\mu = \gamma_\mu\gamma_5 \end{cases} , \qquad \begin{cases} s^V = +1 \\ s^A = -1 \end{cases} , \tag{A.2}$$

Turning now to the actual representation, the Euclidean gamma matrices in the chiral representation γ_μ^E, with $\mu = 1, 2, 3, 4$, are given by

$$\gamma_1^E = \begin{pmatrix} 0 & 0 & 0 & -i \\ 0 & 0 & -i & 0 \\ 0 & i & 0 & 0 \\ i & 0 & 0 & 0 \end{pmatrix}, \qquad \gamma_2^E = \begin{pmatrix} 0 & 0 & 0 & -1 \\ 0 & 0 & 1 & 0 \\ 0 & 1 & 0 & 0 \\ -1 & 0 & 0 & 0 \end{pmatrix}, \tag{A.3}$$

$$\gamma_3^E = \begin{pmatrix} 0 & 0 & -i & 0 \\ 0 & 0 & 0 & i \\ i & 0 & 0 & 0 \\ 0 & -i & 0 & 0 \end{pmatrix}, \qquad \gamma_4^E = \begin{pmatrix} 0 & 0 & 1 & 0 \\ 0 & 0 & 0 & 1 \\ 1 & 0 & 0 & 0 \\ 0 & 1 & 0 & 0 \end{pmatrix},$$

together with $\gamma_5^E = \gamma_1^E \gamma_2^E \gamma_3^E \gamma_4^E$, which reads

$$\gamma_5^E = \begin{pmatrix} 1 & 0 & 0 & 0 \\ 0 & 1 & 0 & 0 \\ 0 & 0 & -1 & 0 \\ 0 & 0 & 0 & -1 \end{pmatrix}. \tag{A.4}$$

These matrices are hermitian and satisfy

$$\gamma_\mu^{E\dagger} = (\gamma_\mu^E)^{-1} = \gamma_\mu^E\,, \qquad \gamma_5^{E\dagger} = (\gamma_5^E)^{-1} = \gamma_5^E\,, \tag{A.5}$$

as well as the anti-commutation relation

$$\{\gamma_\mu^E, \gamma_\nu^E\} = 2\delta_{\mu\nu}\,, \qquad \{\gamma_\mu^E, \gamma_5^E\} = 0\,. \tag{A.6}$$

The relation with the Minkowski matrices γ_μ^M, $\mu = 0, 1, 2, 3$ are given by

$$\gamma_0^M = \gamma_4^E\,, \qquad \gamma_k^E = -i\gamma_k^M\,, \qquad \gamma_5^E = -\gamma_5^M\,. \tag{A.7}$$

A.2 Euclidean operators

We now consider the relation between Euclidean and Minkowski operators. Let us first recall the relation for position space. The time variable is Wick rotated in Euclidean space, i.e. $t^E = it^M$ such that the four-vector x in position space reads

$$x^M = (x_0, \boldsymbol{x}) = (-ix_4, \boldsymbol{x})\,, \qquad x^E = (\boldsymbol{x}, x_4) = (\boldsymbol{x}, ix_0)\,, \tag{A.8}$$

In the next sections, we specify the relation between the two formulations for scalar, pseudoscalar, vector and axial operators. We consider two different quark fields Q and

q, where the relation between their Euclidean and Minkowski representation is given by

$$q^M(x_0, \boldsymbol{x}) = q^M(-ix_4, \boldsymbol{x}) \equiv q^E(\boldsymbol{x}, x_4)\,, \tag{A.9}$$

and similarly for Q.

A.2.1 Scalar and pseudoscalar operators

For a scalar or pseudoscalar operator $\mathcal{P} = \bar{Q}\Gamma^J q$ the relation between the two formulations is given by

$$\begin{aligned} \mathcal{P}^M(x_0, \boldsymbol{x}) &= \bar{Q}^M(x_0, \boldsymbol{x})\Gamma^{J,M} q^M(x_0, \boldsymbol{x}) \\ &= s^J \bar{Q}^M(-ix_4, \boldsymbol{x})\Gamma^{J,E} q^M(-ix_4, \boldsymbol{x}) \\ &= s^J \bar{Q}^E(\boldsymbol{x}, x_4)\Gamma^{J,E} q^E(\boldsymbol{x}, x_4) \\ &\equiv s^J \mathcal{P}^E(\boldsymbol{x}, x_4)\,, \end{aligned} \tag{A.10}$$

where we recall that

$$\Gamma^{J,M} = s^J \Gamma^{J,E}\,. \tag{A.11}$$

A.2.2 Vector and axial operators

For a generic vector or axial operator $J_\mu = \bar{Q}\Gamma^J_\mu q = \bar{Q}\gamma_\mu\Gamma^J q$ we consider temporal and spatial component separately. For the time component we have

$$\begin{aligned} J_0^M(x_0, \boldsymbol{x}) &= \bar{Q}^M(x_0, \boldsymbol{x})\gamma_0^M\Gamma^{J,M} q^M(x_0, \boldsymbol{x}) \\ &= s^J \bar{Q}^M(-ix_4, \boldsymbol{x})\gamma_4^E\Gamma^{J,E} q^M(-ix_4, \boldsymbol{x}) \\ &= s^J \bar{Q}^E(\boldsymbol{x}, x_4)\gamma_4^E\Gamma^{J,E} q^E(\boldsymbol{x}, x_4) \\ &\equiv s^J J_4^E(\boldsymbol{x}, x_4)\,, \end{aligned} \tag{A.12}$$

whereas for the spatial one

$$\begin{aligned} J_k^M(x_0, \boldsymbol{x}) &= \bar{Q}^M(x_0, \boldsymbol{x})\gamma_k^M\Gamma^{J,M} q^M(x_0, \boldsymbol{x}) \\ &= is^J \bar{Q}^M(-ix_4, \boldsymbol{x})\gamma_k^E\Gamma^{J,E} q^M(-ix_4, \boldsymbol{x}) \\ &= is^J \bar{Q}^E(\boldsymbol{x}, x_4)\gamma_k^E\Gamma^{J,E} q^E(\boldsymbol{x}, x_4) \\ &\equiv is^J J_k^E(\boldsymbol{x}, x_4)\,. \end{aligned} \tag{A.13}$$

A.2.3 General operator

We can write in a general way the consideration of previous section for a generic operator $\mathcal{O}$. In particular we can write

$$\mathcal{O}^M = s^E_{\mathcal{O}} \mathcal{O}^E \,, \qquad\qquad \mathcal{O}^E = s^M_{\mathcal{O}} \mathcal{O}^M \tag{A.14}$$

where $s^E_{\mathcal{O}} = 1/s^M_{\mathcal{O}}$ are in general complex coefficients. The expectation value of the product of n operators $\mathcal{O}_j$, $j = 1, \ldots, n$ can be easily mapped from Euclidean to Minkowski as

$$\langle \mathcal{O}^M_1 \mathcal{O}^M_2 \ldots \mathcal{O}^M_n \rangle = s^E_{\mathcal{O}_1} s^E_{\mathcal{O}_2} \ldots s^E_{\mathcal{O}_n} \langle \mathcal{O}^E_1 \mathcal{O}^E_2 \ldots \mathcal{O}^E_n \rangle \tag{A.15}$$

where the Euclidean version is computed through a n-point correlators $C_{n\text{pt}}$ on a lattice,

$$C_{n\text{pt}} \propto \langle \mathcal{O}^E_1 \mathcal{O}^E_2 \ldots \mathcal{O}^E_n \rangle \,. \tag{A.16}$$

A.3 Matrix elements and correlators

We now show the relation between Euclidean and Minkowski matrix elements, from which also follow the relation between correlators. This is helpful to understand where the physical signals appear in the correlation functions computed in practice on the lattice, i.e. either in the real or imaginary part of the Euclidean correlator. Indeed, while we work in Euclidean space on the lattice, physics lives in Minkowski space and we have to relate our computation to it. We consider the case of a three-point function, as the four-point function case can be straightforwardly obtained from the following discussion recalling Eq. (4.22).

Let us consider the process for two pseudoscalar meson $\mathcal{P}_i \to \mathcal{P}_f$ mediated by the current J_μ: the relevant matrix element $\langle \mathcal{P}_f | \, J_\mu \, | \mathcal{P}_i \rangle$ can be extracted from an Euclidean three-point correlation function

$$C^E_{P_f P_i, \mu} \propto \left\langle \mathcal{P}^E_f \right| J^E_\mu \left| \mathcal{P}^E_i \right\rangle \,. \tag{A.17}$$

The corresponding physical matrix element in Minkowski space is $\langle \mathcal{P}^M_f | J^M_\mu | \mathcal{P}^M_i \rangle$. Since there are two pseudoscalar operators which both get a minus sign when switching between the two formulations (see Eq. (A.10)) we omit their superscript and focus only on the current J_μ. Considering the spatial and temporal components separately we obtain

$$\langle \mathcal{P}_f | \, J^M_0(x_0, \boldsymbol{x}) \, | \mathcal{P}_i \rangle = s^J \, \langle \mathcal{P}_f | \, J^E_4(\boldsymbol{x}, x_4) \, | \mathcal{P}_i \rangle \tag{A.18}$$

$$\langle \mathcal{P}_f | \, J^M_k(x_0, \boldsymbol{x}) \, | \mathcal{P}_i \rangle = i s^J \, \langle \mathcal{P}_f | \, J^E_k(\boldsymbol{x}, x_4) \, | \mathcal{P}_i \rangle \,. \tag{A.19}$$

From the above equation is immediate to see the the physics signal of the Euclidean correlator lies in its real part for the temporal components and in the imaginary part for the spatial ones.

APPENDIX B

DISCRETE SYMMETRIES

In this appendix we list some properties and discrete symmetries of Wilson-type fermions, that apply in particular to the DWF and RHQ formulations used in this work. We follow [93, 94] and refer to those sources for more details. Discrete symmetries are useful for matrix element calculations, as they can be used to determine which elements (e.g. which type of currents) contribute in a given process. We illustrate them considering a quark fermion field $q(x)$ and a gauge field $U_\mu(x)$. We indicate explicitly the dependence on the gauge field in the quark propagator $G(y, x; U) = \langle q(y)\bar{q}(x)\rangle$ in order to point out precisely how G transforms under these symmetries.

B.1 Parity

The parity operator P has the effect of reversing the spatial coordinates, i.e.

$$P \,:\, x = (\boldsymbol{x}, x_4) \to x^P = (-\boldsymbol{x}, x_4)\,. \tag{B.1}$$

It acts on the quark and gauge fields as

$$\begin{aligned} P \,:\quad q(x) &\to q^P(x) = \gamma_4 q(x^P)\,, \\ \bar{q}(x) &\to \bar{q}^P(x) = \bar{q}(x^P)\gamma_4\,, \\ U_4(x) &\to U_4^P(x) = U_4(x^P)\,, \\ U_j(x) &\to U_j^P(x) = -U_{-j}(x^P)\,, \end{aligned} \tag{B.2}$$

and the propagator transforms as

$$P \,:\, G(y, x; U) \to \gamma_4 G(y^P, x^P; U^P)\gamma_4\,. \tag{B.3}$$

B.2 Time reversal

The time reversal operator T is the analogous of the parity operator for the time direction

$$T \,:\, x = (\boldsymbol{x}, x_4) \to x^t = (\boldsymbol{x}, -x_4)\,. \tag{B.4}$$

It acts on the quark and gauge fields as

$$\begin{aligned} T \,:\;\; q(x) &\to q^t(x) = \gamma_4\gamma_5 q(x^t)\,, \\ \bar{q}(x) &\to \bar{q}^t(x) = \bar{q}(x^t)\gamma_5\gamma_4\,, \\ U_4(x) &\to U_4^t(x) = -U_{-4}(x^t)\,, \\ U_j(x) &\to U_j^t(x) = U_j(x^t)\,, \end{aligned} \tag{B.5}$$

and the propagator transforms as

$$T \,:\, G(y,x;U) \to \gamma_4\gamma_5 G(y^t, x^t; U^t)\gamma_5\gamma_4\,. \tag{B.6}$$

B.3 Charge conjugation

Charge conjugation transforms particles into antiparticles and the corresponding operator C acts on the fermion field as

$$C \,:\; q(x) \to q^C(x) = C\bar{q}(x)^T\,, \tag{B.7}$$

$$\bar{q}(x) \to \bar{q}^C(x) = -q(x)^T C^{-1}\,, \tag{B.8}$$

$$U_\mu(x) \to U_\mu^C(x) = U_\mu^*(x)\,. \tag{B.9}$$

where the transpose "T" transforms a column spinor into a row spinor and vice versa. The propagator G transforms as

$$G(y,x;U) \;\to\; G^C(y,x;U) = C\,G(y,x;U^C)^T\,C^{-1}\,. \tag{B.10}$$

The specific form of C depends on the chosen representation of the gamma matrices. A common choice is the chiral representation as in App. A.1, for which $C = i\gamma_2\gamma_4$. Regardless of the representation, the following relations hold true

$$C\Gamma^J C^{-1} = (\Gamma^J)^T\,, \tag{B.11}$$

$$C\Gamma_\mu^J C^{-1} = -s^J(\Gamma_\mu^J)^T\,, \tag{B.12}$$

where we recall that $s^V = 1$, $s^A = -1$ and $\Gamma^V = \mathrm{I}$, $\Gamma^A = \gamma_5$, $\Gamma_\mu^V = \gamma_\mu$ and $\Gamma_\mu^A = \gamma_\mu\gamma_5$.

B.4 γ_5-hermiticity

The quark propagator $G(y, x; U)$ obeys the property

$$G^\dagger(y, x; U) = \gamma_5 G(x, y; U)\gamma_5 \,, \tag{B.13}$$

which is typical of Wilson-type operators. It can be implement through the operator

$$H \,:\, G(x, y; U) \to \gamma_5 G^\dagger(y, x; U)\gamma_5 \,. \tag{B.14}$$

APPENDIX C

CHEBYSHEV POLYNOMIALS

In this appendix we review some properties of the standard Chebyshev polynomials and generalise them for generic shifted polynomials. We refer to other sources [200, 201] for more details.

C.1 Standard Polynomials

The standard Chebyshev polynomials of the first kind are defined as

$$T_k : [-1,1] \to [-1,1]\,, \quad T_k(x) = \cos\left(k \cos^{-1}(x)\right)\,, \quad k \in \mathbb{N}\,, \tag{C.1}$$

from which it follows that

$$T_k(\cos(\theta)) = \cos(k\theta)\,, \quad \theta \in [0,\pi]\,. \tag{C.2}$$

They are orthogonal with respect the scalar product

$$\int_{-1}^{1} T_r(x) T_s(x) \Omega(x)\, \mathrm{d}x = \pi \delta_{rs} \left(1 - \frac{1}{2}\delta_{r0}\right)\,, \tag{C.3}$$

where $\Omega(x) = 1/\sqrt{1-x^2}$ is a weight function.

We list here some of the most useful properties that have been used explicitly in this thesis.

- *Recurrence relation.* The polynomials satisfy the relation

$$T_{k+1}(x) = 2xT_k(x) - T_{k-1}(x)\,, \tag{C.4}$$

with $T_0(x) = 1$ and $T_1(x) = x$.

- *Zeros.* $T_k(x)$ has k zeros in $(-1, 1)$ given by

$$x_j^0 = \cos\left(\frac{2j+1}{2k}\pi\right), \quad j = 0, 1, \ldots, k-1\,. \tag{C.5}$$

- *Extrema.* $T_k(x)$ has $k+1$ extrema in $[-1, 1]$ given by

$$x'_j = \cos\left(\frac{j}{k}\pi\right), \quad j = 0, 1, \ldots, k\,. \tag{C.6}$$

The values of the polynomials in the extrema are given by $T_k(x'_j) = (-1)^j$.

C.1.1 Polynomial representation

The expansion of the Chebyshev polynomials in x^k is given by

$$T_n(x) = \sum_{k=0}^{[n/2]} d_k^{(n)} x^{n-2k}\,, \tag{C.7}$$

with

$$\begin{cases} d_k^{(n)} & = (-1)^k 2^{n-2k-1} \frac{n}{n-k}\binom{n-k}{k} \quad \text{if} \quad k \neq \frac{n}{2} \\ d_k^{(n)} & = (-1)^k \quad \text{if} \quad k = \frac{n}{2} \end{cases}. \tag{C.8}$$

Note that if n is even the powers of x are all even, and vice versa if n is odd. We can rewrite this expression setting $k = (n-j)/2$ and $t_j^{(n)} = d_{(n-j)/2}^{(n)}$ as

$$T_n(x) = \sum_{j=0}^{n} t_j^{(n)} x^j\,, \tag{C.9}$$

with

$$\begin{cases} t_0^{(n)} = (-1)^{n/2} & \text{if } n \text{ even} \\ t_k^{(n)} = 0 & \text{if } n-k \text{ odd} \\ t_k^{(n)} = (-1)^{(n-k)/2}\, 2^{k-1} \frac{n}{\frac{n+k}{2}} \binom{\frac{n+k}{2}}{\frac{n-k}{2}} & \text{if } k \neq 0 \text{ and } n-k \text{ even} \end{cases}. \tag{C.10}$$

C.1.2 Power representation

A useful property involves the power representation of the standard Chebyshev polynomial

$$p_n(x) \equiv x^n = 2^{1-n} \sum_{\substack{k=0 \\ n-k \text{ even}}}^{n}{}' \binom{n}{\frac{n-k}{2}} T_k(x)\,, \quad x \in [-1,1]\,, \tag{C.11}$$

where the prime indicates that the first term is halved.

C.1.3 Chebyshev interpolation

The strength of the Chebyshev polynomials relies on the fact that they provide the best approximation of the function $f : [-1,1] \to \mathbb{R}$ to any given order N in terms of the L_∞-norm. In other words, the *minmax* error, i.e. the maximum difference between the target function and the reconstructed one, is minimised. In particular, for the functions considered in this work, it is guaranteed that the Chebyshev approximation converges when $N \to \infty$. The polynomial approximation reads

$$f(x) \simeq \frac{1}{2} c_0 T_0(x) + \sum_{k=1}^{N} c_k T_k(x)\,, \quad c_k = \frac{2}{\pi} \int_{-1}^{1} \mathrm{d}x\, f(x) T_k(x) \Omega(x)\,, \tag{C.12}$$

where we recall that $T_0(x) = 1$ by definition. The coefficients are given by the projection of the target function f on the basis of Chebyshev polynomials.

C.2 Shifted Polynomials

Let us now address the generalisation of the standard Chebyshev polynomials. In the most general case, we want to consider a generic function $f(x)$ defined in an interval $[a,b]$ and we want to approximate it with Chebyshev polynomials. In order to achieve that we can define some shifted polynomials $\tilde{T}_n(x)$ with $x \in [a,b]$ and look for an approximation of the function at order N

$$f(x) = \frac{1}{2} \tilde{c_0} \tilde{T}_0(x) + \sum_{k=1}^{N} \tilde{c_k} \tilde{T}_k(x)\,. \tag{C.13}$$

The shifted Chebyshev polynomials are related to the standard ones by

$$\tilde{T}_n(x) = T_n(h(x))\,, \tag{C.14}$$

where $h : [a, b] \to [-1, 1]$, $y = h(x)$ is a invertible function that maps the new domain into the domain of the standard Chebyshev polynomials, with

$$h(a) = -1\,, \quad h(b) = +1\,. \tag{C.15}$$

We can then redefine the properties of the polynomials in a more general way. In particular, the orthogonality relation now reads

$$\int_a^b \mathrm{d}x\, \tilde{T}_r(x)\tilde{T}_s(x)\Omega_h(x) = \int_a^b \mathrm{d}x\, T_r(h(x))T_s(h(x))\Omega_h(x)\,, \tag{C.16}$$

where $\Omega_h(x)$ is the new weight for the shifted $\tilde{T}_n(x)$ which depends on the map h. To show this and determine the form of $\Omega_h(x)$, we can set $x = h^{-1}(y)$, $\mathrm{d}x = \frac{1}{h'(h^{-1}(y))}\mathrm{d}y$ such that

$$\int_{h(a)}^{h(b)} \mathrm{d}y\, T_r(y)T_s(y)\frac{\Omega(h^{-1}(y))}{h'(h^{-1}(y))}\,. \tag{C.17}$$

From this equation, it is immediate to see that choosing

$$\Omega_h(x) = \Omega(h(x))|h'(x)| \tag{C.18}$$

we obtain

$$\int_a^b \mathrm{d}x\, \tilde{T}_r(x)\tilde{T}_s(x)\Omega_h(x) = \int_{-1}^1 \mathrm{d}y\, T_r(y)T_s(y)\Omega(y)\,, \tag{C.19}$$

which indeed recovers the original orthogonality relation in Eq. (C.3). The coefficients are then given by

$$\begin{aligned}\tilde{c}_k &= \frac{2}{\pi}\int_a^b \mathrm{d}x\, f(x)\tilde{T}_k(x)\Omega_h(x) = \frac{2}{\pi}\int_a^b \mathrm{d}x\, f(x)T_k(h(x))\Omega(h(x))|h'(x)| \\ &\overset{h(x)=y}{=} \frac{2}{\pi}\int_{-1}^1 \mathrm{d}y\, f(h^{-1}(y))T_k(y)\Omega(y) \overset{y=\cos\theta}{=} \frac{2}{\pi}\int_0^\pi \mathrm{d}\theta\, f(h^{-1}(\cos\theta))(\cos k\theta)\,.\end{aligned} \tag{C.20}$$

The recursion relation $T_{n+1}(x) = 2xT_n(x) - T_{n-1}(x)$ becomes

$$\tilde{T}_{n+1}(x) = T_{n+1}(h(x)) = 2h(x)T_n(h(x)) - T_{n-1}(h(x)) = 2h(x)\tilde{T}_n(x) - \tilde{T}_{n-1}(x)\,. \tag{C.21}$$

Let us consider some of the possible maps in the following sections. We focus on maps of the form

$$h(x) = A(x) + B = Aa(x) + B\,, \tag{C.22}$$

where A and B are constants that depend on the values a and b of the domain of the function f.

C.2.1 Linear map

The simplest map is given by the linear shift with

$$h : [a, b] \to [-1, 1] \,, \qquad h(x) = Ax + B \,, \qquad a(x) = x \,, \tag{C.23}$$

where

$$A = \frac{2}{b-a} \,, \qquad B = -\frac{b+a}{b-a} \,. \tag{C.24}$$

If we set $y = h(x)$ we get

$$x = h^{-1}(y) = \frac{1}{A} y - \frac{B}{A} = \frac{b-a}{2} y + \frac{b+a}{2} \,,$$

such that a generic function f in $[a, b]$ can be approximated by

$$f(x) = \frac{1}{2} \tilde{c_0} \tilde{T}_0(x) + \sum_{k=1}^{N} \tilde{c_k} \tilde{T}_k(x) \,, \quad \tilde{c_k} = \frac{2}{\pi} \int_0^\pi \mathrm{d}\theta \, f\left(\frac{b-a}{2} \cos\theta + \frac{b+a}{2} \right) \cos(k\theta) \,. \tag{C.25}$$

C.2.2 Exponential map

Another way of shifting the polynomials can be achieved through

$$h : [a, b] \to [-1, 1] \,, \qquad h(x) = Ae^{-x} + B \,, \qquad a(x) = e^{-x} \,, \tag{C.26}$$

where in this case the resulting polynomial is in term of exponentials $(e^{-x})^k$. Setting again $y = h(x)$ and inverting we find

$$x = h^{-1}(y) = -\log\left(\frac{y-B}{A} \right) \,. \tag{C.27}$$

Requiring $h(a) = -1$ and $h(b) = +1$ we can determine the coefficients as

$$A = -\frac{2}{e^{-a} - e^{-b}} \,, \qquad B = \frac{e^{-a} - e^{-b}}{e^{-a} + e^{-b}} \,. \tag{C.28}$$

A generic function f in $[a, b]$ is then approximated by

$$f(x) = \frac{1}{2} \tilde{c_0} \tilde{T}_0(x) + \sum_{k=1}^{N} \tilde{c_k} \tilde{T}_k(x) \,, \quad \tilde{c_k} = \frac{2}{\pi} \int_0^\pi \mathrm{d}\theta \, f\left(-\ln\left(\frac{\cos\theta - B}{A} \right) \right) \cos(k\theta) \,. \tag{C.29}$$

Note that this case is interesting because it allows us to easily consider an unbounded function defined in an interval $[a, \infty]$ simply by considering the limit $b \to \infty$.

C.2.3 Polynomial representation

For a generic shifted polynomial with map $h(x) = A(x) + B$ and $A(x) = Aa(x)$, where $a(x) = x$ for a linear map and $a(x) = e^{-x}$ for an exponential map, the polynomial representation reads

$$\tilde{T}_n(x) = \sum_{j=0}^{n} t_j^{(n)} h(x)^j = \sum_{j=0}^{n} t_j^{(n)} (A(x) + B)^j = \sum_{j=0}^{n} t_j^{(n)} \sum_{k=0}^{j} \binom{j}{k} A(x)^k B^{j-k} . \tag{C.30}$$

We can expand this sum explicitly and re-sum it in order to isolate the coefficients of $A(x)^j$

$$\begin{aligned}
\tilde{T}_n(x) &= \sum_{j=0}^{n} t_j^{(n)} \sum_{k=0}^{j} \binom{j}{k} A(x)^k B^{j-k} \qquad (C.31)\\
&= A(x)^n \left[\binom{n}{n} t_n^{(n)} \right] + A(x)^{n-1} \left[\binom{n-1}{n-1} t_{n-1}^{(n)} + \binom{n}{n-1} t_n^{(n)} B^1 \right] \\
&+ A(x)^{n-2} \left[\binom{n-2}{n-2} t_{n-2}^{(n)} + \binom{n-1}{n-2} t_{n-1}^{(n)} B^1 + \binom{n}{n-2} t_n^{(n)} B^2 \right] + \cdots \\
&+ A(x) \left[\binom{1}{1} t_1^{(n)} + \binom{2}{1} t_2^{(n)} B + \cdots + \binom{n}{1} t_n^{(n)} B^{n-1} \right] \\
&+ \left[\binom{0}{0} t_0^{(n)} + \binom{1}{0} t_1^{(n)} B + \cdots + \binom{n}{0} t_n^{(n)} B^n \right] ,
\end{aligned}$$

and we get

$$\tilde{T}_n(x) = \sum_{k=0}^{n} A(x)^k \sum_{j=k}^{n} \binom{j}{k} t_j^{(n)} B^{j-k} . \tag{C.32}$$

Recalling that $A(x) = Aa(x)$ with $A = const$ and redefining the coefficients we finally get

$$\tilde{T}_n(x) = \sum_{k=0}^{n} \tilde{t}_k^{(n)} a(x)^k , \qquad \tilde{t}_k^{(n)} = A^k \sum_{j=k}^{n} \binom{j}{k} t_j^{(n)} B^{j-k} . \tag{C.33}$$

We can also write this expression through the help of a matrix as

$$\begin{pmatrix} \tilde{T}_0(x) \\ \tilde{T}_1(x) \\ \vdots \\ \vdots \\ \tilde{T}_n(x) \end{pmatrix} = \begin{pmatrix} \tilde{t}_0^{(0)} & 0 & \cdots & \cdots & 0 \\ \tilde{t}_0^{(1)} & \tilde{t}_1^{(1)} & 0 & \cdots & 0 \\ \vdots & \vdots & \ddots & \ddots & \vdots \\ \vdots & \vdots & & \ddots & 0 \\ \tilde{t}_0^{(n)} & \tilde{t}_1^{(n)} & \cdots & \cdots & \tilde{t}_n^{(n)} \end{pmatrix} \begin{pmatrix} 1 \\ a(x)^1 \\ \vdots \\ \vdots \\ a(x)^n \end{pmatrix} , \tag{C.34}$$

where the matrix can be written in a compact notation as $\tilde{\boldsymbol{t}}$ with $(\tilde{\boldsymbol{t}})_{ij} = \tilde{t}_j^{(i)}$.

C.2.4 Power representation

We also generalise the power representation as

$$\tilde{p}_n(x) \equiv h(x)^n = 2^{1-n} \sum_{\substack{j=0 \\ n-j \text{ even}}}^{n}{}' \binom{n}{\frac{n-j}{2}} \tilde{T}_j(x)\,, \quad x \in [a,b]\,, \tag{C.35}$$

which implies that $(A(x)+B)^n = \tilde{p}_n(x)$. Using

$$\tilde{p}_n(x) = (A(x)+B)^n = \sum_{k=0}^{n} \binom{n}{k} A(x)^k B^{n-k} \tag{C.36}$$

we can work out iteratively the general expression for $A(x)$ as

$$A(x)^n = \tilde{p}_n(x) - \sum_{k=0}^{n-1} \binom{n}{k} A(x)^k B^{n-k}\,, \quad a(x)^n = \frac{A(x)^n}{A^n}\,. \tag{C.37}$$

We can now rewrite $a(x)^n$ in a more compact form as

$$a(x)^n = \sum_{j=0}^{n} \tilde{a}_j^{(n)} \tilde{T}_j(x)\,. \tag{C.38}$$

The set of coefficients $\tilde{a}_j^{(n)}$ can be easily found numerically. In a more compact way, the above equation can be expressed in matrix form as

$$\begin{pmatrix} 1 \\ a(x)^1 \\ \vdots \\ \vdots \\ a(x)^n \end{pmatrix} = \begin{pmatrix} \tilde{a}_0^{(0)} & 0 & \cdots & \cdots & 0 \\ \tilde{a}_0^{(1)} & \tilde{a}_1^{(1)} & 0 & \cdots & 0 \\ \vdots & \vdots & \ddots & \ddots & \vdots \\ \vdots & \vdots & & \ddots & 0 \\ \tilde{a}_0^{(n)} & \tilde{a}_1^{(n)} & \cdots & \cdots & \tilde{a}_n^{(n)} \end{pmatrix} \begin{pmatrix} \tilde{T}_0(x) \\ \tilde{T}_1(x) \\ \vdots \\ \vdots \\ \tilde{T}_n(x) \end{pmatrix}, \tag{C.39}$$

where the above matrix can again be written in a compact notation as $\tilde{\boldsymbol{a}}$ with $(\tilde{\boldsymbol{a}})_{ij} = \tilde{a}_j^{(i)}$. It is immediate to see that the matrix $\tilde{\boldsymbol{a}}$ and $\tilde{\boldsymbol{t}}$ in Eq. (C.34) are related by

$$\tilde{\boldsymbol{a}} = \tilde{\boldsymbol{t}}^{-1}\,, \quad \tilde{\boldsymbol{a}}^{-1} = \tilde{\boldsymbol{t}}\,. \tag{C.40}$$

APPENDIX D

GENERALISED BACKUS-GILBERT

In this appendix we reformulate and generalise the modified Backus-Gilbert approach proposed in [28,175]. The idea is to provide a more general framework, which allows for the use of an arbitrary basis, and to explore the properties and numerical advantages of different choices.

D.1 The method

The problem we want to address is the evaluation of a generic observable O of the form

$$O = \int_a^b \mathrm{d}\omega\, \rho(\omega) K(\omega)\,, \tag{D.1}$$

where $K(\omega)$ is a function we will refer to as *kernel* and $\rho(\omega)$ is the spectral function related to a given correlation function through the Källén-Lehmann representation [202, 203]

$$C(t) = \int_a^b \mathrm{d}\omega\, \rho(\omega) e^{-\omega t}\,. \tag{D.2}$$

While typically the range of integration is $a = 0$ and $b = \infty$, here we chose to leave it generic to keep the discussion general. The idea to address the computation is to approximate the kernel in polynomials in $e^{-\omega}$ (in lattice units $a = 1$) up to some degree N, i.e. $K(\omega) = \sum_{j=0}^{N} g_j e^{-\omega j}$, such that the target observable can be estimated as

$$O \simeq \sum_{j=0}^{N} g_j \int_a^b \mathrm{d}\omega\, \rho(\omega) e^{-\omega j} = \sum_{j=0}^{N} g_j C(j). \tag{D.3}$$

For example, a typical problem consists in the extraction of the spectral density of a correlator, in which case one would consider the kernel to be a smoothed Dirac delta $K(\omega) = \delta_\sigma(\omega)$ with a finite width σ, as for example a Gaussian.

The approach consists of weighting the two functionals $A[g]$ and $B[g]$ against each other, where the first one provides a measure for the systematic effects coming from the polynomial approximation, and the second one provides a measure for the variance σ_O^2 of the observable O, in particular, $B[g] = \sigma_O^2 = \sum_{i,j} g_i \sigma_{ij} g_j$, where we defined $\sigma_{ij} = \mathrm{Cov}(C(i), C(j))$. This is equivalent to solving a minimisation problem with constraints. We can then define a new functional F_θ as

$$F_\theta[g] = A[g] + \theta^2 B[g]\,, \tag{D.4}$$

and determine the coefficients by variational principle $\partial F_\theta[g]/\partial g_j = 0$ at different values of θ^2. The value $\theta^2 = 0$ corresponds to addressing exclusively the polynomial approximation, as prescribed by the choice of $A[g]$, whereas the choices $\theta^2 \to \infty$ would correspond to dealing purely with the variance minimisation and would result in $g_j = 0$. Note that we can map $\theta^2 = \lambda/(1-\lambda)$ for simplicity, such that $\lambda \in [0, 1)$ and $\theta^2 \to \infty$ for $\lambda \to 1$. Furthermore, any relative normalisation term between the two functionals can be reabsorbed into θ^2. Depending on the choice of the basis, the coefficients g_j may grow over different orders of magnitude and numerical instabilities may appear. This can be addressed in practice by using arbitrary precision arithmetic.

We now discuss in detail how to generalise the modified Backus-Gilbert [28] for a generic basis of functions, starting from the construction of $A[g]$. Following the original paper we can generalise the L_2-norm of the difference between the target function and the polynomial reconstruction using an arbitrary family of basis functions $P_k(x) = \sum_{j=0}^k p_j^{(k)} x^j$ defined in an interval $x \in [p_-, p_+]$. As for the Chebyshev, we will deal in general with a shifted version of this family of polynomials in e^{-x} defined in a generic interval $[a, b]$

$$\tilde{P}_k(x) = \sum_{j=0}^{k} \tilde{p}_j^{(k)} e^{-jx}\,, \quad x \in [a, b]\,, \tag{D.5}$$

where $\tilde{P}_k(x) = P_k(h(x))$ and $h(x) = Ae^{-x} + B$ is an invertible map that satisfies $h(a) = p_-$ and $h(b) = p_+$. The interval $[a, b]$ has to match the range of integration of the observable O in Eq. (D.1). The functional $A[g]$ now reads

$$A[g] = \int_a^b \mathrm{d}\omega\, \Omega(\omega) \left[K(\omega) - \sum_{j=0}^{N} g_j \tilde{P}_j(\omega) \right]^2 . \tag{D.6}$$

With respect to the original version we now have introduced a generic weight $\Omega(\omega)$; note that we start the approximation at $\tilde{P}_0(\omega)$ (as long as $\Omega(\omega)$ can be integrated in $[a, b]$).

If we consider only the $A[g]$ term, the solution of the system by variational principle is given by

$$\boldsymbol{A} \cdot \boldsymbol{g} = \boldsymbol{K} \quad \longleftrightarrow \quad \boldsymbol{g} = \boldsymbol{A}^{-1} \cdot \boldsymbol{K} \tag{D.7}$$

where

$$A_{ij} = \int_a^b \mathrm{d}\omega\, \Omega(\omega) \tilde{P}_i(\omega) \tilde{P}_j(\omega)\,, \tag{D.8}$$

$$K_i = \int_a^b \mathrm{d}\omega\, \Omega(\omega) \tilde{P}_i(\omega) K(\omega)\,, \tag{D.9}$$

and $\boldsymbol{g}$ is a vector of parameters.

With this setup, the convenient choice consists in picking a set of (shifted) orthogonal polynomials

$$\langle \tilde{P}_i, \tilde{P}_j \rangle = \int_a^b \mathrm{d}x\, \Omega(x) \tilde{P}_i(x) \tilde{P}_j(x) \propto \delta_{ij}\,, \tag{D.10}$$

with Ω being the actual weight that defines the scalar product. The advantage is immediately clear, as the matrix $\boldsymbol{A}$ becomes

$$A_{ij} = \langle \tilde{P}_i, \tilde{P}_j \rangle\,, \tag{D.11}$$

and the coefficients are given by

$$g_i = \frac{1}{\langle \tilde{P}_i, \tilde{P}_i \rangle} \int_a^b \mathrm{d}\omega\, \Omega(\omega) \tilde{P}_i(\omega) K(\omega)\,. \tag{D.12}$$

Since the matrix $\boldsymbol{A}$ is now diagonal, the inverse required to compute Eq. (D.7) is analytically known. Furthermore, the solution is now equivalent to the projection on the polynomial basis.

We can now include the B term, i.e. the covariance matrix of the data. Note that in general we now need to consider a linear combination of the correlator at different time slices according to the polynomial basis, i.e.

$$C^P(k) = \int_a^b \mathrm{d}\omega\, \rho(\omega) \tilde{P}_k(\omega) = \int_a^b \mathrm{d}\omega\, \rho(\omega) \sum_{j=0}^{k} \tilde{p}_j^{(k)} e^{-j\omega} = \sum_{j=0}^{k} \tilde{p}_j^{(k)} C(j)\,, \tag{D.13}$$

such that

$$B[g] = \sum_{i,j} g_i\, \sigma_{ij}^P\, g_j\,, \qquad \sigma_{ij}^P = \mathrm{Cov}(C^P(i), C^P(j))\,. \tag{D.14}$$

The full functional is then

$$F_\theta[g] = A[g] + \theta^2 B[g] \tag{D.15}$$

and the final solution is

$$\boldsymbol{g}_\theta = \boldsymbol{F}_\theta^{-1} \cdot \boldsymbol{K} \tag{D.16}$$

with

$$\boldsymbol{F}_\theta = \boldsymbol{A} + \theta^2 \boldsymbol{B}\,, \tag{D.17}$$

where $B_{ij} = \sigma_{ij}^P$. The steps considered here are mathematically equivalent to the approach in [176]. However, while the matrix considered in [176] is ill-conditioned by construction and requires the use of arbitrary precision arithmetic to perform the inversion, our formulation relies on the construction of a diagonal matrix $\boldsymbol{A}$, in the case where an orthogonal polynomial basis is chosen. Therefore, in this scenario the inversion of the matrix $\boldsymbol{F}$ in Eq. (D.17) may be better conditioned and possible numerical instabilities may be avoided.

On top of that we could also implement some constraints that our approximation has to fulfil. In particular, following what was done for the spectral function in [28, 175], we can require that the polynomial approximation preserve the (weighted) area of the target function, i.e.

$$\int_a^b \mathrm{d}\omega\, \Omega(\omega) \sum_{k=0}^{N} g_k\, \tilde{P}_k(\omega) = \int_a^b \mathrm{d}\omega\, \Omega(\omega) K(\omega)\,. \tag{D.18}$$

This can be expressed as

$$\boldsymbol{R}^T \cdot \boldsymbol{g}_\theta = r\,, \tag{D.19}$$

where

$$R_k = \int_a^b \mathrm{d}\omega\, \Omega(\omega) \tilde{P}_k(\omega)\,, \qquad r = \int_a^b \mathrm{d}\omega\, \Omega(\omega) K(\omega)\,. \tag{D.20}$$

Taking into account these constraints, the solution becomes

$$\boldsymbol{g}_\theta = \boldsymbol{F}_\theta^{-1} \cdot \boldsymbol{K} + \boldsymbol{F}_\theta^{-1} \cdot \boldsymbol{R} \frac{r - \boldsymbol{R}^T \cdot \boldsymbol{F}_\theta^{-1} \cdot \boldsymbol{K}}{\boldsymbol{R}^T \cdot \boldsymbol{F}_\theta^{-1} \cdot \boldsymbol{R}}\,. \tag{D.21}$$

The final observable then reads

$$O_\theta \simeq \sum_{j=0}^{N} g_{\theta,j} C^P(j)\,, \tag{D.22}$$

for a given value of θ. The choice of θ is in principle arbitrary. A common choice is to take the value θ^* that gives equal weight to the A and B functional, $A[g_{\theta^*}] = B[g_{\theta^*}]$, i.e. an equal weight to statistical and systematic error. For a given choice of θ, it is important to make sure that the value of the final observable is stable for small changes in θ, in order to make sure that the procedure did not introduce any bias.

To conclude, note that this recovers the method first proposed in [28] if we consider the following substitutions

$$\begin{aligned} \tilde{P}_j(\omega) &\to e^{-(j+1)\omega}\,, \\ \Omega(\omega) &\to 1\,, \\ \theta^2 &\to \lambda/(1-\lambda)\,, \\ F[g] &\to (1-\lambda)F[g]\,. \end{aligned} \tag{D.23}$$

D.2 A different perspective

The previous reformulation in App. D.1 allows us to rely on arbitrary polynomials for the approximation. In this general picture it is useful to consider a different perspective to the method: we can reduce the problem to finding a suitable correction to the optimal coefficients, i.e.

$$g_j = \gamma_j + \epsilon_j\,, \tag{D.24}$$

where γ_j are the coefficients of the polynomial approximation coming purely from the functional $A[\gamma]$, i.e. $\boldsymbol{\gamma} = \boldsymbol{A}^{-1}\boldsymbol{K}$ as in Eq. (D.7), and ϵ_j a correction that takes into account the data. We can then rewrite the functional as

$$F_\theta[g] = F_\theta[\gamma+\epsilon] = F_\theta[\gamma] + \delta F_\theta[\epsilon]\,, \tag{D.25}$$

and explicitly

$$\delta F_\theta[\epsilon] = \int_a^b \mathrm{d}\omega\,\Omega(\omega)\left[\sum_{k=0}^{N}\epsilon_k\tilde{P}_k(\omega)\right]^2 + \theta^2\left(2\gamma_i\sigma^P_{ij}\epsilon_j + \epsilon_i\sigma^P_{ij}\epsilon_j\right)\,. \tag{D.26}$$

The minimisation of $\delta F_\theta[\epsilon]$ gives

$$\boldsymbol{\epsilon}_\theta = -\theta^2\left(\boldsymbol{A} + \theta^2\boldsymbol{\sigma^P}\right)^{-1}\boldsymbol{\sigma^P}\boldsymbol{\gamma}\,, \tag{D.27}$$

which is equivalent to the previous approach. It is then clear that ϵ_j are by construction coefficients that should not modify the quality of the polynomial approximations but take care of the reduction of the statistical noise. In practice, this will of course depend on the choice of θ.

APPENDIX E

FIT STRATEGY

In this appendix we discuss the fit strategy adopted in this work, reviewing in particular the Maximum Likelihood method in App. E.1, the Maximum a Posteriori approach in App. E.2 and the application of the latter with a boostrap analysis in App. E.3. Thorough discussions about data fitting can be found, e.g., in [192, 193, 196, 204–207]

To keep the discussion very general we consider a generic linear model of the form

$$y(x) = \sum_{\alpha=1}^{M} p_\alpha X_\alpha(x)\,, \tag{E.1}$$

where $X_\alpha(x)$ are known data and p_α are the parameters to be determined.

E.1 Maximum likelihood (ML)

In the standard frequentist approach, we define the χ^2 distribution as

$$\chi^2 = \sum_{i,j=1}^{N} \left(y_i - \sum_{\alpha=1}^{M} p_\alpha X_\alpha(x_i) \right) \mathrm{Cov}_{ij}^{-1} \left(y_j - \sum_{\beta=1}^{M} p_\beta X_\beta(x_j) \right) \tag{E.2}$$

where $\mathrm{Cov}_{ij} = \langle (y_i - \langle y_i \rangle)(y_j - \langle y_j \rangle) \rangle$ is the covariance matrix of the data. To obtain the parameters p_α we need to minimise the χ^2 with respect to those parameters. Indeed, the probability of the *data (D) given the fit (F)* is given by the probability distribution

$$P(D|F) = \frac{1}{(2\pi)^{N/2}\sqrt{\det[\mathrm{Cov}]}} e^{-\frac{1}{2}\chi^2}\,. \tag{E.3}$$

Maximising this probability (the *maximum likelihood* (ML) method) is equivalent to minimizing the χ^2.

We can now take the derivative

$$\left.\frac{\partial\chi^2}{\partial p_\gamma}\right|_{\hat{p}} = 2\sum_{i,j=1}^{N}\left(y_i - \sum_{\alpha=1}^{M}\hat{p}_\alpha X_\alpha(x_i)\right)\mathrm{Cov}_{ij}^{-1}(-X_\gamma(x_j)) = 0\,, \tag{E.4}$$
$$\Rightarrow \sum_{i,j=1}^{N} y_i \mathrm{Cov}_{ij}^{-1} X_\gamma(x_j) = \sum_{\alpha=1}^{M}\hat{p}_\alpha \sum_{i,j=1}^{N} X_\alpha(x_i)\mathrm{Cov}_{ij}^{-1}X_\gamma(x_j)\,,$$

and defining

$$\begin{cases} v_\gamma &= \sum_{i,j=1}^{N} y_i \mathrm{Cov}_{ij}^{-1} X_\gamma(x_j) \\ U_{\alpha\gamma} &= \sum_{i,j=1}^{N} X_\alpha(x_i)\mathrm{Cov}_{ij}^{-1}X_\gamma(x_j) \end{cases} \tag{E.5}$$

we get the final value for the parameters $\hat{p}_\alpha$

$$\hat{p}_\alpha = \sum_{\gamma=1}^{M}(U^{-1})_{\gamma\alpha}v_\gamma\,. \tag{E.6}$$

Note that Cov_{ij} is symmetric and so is its inverse Cov_{ij}^{-1}. By definition, then, also U and its inverse are symmetric. Furthermore, we note that U is the Hessian matrix of the χ^2: taking another derivative in Eq. (E.4) it is straightforward to see that

$$U_{\alpha\gamma} = \frac{1}{2}\frac{\partial^2\chi^2}{\partial p_\alpha \partial p_\gamma}\,. \tag{E.7}$$

U is also known as *curvature matrix*: for a linear model it is constant and independent of the fit parameters. U^{-1} represents the covariance matrix of the parameters, i.e. $\mathrm{Cov}(p_\alpha, p_\beta) = (U^{-1})_{\alpha\beta}$.

Let us prove that this is really the covariance. Assuming we only have one set of data y_i with the covariance Cov_{ij} we can consider simulated values y_i^S of the data points, with $\delta y_i^S = y_i^S - y_i$. The deviation of the parameters calculated on the simulated data set $\delta p_\alpha = p_\alpha^S - p_\alpha$ is then

$$\delta p_\alpha^S = \sum_{i=0}^{N}\frac{\partial p_\alpha}{\partial y_i}\delta y_i^S\,, \tag{E.8}$$

and the corresponding covariance $\sigma_{\alpha\beta}^S = \mathrm{Cov}(p_\alpha, p_\beta)$ is

$$\sigma_{\alpha\beta}^S = \langle \delta p_\alpha^S \delta p_\beta^S\rangle = \sum_{i,j=1}^{N}\frac{\partial p_\alpha}{\partial y_i}\mathrm{Cov}_{ij}\frac{\partial p_\beta}{\partial y_j}\,, \tag{E.9}$$

since $\mathrm{Cov}_{ij} = \langle \delta y_i^S \delta y_j^S \rangle$. Recalling Eqs. (E.5) and (E.6) we have

$$\frac{\partial p_\alpha}{\partial y_i} = \sum_{\gamma=1}^{M} \sum_{k=1}^{N} (U^{-1})_{\gamma\alpha} \mathrm{Cov}_{ik}^{-1} X_\gamma(x_k) \,. \tag{E.10}$$

Substituting this into the above equation we finally get

$$\begin{aligned} \sigma_{\alpha\beta}^S &= \sum_{\gamma,\delta=1}^{M} \sum_{i,j=1}^{N} (U^{-1})_{\gamma\alpha} (U^{-1})_{\delta\beta} \mathrm{Cov}_{ij}^{-1} X_\gamma(x_i) X_\delta(x_j) \\ &= \sum_{\gamma,\delta=1}^{M} (U^{-1})_{\gamma\alpha} (U^{-1})_{\delta\beta} \underbrace{\sum_{i,j=1}^{N} X_\gamma(x_i) \mathrm{Cov}_{ij}^{-1} X_\delta(x_j)}_{U_{\gamma\delta}} \\ &= (U^{-1})_{\alpha\beta} \end{aligned} \tag{E.11}$$

We have thus shown that $\mathrm{Cov}(\hat{p_\alpha}, \hat{p_\beta}) = (U^{-1})_{\alpha\beta}$. It is important to notice that we would have obtained the exact same result if we had considered a large number of data set $y_i^{(d)}$ and calculated the covariance with respect the the true value y_i^{true}, with deviation $\delta y_i^{(d)} = y_i^{(d)} - y_i^{\mathrm{true}}$. Indeed, the calculation would follow exactly the step above and would lead to the same result.

For a non-linear model, the curvature matrix is no more independent from the fit parameters. It is, however, generally assumed that the estimated standard deviation corresponds to the standard deviation of the model. The covariance matrix is then estimated in this case as the inverse of the curvature matrix at the minimum of the χ^2.

This is indeed the case when we "wrap" the parameters p_α in some non-linear invertible function $p_\alpha = f(\pi_\alpha)$ to enforce some constraint. For example, if we know a priori that the parameters must be positive, we may consider fitting some new parameters $\pi_\alpha = \log(p_\alpha)$ and convert the final results in term of $p_\alpha = \exp(\pi_\alpha)$ after the fit. In such a case the χ^2 looks like

$$\chi^2 = \sum_{i,j=1}^{N} \left(y_i - \sum_{\alpha=1}^{M} f(\pi_\alpha) X_\alpha(x_i) \right) \mathrm{Cov}_{ij}^{-1} \left(y_j - \sum_{\alpha=1}^{M} f(\pi_\alpha) X_\alpha(x_j) \right) . \tag{E.12}$$

The optimal parameters $\hat{\pi}_\alpha$ can be found as usual by minimising the χ^2 and solving for π_α. However, due to the fact that f is in general non-linear, in this case the parameters have to be determined numerically.

E.2 Maximum a posteriori (MAP) estimation

The frequentist approach gives information about the *probability of the data given the fit* $P(D|F)$. Instead, we would like to consider the *probability of the fit given the data*

$P(F|D)$: this can be achieved through Bayes theorem. Indeed, we can relate the probabilities as

$$P(F|D) = \frac{P(D|F)P(F)}{P(D)}\,, \tag{E.13}$$

where $P(F)$ is a *prior distribution*, which encodes the "a priori" knowledge about the fit parameters, whereas $P(F|D)$ is the *posterior distribution*. Bayesian statistics may seem either subjective or determined by mathematical convenience, but it is indeed a powerful tool to introduce bounds or other a priori information about the parameters.

In more details, $P(D|F)$ is taken to be the usual likelihood as above and $P(F)$ is usually taken gaussian for mathematical convenience. A common choice for the latter is a gaussian with mean $\mu = 0$ and variance $\sigma = 1$. The probability $P(D)$ is a constant independent from the parameters and acts as a normalization, as it can be rewritten as

$$P(D) = \sum_F P(D|F)P(F)\,. \tag{E.14}$$

The easiest and most convenient case is to consider a Gaussian distribution for the parameters such that

$$P(F) \propto \Pi_{\alpha=1}^{M} \exp\left(-\frac{1}{2}\frac{(p_\alpha - \bar{p}_\alpha)^2}{\bar{\sigma}_\alpha^2}\right) \equiv \exp\left(-\frac{1}{2}\chi^2_{\text{prior}}\right), \tag{E.15}$$

where we introduced some arbitrary mean values $\bar{p}_\alpha$ and standard deviations $\bar{\sigma}_\alpha$ based on our prior knowledge of the parameter distributions. We can build in this way an *augmented* $\chi^2_{\text{aug}} = \chi^2 + \chi^2_{\text{prior}}$, which is now made of the usual frequentist χ^2 and of a new "prior" χ^2_{prior}, i.e.

$$\chi^2_{\text{aug}} = \sum_{i,j=1}^{N} \left(y_i - \sum_{\alpha=1}^{M} p_\alpha X_\alpha(x_i)\right) \text{Cov}_{ij}^{-1} \left(y_j - \sum_{\alpha=1}^{M} p_\alpha X_\alpha(x_j)\right) + \sum_{\alpha=1}^{M} \frac{(p_\alpha - \bar{p}_\alpha)^2}{\bar{\sigma}_\alpha^2}\,. \tag{E.16}$$

The parameters that minimizes the new χ^2_{aug} can be found as usual as requiring $\frac{\partial \chi^2_{\text{aug}}}{\partial p_\gamma} = 0$

$$\begin{aligned} \frac{\partial \chi^2_{\text{aug}}}{\partial p_\gamma} &= \frac{\partial \chi^2}{\partial p_\gamma} + \frac{\partial}{\partial p_\gamma} \sum_{\alpha=1}^{M} \frac{(p_\alpha - \bar{p}_\alpha)^2}{\bar{\sigma}_\alpha^2} \\ &= \frac{\partial \chi^2}{\partial p_\gamma} + 2\left(\frac{p_\gamma}{\bar{\sigma}_\gamma^2} - \frac{\bar{p}_\gamma}{\bar{\sigma}_\gamma^2}\right) = 0\,. \end{aligned} \tag{E.17}$$

The parameters are given by $\hat{p}_\alpha = \sum_{\gamma=1}^{M} (\bar{U}^{-1})_{\gamma\alpha} \bar{v}_\gamma$ where in this case

$$\begin{cases} \bar{v}_\gamma & = \sum_{i,j=1}^{N} y_i \mathrm{Cov}_{ij}^{-1} X_\gamma(x_j) + \dfrac{\bar{p}_\gamma}{\bar{\sigma}_\gamma^2} \\ \bar{U}_{\alpha\gamma} & = \sum_{i,j=1}^{N} X_\alpha(x_i) \mathrm{Cov}_{ij}^{-1} X_\gamma(x_j) + \dfrac{\delta_{\alpha\gamma}}{\bar{\sigma}_\gamma^2} \end{cases} . \tag{E.18}$$

The same considerations as before apply here, as $\bar{U}$ and $\bar{v}_\alpha$ are still independent from the parameters p_α and the data y_i. In particular, it is still true that

$$\mathrm{Cov}(\hat{p}_\alpha, \hat{p}_\beta) = (\bar{U}^{-1})_{\alpha\beta} . \tag{E.19}$$

E.2.1 Most general MAP

We now consider the case where we "wrap" the parameters in a function $p_\alpha = f(\pi_\alpha)$ in a Bayesian context. In this case, the fit is performed on the new parameters π_α, and the prior is then introduced accordingly. The augmented χ^2 looks like

$$\chi^2_{\mathrm{aug}} = \sum_{i,j=1}^{N} \left(y_i - \sum_{\alpha=1}^{M} f(\pi_\alpha) X_\alpha(x_i) \right) \mathrm{Cov}_{ij}^{-1} \left(y_j - \sum_{\alpha=1}^{M} f(\pi_\alpha) X_\alpha(x_j) \right) + \sum_{\alpha=1}^{M} \frac{(\pi_\alpha - \bar{\pi}_\alpha)^2}{\bar{\sigma}_\alpha^2} . \tag{E.20}$$

Imposing $\frac{\partial \chi^2_{\mathrm{aug}}}{\partial \pi_\gamma} = 0$ we get

$$\left. \frac{\partial \chi^2_{\mathrm{aug}}}{\partial \pi_\gamma} \right|_{\hat{\pi}} = 2 \sum_{i,j=1}^{N} \left(y_i - \sum_{\alpha=1}^{M} f(\hat{\pi}_\alpha) X_\alpha(x_i) \right) \mathrm{Cov}_{ij}^{-1} (-X_\gamma(x_j) f'(\hat{\pi}_\gamma)) + 2 \left(\frac{\hat{\pi}_\gamma - \bar{\pi}_\gamma}{\bar{\sigma}_\gamma^2} \right) = 0 \tag{E.21}$$

from which we obtain

$$\sum_{i,j=1}^{N} y_i \mathrm{Cov}_{ij}^{-1} X_\gamma(x_j) - \left(\frac{\hat{\pi}_\gamma - \bar{\pi}_\gamma}{\bar{\sigma}_\gamma^2} \right) = \sum_{\alpha=1}^{M} f(\hat{\pi}_\alpha) \sum_{i,j=1}^{N} X_\alpha(x_i) \mathrm{Cov}_{ij}^{-1} X_\gamma(x_j) f'(\hat{\pi}_\gamma) . \tag{E.22}$$

In general, this equation is now non-linear and the optimal value for the parameters $\hat{\pi}_\alpha$ can be determined numerically. The error can be calculated as usual inverting the

curvature matrix. For the internal parameters π_α we get

$$\begin{aligned}\frac{1}{2}\frac{\partial^2\chi^2}{\partial\pi_\alpha\partial\pi_\beta}\bigg|_{\hat{\pi}} =& f'(\hat{\pi}_\alpha)\left[\sum_{i,j=1}^{N} X_\alpha(x_i)\mathrm{Cov}_{ij}^{-1}X_\gamma(x_j)\right]f'(\hat{\pi}_\beta) \\ &+\sum_{i,j=1}^{N}\left(y_i-\sum_{\alpha=1}^{M}f(\hat{\pi}_\alpha)X_\alpha(x_i)\right)\mathrm{Cov}_{ij}^{-1}(-X_\beta(x_j)f''(\hat{\pi}_\beta))\delta_{\alpha\beta}+\delta_{\alpha\beta}\frac{1}{\sigma_\alpha^2} \\ =& f'(\hat{\pi}_\alpha)U_{\alpha\beta}f'(\hat{\pi}_\beta)+\delta_{\beta\alpha}\left[\frac{1}{\sigma_\alpha^2}-\frac{f''(\hat{\pi}_\alpha)}{f'(\hat{\pi}_\alpha)}\frac{\hat{\pi}_\alpha-\bar{\pi}_\alpha}{\bar{\sigma}_\alpha^2}\right],\end{aligned} \tag{E.23}$$

where in the last line we used Eq. (E.21). For the final parameters $\hat{p}_\alpha$ we then get the covariance matrix

$$\begin{aligned}\mathrm{Cov}(p_\alpha,p_\beta)=\frac{1}{2}\frac{\partial^2\chi^2}{\partial p_\alpha\partial p_\beta}\bigg|_{\hat{p}} &= \frac{1}{f'(\hat{\pi}_\alpha)}\,\frac{1}{2}\frac{\partial^2\chi^2}{\partial\pi_\alpha\partial\pi_\beta}\bigg|_{\hat{\pi}}\,\frac{1}{f'(\hat{\pi}_\beta)} \\ &= U_{\alpha\beta}+\delta_{\alpha\beta}\frac{1}{f'(\hat{\pi}_\alpha)}\left[\frac{1}{\sigma_\alpha^2}-\frac{f''(\hat{\pi}_\alpha)}{f'(\hat{\pi}_\alpha)}\frac{\hat{\pi}_\alpha-\bar{\pi}_\alpha}{\bar{\sigma}_\alpha^2}\right]\frac{1}{f'(\hat{\pi}_\alpha)}\,.\end{aligned} \tag{E.24}$$

E.3 MAP estimation with bootstrap analysis

As discussed in the previous sections, the inclusion of a "wrapping" function on the parameters p_α indicates that the distribution of these parameters is generally not Gaussian. This conclusion arises from our assumption that the internal parameters π_α follow a Gaussian distribution, while the wrapping function introduces constraints that limit the domain of p_α. Rather than determining the central value of the data and estimating error through the inverse of the curvature matrix (the Hessian of the χ^2 with respect to the parameters), a more suitable strategy is to employ a bootstrap approach. This approach automatically accommodates any deviations from Gaussian behaviour. In practice, this involves fitting all the bootstrap bins and constructing the parameter distribution while handling the associated errors accordingly.

Our chosen methodology involves assuming a normal distribution for the internal parameters $\pi_\alpha \sim \mathcal{N}(\mu,\sigma)$ such that $p_\alpha = f(\pi_\alpha)$ follow a distribution based on our prior knowledge of the parameters. To implement this approach, we consider a set of N_b bootstrap bins, each associated with data points y_i^b. For each bin, we perform a separate fit that employs a distinct prior value $\bar{\pi}_\alpha^b$ sampled from the normal distribution $\mathcal{N}(\mu,\sigma)$. This ensures that the appropriate prior information is included into p_α. In cases where the data contain limited information, leading to $min(\chi^2_{\mathrm{aug}}) \approx min(\chi^2_{\mathrm{prior}})$, the fitting process effectively returns the prior information we introduced by hand.

REFERENCES

[1] A. Barone, A. Jüttner, S. Hashimoto, T. Kaneko and R. Kellermann, *Inclusive semi-leptonic $B_{(s)}$ mesons decay at the physical b quark mass*, *PoS* **LATTICE2022** (2023) 403 [2211.15623].

[2] R. Kellermann, A. Barone, S. Hashimoto, A. Jüttner and T. Kaneko, *Inclusive semi-leptonic decays of charmed mesons with Möbius domain wall fermions*, *PoS* **LATTICE2022** (2023) 414 [2211.16830].

[3] A. Barone, S. Hashimoto, A. Jüttner, T. Kaneko and R. Kellermann, *Approaches to inclusive semileptonic $B_{(s)}$-meson decays from Lattice QCD*, *JHEP* **07** (2023) 145 [2305.14092].

[4] Heavy Flavor Averaging Group, HFLAV collaboration, *Averages of b-hadron, c-hadron, and τ-lepton properties as of 2021*, *Phys. Rev. D* **107** (2023) 052008 [2206.07501].

[5] Flavour Lattice Averaging Group (FLAG) collaboration, *FLAG Review 2021*, *Eur. Phys. J. C* **82** (2022) 869 [2111.09849].

[6] BaBar collaboration, *Measurement of an Excess of $\bar{B} \to D^{(*)}\tau^-\bar{\nu}_\tau$ Decays and Implications for Charged Higgs Bosons*, *Phys. Rev. D* **88** (2013) 072012 [1303.0571].

[7] Belle collaboration, *Measurement of the branching ratio of $\bar{B} \to D^{(*)}\tau^-\bar{\nu}_\tau$ relative to $\bar{B} \to D^{(*)}\ell^-\bar{\nu}_\ell$ decays with hadronic tagging at Belle*, *Phys. Rev. D* **92** (2015) 072014 [1507.03233].

[8] Belle collaboration, *Measurement of the τ lepton polarization and $R(D^*)$ in the decay $\bar{B} \to D^*\tau^-\bar{\nu}_\tau$*, *Phys. Rev. Lett.* **118** (2017) 211801 [1612.00529].

[9] Belle collaboration, *Measurement of $\mathcal{R}(D)$ and $\mathcal{R}(D^*)$ with a semileptonic tagging method*, *Phys. Rev. Lett.* **124** (2020) 161803 [1910.05864].

[10] LHCb collaboration, *Measurement of the ratio of branching fractions* $\mathcal{B}(\bar{B}^0 \to D^{*+}\tau^-\bar{\nu}_\tau)/\mathcal{B}(\bar{B}^0 \to D^{*+}\mu^-\bar{\nu}_\mu)$, *Phys. Rev. Lett.* **115** (2015) 111803 [1506.08614].

[11] LHCb collaboration, *Test of Lepton Flavor Universality by the measurement of the* $B^0 \to D^{*-}\tau^+\nu_\tau$ *branching fraction using three-prong* τ *decays*, *Phys. Rev. D* **97** (2018) 072013 [1711.02505].

[12] LHCb collaboration, *Measurement of Form-Factor-Independent Observables in the Decay* $B^0 \to K^{*0}\mu^+\mu^-$, *Phys. Rev. Lett.* **111** (2013) 191801 [1308.1707].

[13] LHCb collaboration, *Test of lepton universality using* $B^+ \to K^+\ell^+\ell^-$ *decays*, *Phys. Rev. Lett.* **113** (2014) 151601 [1406.6482].

[14] BaBar collaboration, *Evidence for an excess of* $\bar{B} \to D^{(*)}\tau^-\bar{\nu}_\tau$ *decays*, *Phys. Rev. Lett.* **109** (2012) 101802 [1205.5442].

[15] P. Gambino, K.J. Healey and S. Turczyk, *Taming the higher power corrections in semileptonic B decays*, *Physics Letters, Section B: Nuclear, Elementary Particle and High-Energy Physics* **763** (2016) 60 [1606.06174].

[16] BaBar collaboration, *Measurement of* $|V(cb)|$ *and the Form-Factor Slope in* $\overline{B} \to D\ell^-\overline{\nu}_\ell$ *Decays in Events Tagged by a Fully Reconstructed B Meson*, *Phys. Rev. Lett.* **104** (2010) 011802 [0904.4063].

[17] Belle collaboration, *Measurement of the decay* $B \to D\ell\nu_\ell$ *in fully reconstructed events and determination of the Cabibbo-Kobayashi-Maskawa matrix element* $|V_{cb}|$, *Phys. Rev.* **D93** (2016) 032006 [1510.03657].

[18] MILC collaboration, *B→Dℓν form factors at nonzero recoil and —*V_{cb}*— from 2+1-flavor lattice QCD*, *Phys. Rev. D* **92** (2015) 034506 [1503.07237].

[19] HPQCD collaboration, $B \to Dl\nu$ *form factors at nonzero recoil and extraction of* $|V_{cb}|$, *Phys. Rev. D* **92** (2015) 054510 [1505.03925].

[20] T. Kaneko, *Heavy flavor physics from lattice QCD*, *PoS* **LATTICE2022** (2023) 238 [2304.01618].

[21] M. Fael, K. Schönwald and M. Steinhauser, *Third order corrections to the semileptonic b→c and the muon decays*, *Phys. Rev. D* **104** (2021) 016003 [2011.13654].

[22] M. Bordone, B. Capdevila and P. Gambino, *Three loop calculations and inclusive Vcb*, *Phys. Lett. B* **822** (2021) 136679 [2107.00604].

[23] S. Hashimoto, *Inclusive semi-leptonic B meson decay structure functions from lattice QCD*, *Progress of Theoretical and Experimental Physics* **2017** (2017) 53 [1703.01881].

[24] M.T. Hansen, H.B. Meyer and D. Robaina, *From deep inelastic scattering to heavy-flavor semileptonic decays: Total rates into multihadron final states from lattice QCD*, *Phys. Rev. D* **96** (2017) 094513 [1704.08993].

[25] P. Gambino and S. Hashimoto, *Inclusive Semileptonic Decays from Lattice QCD*, *PHYSICAL REVIEW LETTERS* **125** (2020) 32001 [2005.13730].

[26] J.C.A. Barata and K. Fredenhagen, *Particle scattering in Euclidean lattice field theories*, *Commun. Math. Phys.* **138** (1991) 507.

[27] G. Bailas, S. Hashimoto and T. Ishikawa, *Reconstruction of smeared spectral functions from Euclidean correlation functions*, *Progress of Theoretical and Experimental Physics* **2020** (2020) 43 [2001.11779].

[28] M. Hansen, A. Lupo and N. Tantalo, *Extraction of spectral densities from lattice correlators*, *Physical Review D* **99** (2019) [1903.06476].

[29] P. Gambino, S. Hashimoto, S. Mächler, M. Panero, F. Sanfilippo, S. Simula et al., *Lattice QCD study of inclusive semileptonic decays of heavy mesons*, *JHEP* **07** (2022) 083 [2203.11762].

[30] C.N. Yang and R.L. Mills, *Conservation of isotopic spin and isotopic gauge invariance*, *Phys. Rev.* **96** (1954) 191.

[31] S.L. Glashow, *The renormalizability of vector meson interactions*, *Nuclear Physics* **10** (1959) 107.

[32] S.L. Glashow, *Partial-symmetries of weak interactions*, *Nuclear Physics* **22** (1961) 579.

[33] A. Salam and J.C. Ward, *Weak and electromagnetic interactions*, *Nuovo Cim.* **11** (1959) 568.

[34] A. Salam and J.C. Ward, *Electromagnetic and weak interactions*, *Phys. Lett.* **13** (1964) 168.

[35] S. Weinberg, *A model of leptons*, *Phys. Rev. Lett.* **19** (1967) 1264.

[36] P.W. Higgs, *Broken symmetries and the masses of gauge bosons*, *Phys. Rev. Lett.* **13** (1964) 508.

[37] P. Higgs, *Broken symmetries, massless particles and gauge fields*, *Physics Letters* **12** (1964) 132.

[38] F. Englert and R. Brout, *Broken symmetry and the mass of gauge vector mesons*, *Phys. Rev. Lett.* **13** (1964) 321.

[39] M. Gell-Mann, *The Eightfold Way: A Theory of strong interaction symmetry*, .

[40] H. Fritzsch, M. Gell-Mann and H. Leutwyler, *Advantages of the Color Octet Gluon Picture*, *Phys. Lett. B* **47** (1973) 365.

[41] H.D. Politzer, *Reliable Perturbative Results for Strong Interactions?*, *Phys. Rev. Lett.* **30** (1973) 1346.

[42] D.J. Gross and F. Wilczek, *Ultraviolet behavior of non-abelian gauge theories*, *Phys. Rev. Lett.* **30** (1973) 1343.

[43] M.E. Peskin and D.V. Schroeder, *An Introduction to quantum field theory*, Addison-Wesley, Reading, USA (1995).

[44] M. Thomson, *Modern particle physics*, Cambridge University Press, New York (2013), 10.1017/CBO9781139525367.

[45] M.D. Schwartz, *Quantum Field Theory and the Standard Model*, Cambridge University Press (3, 2014).

[46] E. Noether, *Invariante variationsprobleme*, *Nachrichten von der Gesellschaft der Wissenschaften zu Göttingen, Mathematisch-Physikalische Klasse* **1918** (1918) 235.

[47] R.P. Feynman, *Space-time approach to quantum electrodynamics*, *Phys. Rev.* **76** (1949) 769.

[48] R.P. Feynman, *Mathematical formulation of the quantum theory of electromagnetic interaction*, *Phys. Rev.* **80** (1950) 440.

[49] Y. Nambu, *Quasi-particles and gauge invariance in the theory of superconductivity*, *Phys. Rev.* **117** (1960) 648.

[50] J. Goldstone, *Field Theories with Superconductor Solutions*, *Nuovo Cim.* **19** (1961) 154.

[51] S. Weinberg, *Physical processes in a convergent theory of the weak and electromagnetic interactions*, *Phys. Rev. Lett.* **27** (1971) 1688.

[52] S. Weinberg, *General theory of broken local symmetries*, *Phys. Rev. D* **7** (1973) 1068.

[53] P. Minkowski, $\mu \to e\gamma$ *at a rate of one out of 109 muon decays?*, *Physics Letters B* **67** (1977) 421.

[54] M. Gell-Mann, P. Ramond and R. Slansky, *Complex Spinors and Unified Theories*, *Conf. Proc. C* **790927** (1979) 315 [1306.4669].

[55] T. Yanagida, *Horizontal symmetry and mass of the t quark*, *Phys. Rev. D* **20** (1979) 2986.

[56] S.L. Glashow, *The Future of Elementary Particle Physics*, *NATO Sci. Ser. B* **61** (1980) 687.

[57] R.N. Mohapatra and G. Senjanovic, *Neutrino Mass and Spontaneous Parity Nonconservation*, *Phys. Rev. Lett.* **44** (1980) 912.

[58] J. Schechter and J.W.F. Valle, *Neutrino masses in su(2) $\bigotimes$ u(1) theories*, *Phys. Rev. D* **22** (1980) 2227.

[59] J. Schechter and J.W.F. Valle, *Neutrino decay and spontaneous violation of lepton number*, *Phys. Rev. D* **25** (1982) 774.

[60] N. Cabibbo, *Unitary symmetry and leptonic decays*, *Phys. Rev. Lett.* **10** (1963) 531.

[61] M. Kobayashi and T. Maskawa, *CP-Violation in the Renormalizable Theory of Weak Interaction*, *Progress of Theoretical Physics* **49** (1973) 652.

[62] L. Wolfenstein, *Parametrization of the kobayashi-maskawa matrix*, *Phys. Rev. Lett.* **51** (1983) 1945.

[63] Particle Data Group collaboration, *Review of Particle Physics*, *Progress of Theoretical and Experimental Physics* **2022** (2022) 083C01.

[64] UTfit collaboration, *The 2004 UTfit collaboration report on the status of the unitarity triangle in the standard model*, *JHEP* **07** (2005) 028 [hep-ph/0501199].

[65] UTfit collaboration, *Model-independent constraints on $\Delta F = 2$ operators and the scale of new physics*, *JHEP* **03** (2008) 049 [0707.0636].

[66] CKMfitter Group collaboration, *CP violation and the CKM matrix: Assessing the impact of the asymmetric B factories*, *Eur. Phys. J. C* **41** (2005) 1 [hep-ph/0406184].

[67] UTfit collaboration, *New UTfit Analysis of the Unitarity Triangle in the Cabibbo-Kobayashi-Maskawa scheme*, *Rend. Lincei Sci. Fis. Nat.* **34** (2023) 37 [2212.03894].

[68] B. Pontecorvo, *Inverse beta processes and nonconservation of lepton charge*, *Zh. Eksp. Teor. Fiz.* **34** (1957) 247.

[69] Z. Maki, M. Nakagawa and S. Sakata, *Remarks on the unified model of elementary particles*, *Prog. Theor. Phys.* **28** (1962) 870.

[70] M. Gell-Mann, *Symmetries of baryons and mesons*, *Phys. Rev.* **125** (1962) 1067.

[71] H.D. Politzer, *Reliable perturbative results for strong interactions?*, *Phys. Rev. Lett.* **30** (1973) 1346.

[72] D.J. Gross and F. Wilczek, *Ultraviolet behavior of non-abelian gauge theories*, *Phys. Rev. Lett.* **30** (1973) 1343.

[73] LHCb collaboration, *Observation of $J/\psi\phi$ structures consistent with exotic states from amplitude analysis of $B^+ \to J/\psi\phi K^+$ decays*, *Phys. Rev. Lett.* **118** (2017) 022003 [1606.07895].

[74] LHCb collaboration, *Amplitude analysis of $B^+ \to J/\psi\phi K^+$ decays*, *Phys. Rev. D* **95** (2017) 012002 [1606.07898].

[75] LHCb collaboration, *Observation of structure in the J/ψ -pair mass spectrum*, *Sci. Bull.* **65** (2020) 1983 [2006.16957].

[76] LHCb collaboration, *Observation of New Resonances Decaying to $J/\psi K^+$+ and $J/\psi\phi$*, *Phys. Rev. Lett.* **127** (2021) 082001 [2103.01803].

[77] LHCb collaboration, *Observation of $J/\psi p$ Resonances Consistent with Pentaquark States in $\Lambda_b^0 \to J/\psi K^- p$ Decays*, *Phys. Rev. Lett.* **115** (2015) 072001 [1507.03414].

[78] LHCb Collaboration collaboration, *Observation of a $j/\psi\Lambda$ resonance consistent with a strange pentaquark candidate in $B^- \to j/\psi\Lambda\overline{p}$ decays*, *Phys. Rev. Lett.* **131** (2023) 031901.

[79] E. Eichten, K. Gottfried, T. Kinoshita, J. Kogut, K.D. Lane and T.M. Yan, *Spectrum of charmed quark-antiquark bound states*, *Phys. Rev. Lett.* **34** (1975) 369.

[80] E. Eichten, K. Gottfried, T. Kinoshita, K.D. Lane and T.M. Yan, *Charmonium: The model*, *Phys. Rev. D* **17** (1978) 3090.

[81] A. Deur, S.J. Brodsky and G.F. de Teramond, *The QCD Running Coupling*, *Nucl. Phys.* **90** (2016) 1 [1604.08082].

[82] R.P. Feynman, *The behavior of hadron collisions at extreme energies*, *Conf. Proc. C* **690905** (1969) 237.

[83] T. Mannel, *Effective theory for heavy quarks*, *Lect. Notes Phys.* **479** (1997) 387 [hep-ph/9606299].

[84] M. Neubert, *Effective field theory and heavy quark physics*, in *Theoretical Advanced Study Institute in Elementary Particle Physics: Physics in $D \geqq 4$*, pp. 149–194, 12, 2005, DOI [hep-ph/0512222].

[85] A.V. Manohar and M.B. Wise, *Heavy quark physics*, vol. 10, Camb. Monogr. Part. Phys. Nucl. Phys. Cosmol (2000).

[86] A. Khodjamirian, *Hadron Form Factors: From Basic Phenomenology to QCD Sum Rules*, CRC Press, Taylor & Francis Group, Boca Raton, FL, USA (2020).

[87] M.A. Shifman, A.I. Vainshtein and V.I. Zakharov, *QCD and Resonance Physics: Applications*, *Nucl. Phys. B* **147** (1979) 448.

[88] V. Novikov, L. Okun, M. Shifman, A. Vainshtein, M. Voloshin and V. Zakharov, *Charmonium and gluons*, *Physics Reports* **41** (1978) 1.

[89] L. Reinders, H. Rubinstein and S. Yazaki, *Hadron properties from qcd sum rules*, *Physics Reports* **127** (1985) 1.

[90] J. Gasser and H. Leutwyler, *Quark masses*, *Physics Reports* **87** (1982) 77.

[91] P.T. Matthews and A. Salam, *The Green's functions of quantized fields*, *Nuovo Cim.* **12** (1954) 563.

[92] P.T. Matthews and A. Salam, *Propagators of quantized field*, *Nuovo Cim.* **2** (1955) 120.

[93] C. Gattringer and C.B. Lang, *Quantum chromodynamics on the lattice*, vol. 788, Springer, Berlin (2010), 10.1007/978-3-642-01850-3.

[94] T. DeGrand and C.E. Detar, *Lattice methods for quantum chromodynamics* (2006).

[95] K. Symanzik, *Continuum limit and improved action in lattice theories: (i). principles and φ^4 theory*, *Nuclear Physics B* **226** (1983) 187.

[96] K. Symanzik, *Continuum limit and improved action in lattice theories: (ii). o(n) non-linear sigma model in perturbation theory*, *Nuclear Physics B* **226** (1983) 205.

[97] M. Lüscher and P. Weisz, *Computation of the action for on-shell improved lattice gauge theories at weak coupling*, *Physics Letters B* **158** (1985) 250.

[98] G.M. de Divitiis, R. Petronzio and N. Tantalo, *On the discretization of physical momenta in lattice QCD*, *Phys. Lett. B* **595** (2004) 408 [hep-lat/0405002].

[99] C.T. Sachrajda and G. Villadoro, *Twisted boundary conditions in lattice simulations*, *Phys. Lett. B* **609** (2005) 73 [hep-lat/0411033].

[100] Y. Iwasaki, *Renormalization group analysis of lattice theories and improved lattice action: Two-dimensional non-linear o(n) sigma model*, *Nuclear Physics B* **258** (1985) 141.

[101] Y. Iwasaki, *Renormalization Group Analysis of Lattice Theories and Improved Lattice Action. II. Four-dimensional non-Abelian SU(N) gauge model*, 1111.7054.

[102] K.G. Wilson, *Confinement of quarks*, *Phys. Rev. D* **10** (1974) 2445.

[103] H.B. Nielsen and M. Ninomiya, *No Go Theorem for Regularizing Chiral Fermions*, *Phys. Lett. B* **105** (1981) 219.

[104] N.H. Christ, M. Li and H.-W. Lin, *Relativistic Heavy Quark Effective Action*, *Phys. Rev. D* **76** (2007) 074505 [hep-lat/0608006].

[105] H.W. Lin and N. Christ, *Nonperturbatively determined relativistic heavy quark action*, *Physical Review D - Particles, Fields, Gravitation and Cosmology* **76** (2007) [hep-lat/0608005].

[106] A.X. El-Khadra, A.S. Kronfeld and P.B. Mackenzie, *Massive fermions in lattice gauge theory*, *Physical Review D - Particles, Fields, Gravitation and Cosmology* **55** (1997) 3933 [hep-lat/9604004].

[107] RBC, UKQCD collaboration, *Nonperturbative tuning of an improved relativistic heavy-quark action with application to bottom spectroscopy*, *Phys. Rev. D* **86** (2012) 116003 [1206.2554].

[108] N.H. Christ, J.M. Flynn, T. Izubuchi, T. Kawanai, C. Lehner, A. Soni et al., *B-meson decay constants from 2+1-flavor lattice QCD with domain-wall light quarks and relativistic heavy quarks*, *Physical Review D* **91** (2015) .

[109] G.P. Lepage and P.B. Mackenzie, *Viability of lattice perturbation theory*, *Phys. Rev. D* **48** (1993) 2250.

[110] D.B. Kaplan, *A Method for simulating chiral fermions on the lattice*, *Phys. Lett. B* **288** (1992) 342 [hep-lat/9206013].

[111] Y. Shamir, *Chiral Fermions from Lattice Boundaries*, *Nuclear Physics, Section B* **406** (1993) 90 [hep-lat/9303005v1].

[112] Y. Shamir, *Constraints on the existence of chiral fermions in interacting lattice theories*, *Phys. Rev. Lett.* **71** (1993) 2691.

[113] Y. Shamir, *Anomalies and chiral defects fermions*, *Nucl. Phys. B* **417** (1994) 167 [hep-lat/9310006].

[114] V. Furman and Y. Shamir, *Axial symmetries in lattice QCD with Kaplan fermions*, *Nuclear Physics, Section B* **439** (1994) 54 [hep-lat/9405004v2].

[115] P.H. Ginsparg and K.G. Wilson, *A remnant of chiral symmetry on the lattice*, *Phys. Rev. D* **25** (1982) 2649.

[116] R. Narayanan and H. Neuberger, *Infinitely many regulator fields for chiral fermions*, *Phys. Lett. B* **302** (1993) 62 [hep-lat/9212019].

[117] R. Narayanan and H. Neuberger, *Chiral fermions on the lattice*, *Phys. Rev. Lett.* **71** (1993) 3251 [hep-lat/9308011].

[118] R. Narayanan and H. Neuberger, *Chiral determinant as an overlap of two vacua*, *Nucl. Phys. B* **412** (1994) 574 [hep-lat/9307006].

[119] R. Narayanan and H. Neuberger, *A Construction of lattice chiral gauge theories*, *Nucl. Phys. B* **443** (1995) 305 [hep-th/9411108].

[120] H. Neuberger, *Exactly massless quarks on the lattice*, *Phys. Lett. B* **417** (1998) 141 [hep-lat/9707022].

[121] S. Chandrasekharan and U.J. Wiese, *An Introduction to chiral symmetry on the lattice*, *Prog. Part. Nucl. Phys.* **53** (2004) 373 [hep-lat/0405024].

[122] D.B. Kaplan, *Chiral Symmetry and Lattice Fermions*, in *Les Houches Summer School: Session 93: Modern perspectives in lattice QCD: Quantum field theory and high performance computing*, pp. 223–272, 12, 2009 [0912.2560].

[123] A. Borici, *Truncated overlap fermions: The Link between overlap and domain wall fermions*, *NATO Sci. Ser. C* **553** (2000) 41 [hep-lat/9912040].

[124] A.D. Kennedy, *Algorithms for dynamical fermions*, hep-lat/0607038.

[125] M.R. Hestenes and E. Stiefel, *Methods of conjugate gradients for solving linear systems*, *Journal of research of the National Bureau of Standards* **49** (1952) 409.

[126] W.H. Press, S.A. Teukolsky, W.T. Vetterling and B.P. Flannery, *Numerical Recipes 3rd Edition: The Art of Scientific Computing*, Cambridge University Press, USA, 3 ed. (2007).

[127] S.-J. Dong and K.-F. Liu, *Stochastic estimation with Z(2) noise*, *Phys. Lett. B* **328** (1994) 130 [hep-lat/9308015].

[128] P.C. Hohenberg and B.I. Halperin, *Theory of dynamic critical phenomena*, *Rev. Mod. Phys.* **49** (1977) 435.

[129] E. Nelson, *Derivation of the schrödinger equation from newtonian mechanics*, *Phys. Rev.* **150** (1966) 1079.

[130] G. Parisi and Y.-s. Wu, *Perturbation Theory Without Gauge Fixing*, *Sci. Sin.* **24** (1981) 483.

[131] UKQCD collaboration, *Quark mass dependence of hadron masses from lattice QCD*, *Phys. Rev. D* **59** (1999) 074503 [hep-lat/9810021].

[132] P.A. Boyle, A. Juttner, C. Kelly and R.D. Kenway, *Use of stochastic sources for the lattice determination of light quark physics*, *JHEP* **08** (2008) 086 [0804.1501].

[133] C. Best, M. Gockeler, R. Horsley, E.-M. Ilgenfritz, H. Perlt, P.E.L. Rakow et al., *Pion and rho structure functions from lattice QCD*, *Phys. Rev. D* **56** (1997) 2743 [hep-lat/9703014].

[134] S. Güsken, *A study of smearing techniques for hadron correlation functions*, *Nuclear Physics B - Proceedings Supplements* **17** (1990) 361.

[135] UKQCD collaboration, *Gauge invariant smearing and matrix correlators using Wilson fermions at Beta = 6.2*, *Phys. Rev. D* **47** (1993) 5128 [hep-lat/9303009].

[136] G.C. Wick, *The evaluation of the collision matrix*, *Phys. Rev.* **80** (1950) 268.

[137] G. Kilcup, S. Sharpe, R. Gupta, G. Guralnik, A. Patel and T. Warnock, *ϵ beyond the naive mass spectrum*, *Physics Letters B* **164** (1985) 347.

[138] M. Wirbel, B. Stech and M. Bauer, *Exclusive Semileptonic Decays of Heavy Mesons*, *Z. Phys. C* **29** (1985) 637.

[139] J. Chay, H. Georgi and B. Grinstein, *Lepton energy distributions in heavy meson decays from QCD*, *Phys. Lett. B* **247** (1990) 399.

[140] I.I.Y. Bigi, N.G. Uraltsev and A.I. Vainshtein, *Nonperturbative corrections to inclusive beauty and charm decays: QCD versus phenomenological models*, *Phys. Lett. B* **293** (1992) 430 [hep-ph/9207214].

[141] I.I. Bigi, M. Shifman, N.G. Uraltsev and A. Vainshtein, *Qcd predictions for lepton spectra in inclusive heavy flavor decays*, *Phys. Rev. Lett.* **71** (1993) 496.

[142] B. Blok, L. Koyrakh, M.A. Shifman and A.I. Vainshtein, *Differential distributions in semileptonic decays of the heavy flavors in QCD*, *Phys. Rev. D* **49** (1994) 3356 [hep-ph/9307247].

[143] A.V. Manohar and M.B. Wise, *Inclusive semileptonic B and polarized Lambda(b) decays from QCD*, *Phys. Rev. D* **49** (1994) 1310 [hep-ph/9308246].

[144] T. Mannel, *Operator product expansion for inclusive semileptonic decays in heavy quark effective field theory*, *Nucl. Phys. B* **413** (1994) 396 [hep-ph/9308262].

[145] K.G. Wilson, *Non-lagrangian models of current algebra*, *Phys. Rev.* **179** (1969) 1499.

[146] K.G. Wilson and W. Zimmermann, *Operator product expansions and composite field operators in the general framework of quantum field theory*, *Commun. Math. Phys.* **24** (1972) 87.

[147] W. Zimmermann, *Normal products and the short distance expansion in the perturbation theory of renormalizable interactions*, *Annals of Physics* **77** (1973) 570.

[148] E. McLean, C.T.H. Davies, J. Koponen and A.T. Lytle, *$B_s \to D_s \ell \nu$ Form Factors for the full q^2 range from Lattice QCD with non-perturbatively normalized currents*, *Phys. Rev. D* **101** (2020) 074513 [1906.00701].

[149] B. Blossier, P.-H. Cahue, J. Heitger, S. La Cesa, J. Neuendorf and S. Zafeiropoulos, *Extraction of $B_s \to D_s^{(*)}$ form factors from N_f=2 lattice QCD*, *Phys. Rev. D* **105** (2022) 054515 [2110.10061].

[150] J. Flynn, R. Hill, A. Juettner, A. Soni, J.T. Tsang and O. Witzel, *Form factors for semileptonic $B \to \pi$, $B_s \to K$ and $B_s \to D_s$ decays*, *PoS* **LATTICE2021** (2022) 306 [2112.10580].

[151] I.I. Bigi, B. Blossier, A. Le Yaouanc, L. Oliver, O. Pene, J.C. Raynal et al., *Memorino on the '1/2 versus 3/2 puzzle' in $\overline{B} \to l\overline{\nu}X_c$ - a year later and a bit wiser*, *Eur. Phys. J. C* **52** (2007) 975 [0708.1621].

[152] F.U. Bernlochner and Z. Ligeti, *Semileptonic $B_{(s)}$ decays to excited charmed mesons with e, μ, τ and searching for new physics with $R(D^{**})$*, *Phys. Rev. D* **95** (2017) 014022 [1606.09300].

[153] JLQCD collaboration, *Study of intermediate states in the inclusive semi-leptonic $B \to X_c \ell\nu$ decay structure functions*, *PoS* **LATTICE2019** (2019) 148 [2001.11678].

[154] M. Jeżabek and J. Kühn, *Qcd corrections to semileptonic decays of heavy quarks*, *Nuclear Physics B* **314** (1989) 1.

[155] V. Aquila, P. Gambino, G. Ridolfi and N. Uraltsev, *Perturbative corrections to semileptonic b decay distributions*, *Nucl. Phys. B* **719** (2005) 77 [hep-ph/0503083].

[156] T. Becher, H. Boos and E. Lunghi, *Kinetic corrections to $B \to X_c \ell\bar{\nu}$ at one loop*, *JHEP* **12** (2007) 062 [0708.0855].

[157] A. Pak and A. Czarnecki, *Heavy-to-heavy quark decays at NNLO*, *Phys. Rev. D* **78** (2008) 114015 [0808.3509].

[158] K. Melnikov, *O(alpha(s)**2) corrections to semileptonic decay b —> cl anti-nu(l)*, *Phys. Lett. B* **666** (2008) 336 [0803.0951].

[159] A. Alberti, P. Gambino and S. Nandi, *Perturbative corrections to power suppressed effects in semileptonic B decays*, *JHEP* **01** (2014) 147 [1311.7381].

[160] T. Mannel, A.A. Pivovarov and D. Rosenthal, *Inclusive semileptonic B decays from QCD with NLO accuracy for power suppressed terms*, *Phys. Lett. B* **741** (2015) 290 [1405.5072].

[161] BaBar collaboration, *Measurement of the electron energy spectrum and its moments in inclusive $B \to Xe\nu$ decays*, *Phys. Rev. D* **69** (2004) 111104 [hep-ex/0403030].

[162] CDF collaboration, *Measurement of the moments of the hadronic invariant mass distribution in semileptonic B decays*, *Phys. Rev. D* **71** (2005) 051103 [hep-ex/0502003].

[163] DELPHI collaboration, *Determination of heavy quark non-perturbative parameters from spectral moments in semileptonic B decays*, *Eur. Phys. J. C* **45** (2006) 35 [hep-ex/0510024].

[164] Belle collaboration, *Moments of the electron energy spectrum and partial branching fraction of B —> X(c) e nu decays at Belle*, *Phys. Rev. D* **75** (2007) 032001 [hep-ex/0610012].

[165] Belle collaboration, *Moments of the Hadronic Invariant Mass Spectrum in $B \to X_c \ell \nu$ Decays at BELLE*, *Phys. Rev. D* **75** (2007) 032005 [hep-ex/0611044].

[166] BaBar collaboration, *Measurement and interpretation of moments in inclusive semileptonic decays anti-B —> X(c) l- anti-nu*, *Phys. Rev. D* **81** (2010) 032003 [0908.0415].

[167] M. Asakawa, T. Hatsuda and Y. Nakahara, *Maximum entropy analysis of the spectral functions in lattice QCD*, *Prog. Part. Nucl. Phys.* **46** (2001) 459 [hep-lat/0011040].

[168] Y. Nakahara, M. Asakawa and T. Hatsuda, *Hadronic spectral functions in lattice QCD*, *Phys. Rev. D* **60** (1999) 091503 [hep-lat/9905034].

[169] G. Aarts, C. Allton, J. Foley, S. Hands and S. Kim, *Spectral functions at small energies and the electrical conductivity in hot, quenched lattice QCD*, *Phys. Rev. Lett.* **99** (2007) 022002 [hep-lat/0703008].

[170] Y. Burnier and A. Rothkopf, *Bayesian Approach to Spectral Function Reconstruction for Euclidean Quantum Field Theories*, *Phys. Rev. Lett.* **111** (2013) 182003 [1307.6106].

[171] E. Itou and Y. Nagai, *Sparse modeling approach to obtaining the shear viscosity from smeared correlation functions*, *JHEP* **07** (2020) 007 [2004.02426].

[172] G. Parisi, *The strategy for computing the hadronic mass spectrum*, *Physics Reports* **103** (1984) 203.

[173] G.P. Lepage, *The Analysis of Algorithms for Lattice Field Theory*, in *Theoretical Advanced Study Institute in Elementary Particle Physics*, 6, 1989.

[174] G. Backus and F. Gilbert, *The Resolving Power of Gross Earth Data*, *Geophysical Journal of the Royal Astronomical Society* **16** (1968) 169.

[175] J. Bulava, M.T. Hansen, M.W. Hansen, A. Patella and N. Tantalo, *Inclusive rates from smeared spectral densities in the two-dimensional O(3) non-linear σ-model*, *JHEP* **07** (2022) 034 [2111.12774].

[176] Extended Twisted Mass Collaboration (ETMC) collaboration, *Probing the Energy-Smeared R Ratio Using Lattice QCD*, *Phys. Rev. Lett.* **130** (2023) 241901 [2212.08467].

[177] C. Allton, D.J. Antonio, Y. Aoki, T. Blum, P.A. Boyle, N.H. Christ et al., *Physical results from 2+1 flavor domain wall QCD and SU(2) chiral perturbation theory*, *Physical Review D - Particles, Fields, Gravitation and Cosmology* **78** (2008) [0804.0473].

[178] P. Boyle, A. Yamaguchi, G. Cossu and A. Portelli, "Grid: Data parallel C++ mathematical object library." https://github.com/paboyle/Grid.

[179] P.A. Boyle, G. Cossu, A. Yamaguchi and A. Portelli, *Grid: A next generation data parallel C++ QCD library*, *PoS* **LATTICE2015** (2016) 023 [1512.03487].

[180] A. Yamaguchi, P. Boyle, G. Cossu, G. Filaci, C. Lehner and A. Portelli, *Grid: OneCode and FourAPIs*, *PoS* **LATTICE2021** (2022) 035 [2203.06777].

[181] A. Portelli, R. Abott, N. Asmussen, A. Barone, P.A. Boyle, F. Erben et al., *aportelli/hadrons: Hadrons v1.3*, Mar., 2022. 10.5281/zenodo.6382460.

[182] J.M. Flynn, R.C. Hill, A. Jüttner, A. Soni, J.T. Tsang and O. Witzel, *Semi-leptonic form factors for $B_s \to K\ell\nu$ and $B_s \to D_s\ell\nu$*, *PoS* **LATTICE2018** (2019) 290 [1903.02100].

[183] J. Flynn, R. Hill, A. Jüttner, A. Soni, J.T. Tsang and O. Witzel, *Semileptonic $B \to \pi\ell\nu$, $B \to D\ell\nu$, $B_s \to K\ell\nu$, and $B_s \to D_s\ell\nu$ decays*, *PoS* **LATTICE2019** (2019) 184 [1912.09946].

[184] J.M. Flynn, R.C. Hill, A. Jüttner, A. Soni, J.T. Tsang and O. Witzel, *Exclusive semileptonic $B_s \to K\ell\nu$ decays on the lattice*, 2303.11280.

[185] Y.-G. Cho, S. Hashimoto, A. Jüttner, T. Kaneko, M. Marinkovic, J.-I. Noaki et al., *Improved lattice fermion action for heavy quarks*, *JHEP* **05** (2015) 072 [1504.01630].

[186] R.C. Brower, H. Neff and K. Orginos, *The Möbius domain wall fermion algorithm*, *Comput. Phys. Commun.* **220** (2017) 1 [1206.5214].

[187] UKQCD collaboration, *Decay width of light quark hybrid meson from the lattice*, *Phys. Rev. D* **73** (2006) 074506 [hep-lat/0603007].

[188] M.G. Alford, T. Klassen and P. Lepage, *The D234 action for light quarks*, *Nucl. Phys. B Proc. Suppl.* **47** (1996) 370 [hep-lat/9509087].

[189] A.C. Lichtl, *Quantum Operator Design for Lattice Baryon Spectroscopy*, other thesis, 9, 2006, 10.2172/917690, [hep-lat/0609019].

[190] J.M. Flynn, T. Izubuchi, T. Kawanai, C. Lehner, A. Soni, R.S. Van de Water et al., *$B \to \pi \ell \nu$ and $B_s \to K \ell \nu$ form factors and $|V_{ub}|$ from 2+1-flavor lattice QCD with domain-wall light quarks and relativistic heavy quarks*, *Phys. Rev. D* **91** (2015) 074510 [1501.05373].

[191] RBC and UKQCD Collaborations collaboration, *Nonperturbative tuning of an improved relativistic heavy-quark action with application to bottom spectroscopy*, *Phys. Rev. D* **86** (2012) 116003.

[192] J.R. Taylor, *An Introduction to Error Analysis: The Study of Uncertainties in Physical Measurements*, University Science Books, 2 sub ed. (1996).

[193] P. Young, *Everything you wanted to know about data analysis and fitting but were afraid to ask*, 1210.3781.

[194] B. Efron, *Bootstrap Methods: Another Look at the Jackknife*, *Annals Statist.* **7** (1979) 1.

[195] P. Lepage and C. Gohlke, *gplepage/lsqfit: lsqfit version 12.0.3*, Dec., 2021. 10.5281/zenodo.5777652.

[196] G.P. Lepage, B. Clark, C.T.H. Davies, K. Hornbostel, P.B. Mackenzie, C. Morningstar et al., *Constrained curve fitting*, *Nucl. Phys. B Proc. Suppl.* **106** (2002) 12 [hep-lat/0110175].

[197] A. Barone, "LatticeABC (labc)." https://github.com/ale-barone/labc.

[198] J.M. Flynn, A. Juttner, C.T. Sachrajda, P.A. Boyle and J.M. Zanotti, *Hadronic form factors in Lattice QCD at small and vanishing momentum transfer*, *JHEP* **05** (2007) 016 [hep-lat/0703005].

[199] A.X. El-Khadra, A.S. Kronfeld, P.B. Mackenzie, S.M. Ryan and J.N. Simone, *The Semileptonic decays B —> pi lepton neutrino and D —> pi lepton neutrino from lattice QCD*, *Phys. Rev. D* **64** (2001) 014502 [hep-ph/0101023].

[200] *3. Chebyshev Expansions*, in *Numerical Methods for Special Functions*, pp. 51–86 DOI [https://epubs.siam.org/doi/pdf/10.1137/1.9780898717822.ch3].

[201] A. Weiße, G. Wellein, A. Alvermann and H. Fehske, *The kernel polynomial method*, *Rev. Mod. Phys.* **78** (2006) 275 [cond-mat/0504627].

[202] G. Kallen, *On the definition of the Renormalization Constants in Quantum Electrodynamics*, *Helv. Phys. Acta* **25** (1952) 417.

[203] H. Lehmann, *On the Properties of propagation functions and renormalization contants of quantized fields*, *Nuovo Cim.* **11** (1954) 342.

[204] T. Strutz, *Data Fitting and Uncertainty*, Springer Vieweg Wiesbaden, 2 ed. (2015).

[205] C. Michael, *Fitting correlated data*, *Phys. Rev. D* **49** (1994) 2616 [hep-lat/9310026].

[206] R. Bassett and J. Deride, *Maximum a posteriori estimators as a limit of bayes estimators*, *Mathematical Programming* **174** (2018) 129.

[207] W.I. Jay and E.T. Neil, *Bayesian model averaging for analysis of lattice field theory results*, *Phys. Rev. D* **103** (2021) 114502 [2008.01069].